UNIVERSITY OF BIRMINGHAM

ENHANCED DESIGN APPROACHES FOR RIGID AND FLEXIBLE BURIED PIPES USING ADVANCED NUMERICAL MODELLING

by

Saif Alzabeebee

A thesis submitted to The University of Birmingham for the degree of **DOCTOR OF PHILOSOPHY**

Department of Civil Engineering
School of Engineering
College of Engineering and Physical Science
The University of Birmingham
July 2017

ABSTRACT

Buried pipelines are a vital element in maintaining modern life, as they provide a convenient way for transporting products such as gas, potable water, storm water and waste water. These buried structures have to resist external forces due to backfill soil weight and traffic loading. Therefore, the buried pipe needs to be designed properly to withstand these forces. However, careful examination of the current design standards showed significant issues with the existing design methodology for both rigid and flexible pipes. Additionally, limitations and missing information were also found in the literature concerning buried pipes, where the previous studies neglected the effect of the pipe diameter, pipe thickness, installation conditions, backfill height and British Standard traffic loading. Therefore, a full understanding of the behaviour, and hence the design, of buried pipes cannot be achieved based on the previous studies. Thus, this research aimed to use advanced finite element modelling and novel advanced machine learning techniques (namely evolutionary polynomial regression (EPR)) to improve the understanding and propose improvements in the design methods for buried rigid (concrete) and flexible (unplasticized polyvinyl chloride (PVCu)) pipes, to aid with the achievement of a more economic and robust design.

A robust finite element model was developed in this research, where the accuracy of the developed model was validated against real laboratory and field tests of buried pipes under surface static and moving loads. The model was then taken forwards to conduct extensive parametric studies on the effect of the pipe diameter, pipe thickness, backfill height, loading condition and installation condition for both

concrete and PVCu pipes. The obtained results were discussed thoroughly to provide a comprehensive understanding of the response of buried pipes under backfill soil load only and combined backfill soil and traffic loads.

Ultimately, the results obtained from the analyses were linked to the design standards to investigate the robustness of the current design methodologies, where significant issues were found in these standards. Therefore, new modifications (new design models and new design chart) have been proposed using the results of the finite element modelling, utilising the evolutionary polynomial regression analysis.

In summary, the outcomes of this research are a critical literature review, highlighting issues in the previous studies; an improved understanding of the behaviour of buried concrete and PVCu pipes; novel design models for buried concrete pipes; and a novel design chart for buried PVCu pipes. These design models and chart could be easily used by designers for an economic and robust design of buried concrete and PVCu pipes.

PUBLICATIONS

The following publications were prepared from this thesis during the course of the author's study:

Journal papers:

- Alzabeebee, S., Chapman, D., Jefferson, I. and Faramarzi, A. (2017) The response of buried pipes to UK standard traffic loading. **Proceedings of the Institution of Civil Engineers - Geotechnical Engineering**, 170 (1): 38-50.

- Alzabeebee, S., Chapman, D. and Faramarzi, A. Development of a novel model to estimate bedding factors to ensure the economic and robust design of rigid pipe under soil loads. **Tunnelling and Underground Space Technology,** (accepted)**.**

- Alzabeebee, S., Chapman, D. and Faramarzi, A. Economical design of buried concrete pipes subjected to UK standard traffic loading. **Proceedings of the Institution of Civil Engineers – Structures and Buildings,** (accepted)**.**

- Alzabeebee, S., Chapman, D. and Faramarzi, A. Innovative approach to determine the minimum wall thickness of flexible buried pipes. **Geomechanics and Engineering,** (under review)**.**

Conference papers:

- Alzabeebee, S., Chapman, D., Faramarzi, A., 2017. Numerical investigation of the bedding factors associated with the design of buried concrete pipes subjected to traffic loading. Proceeding of the 25th UKACM Conference on Computational Mechanics, Birmingham, UK, pp. 183-186.

- Alzabeebee, S., Chapman, D.N. and Faramarzi, A., 2017, Numerical investigation of the bedding factor of concrete pipes under deep soil fill. Proceeding of the 2nd World Congress on Civil, Structural, and Environmental Engineering (CSEE'17), Barcelona, Spain, paper number 119.

- Alzabeebee, S., Chapman, D.N., Jefferson, I. and Faramarzi, A., 2016. Investigating the maximum soil pressure on a concrete pipe with poor haunch support subjected to traffic live load using numerical modelling. Proceeding of the 11th Pipeline Technology Conference, Berlin, Germany, 11 pages.

This work is dedicated to my mother

ACKNOWLEDGMENTS

I am thankful for my mother, Sameerah, my father, Imad, my sister, Aoula, and my brother, Mohammed, for the unconditional love, endless encouragements and unending support. Your support, prayers and wishes helped me to pass all the difficulties I have come through during the stages of this stressful study. No words can describe how thankful I am.

I would also like to express my deep appreciations to my supervisors Prof. David Chapman and Dr Asaad Faramarzi for their robust guidance and continuous wise advices. Their support helped me to improve my academic writing, presentation skills and critical thinking. Thank you.

I am also grateful for the help provided by Prof. Ian Moore, Queen's University, Canada. The useful discussions with him have increased my confidence in my approach and helped me to identify the issues in the previous studies. He also provided experimental data for validating my finite element model.

I am also thankful for my third supervisor Prof. Ian Jefferson for the useful suggestions and encouragements during the early stages of the research.

I must thank my friends from the University of Al-Qadisiyah, Dr Adnan Al-Sibahy, Mr Hamid Kadim, Dr Jallal Al-Obaedi and Dr Basim Al-Humeidawi for their encouragements. They also helped me to meet the difficult requirements of the sponsor by being my guarantors.

I also acknowledge the Higher Committee for Education Development in Iraq (HCED) for making my dream of studying abroad comes true.

I also thank my fiends Ali Abbas, Wisam Al-Shohani, Yasameen Al-Ameen, Raid Kraidi, Dr Nesreen Al-Obaidy and Harith Ayoob. They have supported, helped and encouraged me during the critical times of this study. I would also like to thank my colleagues in the Department of Civil Engineering Chris Shaw and Dr Giulio Curioni and for the useful discussions and encouragements. Finally, I would like to thank Mrs Janet Hingley for proofreading my thesis.

TABLE OF CONTENTS

LIST OF FIGURES

LIST OF TABLES

LIST OF SYMBOLS

AASHTO	American Association of State Highway and Transportation Officials
ACPA	American Concrete Pipe Association
BF	bedding factor
BS	British Standards
C_c	soil load factor for the case of the wide trench condition
CD	coefficient of determination
C_d	soil load factor for the case of a narrow trench condition
CLSM	controlled low strength material
CL90	silty clay with a minimum degree of compaction of 90% of the standard Proctor density
CL80	silty clay with a minimum degree of compaction of 80% of the standard Proctor density
c'(kPa)	cohesion of the soil
D (m)	inside diameter of the pipe
DC	Duncan-Chang hyperbolic soil model
$Disp.$ (m)	maximum displacement of the buried pipe according to the British Standard
D_L	displacement lag factor
$Dmean$ (m)	mean diameter of the pipe
D_{out} (m)	outside diameter of the pipe
$D-load$ (kN/m)	required three-edge bearing load
D/t	normalized diameter
E (kPa)	modulus of elasticity
EPR	evolutionary polynomial regression analysis
EPR-MOGA	multi-objective evolutionary polynomial regression analysis
E' (kPa)	overall modulus of soil reaction
f_c' (kPa)	compressive strength of the concrete
FEM	finite element analysis

FS	factor of safety
GP90	poorly-graded gravelly sand with a minimum degree of compaction of 90% of the standard Proctor density
H (m)	backfill height
HAF	horizontal soil arching factor
H_c (m)	critical backfill height
H_e (m)	height of the plane of equal settlement above the top of the pipe
I_P (mm^4/mm)	moment of inertia of the pipe
K	modulus number
Ka	lateral active earth pressure coefficient
K_X	coefficient of displacement
LE	linear elastic model
M (kN.m/m)	bending moment of the buried pipe calculated from the finite element modelling
Max	maximum value
MC	Mohr-Coulomb elastic-perfectly plastic model
$mean$	mean value
Min	minimum value
M_{lab} (kN.m/m)	laboratory bending moment
ML49	sandy silt soil with a degree of compaction of 49% of the standard Proctor density
ML80	sandy silt soil with a degree of compaction of 80% of the standard Proctor density
ML90	sandy silt soil with a degree of compaction of 90% of the standard Proctor density
ML95	sandy silt soil with a degree of compaction of 95% of the standard Proctor density
MR-BSI	loading configuration for main road according to the British Standards
n	modulus exponent
P_a (kPa)	atmospheric pressure

Pcr (kPa)	critical buckling pressure
Pe (kPa)	maximum soil pressure due to soil weight
P_s (kPa)	maximum soil pressure developed due to traffic loading
PVCu	unplasticised polyvinyl chloride
r (m)	radius of the pipe measured to the centre of the pipe wall
Rf	failure ratio
$\boldsymbol{S}$ (m)	horizontal distance between the centreline of the pipe and the first set of wheels for the truck travelling parallel to the pipe or the distance between the centreline of the pipe and the right-hand truck axle for the case of a truck travelling perpendicular to the pipe
$Smax$ (kPa)	maximum pipe wall stress according to the British Standard
$STDV$	standard deviation
SW80	Well-graded sandy soil with a degree of compaction of 80% of the standard Proctor density
SW85	Well-graded sandy soil with a degree of compaction of 85% of the standard Proctor density
SW90	Well-graded sandy soil with a degree of compaction of 90% of the standard Proctor density
SW95	Well-graded sandy soil with a degree of compaction of 95% of the standard Proctor density
S_3 (kPa)	lateral stress
t (m)	pipe wall thickness
T (kPa)	maximum wall stress for the poor installation condition
To (kPa)	maximum wall stress for the good installation condition
T_W (m)	trench width
VAF	vertical soil arching factor
$W_{backfill}$ (kN/m)	force applied on the pipe due to soil weight
W_t (kN/m)	total force applied on the pipe
$W_{traffic}$ (kN/m)	traffic load applied on the pipe

γ (kN/m^3)	unit weight of soil
υ	Poisson's ratio
μ	coefficient of friction within the soil mass
μ'	coefficient of friction at the trench wall
ϕ'(°)	angle of internal friction

Chapter 1
INTRODUCTION

1.1. The importance of pipelines

According to the Cambridge English dictionary, a pipeline is defined as “a very long large tube, often underground, through which liquid or gas can flow for long distances”. Historically, pipelines have been used for thousands of years by ancient peoples, probably since civilization as we know it commenced. The oldest known use of pipelines dates back to about 3800 years before Christ. For example, archaeological excavations showed the ruins of brick sewer systems in Eshnunna city (an ancient Sumerian city which dates back to 3000-1700 BC) (Gray, 1940); a developed sanitary system in the Indus and Aegean civilizations (2600 BC-1900 BC); and a well-made drainage and sewage networks in Ur city (an ancient Sumerian city which dates back to 3800 BC-500 BC) (The sewage networks in UR city 4000 BC, 2016).

Nowadays, pipelines can be considered as one of the vital elements in maintaining modern life as they provide a convenient way to transport products such as gas, oil, drinking water, sewage and storm water (Balkaya et al., 2012a; Mohamedzein and Al-Aghbari, 2016). Pipelines can also be used as economical and safe conduits for electricity and telecommunication lines (Moser and Folkman, 2008). These pipelines are usually buried in the ground to protect them from damage due to natural hazards and/or vandalism. Moreover, these pipelines can potentially extend over thousands of metres as they are an essential component of the distribution and/or collection networks (García and Moore, 2015a).

As a result of burying a pipe in the ground, during their service life, pipelines need to resist external forces from the soil overburden pressure, ground movement and traffic load, if buried at a shallow depth. Therefore, the buried pipe needs to be designed properly to withstand these forces. Correctly designed pipelines play an important role in the economic development of countries, where over-conservative design may cause financial problems. However, under-conservative design decreases the design life of the pavement if these pipelines are buried underneath a pavement, due to water leakage from broken pipes (for water, sewage and drainage pipes) (Cui et al., 2012). It can also cause the failure of nearby utilities due to the loss of support for these utilities during the excavation to replace the pipeline (Nath, 1983). Therefore, achieving an economical and robust design for buried pipes is a key factor in the development of countries. Hence, it is the subject of this research.

1.2. Terminology of pipe sections

The terminology commonly used to describe the pipe sections has been considered in this research and is shown in Figure 1.1. The ‘crown’ of the pipe is the top point of the pipe’s perimeter and the ‘invert’ is the bottom point of the pipe’s perimeter. The ‘springings’ of the pipe are the left and right points on the pipe’s perimeter that lie on the horizontal axis of the pipe. Therefore, the pipe’s horizontal axis is called the ‘springline’. The pipe’s ‘shoulders’ are the zones bounded by the crown and the springline and the pipe’s ‘haunches’ are the zones bounded by the springline and the invert.

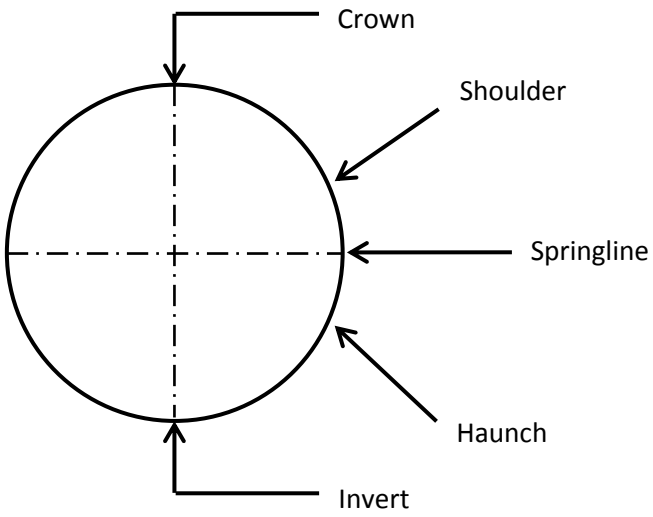

Figure 1.1: Pipe terminology (Rogers, 1987)

1.3. Classifications of pipes

Pipes are usually categorized as either rigid or flexible. Rigid pipes experience small displacements due to loading, where these pipes withstand the load applied from the soil overburden pressure and traffic load without relying on the stiffness of the surrounding soil at the shoulders and springline of the pipe (Robert et al., 2016). However, the performance of rigid pipes is significantly affected by the support condition in the haunch and invert zones (Pettibone and Howard, 1967; Wong et al., 2006). Therefore, these pipes are designed based on the yield strength only. Pipes manufactured from stiff materials such as verified clay, reinforced concrete, concrete and cast iron are considered as stiff pipes (BSI, 2010).

In contrast to rigid pipes, flexible pipes displace significantly due to the applied load (BSI, 2010). This displacement induces a significant increase in the horizontal soil pressure in the surrounding soil; hence it mobilizes additional support from the

surrounding soil (Robert, 2016). Therefore, the behaviour of flexible pipes is significantly affected by the soil's stiffness at the shoulders and the haunch zone (Rogers, 1987; Rogers et al., 1996; Chapman et al., 2007). Thus, the design of flexible pipes is based on displacement, buckling and yield strength (BSI, 2010). Pipes manufactured from flexible materials such as thermoplastic, polyvinyl chloride and glass reinforced plastics are considered as flexible pipes (BSI, 2010).

1.4. Forces on buried pipes

Buried pipes are subjected to different types of forces during their service life depending on the pipe functionality, surrounding soil type and installation conditions. The forces can be divided into internal forces, external forces and additional forces caused by different conditions as follows:

- Internal forces due to the internal fluid pressure for the case of pressurized pipes (Balkaya et al., 2012a).
- External forces due to the backfill soil weight (Moore, 2001).
- External forces due to the traffic loading if the pipe is buried under a paved or unpaved road (Moore, 2001).
- External forces due to shrinking and swelling of reactive soil, if the pipe is buried in a reactive soil (Gallage et al., 2012).
- External forces due to seismic activities (Katona, 2010).
- External forces due to lateral soil movement (Robert, 2010).
- External forces due to geological fault movement (Robert, 2010).
- Additional longitudinal forces due to non-uniform bedding support (Balkaya et al., 2012a, b).

- Additional forces due to wall degradation if the pipe is buried in a chemically active soil (Robert et al., 2016).
- Additional forces caused by cleaning operations.
- Additional forces due to change of support condition caused by voids formation due to pipe leakage (Kamel and Meguid, 2013; Meguid and Kamel, 2014).

1.5. Soil arching in buried pipes

Soil arching is a mechanism in the soil that creates stress changes in the buried structure, due to the significant difference in its stiffness compared to the surrounding soil (Kang et al., 2013a). Buried structures which are stiffer than the surrounding soil (for example concrete pipes) tend to attract more stresses than the surrounding soil. This type of arching is called negative soil arching (Kang et al., 2013a). However, if the stiffness of the buried structure is less than the stiffness of the surrounding soil (for example in the case of a flexible pipe), then the stress in the surrounding soil will be greater than the stress applied on the buried structure. This type of arching is called positive arching (Kang et al., 2013a).

The increase or decrease in the soil stress applied on the buried structure due to soil arching is quantified by a factor called the soil arching factor. The vertical soil arching factor (VAF) gives the percentage of the soil stress attracted by the buried structure as a ratio of the overburden pressure (i.e. $\gamma \times H$, where, γ is the unit weight of the soil and H is the backfill height above the buried structure); and the horizontal arching factor (HAF) gives the percentage of the horizontal soil stress attracted by the buried structure as a ratio of the overburden pressure. The soil arching factor is less than

unity for the case of positive arching, where the applied soil stress on the buried structure will be less than the overburden pressure, as discussed in the previous section (Talby, 1997). In addition, the soil arching factor is greater than unity for the case of negative arching, meaning that the soil stress applied on the buried pipe is greater than the overburden pressure (Talby, 1997).

1.6. Current design practice

1.6.1. Design of concrete pipes

According to the British Standard (BS) (BSI, 1997, 2010) and the American Association of State Highway and Transportation Officials (AASHTO) (AASHTO, 2016), buried concrete pipes are designed using the indirect design method. This method is based on linking the required strength of the buried concrete pipe to the laboratory strength of the pipe by using an empirical factor called a bedding factor (BF). The laboratory strength of the pipe is obtained from a test called the three-edge bearing test, which involves the pipe being supported at the invert only and loaded by a line load at the pipe crown as shown in Figure 1.2 (Moser and Folkman, 2008). The applied force which causes a crack width of 0.254 mm is considered as the laboratory capacity of the pipe (MacDougall et al., 2016).

The bedding factor depends on the installation condition of the buried pipe (AASHTO, 2016). In the AASHTO standard (AASHTO, 2016), there are four standard types of installation depending on the quality of the backfill: Type 1 is the highest quality, where the pipe is fully supported in the haunch zone; while Type 4 is the poorest quality, where the pipe is installed directly on the native soil with poor compaction provided in the haunch zone. Furthermore, the bedding factor value in

the AASHTO standard depends on the diameter of the pipe and the loading conditions (i.e. backfill soil weight only or combined backfill soil weight and traffic load). Figure 1.3 shows the condition of the haunch and bedding soils for each installation type. Table 1.1 shows the soil load bedding factor values (i.e. for the backfill soil weight only) currently adopted in the AASHTO standard (AASHTO, 2016).

The bedding factors used in the BS (BSI, 2010) also depend on the installation quality, but are independent of the diameter of the pipe and the loading condition (i.e. soil load only or combined soil and traffic loads). Currently, there are two general installation types. The first type is called concrete bedding, where the pipe is supported by reinforced or plain concrete in the bedding and haunch zone (Young and O'Reilly, 1987). The second type is called granular bedding or natural base (Young and O'Reilly, 1987). Each of these installation types are divided into classes depending on the quality of the pipe surrounding materials. Only the second type will be reviewed here as it is more practical and is comparable to the AASHTO installation types. Table 1.2 shows the installation classes and the current bedding factor values for each class of granular bedding or natural base installation (BSI, 2010; Young and O'Reilly, 1987).

It is worth mentioning here that in the AASHTO Type 1 installation, the pipe is fully supported and hence it is equivalent to class S in the BS. In addition, in class F the pipe is partially supported in the haunch zone, which is similar to Type 3. Furthermore, in classes N and DD the pipe is directly installed on stiff soil, hence it is similar to the AASHTO Type 4 installation. Finally, the minimum support condition of

class B (i.e. BF = 1.9) can be considered similar to Type 2; where the pipe is well supported, but not quite as well supported as for class S. Hence, it can be assumed that the design installation of AASHTO is similar to the BS design installation. However, the bedding factors for both design standards are different.

The following outlines the design steps for concrete pipes:

Step 1: the total force applied on the pipe in the field is calculated depending on the backfill height, installation condition and the presence of traffic load. The total force applied on the pipe (W_t) is the summation of the load due to the backfill soil weight ($W_{backfill}$) and the traffic load ($W_{traffic}$) (if there is any) as shown in Equation 1.1 (BSI, 1997; BSI, 2010). The backfill soil weight ($W_{backfill}$) is calculated based on the Marston solution (BSI, 1997; BSI, 2010), where the cases of narrow and wide trenches should be compared and the minimum force should be considered as shown in Equation 1.2 (and Equations 1.3 and 1.4). Finally, the traffic load is calculated by multiplying the maximum soil pressure developed due to traffic loading (P_s) by the pipe diameter as shown in Equation 1.5 (BSI, 2010). The details of the BS traffic loading configurations and the calculation of the soil pressure (P_s) are described in Section 1.6.3.

For the AASHTO (2016) standard, the soil weight is calculated utilising a constant vertical arching factor (VAF) as shown in Equation 1.6. The VAF = 1.35 for Type 1; 1.40 for Types 2 and 3; and 1.45 for Type 4 (AASHTO, 2016). The AASHTO design trucks and the method of traffic load calculation of these trucks are not covered in this section as it is outside the scope of this research, because this study focuses on the effect of the UK traffic loading on the behaviour and design of buried pipes. In

addition, the effect of the AASHTO design trucks on the buried pipes have been comprehensively investigated in the literature, as will be discussed in detail in Sections 2.2.4 and 2.3.4.

$$W_t = W_{backfill} + W_{traffic} \tag{1.1}$$

$$W_{backfill} = the\ minimum\ of\ (C_c \times \gamma \times D_{out}^2)\ and\ (C_d \times \gamma \times T_w^2) \tag{1.2}$$

$$C_c = the\ minimum\ of\ (\frac{e^{2\times Ka\times \mu\times \frac{H}{D_{out}}} - 1}{2 \times Ka \times \mu})\ and\ (\frac{e^{2\times Ka\times \mu\times \frac{H_e}{D_{out}}} - 1}{2 \times Ka \times \mu} + (\frac{H}{D_{out}} - \frac{H_e}{D_{out}}) \times e^{2\times Ka\times \mu\times \frac{H_e}{D_{out}}}) \tag{1.3}$$

$$C_d = \frac{1 - e^{-2\times Ka\times \mu'\times \frac{H}{T_W}}}{2 \times Ka \times \mu'} \tag{1.4}$$

$$W_{traffic} = P_s \times D_{out} \tag{1.5}$$

$$W_t = VAF \times \gamma \times H \times D_{out} \tag{1.6}$$

Where, C_c is the soil load factor for the case of the wide trench condition; γ is the unit weight of the soil; D_{out} is the outside diameter of the pipe; Ka is the lateral active earth pressure coefficient; μ is the coefficient of friction within the soil mass; H is the backfill height above the pipe crown; H_e is the height of the plane of equal settlement above the top of the pipe; C_d is the soil load factor for the case of a narrow trench condition; T_W is the trench width; μ' is the coefficient of friction at the trench wall; and VAF is the vertical arching factor.

Step 2: in this step the required three-edge pipe capacity (D-load) is obtained by dividing the force obtained from Equation 1.1 for the BS or Equation 1.6 for the AASHTO standard by the bedding factor, depending on the installation conditions (obtained from Table 1.1 for the AASHTO or Table 1.2 for the BS) and multiplying the result by a factor of safety (FS) (1.25 according to the BSI (2010)), as shown in Equation 1.7. The pipe is then tested in the laboratory to make sure it is able to withstand the calculated force. Surprisingly (to the best of the author's knowledge), there is no guideline in the BS (BSI, 1997; BSI, 2010) as to the necessary pipe wall thickness and reinforcement configuration to achieve the required three-edge bearing load, i.e. the structural design of the pipeline is done based on experience or by trial and error (assuming a wall thickness and reinforcement configuration and verifying the design by using the three-edge bearing test). However, the ASTM C76 (ASTM, 2016) gives the required pipe wall thickness, concrete strength and reinforcement configuration to achieve the required three-edge bearing load ($D-load$).

$$D-load=\frac{W_t\times FS}{BF} \tag{1.7}$$

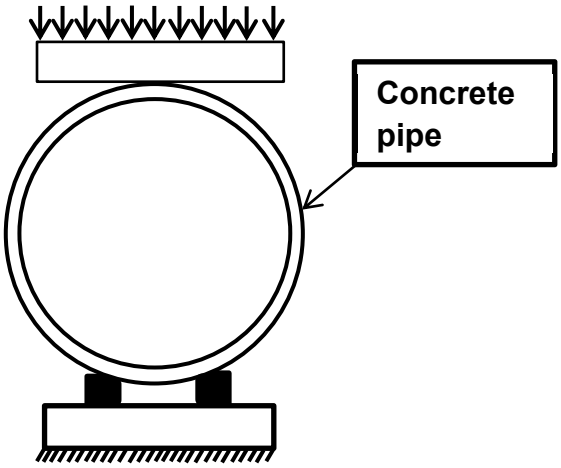

Figure 1.2: Illustration of the three-edge bearing test (Moser and Folkman, 2008)

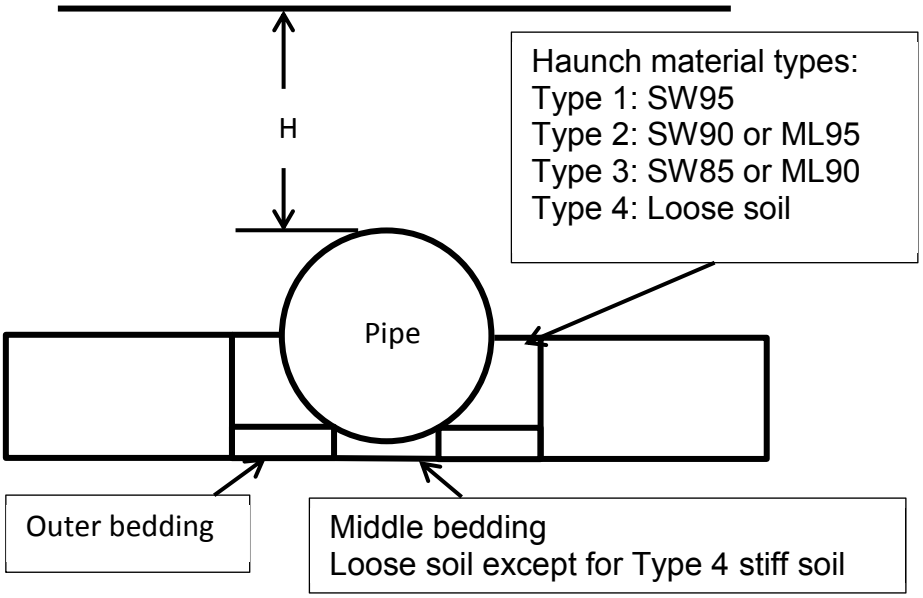

Figure 1.3: AASHTO installation types (AASHTO, 2016) (Note: SW95 is well-graded sandy soil with a degree of compaction of 95% of the standard Proctor density; SW90 is well-graded sandy soil with a degree of compaction of 90% of the standard Proctor density; SW85 is well-graded sandy soil with a degree of compaction of 85% of the standard Proctor density; ML95 is Sandy silt soil with a degree of compaction of 95% of the standard Proctor density; ML90 is Sandy silt soil with a degree of compaction of 90% of the standard Proctor density)

Table 1.1: Bedding factors adopted in the current AASHTO standard (AASHTO, 2016)

Pipe diameter (m)	Standard installations			
	Type 1	Type 2	Type 3	Type 4
0.3	4.4	3.2	2.5	1.7
0.6	4.2	3.0	2.4	1.7
0.9	4.0	2.9	2.3	1.7
1.8	3.8	2.8	2.2	1.7
3.7	3.6	2.8	2.2	1.7

Table 1.2: Installation classes of granular bedding or natural base installation according to the British Standard (Young and O'Reilly, 1987; BSI, 2010)

Installation configuration	Installation class	Bedding factor
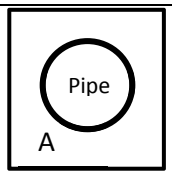	S	2.2
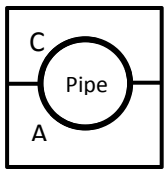	B	1.9 to 2.3
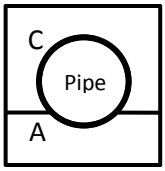	F	1.5 to 1.9
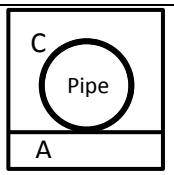	N	1.1 to 1.3
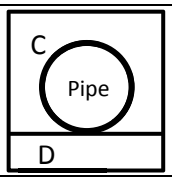	DD	1.1 to 1.3

(Note: A, single size granular material; C, backfill soil free of tree roots, frozen soil, clay lamps, stones larger than 40 mm or any material larger than 75 mm; D, natural soil)

1.6.2. Design of flexible pipes

According to the British Standard (BS), buried flexible pipes are designed based on the following:

- Displacement: the BS recommends calculating the peak displacement of the pipe due to the combined backfill soil weight and traffic load. The displacement should not exceed 5.00-10.00% of the diameter of the pipe (BSI, 2016). However, the pipe displacement limitation has been established based on serviceability requirements and does not represent the overall collapse condition of the pipe (Gumbel et al., 1982). The BS (BSI, 1997) recommends using Equation 1.8 to calculate the maximum displacement ($Disp.$) depending on the maximum soil pressure due to backfill soil weight and traffic load. The maximum soil pressure due to backfill soil weight (Pe) is calculated using the traditional overburden pressure formula (Equation 1.9), where the BS neglects the beneficial effect of positive arching. The maximum soil pressure due to traffic load (P_S) is calculated depending on the truck type, as will be discussed in detail in Section 1.6.3.

$$\frac{Disp.}{Dmean} = \frac{K_X \times (D_L \times P_e + P_S)}{8 \times \frac{E \times I_P}{Dmean^3} + 0.061 \times E'} \quad (1.8)$$

$$Pe = \gamma \times H \quad (1.9)$$

Where, $Dmean$ is the mean diameter of the pipe; K_X is the coefficient of displacement; D_L is the displacement lag factor; E is the modulus of elasticity of the pipe; I_P is the moment of inertia of the pipe; E' is the overall modulus of soil reaction; and H is the backfill height.

- Critical buckling: buckling failure is an excessive inward pipe deformation and happens when the tangential compressive stress exceeds a limit value (Tee et

al., 2013). Exceeding the buckling limit means that the pipe cannot retain its original shape (Tee et al., 2013). Buckling is considered as a failure condition even if the pipe material collapse has not occurred (Gumbel et al., 1982). According to the BS (BSI, 2010), buckling of the pipe is evaluated based on the maximum soil pressure applied on the pipe. The critical buckling pressure (Pcr) is calculated using Equation 1.10 for the supported pipe and Equation 1.11 for the unsupported pipe. The value obtained is then compared with the maximum soil pressure applied on the pipe. According to BS (BSI, 1997), the factor of safety against buckling should be ≥ 1.5 for unsupported pipes and ≥ 2 for supported pipes. However, the BS (BSI, 2010) recommends using Equation 1.11 to calculate the critical buckling pressure, and hence the factor of safety, to account for the loss of side support due to trench digging for the installation of future nearby utilities.

$$Pcr = 0.6 \times (\frac{E \times I_P}{Dmean^3})^{0.33}(E')^{0.67} \quad (1.10)$$

$$Pcr = 24 \times \frac{E \times I_P}{Dmean^3} \quad (1.11)$$

- Pipe material failure: the pipe may fail if the pipe wall stress exceeds the yield stress of the pipe material (Moore, 2001). Therefore, the designer should pay attention to the stresses developed in the pipe wall and make sure that these stresses are lower than the material strength with an appropriate factor of safety. The BS (BSI, 1997; BSI, 2010) recommends calculating the maximum pipe wall stress ($Smax$) using Equation 1.12. However, there is no mention of the appropriate factor of safety against pipe material failure.

$$Smax = \frac{(Pe + P_S) \times Dmean}{2 \times t} \quad (1.12)$$

Where, Pe is the maximum soil pressure due to soil weight and t is the pipe wall thickness.

1.6.3. British Standard traffic loading requirements

In the BS (BSI, 2010), three loading configurations are recommended: eight tyres with a tyre load of 113 kN for 'main road' (main highways); two tyres with a tyre load of 105 kN for 'light trafficked road' (lightly trafficked highways); and two tyres with a tyre load of 60 kN for 'field' (agricultural unpaved road).

The main road loading configuration comprises two axles with four wheels in each axle. The centre-to-centre spacing between the wheels is 1.0 m and the centre-to-centre spacing between the axles is 1.8 m as shown in Figure 1.4(a). The total load of each wheel is 113 kN, including a dynamic allowance factor of 1.3. This dynamic allowance factor accounts for the impact load produced due to truck movement on a ridge or bump on the ground surface.

For lightly trafficked road, the loading configuration comprises two tyres spaced by 0.9 m as shown in Figure 1.4(b). The total load of each wheel is 105 kN, including a dynamic allowance factor of 1.5. For agricultural unpaved road, the loading configuration is also composed of two tyres spaced by 0.9 m. However, the total single tyre load is equal to 60 kN, including a dynamic allowance factor of 2.0.

The BS recommends calculating the maximum soil pressure developed due the main road loading, lightly trafficked road loading and agricultural unpaved road loading using Equations 1.13, 1.14 and 1.15, respectively. These equations were derived based on the Boussinesq solution (BSI, 2010).

$$P_s = \frac{54.5}{H} + \frac{42}{1.8^H} \tag{1.13}$$

$$P_s = \frac{39.5}{H^{1.5}} + \frac{59}{2.7^H} \tag{1.14}$$

$$P_s = \frac{22.5}{H^{1.5}} + \frac{42}{2.7^H} \tag{1.15}$$

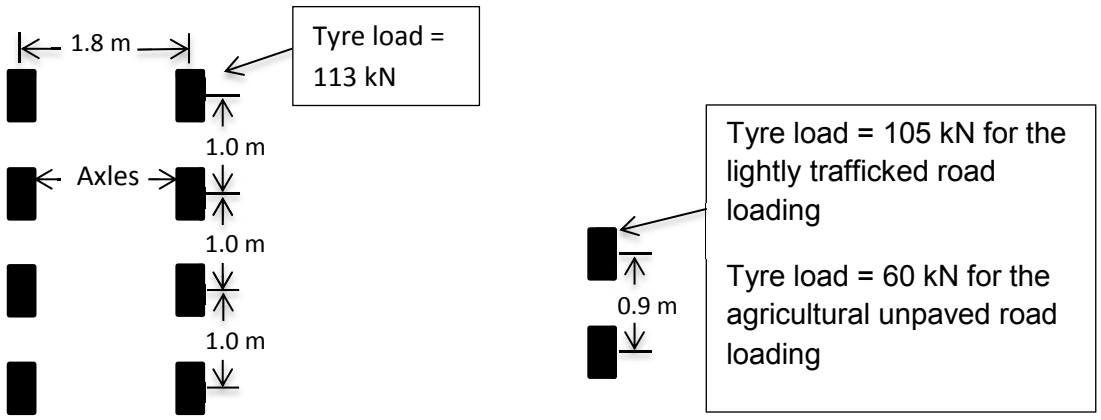

Figure 1.4: (a) The BS main road loading configuration (BSI, 2010); (b) The BS lightly trafficked road loading configuration and agricultural unpaved road loading configuration (BSI, 2010)

1.7. Aim and Objectives

It is evident from the previous sections on current design practice (and from the literature review in **Chapter 2**) that there is much empiricism and potential conservatism in the design of buried pipes. Given the complexity of the problem due to numerous influential factors, simplified and estimated approaches are proven to be inefficient. **The aim of this research is to use numerical modelling and novel advanced machine learning techniques (namely evolutionary polynomial regression (EPR)) to improve understanding and propose improvements in the design methods for buried rigid (concrete) and flexible (unplasticised polyvinyl chloride (PVCu)) pipes, to aid a more economic and robust design**. These types of pipes have been considered as they are the standard pipes used in the UK for drainage and sewerage applications (BSI, 2002; BSI, 2009). For the purposes of this research, these pipes were assumed to be buried in a stable, non-reactive soil, where only the soil overburden pressure and traffic loading were expected to affect the behaviour of the pipes. Other types of forces, such as internal pressure (as discussed in Section 1.4), were outside the scope of the research.

The aim of this research was achieved by following the objectives outlined below. A flow chart for these objectives is also shown in Figure 1.5.

1- To conduct a thorough literature review to understand the current state of the art in relation to the design of buried pipes and to identify gaps in the knowledge.
2- To conduct a thorough literature review to enable a robust and accurate finite element model to be built to simulate the soil-pipe interaction problem.

3- To develop a validated three-dimensional finite element model for buried pipes that captures the key elements of the soil-pipe interaction effects.
4- To understand the methodology of the evolutionary polynomial regression analysis (EPR) and the requirements necessary to develop a robust and accurate model using EPR.
5- To understand the behaviour of buried concrete pipes under soil load by investigating the effect of the pipe diameter, pipe wall thickness, backfill height, and installation conditions. This parametric study was aimed at identifying the parameters affecting the bedding factor.
6- To calculate the bedding factors based on the results from Objective 5 and compare these bedding factors with the BS and AASHTO standard bedding factors, in order to investigate the robustness of these standards.
7- To develop robust models to estimate the bedding factors for buried concrete pipes under the soil weight only using EPR.
8- To investigate the response of buried concrete pipes under the effect of the BS main road traffic loading. This objective aimed to find the critical loading condition of the BS truck and identify the parameters affecting the response of the buried concrete pipes (and hence the bedding factor). The loading configuration for main road was considered, since it represents the worst-case scenario.
9- To calculate the bedding factors for buried concrete pipes under the BS traffic loading based on the results from Objective 8 and compare these bedding factors with the BS bedding factors, in order to investigate the robustness of the BS.

10- To develop robust models to estimate the bedding factors for buried concrete pipes under a combined soil weight and traffic load using EPR.

11- To study the response of buried PVCu pipes under the BS main road traffic loading by conducting a parametric study investigating the effect of the pipe diameter and backfill height on the developed soil pressure, pipe displacement, and pipe wall stress for both good and poorly supported pipes.

12- To investigate the robustness of the BS design equations by comparing the results of the pipe displacement, pipe wall stress and soil pressure obtained from the numerical modelling with the results from these equations (Equations 1.8, 1.11 and 1.12).

13- To use the EPR analysis to develop robust models to estimate the pipe wall stress, pipe displacement and maximum soil pressure for buried flexible pipes.

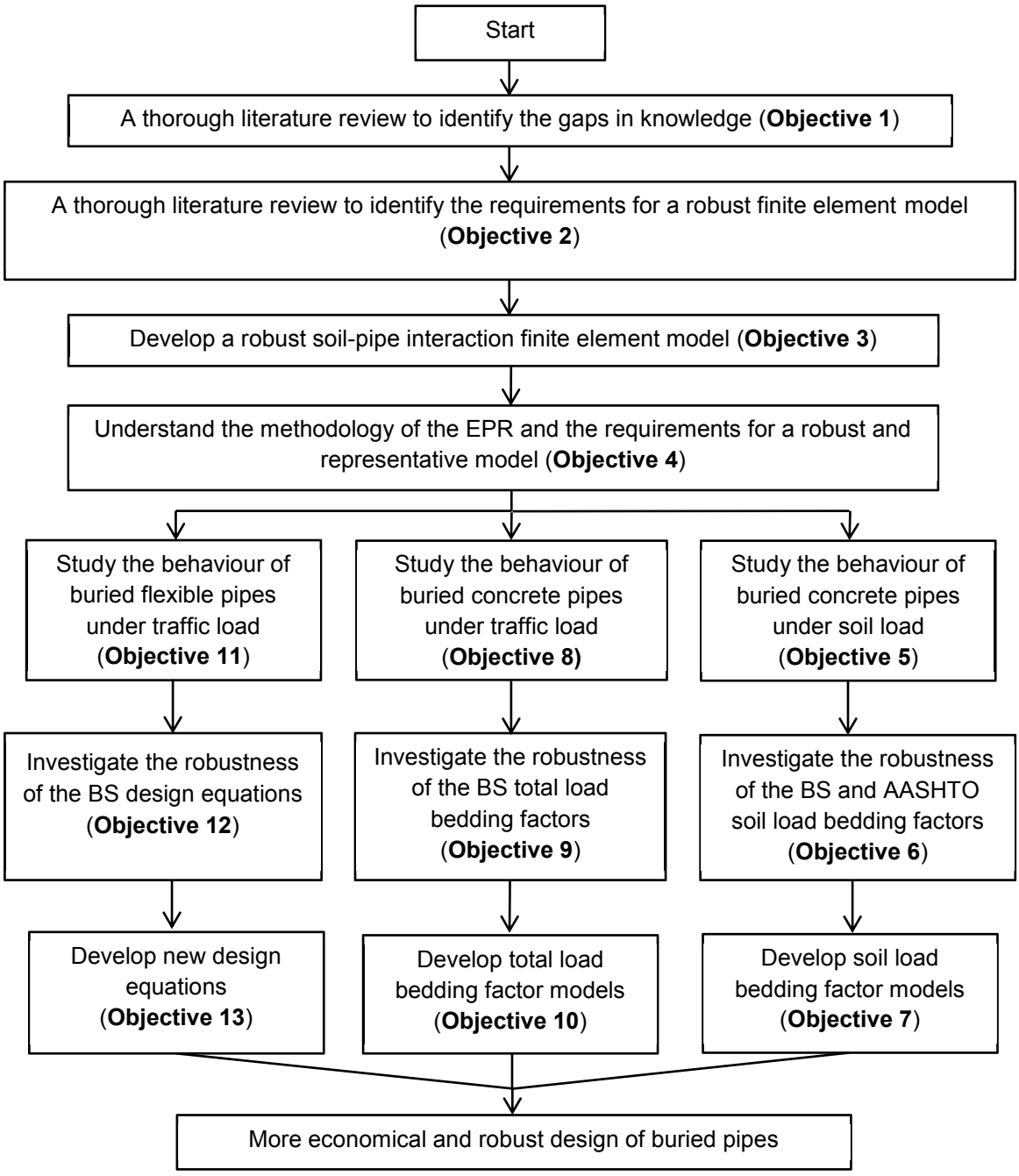

Figure 1.5: Flow chart showing the objectives of the research

1.8. Thesis layout

The thesis consists of seven chapters reporting on published literature, the numerical modelling used for the research and the EPR analysis methodologies, the results from the analysis and the conclusions and the suggestions for future studies. A brief description for each chapter is given below:

Chapter 2 (addressing **Objective 1**) reports on the published literature related to the behaviour of buried concrete and flexible pipes under compaction forces, soil weight and traffic loading. The chapter is divided into two main sections, one section for each pipe type. Each main section finishes with an explicit summary of the gaps in the knowledge and links these gaps to the objectives reported in this chapter; hence justifying the approach taken for the research. Moreover, it ends with a general summary of the overall key points from the chapter.

Chapter 3 (addressing **Objectives 2, 3 and 4**) reports on the development of the finite element modelling and justifies the methodology of the numerical modelling used in this research. The chapter also reports on the results of the model verification using data from previous studies collected from the literature. In addition, the chapter provides a summary of the requirements for a valid soil-pipe interaction model. This summary provides useful information for the approach required for a valid soil-pipe interaction model, which may help researchers who are interested in the numerical modelling of this complex problem. Moreover, the methodology of the EPR analysis and the steps required to obtain a robust and representative model from the input data are also presented in this chapter.

Chapter 4 (addressing **Objectives 5, 6 and 7**) discusses the behaviour of buried concrete pipes under soil load by means of a parametric study; investigating the effect of the pipe diameter, backfill height, pipe thickness and installation condition. In addition, the chapter also investigates the bedding factor by utilising the maximum bending moment obtained from the finite element modelling and discusses the robustness of the BS and AASHTO bedding factors. Finally, the development of a new bedding factors' model is presented.

Chapter 5 (addressing **Objectives 8, 9 and 10**) follows the same order as Chapter 4, but studies the effect of traffic load, particularly the BS main road traffic loading, on the behaviour of buried concrete pipes. This chapter investigates the combined effect of pipe diameter and backfill height, the effect of pipe thickness and the effect of installation conditions on the response of buried concrete pipes under traffic load. In addition, this chapter investigates the robustness of the BS bedding factors and the development of new bedding factor models for buried pipes under the combined action of the soil weight and the BS main road traffic loading.

Chapter 6 (addressing **Objectives 11, 12 and 13**) studies the behaviour of buried flexible pipes under the BS main road traffic loading by means of a parametric study investigating the effect of the pipe diameter, backfill height and installation condition. The chapter also compares the results of the pipe displacement, soil pressure and pipe wall stress with the equations adopted in the BS. A discussion is presented in relation to the derivation of new design equations.

Chapter 7 presents the conclusions from **Chapters 4, 5 and 6**, the contributions to the field of knowledge and the suggestions for future studies.

Chapter 2
LITERATURE REVIEW

2.1. Introduction

This chapter presents a critical review of past research studies, investigating the behaviour of buried concrete and flexible (with emphasis on PVCu) pipes. The aim of the chapter is to illustrate the current state of the art and identify gaps in the knowledge, i.e. areas missing from the previous studies.

The chapter has been divided into two main sections based around the previous studies on buried concrete and flexible pipes. Section 2.2 presents the previous studies on concrete pipes, while Section 2.3 presents the previous studies on flexible pipes. Each of these sections has been divided into subsections covering the behaviour of the buried pipes under compaction forces only, backfill soil weight only and traffic loading. This is done to simplify the review as much as possible as the behaviour of the pipe under these forces is different. Moreover, it was not possible to organise the chapter to explain the behaviour of the buried pipes in general (for example, the effects of pipe diameter, backfill height, installation condition and pipe rigidity), although a significant effort was put in to writing it in this way. This is due to the following:

1- The focus of the previous studies was different (as will be seen in the following sections). For example, some studies investigated the effect of the support condition, while other studies focused on the long-term effect or the trench configuration. Moreover, each study was done considering different parameters (i.e. different trench configurations, different pipe diameters,

different pipe wall thicknesses and different loading conditions (compaction forces, backfill soil weight and combined backfill and traffic load)).

2- The loading configuration for the previous studies under traffic loading was also different; where some studies considered non-standard trucks and other studies considered the Canadian and AASHTO design trucks.
3- The outcomes of the previous studies were also dissimilar; where some studies reported the tensile stresses only, while other studies reported the strains or the displacements only.

Therefore, combining these studies together cannot form a general story describing the developments in the understanding of the behaviour of the buried pipes. However, an effort was made to finish each section with a summary to identify the gaps in the knowledge with regard to the behaviour of the buried pipes under the backfill soil load and traffic loading; hence justifying the approach followed in this research.

2.2. Previous studies on buried concrete pipes

As mentioned in the Introduction, this section is divided into four subsections. The first three subsections present the effect of the compaction force, backfill soil weight and traffic loading. The fourth subsection discusses the gaps in the knowledge and justifies the factors considered in this research.

2.2.1. Effect of compaction forces

The compaction forces applied on the side wall of the buried pipe during construction may add additional stress and lead to pipe failure. Abolmaali and Kararam (2013)

investigated the effect of the compaction forces applied by a HC 920 hydraulic compactor on the behaviour of shallowly buried concrete pipes using three-dimensional finite element analysis. A concrete brittle cracking model was used to model the behaviour of the pipe. Moreover, the steel reinforcement was included in the modelling using a tension stiffening property. This technique allowed the concrete to resist the tensile stresses after cracking by “transferring the forces from the tensile reinforcement to the concrete through the bond” as stated by the authors (Abolmaali and Kararam, 2013, p.199). The accuracy of the developed model was verified by comparing the results of the numerical modelling with the laboratory results of the three-edge bearing tests for concrete pipes with mean diameters of 0.6 m, 0.9 m, and 1.37 m, where very good agreements were achieved as demonstrated in the paper. However, there was no mention in the paper of the model used to simulate the behaviour of the soil (for the case of buried pipes under compaction forces).

Both static and cyclic loads were considered in this study; where the static load represented the compactor weight (200 kPa), while the cyclic load represented the compaction forces applied during the compaction process. The cyclic load was assumed to have an amplitude of 71 kN and a frequency of 2,200 cycles/min. The loaded area was assumed to be with a length of 1.00 m and a width of 0.70 m. A parametric study was carried out to study the influence of the location of the compactor with respect to the pipe, backfill height, and pipe diameter. The induced vertical displacement of the pipe crown and the maximum tensile stress were examined in this study. The results showed that the maximum tensile stress was obtained when the compactor was directly above the pipe. The key finding of this study was that the compaction forces increased the tensile stresses beyond the

tensile strength of the concrete (i.e. it caused cracks in the concrete pipe wall), as shown in Figure 2.1 as an example. However, reinforced concrete pipes are not designed based on the tensile strength of the concrete; therefore the results cannot be directly linked to the design practice of buried concrete pipes.

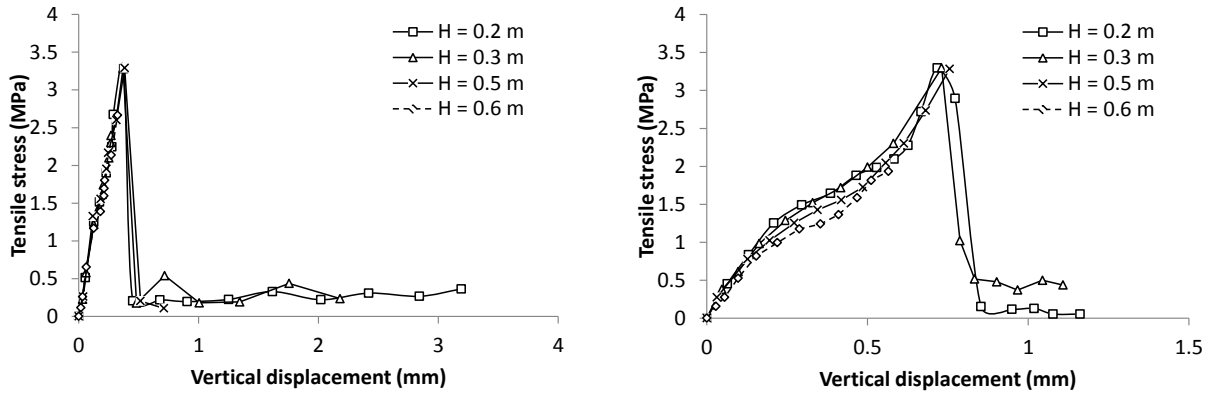

(a) (b)

Figure 2.1: Relationship between the tensile stress and vertical displacement of the concrete pipe crown due to compaction forces: (a) $Dmean$ = 0.6 m; (b) $Dmean$ = 1.2 m (after Abolmaali and Kararam, 2013)

Elshimi and Moore (2013) studied the effect of compaction forces on the behaviour of a concrete pipe with an inside diameter of 2.0 m using two-dimensional finite element analysis. The soil behaviour was simulated using the Mohr-Coulomb elastic-perfectly plastic model; while the concrete pipe behaviour was simulated using the linear elastic model. The compaction forces were modelled by applying a lateral earth pressure on the backfill soil elements beside the buried structure. An empirical factor called the soil kneading factor was introduced and used in this study to account for the increase in the lateral earth pressure due to the effect of the cycles of loading

because of the compaction process. The study found that the effect of compaction forces can be ignored if a vibratory plate compactor was used.

2.2.2. Effect of backfill soil weight only

Pettibone and Howard (1967) produced one of the first studies on the behaviour of buried concrete pipes. The study aimed to understand the effect of the haunch support on the distribution of the soil pressure around the buried pipe. They achieved this aim by monitoring the soil pressure which developed around a 0.5 m inside diameter pipe, using laboratory based tests in a soil box and changing the degree of compaction of haunch soil with respect to the bedding soil. The length, width and height of the box was 2.13 m, 1.83 m and 2.13 m, respectively. A maximum stress of 345 kPa was considered in the tests, which simulates the case of a pipe buried with a maximum backfill height of 16.9 m assuming a soil unit weight of 20.42 kN/m^3. They found that the mobilization of good haunch support occurs if the degree of compaction of the haunch soil is equal to or greater than the degree of compaction of the bedding soil; otherwise, the reaction forces will be concentrated in the bedding zone, creating very high soil pressure at the invert of the pipe.

Wong et al. (2006) investigated the short-term and long-term earth pressure which developed around concrete pipes buried in the AASHTO Type 4 installation condition (i.e. poor support was provided to the pipe in the haunch zone). Four pipes were tested with different trench configurations, as shown in Figure 2.2. The inside diameters of the pipes ranged from 0.6 to 0.9 m. Wong et al. (2006) monitored the soil pressure around the pipes for a period of more than one and a half years (from August 2000 until March 2002). They found that the soil pressure at the invert of the

pipe was significantly higher than the soil pressure at the pipe crown and springline, due to poor haunch support. Moreover, they found that the soil pressure increased with time due to the soil settlement under repeated activities of traffic and snow loads, as shown in Figure 2.3 with trench configuration (d) as an example. However, the authors could not draw a useful conclusion explaining the effect of the pipe diameter on the developed soil pressure, due to the difference of the trenches' configurations and backfill heights considered in the tests (see Figure 2.2).

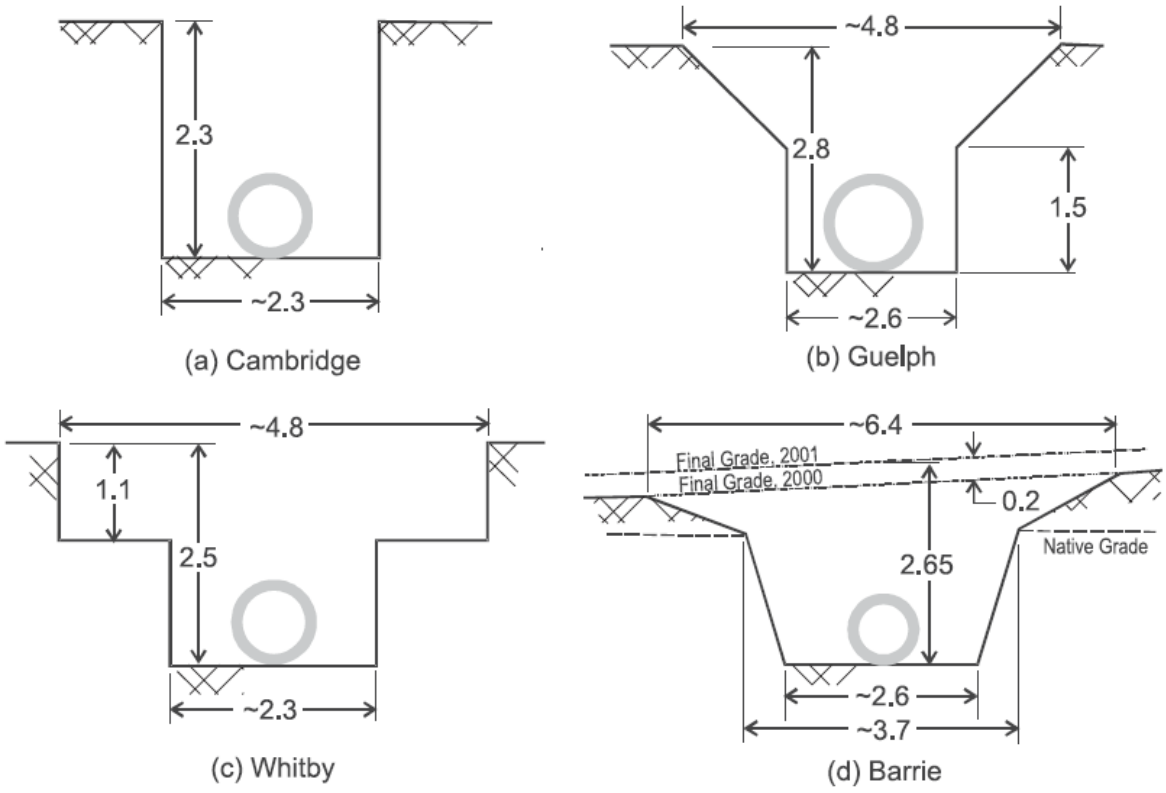

Figure 2.2: Trench configurations considered in Wong et al.'s (2006) study (dimensions are in m)

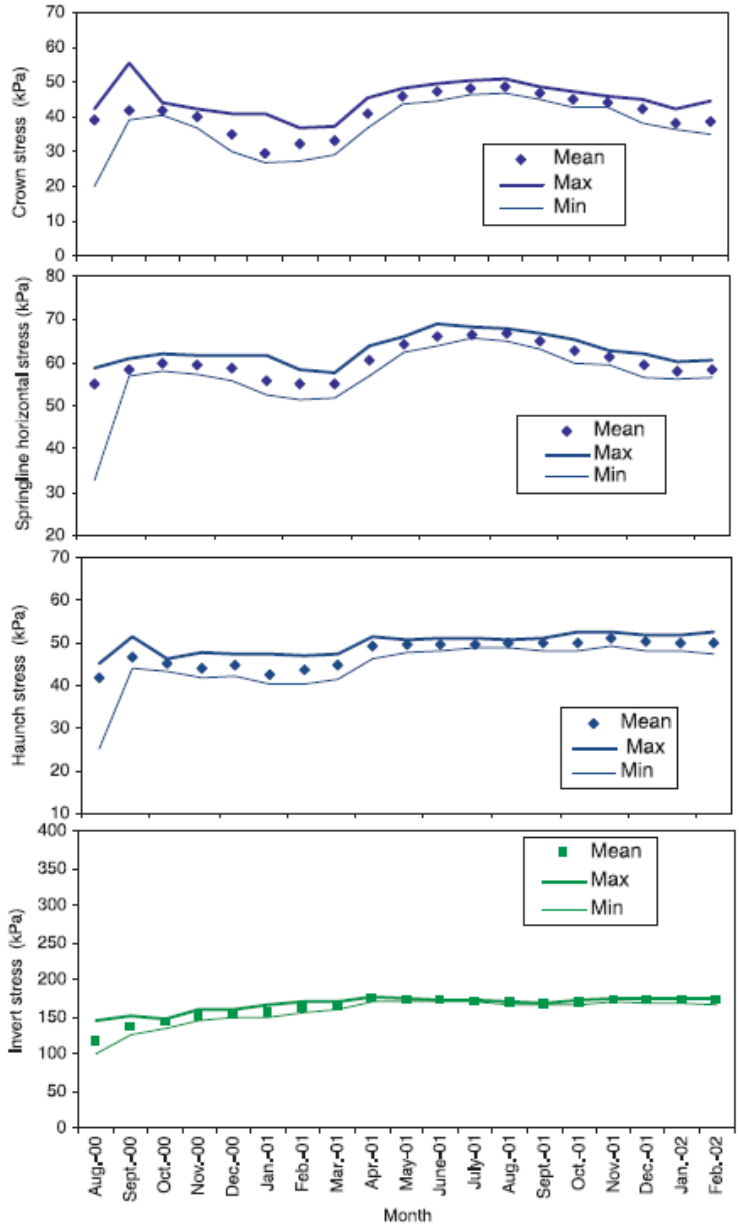

Figure 2.3: Soil pressure around the pipe for trench configuration (d) in Figure 2.2 (Wong et al., 2006)

Kang et al. (2007) investigated the horizontal and vertical arching factor of a buried pipe with an inside diameter of 1.8 m, buried following the requirements of AASHTO Type 3 and Type 4 standard installation conditions and subjected to backfill soil weight using two-dimensional finite element modelling. Kang et al. (2007) modelled

the behaviour of the soil using the hyperbolic soil model, where the dependency of the soil stiffness on the stress level was modelled accurately. The linear elastic model was used to simulate the behaviour of the pipe. Moreover, Kang et al. (2007) simulated the backfill height by using a uniformly distributed pressure applied on the top surface of the model. The considered backfill height ranged from 6.0 m to 27.0 m. They found a decrease in the vertical arching factor (VAF) as the backfill height increased; while the horizontal arching factor (HAF) was found to be independent of the backfill height for both Type 3 and Type 4 installation conditions, as shown in Figures 2.4(a) and (b), respectively.

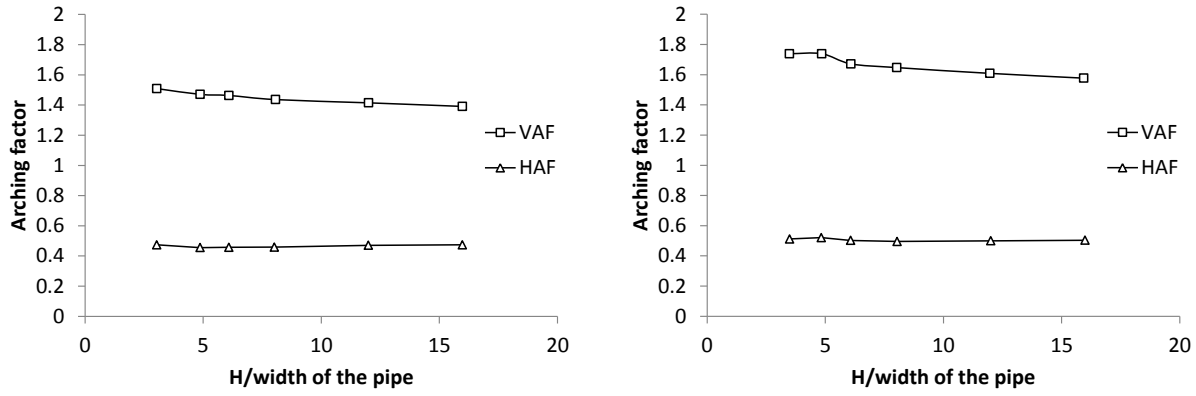

(a) (b)

Figure 2.4: Relationship of vertical and horizontal arching factor with backfill height: (a) AASHTO Type 3 installation; (b) AASHTO Type 4 installation (after Kang et al., 2007)

Abolmaali and Kararam (2010) investigated the effect of the bedding thickness, bedding material stiffness and degree of compaction for the bedding on the tensile stress developed at the invert of a buried concrete pipe using three-dimensional finite element analysis. The concrete behaviour was simulated using a linear elastic soil model, while the soil behaviour was modelled using the Drucker-Prager elastic

perfectly plastic model. Pipes with inside diameters of 0.6 m, 1.5 m and 2.1 m were considered in this study. Moreover, the pipes' wall thicknesses ranged from 0.075 m to 0.225 m. The backfill height considered in this study was from 6.0 m to 30.0 m and the bedding thickness was between 0.075 m and 0.225 m. A gravelly sand with a degree of compaction of 85 and 90 according to standard Proctor test and a sandy silt with a degree of compaction of 70 and 90 according to standard Proctor test were used as bedding materials in the parametric study. They found that the invert tensile stress increased nonlinearly as the backfill height increased, and decreased nonlinearly as the bedding thickness increased. They found also that decreasing the degree of compaction of bedding soil decreased the tensile stress at the pipe invert. This can be justified by the mechanism of the haunch support mobilization described by Pettibone and Howard (1967) and mentioned earlier in this section; where decreasing the degree of compaction of the bedding soil mobilizes greater haunch support and decreases the concentration of reaction forces at the pipe invert. However, Abolmaali and Kararam (2010) did not justify the behaviour they found. Moreover, the authors did not focus on the effect of the pipe diameter or wall thickness on the developed maximum tensile stress; although they considered a diameter range of 0.6 m to 2.1 m and a thickness range of 0.075 m to 0.225 m, the results were poorly presented with the focus on the effect of the bedding thickness only.

Motahari and Abolmaali (2010) investigated the effect of the bedding thickness and bedding soil type on the development of the initial crack and crack opening of buried concrete pipes using a three-dimensional finite element analysis. The behaviour of the concrete and steel was simulated using a brittle-cracking model and isotropic

plasticity model, respectively. Concrete pipes with an inside diameter range of 0.6 m to 1.8 m were considered in the study. Similar conclusions to those reported earlier by Abolmaali and Kararam (2010) were reported in this study, but with justification to the behaviour based on the mechanism of haunch support mobilization. Moreover, they produced design charts for the maximum backfill height limit (critical backfill height (H_c) for different normalized diameters (D/t)). The critical backfill height limit was calculated based on the initial crack limit (Figure 2.5(a)) and crack opening limit (Figure 2.5(b)). However, they did not define the crack width used in producing these design charts. Therefore, it is not obvious if the crack width used was the standard crack width as used in the design standard to define the pipe capacity (i.e. 0.254 mm). Hence, these design charts cannot be directly used without re-evaluation.

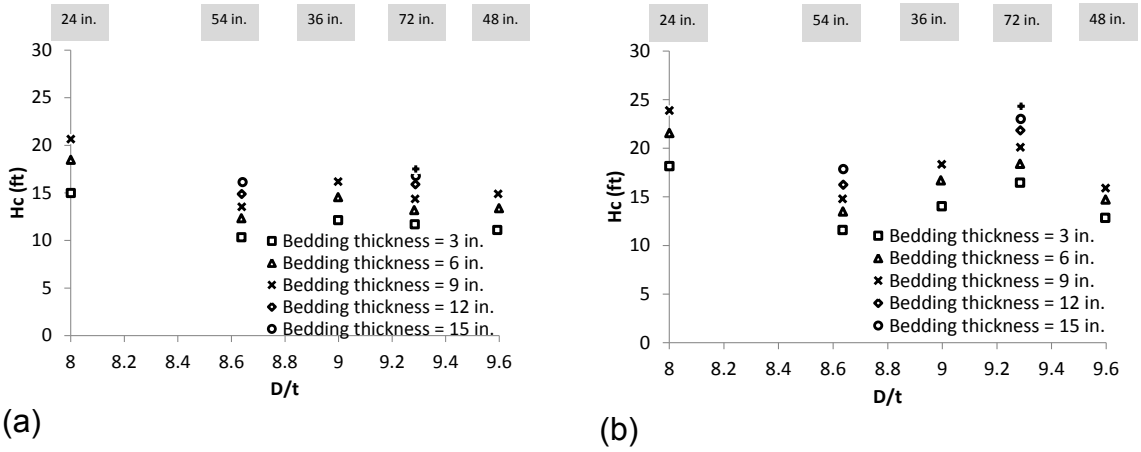

Figure 2.5: Effect of bedding thickness and pipe diameter on the critical backfill height limit for concrete pipes buried in well-graded sandy soil with a degree of compaction of 90% of the standard Proctor density: (a) critical backfill height based on the initial crack development; (b) critical backfill height based on the crack opening development (after Motahari and Abolmaali, 2010)

Allard and El Naggar (2016) studied the effect of the backfill height, trench width, trench inclination and the ratio of the backfill soil stiffness to the surrounding soil stiffness, on the response of a buried concrete pipe with an inside diameter of 1.2 m, using two-dimensional finite element analysis. A backfill height range of 1.2 m to 9.6 m was considered in the study. Allard and El Naggar (2016) modelled the behaviour of the soil and concrete pipe using the hardening soil model and linear elastic model, respectively. The numerical simulation involved calculating the initial stresses for the *in situ* soil, excavating the trench in steps, installing the pipe, and finally adding the backfill soil in steps.

Allard and El Naggar (2016) found that the vertical arching factor significantly decreased as the backfill height above the pipe increased. They also found that the vertical arching factor is significantly affected by the trench configuration; this factor decreased as the trench inclination or the trench width decreased. Furthermore, they found that the ratio of the backfill soil stiffness to the surrounding soil stiffness does not affect this factor.

MacDougall et al. (2016) measured the load capacity of a 0.6 m inside diameter concrete pipe under deep soil fill using a laboratory biaxial cell. The deep soil fill was simulated by applying a uniform pressure on the top surface of the biaxial cell. The length, width and height of the cell was 2.00 m, 2.00 m and 1.60 m, respectively. The maximum applied uniform pressure on the surface was 700 kPa, which is equivalent to a backfill height of 34.3 m assuming a backfill height density of 20.42 kN/m^3. The pipe was installed following the requirements of the AASHTO Type 2 standard installation, where good support was provided for the pipe in the haunch zone.

The pipe was instrumented with eight strain gauges (four were distributed on the inside fibre and four were distributed on the outside fibre of the pipe), displacement transducers and two digital single-lens reflex cameras to record the pipe strain, pipe displacement and development of any crack width under the applied pressure, respectively. The load capacity of the pipe was considered as the load which creates a crack width of 0.254 mm.

MacDougall et al. (2016) found that a uniform pressure of 414 kPa was required to develop a crack width of 0.254 mm. This uniform pressure is equivalent to a backfill height of 20.3 m assuming a backfill unit weight of 20.42 kN/m^3. They calculated the bedding factor by dividing the force which had created a crack width of 0.254 mm in the buried pipe wall, by the pipe capacity measured using the three-edge bearing test (obtained from a previous study conducted by one of the authors). They found that the AASHTO bedding factor for Type 2 design installation is conservative, where the ratio of the calculated bedding factor to the AASHTO design bedding factor was 1.77 (calculated BF was 5.3, while AASHTO BF was 3.0 (Table 1.1)).

2.2.3. Effect of traffic load

Petersen et al. (2010) calculated the bedding factors of buried pipes with different diameters and backfill heights under the effect of AASHTO traffic loading using three-dimensional finite element analysis. The inside diameters of the pipes ranged from 0.3 m to 2.4 m. The maximum backfill height considered in this study was 3.8 m. A single axle load was used in the analysis. The axle consisted of two tyres. Each tyre loading area consisted of a length of 0.50 m and width of 0.25 m, which simulates the foot print specified by AASHTO (2013). The tyre load was 71 kN multiplied by a

dynamic allowance factor depending on the backfill height. The soil was modelled using the Mohr-Coulomb elastic perfectly plastic model; while the pipe was modelled using the linear elastic model. The bedding factor (BF) was calculated by dividing the maximum positive bending moment developed in the pipe wall during the three-edge bearing test, by the maximum positive bending moment developed in the buried pipe obtained from the finite element modelling.

The bedding factor obtained by Petersen et al. (2010) ranged from 1.55 to 4.00, as shown in Figure 2.6. However, Petersen et al. (2010) did not discuss or justify the complex trend in the behaviour of the bedding factors shown in Figure 2.6.

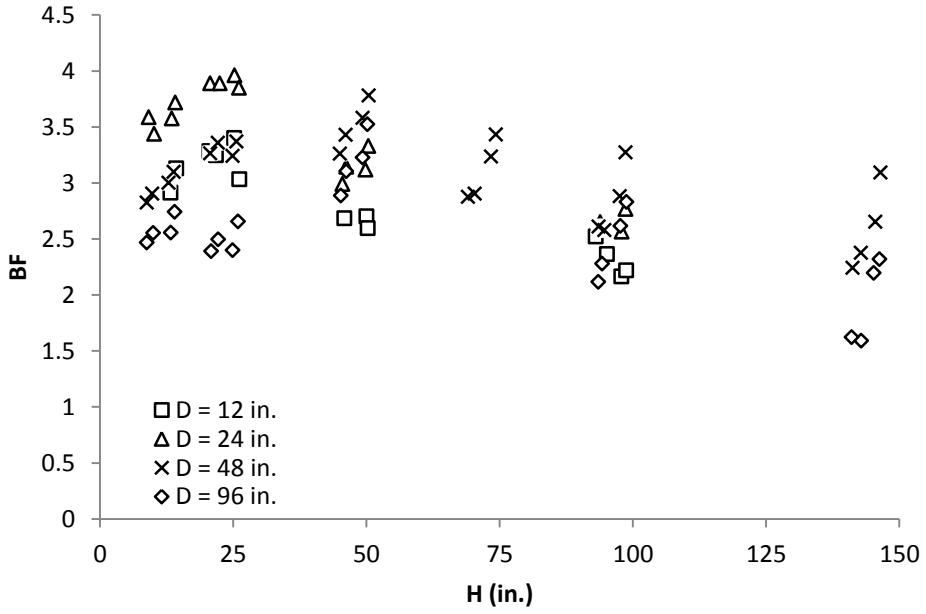

Figure 2.6: The bedding factors obtained from the numerical study of Petersen et al. (2010) for concrete pipes under AASHTO traffic loading (after Petersen et al., 2010)

Kraus et al. (2014) reported the key findings from a research project funded by the Texas Department of Transportation. The aim of the research project was to

investigate the impact of increasing the permitted maximum truck weight on the integrity of in-service buried pipes. For this purpose, Kraus et al. (2014) conducted an experimental and numerical investigation on the response of buried concrete pipes under the effect of traffic loading.

The experimental part aimed to investigate the displacement of jointed concrete pipe buried with a backfill height of 0.5 m and subjected to static and cyclic loads on the surface. A laboratory test box with a length of 2.40 m, width of 3.10 m and height of 2.60 m was manufactured for testing the pipe. The concrete pipe had an inside diameter of 0.5 m. The traffic load was applied using a plate with a length and width of 0.90 m. A maximum load of 107 kN was applied for both static and cyclic tests, which aimed to simulate an AASHTO HS30 truck. The pipe was instrumented with two displacement transducers for measuring the vertical (at the pipe crown) and horizontal (at the pipe springline) displacements. They found that the cyclic load develops a horizontal displacement higher than the static load at the springline of the pipe, as shown in Figures 2.7(a) and (b). Additionally, they noticed the development of a large crack due to the application of cyclic load, as shown in Figure 2.8. They found that the crack was developed due to an error in the installation; where the pipe was supported by the edge of the soil box. This error also led to the differences in the measurements of the horizontal displacement.

The numerical part of the Kraus et al. (2014) study aimed to assess the impact of the backfill height on the crown vertical displacement of the buried concrete pipes. Two-dimensional finite element analysis was used for this purpose. The behaviour of the soil was modelled using the Mohr-Coulomb elastic perfectly plastic model; while the

linear elastic model was used to model the pipe. However, the authors did not mention the details of the traffic loading applied in the finite element analysis. The depth of the soil cover ranged from 0.3 m to 0.9 m. Kraus et al. (2014) found a decrease in the vertical displacement of the pipe crown as the backfill height increased. The ratio of the crown vertical displacement to the pipe diameter was 0.22% for a backfill height of 0.3 m, 0.18% for a backfill height of 0.5 m and less than 0.08% for a backfill height of 0.9 m. However, the study did not recommend a backfill height limit for the safe performance of in-service buried concrete pipes under the AASHTO truck.

It should be noted that this study suffers from two fundamental issues in the methodology as follows:

1- The laboratory tests were conducted by applying a load from a plate with a length and width of 0.90 m. However, the length and width of a standard AASHTO tyre is 0.50 m and 0.25 m, respectively. This means that the stress level applied in the experiment (132 kPa) was significantly lower than the stress level applied from a real AASHTO truck (856 kPa). Therefore, the laboratory model did not correctly simulate the standard truck load.
2- The paper focused only on the horizontal and vertical displacements of the concrete pipes. However, buried concrete pipes are designed based on the load carrying capacity of the buried pipe, or on the bending moment induced in the pipe wall due to the applied load. Hence, the results from the experimental and numerical modelling cannot be directly linked to the design practice of

buried pipes and cannot be used with confidence to recommend a safe backfill height limit.

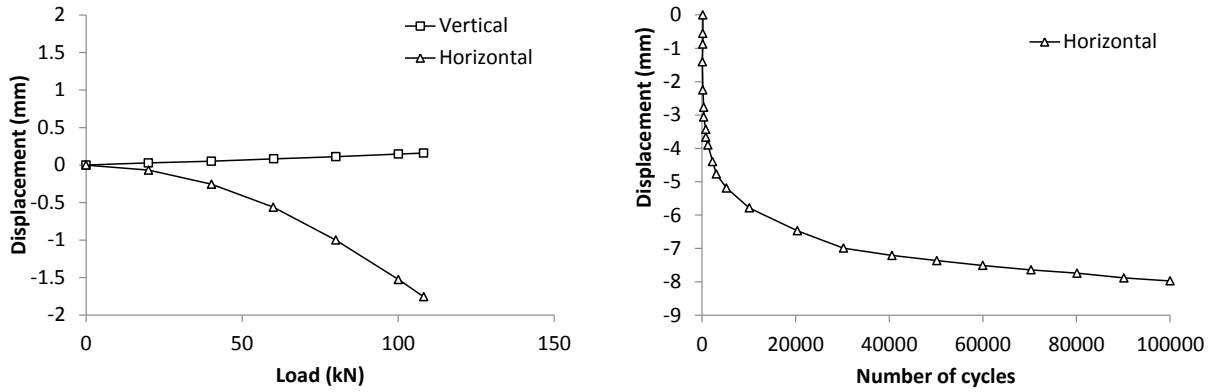

(a) (b)

Figure 2.7: The results of the vertical (at the pipe crown) and horizontal (at the pipe springline) displacements for the buried concrete pipe: (a) due to static load (b) due to cyclic load (after Kraus et al., 2014)

Figure 2.8: Crack development due to the application of cyclic loading (Kraus et al., 2014)

Lay and Brachman (2014) carried out laboratory tests to investigate the strain and the bending moment developed in the wall of a buried concrete pipe with an inside

diameter of 0.6 m under the effect of traffic loading. The pipe was tested in the test pit at the GeoEngineering laboratory at Queen's University, Canada. The laboratory test pit had a length, width and height of 8.00 m, 8.00 m and 3.00 m, respectively. A backfill height range of 0.3 m to 0.9 m was considered in this study. The traffic load was simulated using a two-tyre single axle load. The configuration of the axle simulated the Canadian CL-W truck, where the spacing between the tyres was 1.8 m. The length and width of the tyre footprint was 0.60 m and 0.25 m, respectively, which is the standard footprint recommended by the Canadian design standard (CSA, 2006). The pipe was installed following the requirement of the Type 1 AASHTO installation, where very good support was provided to the pipe in the haunch zone. The pipe was instrumented with eight strain gauges, four distributed on the inside of the pipe wall and four on the outer surface of the pipe.

Six tests were reported in this study, including static and cyclic loads. The details (backfill height and loading magnitude) of these tests are shown in Table 2.1. Lay and Brachman (2014) found that as the backfill height increased, the strain in the pipe wall decreased; the crown moment decreased from 6.0 kN.m/m to 3.9 kN.m/m and 2.1 kN.m/m as the backfill height increased from 0.3 m to 0.6 m and 0.9 m, respectively. In addition, they found that the buried pipe did not fail in any of these experiments. The maximum crack width was 0.150 mm (below the maximum allowable crack width (i.e. 0.254 mm)) and occurred when the backfill height was 0.3 m and the maximum axle load was 400 kN (i.e. test 1).

Table 2.1: Details of tests conducted on buried concrete pipes (Lay and Brachman, 2014)

Test	Backfill height (m)	loading
1	0.3	Increased in steps to a maximum of 400 kN
2	0.3	Ten cycles between 175 kN and 20 kN
3	0.3	Ten cycles between 175 kN and 20 kN
4	0.3	Ten cycles between 175 kN and 20 kN
5	0.9	Increased in steps to a maximum of 465 kN
6	0.6	Increased in steps to a maximum of 500 kN

MacDougall (2014) studied the bending moment of a buried concrete pipe under the effect of traffic loading using laboratory based tests in the test pit at the GeoEngineering laboratory at Queen's University, Canada. The laboratory test pit had a length, width and height of 8.00 m, 8.00 m and 3.00 m, respectively (similar to that used by Lay and Brachman (2014)). The outside diameter of the pipe was 0.8 m. A single AASHTO tyre load of 100 kN with a tyre print area of 0.25 m x 0.50 m was used to simulate the traffic loading. The pipe was installed following the requirement of the Type 2 AASHTO installation, where good support was provided to the pipe in the haunch zone. Three different backfill heights were considered in the tests (0.3 m, 0.6 m and 0.9 m). The maximum bending moment was obtained at the crown. In addition, the maximum bending moment decreased as the backfill height increased: it was equal to 2.9 kN.m/m for a backfill height of 0.3 m and 1.1 kN.m/m for a backfill

height of 0.9 m (i.e. percentage decrease of 61%). Furthermore, no cracks developed in the pipe in all of the reported tests.

Rakitin and Xu (2014) studied the bending moment developed in a concrete pipe with a diameter of 1.4 m subjected to traffic loading by using centrifuge modelling. The study focused on the effect of the location of traffic loading with respect to the pipe and the soil cover on the developed bending moment in the pipe wall. The loading conditions of two trucks, medium and heavy, were considered in this study. The maximum axle load of the medium truck was 95 kN; while the maximum axle load of the heavy truck was 567 kN. Figure 2.9 shows the medium and heavy trucks' configurations. A backfill height range of 1.0 m to 4.0 m was considered in this study. A silty soil was used as a backfill soil for all the tests. Rakitin and Xu (2014) noticed that the highest bending moment in the pipe was recorded when the heaviest axle of the vehicle was directly above the pipe.

They also noticed that the traffic load affected the bending moment in the concrete pipe wall even for a backfill height of 4.0 m, as shown in Figure 2.10 for the buried pipe under the heavy truck loading. They compared this finding with the American Concrete Pipe Association (ACPA) design methodology (ACPA, 2011) and noticed that the ACPA recommended ignoring the effect of traffic load of an AASHTO HS20 truck when the backfill height above the pipe is equal to or greater than 3.0 m. Rakitin and Xu (2014) justified the difference between their results and the recommended ACPA backfill height limit due to the higher axle load used in their experiment (567 kN), which was significantly higher than the HS20 axle load (142 kN). However, only

one tyre was used in the experiment with a maximum tyre stress of 468 kPa, which is lower than the nominal tyre stress of the HS20 truck (568 kPa).

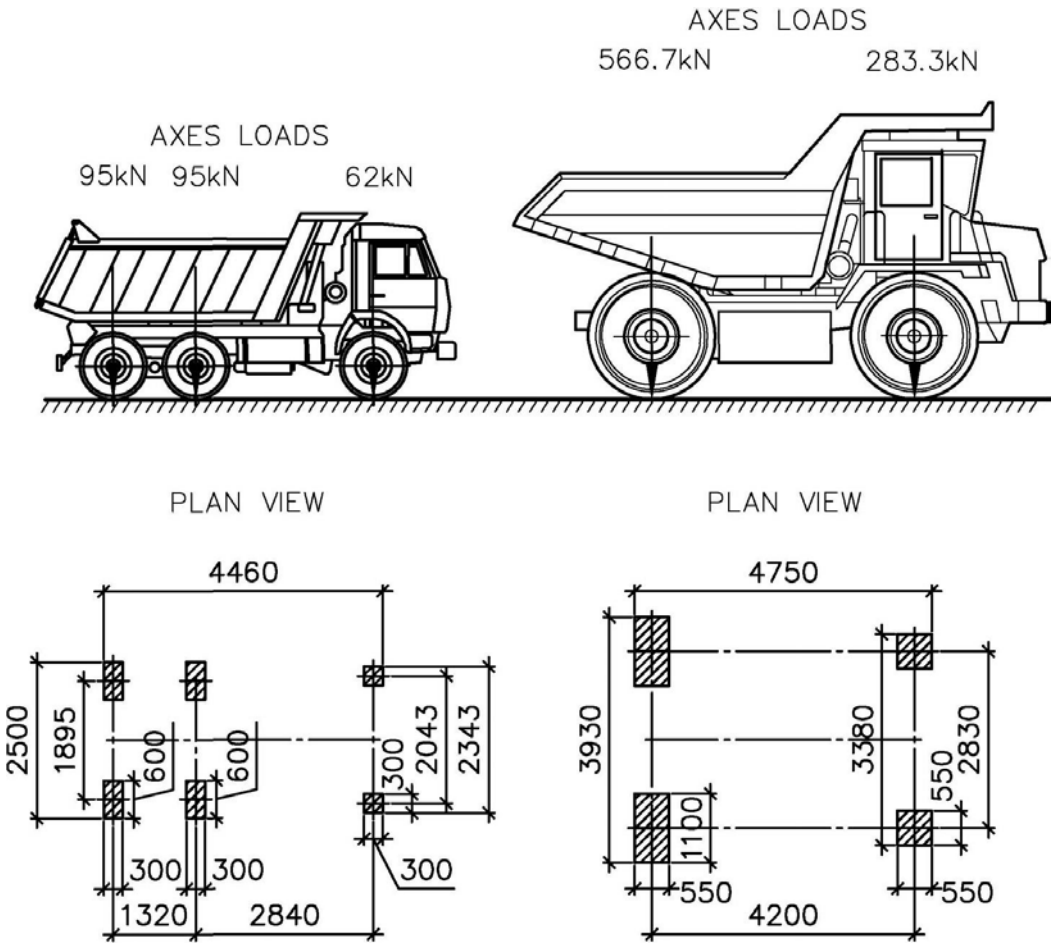

Figure 2.9: Configuration of trucks used in the laboratory analysis of Rakitin and Xu (2014) (dimensions are in mm)

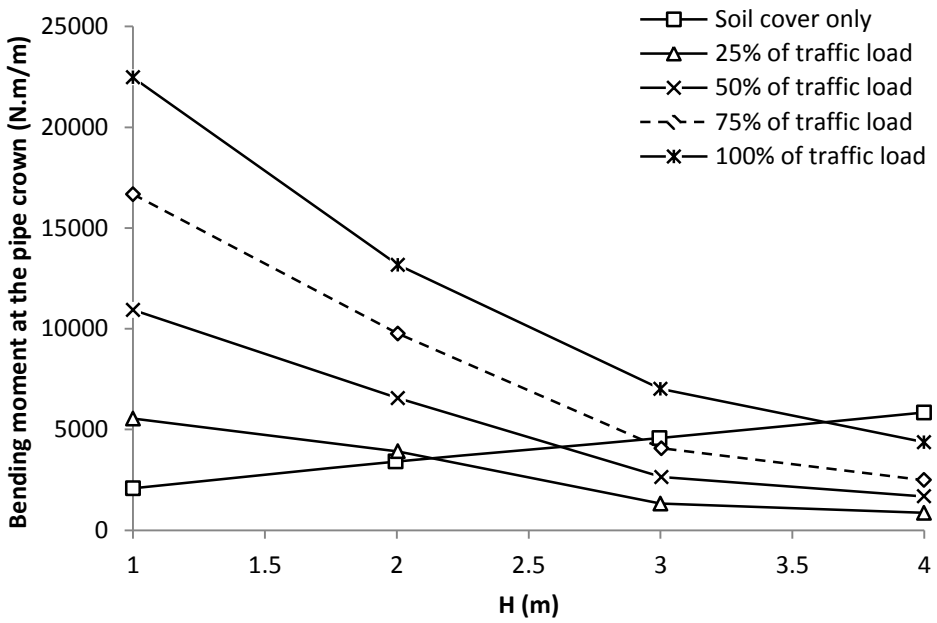

Figure 2.10: Bending moment developed at the pipe crown due to soil weight only and traffic loading only (simulation of heavy truck condition) for different backfill heights (after Rakitin and Xu, 2014)

Sheldon et al. (2015) measured the crown vertical displacement of two in-service buried concrete pipes under static and moving truck loads. The inside diameters of these pipes were 2.1 m and 1.4 m, respectively. The backfill height was 1.4 m for the first pipe and 0.6 m for the second pipe. The test truck had two axles with a maximum axle load of 127 kN (i.e. not a standard truck). Different load cases were investigated for the static loading condition to find the critical loading position of the truck. They found that the maximum displacement (worst-case scenario) was recorded when the heaviest axle was directly above the pipe: the maximum displacement was approximately 0.07 mm for the 2.1 m pipe and 0.13 mm for the 1.4 m pipe. Furthermore, they found that the static load produced higher displacement than the

moving load, where the ratio of moving to static crown vertical displacement ranged from 0.80 to 0.67 depending on the truck speed.

MacDougall et al. (2016) investigated the load capacity of four buried concrete pipes subjected to AASHTO traffic loading requirements. Two pipes had an inside diameter of 0.6 m and a wall thickness of 0.094 m, but with different levels of reinforcement (area of steel of 212 mm^2/m and 380 mm^2/m, respectively). The other two pipes had an internal diameter of 1.2 m and a wall thickness of 0.125 m and 0.144 m, respectively. A laboratory test pit with a length of 8.00 m, width of 8.00 m and height of 3.00 m was used for testing the pipes. The pipes were tested with three different backfill heights (0.3 m, 0.6 m and 1.2 m). Two loading scenarios were considered; the first loading scenario simulated an AASHTO single tyre load, while the second loading simulated an AASHTO single axle load using two plates spaced by 1.8 m. Each plate had a length of 0.50 m and a width of 0.25 m.

Both pipes were installed following the requirements of the AASHTO Type 2 installation. Each pipe was instrumented with eight strain gauges, displacement transducers and two digital single-lens reflex cameras to record the pipe strain, pipe displacement and development of the crack width under the applied soil and traffic loading, respectively.

MacDougall et al. (2016) found that none of the pipes failed under the service loading (i.e. under single axle load with a tyre load of 110 kN). However, the pipes failed (i.e. crack width exceeded 0.254 mm) when the single tyre load exceeded the service load (i.e. 110 kN) by 2.5 to 4.0 times, depending on the pipe diameter, backfill height, pipe thickness and level of reinforcement. In addition, they calculated the bedding

factor for each pipe by dividing the force which had created a crack width of 0.254 mm in the buried pipe wall, by the pipe capacity obtained from the three-edge bearing test (obtained from the manufacturer's data). They also compared the result with the AASHTO total load bedding factors. They found that the AASHTO total load bedding factors are conservative: the ratio of the obtained factors to the AASHTO bedding factors ranged from 1.17 to 1.75. However, the study did not provide an insight into the effect of pipe diameter on the behaviour of buried concrete pipes.

2.2.4. Summary and gaps in knowledge

In summary, it can be concluded that the previous studies on concrete pipes paid significant attention to investigating the soil pressure around the pipe (Pettibone and Howard, 1967; Wong et al., 2006); and the development of tensile stresses in the pipe wall (Abolmaali and Kararam, 2010; Motahari and Abolmaali, 2010); as well as understanding the soil arching in buried concrete pipes in relation to the backfill height and trench configuration (Kang et al., 2007; Allard and El Naggar, 2016). In addition, the previous studies have investigated the response of buried concrete pipes under the Canadian, AASHTO and non-standard trucks (Petersen et al., 2010; Kraus et al., 2014; Lay and Brachman, 2014; MacDougall, 2014; Rakitin and Xu, 2014; Sheldon et al., 2015; MacDougall et al., 2016) and have investigated the effect of the backfill height in relation to the traffic loading (Rakitin and Xu, 2014). However, the following gaps in the knowledge were identified:

1- Little attention has been paid to the real design practice of buried concrete pipes under deep soil fill, where only one published study (MacDougall et al., 2016) has investigated the bedding factor of concrete pipes under a deep

burial condition. However, although the study showed that the current AASHTO bedding factor value for Type 2 installation is conservative, it did not recommend a new bedding factor value. Furthermore, this study did not investigate the bedding factors for AASHTO Type 1, Type 3 and Type 4 installation conditions; nor did it study the effect of the pipe diameter and pipe wall thickness on the bedding factor. **Objectives 5, 6 and 7 of this study (Chapter 4)** will address this gap in knowledge and produce robust and economical bedding factor models for buried concrete pipes under backfill soil weight only.

2- Surprisingly, no study has considered the BS traffic loading requirements, nor investigated the design methodology of the BS, where the previous studies considered AASHTO, Canadian and non-standard trucks as shown in Section 2.2.3. **Objective 8 of this study (Chapter 5)** will address this gap in knowledge by conducting a parametric study to investigate the response of the buried concrete pipes under the BS main road traffic loading.

3- No effort has been made to understand the combined effect of the pipe diameter and backfill height under traffic loading. Moreover, the effect of the concrete pipe wall thickness under traffic load was also neglected in the previous studies. **Objective 8 this study (Chapter 5)** will address this gap in knowledge by studying the effect of the pipe diameter, backfill height and pipe thickness on the response of buried concrete pipes under traffic loading.

4- Different opinions were noted with respect to the recommended backfill height limit for the effect of the traffic load, where the study of Rakitin and Xu (2014) showed that the traffic load affects the bending moment in the concrete pipe

wall, even for a backfill height of 4.0 m. However, the American Concrete Pipe Association (ACPA, 2011) recommended ignoring the effect of the traffic load when the backfill height above the pipe is equal to or greater than 3.0 m. On the other hand, the BS (BSI, 2010) does not recommend a backfill height limit for the effect of traffic load. The BS (BSI, 2010) only provides an equation to predict the maximum soil pressure due to the BS main road traffic loading (Equation 1.13). However, by solving this equation, it can be easily seen that the effect of the traffic load extends to a backfill height of more than 10 m, as shown in Figure 2.11. **Objective 8 of this study (Chapter 5)** will address this gap in knowledge by investigating the response of buried concrete pipes under backfill soil weight only and comparing it with the response under traffic load for different backfill heights, to find the backfill height limit for the traffic load.

5- Little attention has been paid to the real design practice of buried concrete pipes under traffic loading; there are only two published studies concerning the bedding factor of buried concrete pipes under traffic loading. Moreover, these studies only considered the AASHTO traffic loading. Hence, these studies cannot be used to test and improve the current BS bedding factors because of the significant difference of the load configuration and the maximum axle load between the BS main road traffic loading and the AASHTO trucks considered in these studies. This gap in knowledge will be addressed in **Objectives 9 and 10 of this study (Chapter 5),** where the bedding factors for the buried pipes under the BS main road loading will be calculated by utilising the maximum bending moment obtained from finite

element analyses. Moreover, the obtained bedding factors will be used to propose robust models to enable the economic and robust design of buried pipes.

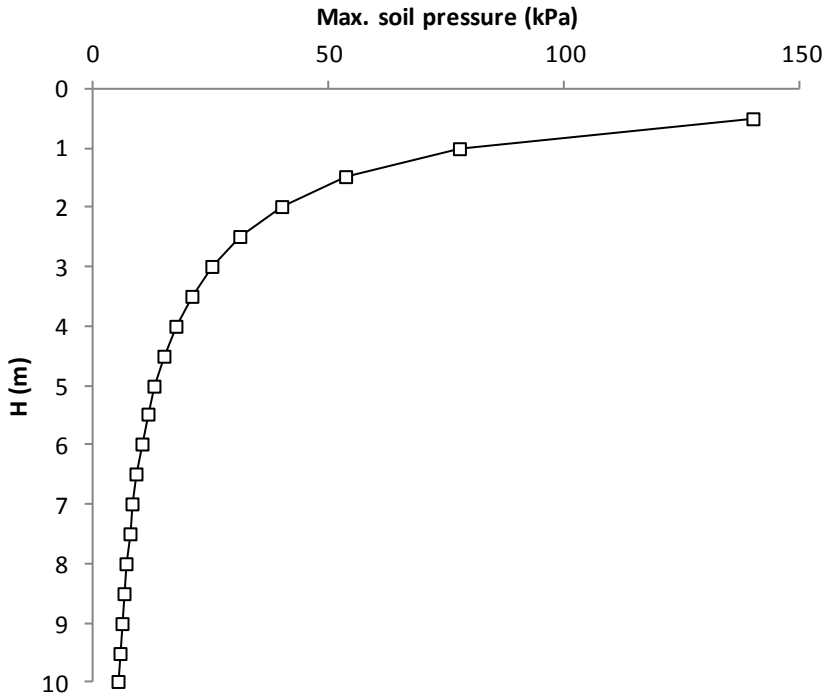

Figure 2.11: The relationship between the backfill height and the maximum soil pressure based on the BS maximum soil pressure design equation (Equation 1.13)

2.3. Previous studies on buried flexible pipes

2.3.1. Effect of compaction forces

Elshimi and Moore (2013) investigated the effect of the compaction forces on the response of a buried flexible pipe using two-dimensional finite element analysis. The pipe had an inside diameter of 2.0 m. The soil and pipe models, as well as the modelling technique of the compaction forces were described in detail in Section

2.2.1. Elshimi and Moore (2013) noticed that the compaction process does not significantly affect the response of the pipe if a vibratory plate compactor was used in the compaction process.

2.3.2. Effect of backfill soil weight only

Rogers et al. (1996) investigated the effect of the installation condition on the response of a buried unplasticized polyvinylchloride (PVCu) pipe under a deep burial condition using laboratory based studies. The length, width and height of the experimental box was 1.88 m, 1.38 m and 1.57 m, respectively. The pipe had an outside diameter of 0.3 m and was buried with a backfill height of 0.3 m. The deep burial condition was simulated by applying a uniform load at the top of the model using water bags. The maximum applied pressure was 150 kPa applied in three equal increments. The maximum applied pressure is equivalent to a backfill height of 7.3 m assuming a backfill soil unit weight of 20.42 kN/m^3. Four installation conditions were considered in this study. The soil was carefully placed at the haunch zone in the first and second installation. However, the soil was compacted in the first installation; while it was not in the second installation. The third and fourth installations were intended to simulate poor site practice, where no support was provided to the pipe in the haunch zone in these tests.

Rogers et al. (1996) noticed a significant effect from the haunch support on the response of the pipe; where providing poor support to the pipe in the haunch zone concentrated the reaction forces at the pipe invert. These reaction forces resulted in a large tensile strain at the pipe invert.

The results of the pipe load versus the applied load and the pipe displacements versus the applied load of the tests conducted by Rogers et al. (1996), in addition to the tests of another PVCu pipe with an outside diameter of 0.2 m, were reported by Chapman et al. (2007). The paper of Chapman et al. (2007) focused on understanding the effect of the installation condition and pipe stiffness on the degree of soil arching. They found that the positive soil arching increased as the installation quality increased or pipe stiffness decreased; where the pipe load and pipe displacement for the case of the good compaction-good haunch support was less than that of the poor compaction-good haunch support. Moreover, they found that the degree of soil arching for the poor haunch support installation was approximately similar to that of the good compaction-good haunch support, where the pipe load was almost similar. However, they noticed an increase in the displacement of the poor haunch supported pipe compared to the good compaction-good haunch supported pipe. They also found that the good compaction-good haunch support and the poor compaction-good haunch supported pipes were deformed to a heart shape under the applied load; while the poor haunch supported pipe was deformed to an inverted heart shape.

Sargand et al. (2001a) reported on the long-term horizontal (at the pipe springline) and vertical (at the pipe crown) displacements of two buried corrugated PVCu pipes measured under a deep burial condition. The PVCu pipes had an internal diameter of 0.8 m and tested under a maximum backfill height of 12.2 m. The moment of inertia of the first pipe and the second pipe was 1770 mm^4/mm and 1819 mm^4/mm, respectively. Displacement potentiometers were used to measure the vertical and horizontal displacement of the pipes. A crushed limestone with a degree of

compaction of 96% according to the standard Proctor test was used in both tests. Sargand et al. (2001a) noticed that the vertical and horizontal displacements of the first pipe steadied 14 days after the completion of the construction process; while the readings of the second pipe steadied 30 days after finishing the backfilling process. The maximum vertical displacement (at the pipe crown) obtained for Pipe 1 and Pipe 2 was 12.70 mm and 10.37 mm, respectively. Figures 2.12(a) and (b) show the trend of the displacement-time relationships obtained by Sargand et al. (2001a) for the first and second pipes, respectively.

The soil pressure above the crown of the second pipe was reported in another publication (Sargand et al., 2001b) under the maximum backfill height (i.e. 12.2 m). The soil pressure was recorded using a pressure cell installed 25 mm above the pipe crown. The result from the pressure cell showed a significant reduction in the soil pressure above the crown of the pipe due to the positive soil arching; where the recorded soil pressure was equal to 161 kPa compared to an overburden pressure value of 240 kPa.

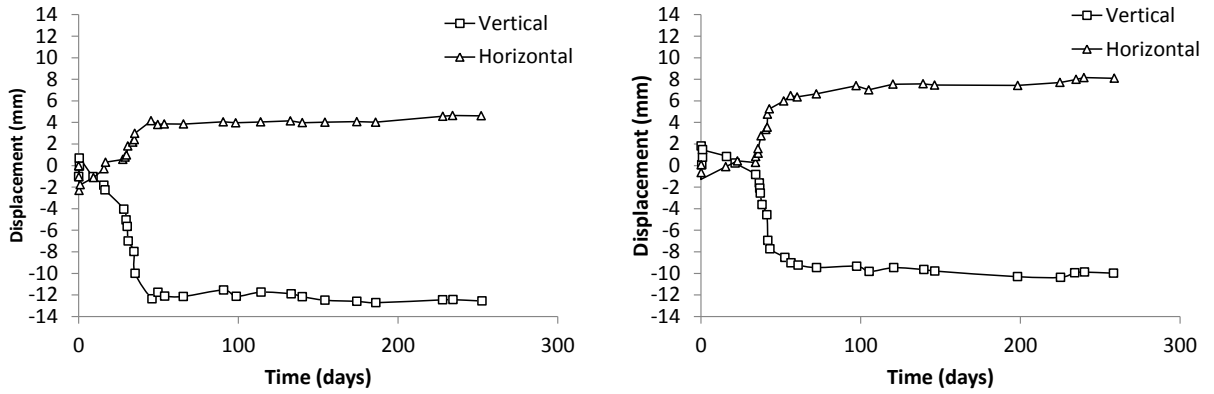

(a) (b)

Figure 2.12: Vertical (at the pipe crown) and horizontal (at the pipe springline) displacements-time relationships of PVCu pipes: (a) Pipe 1 (with a moment of inertia of 1770 mm^4/mm); (b) Pipe 2 (with a moment of inertia of 1819 mm^4/mm) (after Sargand et al., 2001a)

Dhar et al. (2004) studied the vertical (at the pipe crown) and horizontal displacements and strain developed in the wall of a ribbed PVCu pipe using a biaxial pipe test cell and two-dimensional finite element analysis. The length, width and height of the biaxial test box was equal to 2.00 m, 2.00 m and 1.60 m, respectively. The pipe had an inside diameter of 0.6 m. It was backfilled with poorly-graded sandy soil. An incremental static pressure of 500 kPa was applied on the top surface of the soil to simulate the scenario of a buried pipe under deep soil fill. They found that the horizontal displacement at the springline of the pipe and vertical displacement at the pipe crown increased non-linearly as the load (backfill soil weight) increased, as shown in Figure 2.13.

Dhar et al. (2004) used the laboratory test results to validate the finite element model. Half of the laboratory model was considered in the finite element modelling with a width and height equal to the width and height of the laboratory biaxial cell, as shown

in Figure 2.14. The non-linear behaviour of the soil was simulated using a non-linear soil model based on the Janbu stress level-soil stiffness model ($E = K\sigma^n$, where K and n are non-linear fitting parameters; σ is the stress level) (Janbu, 1963) with a Mohr-Coulomb failure criteria and the Mohr-Coulomb elastic-perfectly plastic model. The linear elastic model was used to model the behaviour of the buried pipe. A uniform pressure was applied on the top surface of the model similar to that used in the biaxial test. Dhar et al. (2004) found that both models are able to simulate the applied stress-pipe displacement relationships observed in the laboratory test, as shown in Figure 2.13. However, the non-linear model was better in tracing the non-linear vertical and horizontal displacements of the pipe as can be clearly seen in Figure 2.13. Moreover, they used the developed numerical model to study the effect of poor haunch support on the behaviour of the pipe, by reducing the soil stiffness in a limited part of the haunch zone, as shown in Figure 2.14. They found that poor haunch support caused a redistribution of strains around the circumference of the pipe and increased the pipe's vertical displacement. Additionally, they noticed that the pipe responded to the poor support with an inverted heart shape deformation under the applied loads.

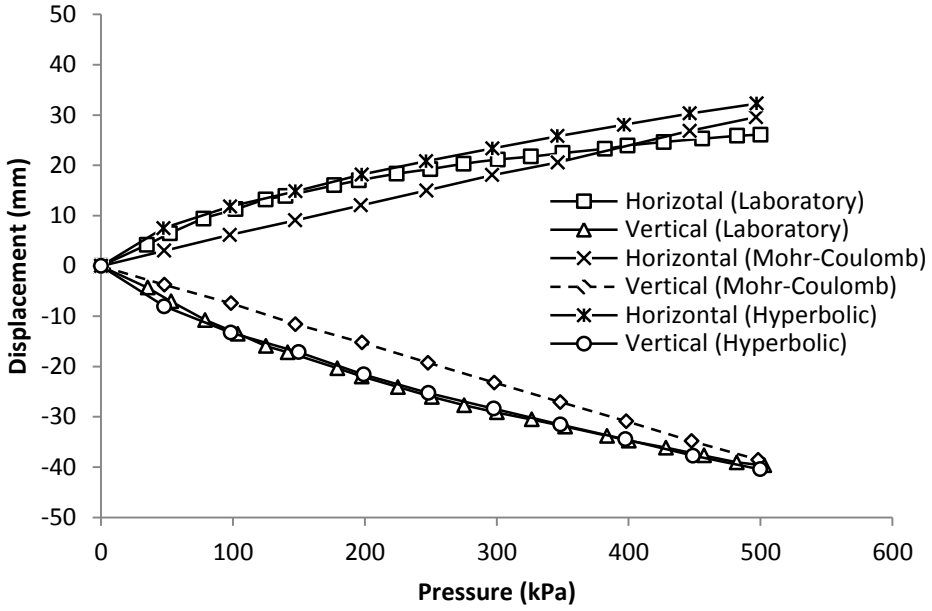

Figure 2.13: The results of the vertical displacement at the pipe crown and the horizontal displacement at the pipe springline obtained from a biaxial laboratory test and finite element analysis reported by Dhar et al. (2004)

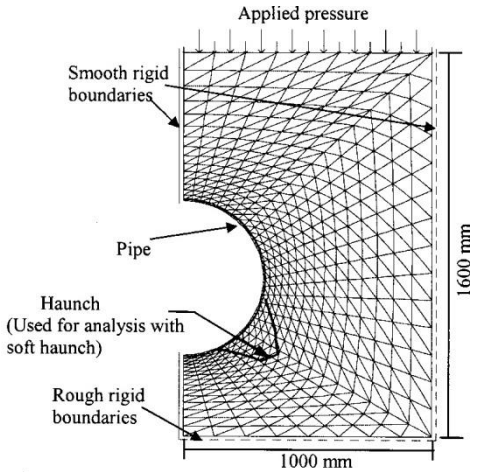

Figure 2.14: Finite element mesh used by Dhar et al. (2004) and the location of poor haunch support considered in his analysis

Kang et al. (2013a) investigated the maximum allowable backfill soil height for the buried PVCu pipes under the backfill soil weight only, using two-dimensional finite element analysis. The behaviour of the soil was simulated using the hyperbolic soil model; while the pipe was assumed to behave following the linear elastic model. The short-term and long-term response of the pipe was evaluated by considering the short and long-term properties of the pipe. A pipe diameter range of 0.3 m to 1.5 m was considered in the finite element analysis. Well-graded sand (SW) and silty sand (ML) were considered in the numerical analysis with two densities (90% and 95% of the standard Proctor density).

The maximum allowable backfill height was calculated based on the pipe wall stress and the crown vertical displacement. The pipe was considered safe if the pipe wall stress did not exceed half of the yield strength of the pipe material and the crown vertical displacement did not exceed 5.00% of the diameter of the pipe. These criteria were considered based on the AASHTO LRFD (2004) requirements for the design of buried flexible pipe, as stated by the authors.

Kang et al. (2013a) noticed an increase in the pipe wall stress as the pipe diameter increased. However, they did not justify this response. Moreover, they found that the long-term material properties of the PVCu pipe governed the maximum fill height (i.e. controlled the design). In summary, they found that for a diameter range of 0.3 m to 1.2 m, the maximum allowable backfill height was 26.0 m, 17.0 m, 18.0 m and 12.0 m for the case of the SW95, SW90, ML95 and ML90 backfill soils, respectively. For a pipe with a diameter larger than 1.2 m, the maximum allowable backfill height was 20.0 m, 14.0 m, 15.0 m and 8.0 m for the case of the SW95, SW90, Ml95 and ML90

backfill soils, respectively. However, these backfill heights were calculated without considering the buckling of the pipe under the applied load; although the buckling is a design parameter. In addition, the methodology which has been used to calculate the pipe wall stresses from the predicted pipe forces using the two-dimensional finite element analysis are not described in the paper. Hence, the results of the maximum wall stress reported in the paper cannot be used in the design without re-evaluation.

2.3.3. Effect of traffic load

Rogers (1985) conducted a parametric study to investigate the crown vertical displacement of a buried PVCu pipe subjected to a surface single tyre load using two-dimensional finite element analysis. The pipe had an inside diameter of 0.2 m and was buried with a backfill height of 0.5 m. The tyre load was simulated as a strip load with a load intensity of 70 kN over a width of 0.32 m. The behaviour of the soil and the pipe was simulated using a linear elastic model. The parametric study involved investigating the effect of the stiffness of the pipe's surrounding soil (i.e. the soil supporting the pipe in the haunches, springline and shoulders), the backfill soil (the soil above the crown of the pipe) and the natural soil on the displacement response of the buried pipe.

Rogers (1985) found that the crown vertical displacement of the pipe decreased as the stiffness of the pipe's surrounding soil or the natural soil increased. Furthermore, he found that the crown vertical displacement increased as the stiffness of the backfill soil increased.

Rogers (1987) conducted one of the first laboratory studies on the response of small diameter PVCu pipes under the effect of surface load. The tests were conducted in a small laboratory box (0.75 m x 0.50 m x 0.55 m) and large test pit (3 m x 2.1 m x 1.9 m). The pipe had an inside diameter of 0.2 m. The testing programme involved testing the pipe under 55 kN static and cyclic loads followed by 70 kN static and cyclic loads. The load was applied using a circular plate in the small-scale and large-scale tests. The diameter of the plate was 0.7 m for the large-scale tests and 0.48 m for the small-scale test; while the backfill height was 0.5 m and 0.3 m, respectively. The study focused on the effect of the type of side fill material (pea gravel, silty clay, concrete ballast, uniform sand, quarry tailings and silty sand); degree of compaction of the side fill material (no compaction, light compaction and thorough compaction); and the bedding thickness (0.000 m, 0.050 m and 0.100 m).

Rogers (1987) found that the crown vertical displacement is significantly affected by the type of the side fill material, where the granular soils (pea gravel, concrete ballast, quarry tailings and uniform sand) were found to provide good support for the pipe, compared to the silty sand and silty clay. Moreover, Rogers (1987) recommended using a thin bedding layer for an optimum design of buried PVCu pipes, as he found that the crown vertical displacement decreased when the bedding thickness increased from 0.000 m to 0.050 m and then increased as the bedding thickness increased to 0.100 m.

Rogers (1988) used the results of the deformed shape and pipe wall strain of the tests described in his earlier work (Rogers, 1987), with additional results from the literature, to establish a general hypothesis describing the behaviour of the buried

flexible pipes under the applied load based on the support condition. This hypothesis can be summarized in the following:

1- The pipe will deform into an elliptical shape (Figure 2.15(a)) if a poor support is provided from the surrounding soil due to poor compaction or poor soil material.
2- The pipe will deform into a heart shape (Figure 2.15(b)) if a good support is provided for the pipe in the haunch zone up to the springline.
3- The pipe will deform into an inverted heart shape (Figure 2.15(c)) if the surrounding soil is poor at the haunch zone and good above the springline.
4- The pipe will deform into a square shape (Figure 2.15(d)) if good support is provided at the springline and poor support is provided at the haunches and shoulders of the pipe.

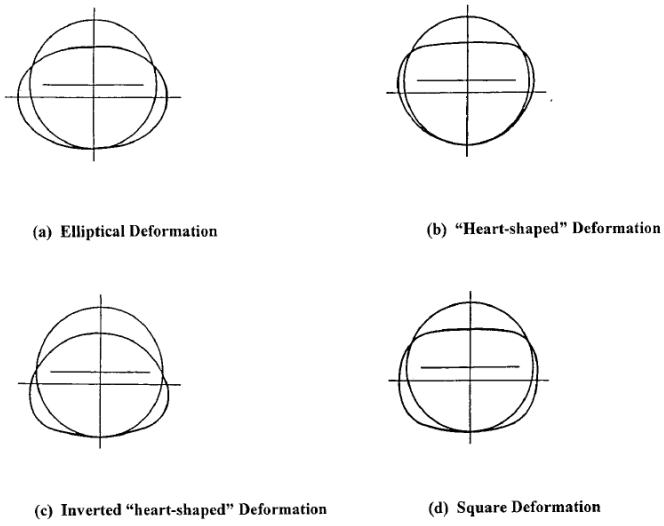

Figure 2.15: The hypothesis of flexible pipe response under the applied load (Rogers, 1988)

Zhan and Rajani (1997) investigated the effect of the backfill soil type and backfill height on the structural response of a buried PVCu pipe under the effect of traffic loading, using two-dimensional finite element analysis. The pipe was modelled using the linear elastic model; while the soil was modelled using the Drucker-Prager elastic-perfectly plastic soil model. Sand, clay and controlled low strength material (CLSM) were used as backfill soils. The CLSM is a type of self-compacted weak cementitious material used as a backfill for buried structures in places where it is difficult to add the traditional backfill soil (i.e. sandy or granular soil) such as pipes buried in narrow trenches. The controlled low strength material was assumed to be stronger than the sand and clay backfills. The pipe had a nominal diameter of 0.2 m and was buried with a backfill height ranging from 1.5 m to 2.5 m. The modulus of elasticity of the sand, clay and CLSM were assumed to be equal to 30,000 kPa, 10,000 kPa and 300,000 kPa, respectively. The traffic load was simulated as a strip load with a maximum pressure of 100 kPa applied over a trench width of 0.80 m.

The study showed that the stresses in the pipe wall decreased significantly when the CLSM material was used as a backfill material or when the backfill height increased as shown in Figure 2.16. Furthermore, the study showed that using clay soil provided more support to the pipe than the sand soil, as the maximum bending stress was higher for the sand backfill, as can be seen in Figure 2.16. However, the authors did not justify the choice for the material properties of the clay; nor did they consider the effect of consolidation of the clay on the behaviour of the pipe. Hence, the conclusion drawn that the clay is better than the sand as a backfill material is questionable.

It should be noted that the authors tried to justify the simulation of the traffic load as an infinite strip load over the trench width with an intensity of 100 kPa, by stating that this load is equivalent to a tyre load of 140 kN with a dynamic allowance factor of 1.5. However, there was no justification of this statement. In addition, the authors did not use the spreading factor in the two-dimensional analysis, nor justified neglecting this factor. Finally, the authors reported the figures for bending hoop stress (Figure 2.16), external and internal hoop stress (which can be seen in the paper) and uniform hoop stress (which can be seen in the paper). However, there was no mention of the methods used to calculate these stresses, as the authors used beam elements in modelling the buried pipe and these elements only have the ability to predict the shear forces and bending moments in the buried pipe. Hence, the results of the pipe wall stresses reported in this study are questionable.

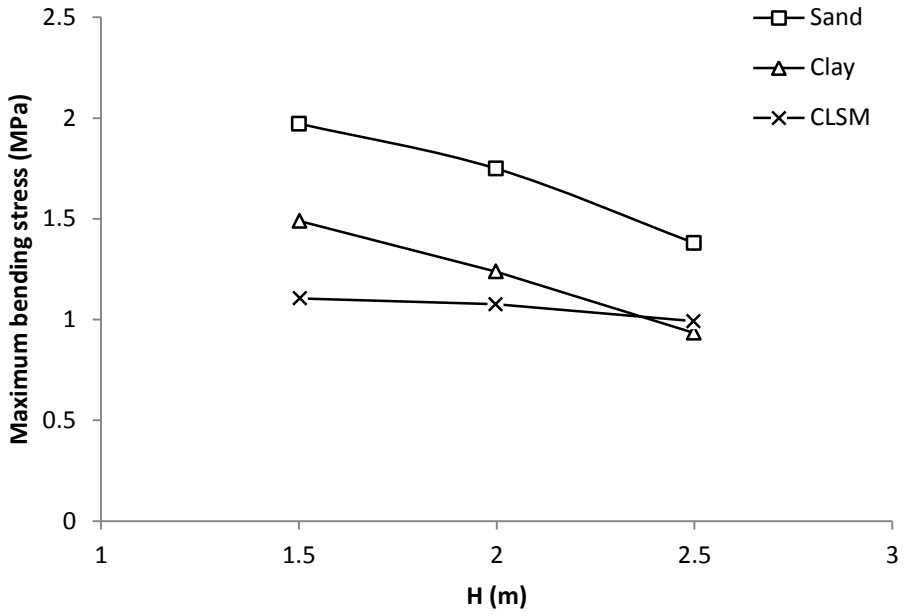

Figure 2.16: Maximum bending stress of PVCu pipe as a function of the burial depth (after Zhan and Rajani, 1997)

Kang et al. (2014) studied numerically the minimum allowable backfill soil height required for buried PVCu pipes under the AASHTO traffic loading requirements using two-dimensional finite element analyses. The soil was modelled using the hyperbolic soil model and the PVCu pipe was modelled using the linear elastic model. The short-term and long-term performance of the buried pipes was investigated in this study. The short-term and long-term behaviour was modelled by changing the parameters of the pipe in the numerical analysis. A pipe diameter range of 0.3 m to 1.5 m was considered in the finite element analysis. These finite element analyses were conducted for three different soil types: (gravely sand (SW), silty sand (ML) and silty clay ()) and with two densities (80% and 90% of the standard Proctor density).

Two loading conditions were considered in this investigation. The first load case simulated a single AASHTO H25 truck (axle load of 178 kN) travelling perpendicular to the pipe direction as shown in Figure 2.17(a); while the second case simulated two HS25 trucks spaced by 1.2 m travelling parallel to the pipeline direction as shown in Figure 2.17(b).

The minimum backfill height was calculated based on the crown vertical displacement and the pipe wall stress, where the pipe was considered safe if the crown vertical displacement did not exceed 5.00% of the pipe diameter and the pipe hoop stress did not exceed half of the yield strength of the pipe material. These criteria were considered based on the AASHTO (2007) requirements for the design of buried flexible pipes as stated by the authors.

The results from the analysis showed that the long-term properties of the PVCu pipe governed the design (i.e. simulate the worst-case scenario). Moreover, the authors

produced design tables for the minimum backfill height required for safe performance of buried PVCu pipes under the two load cases considered, as shown in Table 2.2 and Table 2.3 for load case 1 and 2, respectively. They also investigated the effect of the pavement material type (concrete or asphalt) and pavement thickness on the minimum backfill height required, and produced design tables depending on these factors. However, the buried pipes are usually designed by neglecting the presence of the pavement, as the pavement will deteriorate over time and its beneficial effect in reducing the soil pressure applied on the pipe will be diminished; hence the risk of pipe failure will be increased as the soil pressure will be increased significantly. Moreover, the study did not focus on the impact of the pipe diameter on the pipe behaviour; the authors only reported the results they found without attempts to justify the behaviour observed from the numerical modelling.

It should be noted that these design tables (shown in Table 2.2 and 2.3) were produced by neglecting the buckling of the pipe under the applied load. The authors did not consider the pipe buckling nor justified the reason for neglecting the buckling, even though it is one of the design parameters for buried flexible pipes based on the AASHTO (2007) and the recent AASHTO (2013). Moreover, the authors did not mention the method used to calculate and calibrate the predicted pipe wall stresses, as they used beam elements in modelling the buried pipe. These elements are only able to predict the displacements, bending moments and shear forces in the buried pipes. Finally, the traffic load was applied as an infinite strip loading without multiplying the load by a spreading factor (which is an empirical factor used in two-dimensional modelling to consider the three-dimensional effect of traffic loads on pipes); meaning that the three-dimensional nature of the loading condition has been

neglected. Therefore, these design tables require re-evaluation considering these issues.

(a) (b)

Figure 2.17: Load case considered by Kang et al. (2014): (a) single AASHTO H25 truck (axle load of 178 kN) travelling perpendicular to the pipe direction; (b) two HS25 trucks spaced by 1.2 m travelling parallel to the pipeline direction

Table 2.2: Minimum backfill soil height required for load case a (Kang et al., 2014)

Short-term properties							Long-term properties					
D (m)	SW90	SW80	ML90	ML80	CL90	CL80	SW90	SW80	ML90	ML80	CL90	CL80
0.3	1.0 m	1.2 m	1.0 m	1.5 m	1.3 m	1.6 m	1.0 m	1.5 m	1.0 m	1.7 m	1.2 m	1.8 m
0.9	1.0 m	1.5 m	1.0 m	1.7 m	1.1 m	1.8 m	1.1 m	1.6 m	1.0 m	1.8 m	1.3 m	1.8 m
1.5	0.9 m	1.2 m	1.2 m	1.5 m	1.3 m	1.4 m	0.9 m	1.5 m	1.2 m	1.5 m	1.2 m	1.6 m

Table 2.3: Minimum backfill soil height required for load case b (Kang et al., 2014)

Short-term properties						Long-term properties					
SW90	SW80	ML90	ML80	CL90	CL80	SW90	SW80	ML90	ML80	CL90	CL80
0.4 m	0.5 m	0.4 m	0.6 m	0.6 m	0.8 m	0.4 m	0.5 m	0.5 m	0.8 m	0.8 m	1.0 m

Kraus et al. (2014) reported the results of static and cyclic load tests on jointed and unjointed PVCu pipes using laboratory and finite element analysis-based studies to investigate the minimum backfill height limit for a safe performance of buried PVCu pipes. The laboratory model box, loading condition and numerical modelling details were described in Section 2.2.3. The PVCu pipe had an inside diameter of 0.5 m and was buried with a backfill height of 0.5 m. They noticed that the crown vertical displacement of the unjointed and jointed PVCu pipes under the static loading was 2.80 mm and 6.10 mm, respectively. Moreover, they found that the cyclic loading decreased the crown vertical displacement of the unjointed PVCu pipe and increased the crown vertical displacement of the jointed PVCu pipe, compared to the displacement for both pipes under static loading. However, they did not justify this counterintuitive behaviour.

The numerical study conducted by Kraus et al. (2014) aimed to study the effect of the backfill height and number of axles on the vertical displacement of the pipe crown of buried PVCu pipes using two-dimensional and three-dimensional numerical modelling. They modelled the behaviour of the soil using the Mohr-Coulomb elastic-perfectly plastic model; while the linear elastic model was used to model the behaviour of the pipe. The depth of the soil cover ranged from 0.3 m to 0.9 m and the numbers of axles were between four and nineteen. They found a decrease in the

crown vertical displacement as the backfill height increased. Moreover, they found a non-linear relationship between the number of axles and the crown vertical displacement, where the displacement increased as the number of axles increased. However, the displacement stabilized and slightly decreased when the number of axles exceeded eight, as shown in Figure 2.18. They justified this behaviour by the increase of the soil strength due to the additional confinement provided from the increase of the number of axles. However, the study did not recommend a backfill height limit for safe performance of buried PVCu pipes under the AASHTO truck.

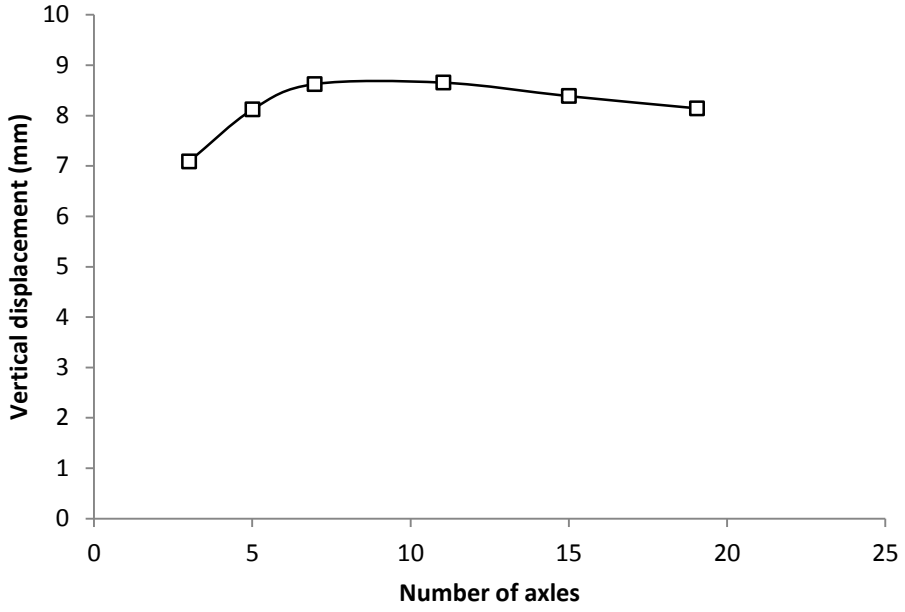

Figure 2.18: Relationship between maximum vertical displacement of the PVCu pipe crown and number of axles (after Kraus et al., 2014)

Chaallal et al. (2015a) conducted field tests to investigate the response of a corrugated PVCu pipe under the effect of traffic loading. The pipe was subjected to surface traffic loads from two axles of two trucks with an axle load of 181 kN. This

axle load simulated the design axle load of the AASHTO HS20 truck. The space between the trucks was 0.91 m. Each truck had two tyres with a tyre footprint area of 0.23 m by 0.23 m. The pipe had an inside diameter of 0.9 m. Three backfill heights were considered in the field test (0.5 m, 0.9 m and 1.8 m). Granular backfill soil was used in these tests with a degree of compaction of 95% of the standard Proctor maximum density. They found that the vertical displacement of the pipe crown decreased as the backfill height increased from 0.5 m to 0.9 m, then increased as shown in Figure 2.19. Moreover, they noticed that the PVCu pipe did not experience any wall crushing or crack development in any of the tests. They also found that the pipes were deformed to a heart shape under the applied load.

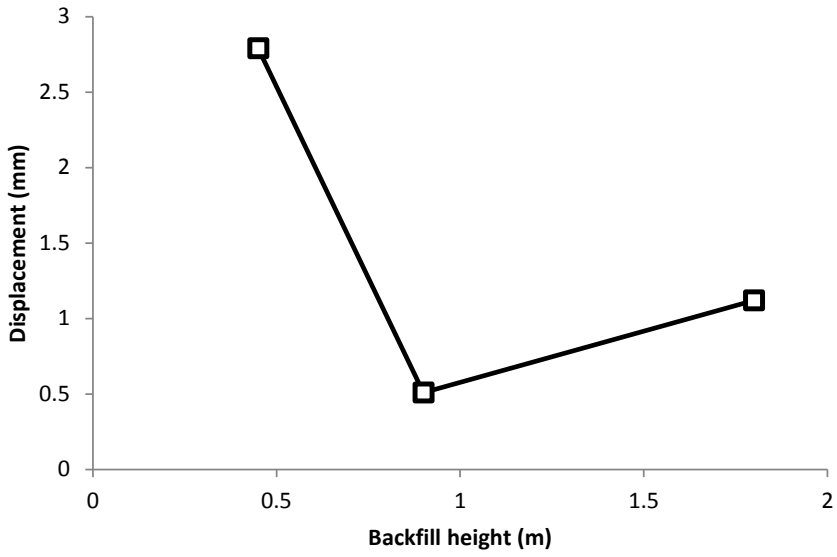

Figure 2.19: Vertical displacement of PVCu pipe crown under the effect of the traffic loading (after Chaallal et al., 2015a)

Mohamedzein and Al-Aghbari (2016) conducted laboratory tests to investigate the behaviour of a small diameter PVCu pipe (inside diameter of 0.2 m) subjected to a

surface load. A laboratory box with a length of 1.00 m, width of 0.32 m and height of 1.00 m was used for this purpose. A maximum surface load of 250 kPa was considered in this study. The surface load was applied over a surface area with a length of 0.34 m and a width of 0.10 m. The study focused on the possibility of using dune sand as a backfill material instead of conventional backfill materials like coarse sand. Therefore, Mohamedzein and Al-Aghbari (2016) compared the behaviour of the pipe installed in coarse sand and dune sand, respectively. They found that the vertical displacement of the pipe crown, pipe hoop strain and pipe bending moment for a pipe buried in dune sand is less than those for the pipe buried in coarse sand. Therefore, they recommended using dune sand as a good backfill material. Moreover, they tested the pipe under the effect of cyclic load with a total number of 20 cycles. They noticed that the vertical displacement of the pipe crown increased slightly under the effect of cyclic load, as shown in Figure 2.20, for the case of a pipe buried in compacted dune sand with a backfill height of 0.4 m.

However, it should be noted that the stress level considered in this study was very low (250 kPa) compared with the stress level applied from AASHTO, BS and Canadian design trucks.

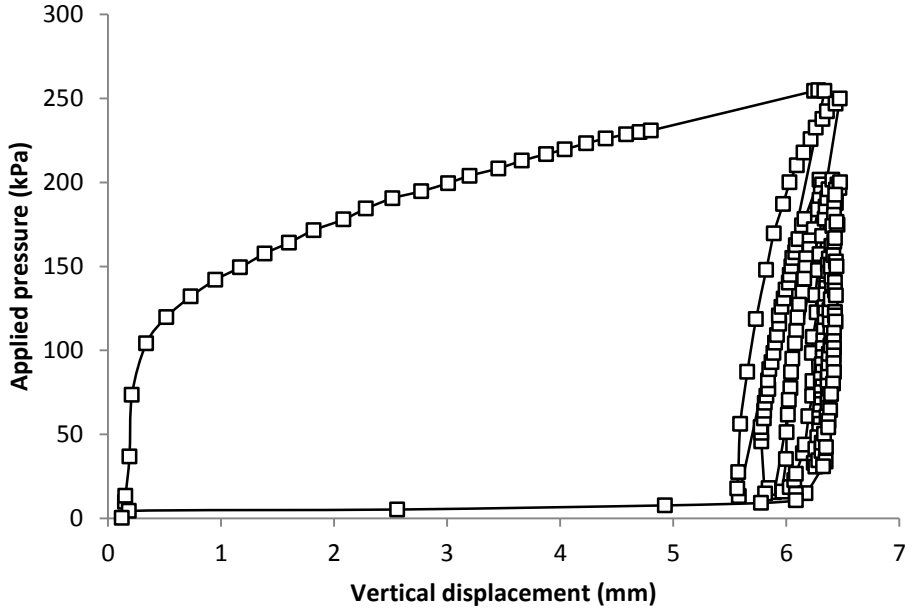

Figure 2.20: Vertical displacement of PVCu pipe crown buried in dune sand under the effect of cyclic loading (after Mohamedzein and Al-Aghbari, 2016)

2.3.4. Summary and gaps in knowledge

In summary, it can be concluded that previous studies have paid significant attention to the effect of the surrounding soil on the behaviour and response of the buried PVCu pipes under the backfill soil weight (Rogers et al., 1996; Sargand et al., 2001a, b; Dhar et al., 2004; Chapman et al., 2007; Kang et al., 2013a) and surface loads (Rogers, 1985, 1987; Zhan and Rajani, 1997; Kang et al., 2014; Kraus et al., 2014; Chaallal et al., 2015a; Mohamedzein and Al-Aghbari, 2016). Additionally, the importance of the haunch support has been demonstrated and the need for a good haunch support has been noted (Dhar et al., 2004; Chapman et al., 2007). However, the following gaps in the knowledge have been identified:

1- Little attention has been paid to the effect of the pipe diameter, where the studies of Kang et al. (2013a, 2014) did not clearly discuss the effect of the pipe diameter. Moreover, the study of Chapman et al. (2007) only considered pipes with a small diameter range (0.2 m and 0.3 m). **Objective 11 of this study (Chapter 6)** will address this gap in the knowledge by conducting a parametric study to investigate the effect of the pipe diameter on the behaviour of the pipe.

2- As noted for the buried concrete pipes, no study has considered the effect of the BS main road traffic loading, nor investigated the critical backfill height for the PVCu pipes under traffic loading. The previous studies on traffic loading were limited and only considered the AASHTO trucks (Kang et al., 2014; Kraus et al., 2014) or non-standard trucks (Rogers, 1987). **Objective 11 of this study (Chapter 6)** will address this gap in the knowledge by conducting a parametric study to investigate the effect of the BS main road traffic loading on the behaviour of the pipe.

3- No study has investigated the effect of the poor installation (poor haunch support) under traffic loading on the behaviour and integrity of buried PVCu pipes; even though proper haunch support is difficult to achieve in practice (Boschert and Howard, 2014; Turney et al., 2015) and the behaviour of the buried PVCu pipe is significantly affected by the condition of the haunch support. **Objective 11 of this study (Chapter 6)** will address this gap in the knowledge by conducting a parametric study to examine the effect of the poor haunch support on the behaviour and integrity of buried PVCu pipes under the BS main road traffic loading.

4- No effort has been made to understand the combined effect of the pipe diameter and poor installation (poor haunch support); as the previous studies which considered the poor haunch support focused on a limited diameter range (Rogers et al., 1996; Dhar et al., 2004; Chapman et al., 2007). **Objective 11 of this study (Chapter 6)** will address this gap in the knowledge by investigating the effect of the pipe diameter and traffic load on the behaviour of the poor haunch supported pipes.

5- No study has investigated the robustness of the design models which are currently adopted in the BS to calculate the soil pressure, pipe displacement and pipe wall stress. **Objective 12 of this study (Chapter 6)** will address this gap in the knowledge by comparing the results from the validated finite element analysis with the BS analytical equations.

2.4. General summary

This chapter has thoroughly reviewed the previous studies concerning the behaviour of buried concrete and flexible (with emphasis on PVCu) pipes under the effect of compaction forces, soil weight and traffic load. The issues in the methodology of some of the previous studies were also discussed with the aim of making this chapter useful for future studies or for young pipeline engineers, i.e. they may follow these studies, which may lead to a misunderstanding of the design philosophy for buried concrete and PVCu pipes.

In general, it was found that some of the previous studies were focused on particular case studies with a limited pipe diameter range and limited backfill height range; while other studies only reported the results of the analysis without paying any

attention to understanding and justifying the behaviour of the buried pipes. Moreover, the review has shown little effort has been paid, in the previous studies, to link the results obtained to the design practice of buried pipes. All of these issues were summarized and the gaps in the knowledge have been highlighted and linked to the objectives of this study. These gaps in the knowledge were the basis for the development of the objectives of this research.

Chapter 3
METHODOLOGY OF THE FEM AND EPR ANALYSES

3.1. Introduction

This chapter describes details of the finite element analysis (FEM) and the evolutionary polynomial regression analysis (EPR). Hence, the chapter has been divided into two main sections to separately discuss these two diverse methods. The first section discusses the requirements for developing a valid and robust finite element model to simulate the behaviour of the buried pipes under the backfill soil load and under a combined backfill soil and traffic load (hereafter referred to as total load). The second section briefly discusses the methodology of the EPR analysis and the steps required to derive a valid and representative model using this method. The chapter finishes with a summary of the key points.

3.2. Development of finite element methodology

Developing a validated finite element model that captures the key elements of the soil-pipe interaction effects was a significant factor of this study. Therefore, the first step in the model's development was to carry out a thorough literature review of the previous numerical studies to investigate the requirements to develop an accurate finite element model. The focus of this review was on the modelling techniques that had been used in the previous studies, including the constitutive models used for simulating the behaviour of the soil and the pipe; the effect of the model extent (i.e. distance to the model boundaries); the effect of the interface conditions; and the technique required to simulate deep soil fill.

The second step focused on conducting a sensitivity analysis to study the effect of the model extent and the soil constitutive models on the behaviour of the pipe, to add additional confidence in the robustness of the modelling approach. Finally, the modelling approach adopted was tested by comparing the results from the finite element analysis with the results of laboratory and field tests collected from the literature. The following subsections detail the development of the finite element methodology.

3.2.1. Requirements for a valid soil-pipe interaction finite element model (conclusions from previous studies)

A thorough literature review of previous studies was conducted to answer the following:

- Can a two-dimensional finite element analysis be used to predict the behaviour of buried pipes under traffic loading?
- What is the required model extent to avoid the boundary effect?
- What is the required degree of complexity of the soil and pipe constitutive models to accurately simulate the soil-pipe interaction problem?
- Is the predictive ability of the soil-pipe interaction finite element model influenced by the interface condition between the soil and the pipe?
- Does a moving traffic load produce a higher deformation compared to a static traffic load?
- What is the best way to simulate the case of a buried pipe under deep soil fill?

The following subsections discuss each of these questions and the decisions made based on previous studies.

3.2.1.1. Two-dimensional versus three-dimensional FE analysis

The thorough literature review showed that the use of two-dimensional finite element analysis to study the behaviour of buried pipes under traffic loading dominated previous studies; which can be clearly seen in **Chapter 2**. This is because two-dimensional finite element analysis is cheaper, faster and easier compared to three-dimensional analysis. However, two-dimensional finite element analysis involves the use of the spreading factor, which is an empirical factor as discussed in **Chapter 2**, to account for the three-dimensional effect of the traffic loading. In addition, the currently available values for the spreading factor were found to provide poor predictions when compared to the results from full-scale tests of buried pipes and arch culverts under traffic loading (Mai et al., 2014; Yeau et al., 2014). Hence, the decision was made to use a three-dimensional finite element analysis to avoid the empiricism associated with the spreading factor and to provide a robust analysis, which can be confidently used to test the design methodology of the AASHTO and the BS.

It should be noted that the idea and the methodology of the spreading factor were developed because the designers in north America use two-dimensional software called CANDE (**C**ulvert **A**nalysis a**N**d **DE**sign) for designing and analysing buried culverts (Katona, 1976). The software has been developed by research funded by the Federal Administration Highway. The first version of this software was released in 1976 (Katona, 1976). Although the software has gone through a lot of updates since

the release of the first version, no attempts have been made to add three-dimensional modelling capabilities. More importantly, recent studies have shown that this software is not capable of simulating the response of buried culverts under three-dimensional loading, even with the use of the spreading factor as discussed in the previous section. Hence, this software was not used in this research due to the aforementioned reasons.

3.2.1.2. Effect of the finite element model extent

Although many studies have investigated soil-pipe interaction using numerical analysis, a relatively limited number of studies have used three-dimensional finite element modelling for this purpose (Trickey and Moore, 2007; Petersen et al., 2010; Bian et al., 2012; García, 2012; Bryden et al., 2015; Mehrjardi et al., 2015; Robert et al., 2016), compared to the studies conducted using two-dimensional finite element modelling.

Careful examination of the model extent from these three-dimensional numerical studies has shown there are different opinions on the effect of the model extent, with studies using different values for the width, length and height of the three-dimensional finite element models, as shown in Table 3.1. In addition, the majority of these studies obtained good agreement with the laboratory and the field results (Petersen et al., 2010; Bian et al., 2012; García, 2012; Bryden et al., 2015; Robert et al., 2016), although the finite element models in these studies were developed with different model extents as can be clearly seen in Table 3.1. This indicates that the model extent does not significantly affect the results. However, as the previous

studies did not explicitly illustrate this conclusion, a sensitivity analysis is required to show the effect of the model extent.

Table 3.1: The width, length and height of the three-dimensional models developed in the previous studies

No.	Reference	Width	Length	Height
1	Trickey and Moore (2007)	62.5 D_{out}	62.5 D_{out}	31.3 D_{out}
2	Petersen et al. (2010)	2.3-14.0 D_{out}	1.9-13.5 D_{out}	2.2-7.9 D_{out}
3	Bian et al. (2012)	1.4 D_{out}	1.7 D_{out}	1.9 D_{out}
4	García (2012)	4.0 D_{out}	6.2 D_{out}	3.3 D_{out}
5	Bryden et al. (2015)	10.0 D_{out}	6.7 D_{out}	10.0 D_{out}
6	Robert et al. (2016)	10.0-3.0 D_{out}	10.0-3.0 D_{out}	5.0-2.0 D_{out}

3.2.1.3. Soil constitutive models

The thorough review of the literature showed that previous studies obtained a good agreement with the experimental results using linear elastic (Chaallal et al., 2015b; Robert et al., 2016), elastic- perfectly plastic (Yoo et al., 1999; Dhar et al., 2004; Elshimi and Moore, 2013) and non-linear elastic soil models (Dhar et al., 2004; Kang et al., 2013a, b; Turan et al., 2013; Kang et al., 2014; Witthoeft and Kim, 2016). In addition, two recent studies have shown that including the soil plasticity does not affect the accuracy of the finite element predictions (Robert et al., 2016; Katona, 2017). Whereas, Dhar et al. (2004) (Figure 2.13) and Katona (2017) have shown that using the non-linear elastic soil model improves the accuracy of the soil-pipe finite element analysis compared to the linear elastic and the elastic-perfectly plastic

models. The latter finding is because of the dependency of the pipe behaviour on the soil stiffness around the pipe (i.e. the support condition) and the ability of the non-linear elastic soil model to accurately simulate the dependency of the soil stiffness on the stress level (Katona, 2017). Therefore, the Duncan-Chang hyperbolic soil model (Duncan and Chang, 1970) was considered because of the following:

1- The model is able to simulate the change of the soil stiffness and the strain hardening as the stress level increases. Hence, this model provides a better prediction.
2- The model has been found to be able to produce good predictions of the behaviour noted in the laboratory and field tests (Dhar et al., 2004; Turan et al., 2013).
3- The results of a sensitivity analysis conducted as part of this study showed that including the soil plasticity does not affect the behaviour of buried pipes, and hence confirmed the conclusions of Robert et al. (2016) and Katona (2017). Thus, there is no need to include the soil plasticity in the analysis. Details of the sensitivity analysis are explained in Section 3.2.2.2.
4- Importantly, the model was found to be able to reproduce the results of the laboratory and field tests from the literature, as will be discussed in the validation section (Section 3.2.3).

3.2.1.4. Pipe modelling

This section discusses requirements for modelling the PVCu and concrete pipes and the decisions made based on the thorough review of previous studies.

3.2.1.4.1. PVCu pipe modelling

The previous studies modelled the behaviour of PVCu buried pipes using a linear elastic soil model with the assumption of a thin shell theory (i.e. using beam elements in the two-dimensional analysis and shell elements in the three-dimensional analysis) and a good agreement between the experimental and numerical results was obtained (Dhar et al., 2004; Petersen et al., 2010; Kang et al., 2013a, b; Kang et al., 2014). Therefore, the initial decision was made to use a linear elastic model with the thin shell theory (i.e. using the shell elements) to simulate the behaviour of the PVCu pipes. Again, this initial decision was rigorously tested in the validation stage by investigating the abilities of this modelling technique in replicating the laboratory and field results.

3.2.1.4.2. Concrete pipe modelling

Only one study was found in the literature that compared the results of finite element analysis with the results of laboratory tests (three-edge bearing test) (Abolmaali and Kararam, 2013). The concrete pipe in the Abolmaali and Kararam's (2013) study was modelled using solid elements with a concrete brittle cracking model used to simulate the behaviour of the pipe. The steel reinforcement was included in the simulation using a tension stiffening property, as discussed in detail in Section 2.2.1. However, the bending moment, which is key in the derivation of the bedding factor, cannot be directly obtained from the finite element analysis if the pipe is modelled using these solid elements.

On the other hand, the use of the bending moment in the derivation of the bedding factor provides a solution independent from the steel reinforcement of the pipe. The

required steel reinforcement would then be specified based on the developed bending moment, as the bedding factor would be derived using the maximum bending moment value. This is similar to the case of drawing a bending moment diagram for a structural member (for example a simply supported beam) and then using the maximum bending moment to design the structural member. Therefore, the buried concrete pipes in this study were modelled using shell elements as the bending moment can be directly obtained from these elements (i.e. employing a thin shell theory). In addition, the thin shell theory was employed to add additional conservatism to the analysis, as it provides a higher bending moment than the thick ring theory (i.e. using solid elements to model the pipe) with a percentage difference ranging from 2% to 10% (Moore et al., 2014). Hence, the bedding factor derived using this theory will be less than that derived following the thick shell theory.

It should be noted that the behaviour of the pipe was simulated using a linear elastic model. This model was used to provide a general solution independent of the yield of the concrete. The yield of the concrete and the effect of the steel reinforcement will be implicitly included, based on the pipe's capacity obtained from the three-edge bearing test, which will be specified based on the bedding factor (i.e. the maximum bending moment used in the derivation of the bedding factor). Therefore, there was no need to include the plasticity of the concrete in the analysis.

This modelling technique (thin shell theory with a linear elastic behaviour) was found to be able to accurately estimate the bending moment around the pipe (as will be discussed in Section 3.2.3.2) and the experimental bedding factor obtained by MacDougall et al. (2016) (as will be discussed in Section 4.4.3).

3.2.1.5. Effect of the interface elements

The previous studies have repeatedly shown that using a full interface bond between the buried structure and the soil gives a good prediction for the behaviour of the buried structure (Dhar et al., 2004; Arockiasamy et al., 2006; García, 2012; Kang et al., 2013a; Kang et al., 2014; Meguid and Kamel, 2014; Chaallal et al., 2015b; Robert et al., 2016). In addition, Robert et al. (2016) compared the results of the finite element analysis of the pipe wall stress for different interface conditions and found a negligible effect (percentage difference less than 1%) from the interface condition on the results. Therefore, a full bond between the pipe and the soil has been considered in this research. However, the robustness of this assumption has been checked in the validation stage, where this modelling technique was found to be able to accurately reproduce the results of laboratory and field tests of buried pipes under surface loads.

3.2.1.6. Method of traffic load application

It was expected, during the initial stages of this research, that moving traffic loading produces higher deformations and stresses in the pipe wall compared with the static traffic loading, due to the vibration induced from trucks moving. Hence, the initial decision was made to consider a moving traffic load in this research. However, a paper comparing the response of buried pipes under static and moving loading using field-based studies was published (Sheldon et al., 2015) during the early stages of the development of the finite element model. The study of Sheldon et al. (2015) illustrated that the static traffic loading produces higher deformation in the pipe wall compared to the moving loading. The ratio of the crown vertical displacement due to

a moving traffic load to the crown vertical displacement due to a static traffic load ranged from 0.80 to 0.67, depending on the truck speed, as discussed earlier in Section 2.2.3. In addition, a field study conducted on a buried cast iron pipe by Robert et al. (2016) showed also that static traffic loading produces stresses in the pipe wall higher than moving traffic loading. Hence, the decision was made to consider static traffic loading instead of moving traffic loading to simulate the worst-case scenario. However, the decision was also reinforced after comparing the results of the developed finite element models for both a static and moving traffic load with the results of Sheldon et al.'s (2015); where the same conclusion was found. The details of the development of the finite element model for moving traffic loading and the comparisons with Sheldon et al.'s work (2015) are discussed in the validation problems 6 and 7.

3.2.1.7. Simulation of soil load

The previous studies conducted on the behaviour of buried infrastructures under a soil load modelled the deep soil fill by applying a uniformly distributed load to the top surface of the model (Dhar et al., 2004; Kang et al., 2007; Kang et al., 2008a, b; Tan and Moore, 2007; Kang et al., 2013a; Balkaya et al., 2012a, b; Balkaya et al., 2013; Masada and Zhu, 2015; Katona, 2017). This technique was considered in the previous studies to reduce the computational time and was shown not to affect the accuracy of the modelling. Kang et al. (2013a, p.669) stated that "no difference occurs in the analysis results between a model using additional soil elements and a model with an equivalent overburden pressure". Hence, this modelling technique was

adopted in the present research to model the behaviour of buried concrete pipes under soil load (**Chapter 4**) to reduce the computational time of the analysis.

3.2.2. Sensitivity analysis

As discussed in the previous section, the thorough literature review of previous studies has shown different opinions on the required length, width and height for a three-dimensional finite element model. In addition, it was also shown that limited studies (only two) were conducted on the effect of including the soil plasticity on the accuracy of the finite element predictions (Section 3.2.1.3). Hence, this section discusses the effect of the extent of the finite element model and the soil plasticity on the accuracy of the finite element predictions by using a sensitivity analysis to thoroughly investigate these parameters.

3.2.2.1. Effect of the finite element model extent

A finite element model for a concrete pipe buried with a backfill height of 1.0 m and subjected to the BS main road traffic loading (Figure 1.4(a)) was used to investigate the effect of the finite element model extent. MIDAS GTS/NX was used to build the numerical models. The pipe had an outside diameter of 1.0 m and a wall thickness of 0.076 m. A well-graded sandy soil with a degree of compaction of 90% of the maximum standard Proctor density (SW90) was used as backfill material and the surrounding soil. The Duncan-Chang hyperbolic soil model (Duncan and Chang, 1970) was used to simulate the behaviour of the soil; while the linear elastic model was used to simulate the behaviour of the pipe. The material properties of the soil were taken from the literature (Boscardin et al., 1990) and are shown in Table 3.2.

The modulus of elasticity (E) and the Poisson's ratio (υ) of the concrete pipe were taken as 24,856,000 kPa and 0.20, respectively (Petersen et al., 2010). An example of the finite element mesh used in the analysis is shown in Figure 3.1.

The effect of the model extent was studied in three-steps. The first step investigated the effect of the model width; the second step investigated the effect of the soil depth below the pipe; and the third step investigated the effect of the model length in the third dimension. The effect of the model width (step 1) and the effect of the soil depth below the pipe (step 2) were investigated under the soil load only and the total load to find the model extent required for these loading conditions. However, the effect of the model length in the third dimension was investigated only under the total load, as the case of a buried pipe under the soil load only is a plane strain problem (Dhar et al., 2004; Kang et al., 2007). Hence, the model length in the third dimension does not affect the results.

In the first step, the length and the height of the model were fixed to 10.0 m and 5.0 m, respectively; while the width of the model was changed with respect to the outside diameter of the pipe, to study the impact of the finite element model width on the results. The considered widths were equal to 3.0, 3.5, 4.0 and 5.0 times the outside diameter of the pipe. A new finite element model was built for each width and the bending moment developed around the pipe was recorded for the case of the soil load only and the total load. Figures 3.2 and 3.3 show the recorded bending moment from the finite element analyses for the soil load only and total load, respectively. It can be seen from Figure 3.2 that changing the model width from 3.0 D_{out} to 3.5 D_{out}, 4.0 D_{out} and 5.0 D_{out} does not affect the results. Figure 3.3 shows that changing the

model width from 3.0 D_{out} to 4.0 D_{out} changes the bending moment at the pipe crown by 59% and the maximum bending moment (at the pipe invert) by 11%. However, the effect of the model width diminishes as the width changes from 4.0 D_{out} to 5.0 D_{out} (the bending moment stabilized). Hence, it can be concluded that the developed model should be built with a width not less than three times the outside diameter of the pipe, for the case of the soil load only; and four times the outside diameter of the pipe, for the case of the total load.

In the second step, the impact of the depth of the soil below the pipe has been investigated. The depth below the pipe was considered instead of the total height of the model because the backfill height above the pipe was one of the parameters investigated in this study, as it plays a significant role in reducing the effect of the traffic load (as will be discussed in **Chapters 5 and 6**). Therefore, it was not possible to propose a limit for the total height of the model, as the backfill height is not constant. In addition, the behaviour of the pipe is significantly affected by the support condition in the invert and haunch zones (Pettibone and Howard, 1967; Wong et al., 2006). Hence, the depth of the soil below the pipe was investigated.

Four finite element models were built with a soil depth below the pipe of 0.5, 1.0, 2.0 and 3.0 times the outside diameter of the pipe. The width and the length of the finite element model were fixed for all of these models; where the width was 4.0 m (4.0 times the diameter of the pipe) and the length was 10.0 m. Figures 3.4 and 3.5 show the effect of the soil depth below the pipe on the bending moment developed in the pipe wall, due to the application of the soil load only and total load, respectively. Figure 3.4 shows the insignificant effect of the soil depth below the pipe on the

results when it is equal to or more than the outside diameter of the pipe for the case of the soil load only. Figure 3.5 shows that the boundary effect ends when the soil depth below the pipe is equal to or more than twice the outside diameter of the pipe for the case of the total load.

In the third step, the effect of the finite element model length was investigated. The length of the model has not been investigated in terms of the pipe diameter, as it is directly related to the configuration of the applied load rather than the diameter of the pipe. This conclusion was found during the validation stage by comparing the results from the finite element analysis with the laboratory and the field results for buried pipes with different diameters; where it was noticed that the length of the model is related to the traffic load on the surface, rather than the outside diameter of the pipe. Furthermore, to explicitly illustrate this, additional finite element models for a buried concrete pipe with an outside diameter of 3.0 m were built and used to investigate the effect of the model length on the results. Therefore, the effect of the model length was investigated by considering finite element models with different lengths (5.0 m, 7.5 m, 10.0 m, 15.0 m and 30.0 m) for buried pipes with an outside diameter of 1.0 m and 3.0 m. Figures 3.6 and 3.7 show the developed bending moment in the pipe wall recorded for the buried pipes with outside diameters of 1.0 m and 3.0 m, respectively. It can be clearly seen from both figures that the effect of the model length diminishes when the length increased from 7.5 m to 10.0 m for both pipes, illustrating the independency of the results of the finite element analysis on the model length when it is equal to or larger than 10.0 m for both pipes.

Table 3.2: The material properties of the SW90 soil used in the analysis (Boscardin et al., 1990)

Property	SW90
γ (kN/m3)	20.99
υ	0.30
c'(kPa)	1
ϕ'(°)	42
K	640
Rf	0.75
n	0.43

Note: γ is the unit weight of the soil; υ is the Poisson's ratio; c' is the cohesion of the soil; $\phi'$is the angle of internal friction; K is the modulus number; n is the modulus exponent; and Rf is the failure ratio.

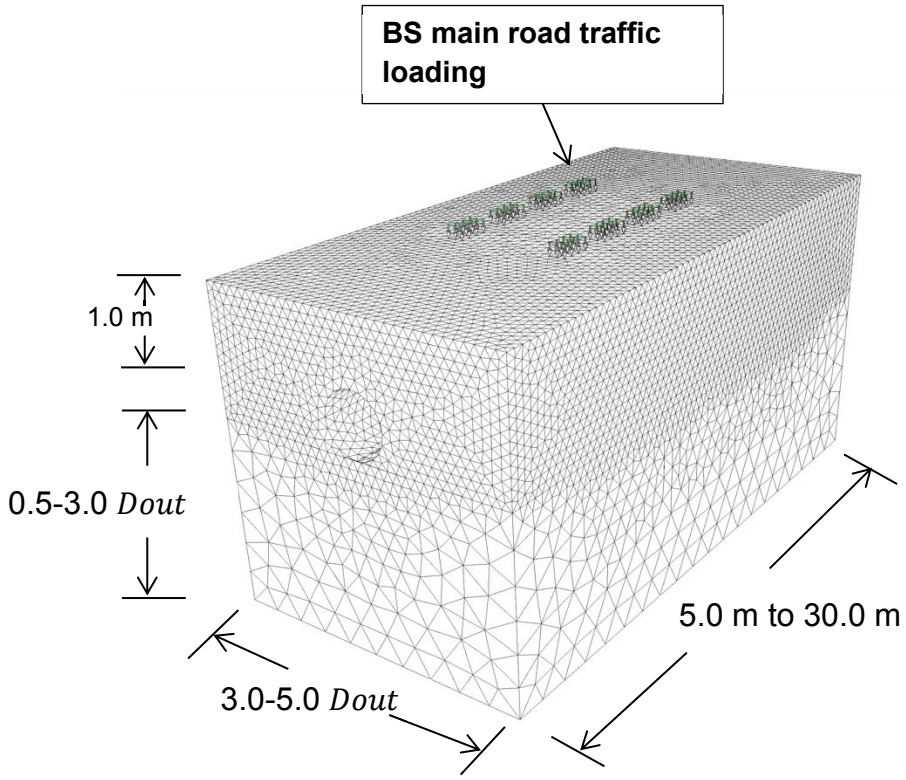

Figure 3.1: A typical finite element mesh used to study the effect of the finite element model extent

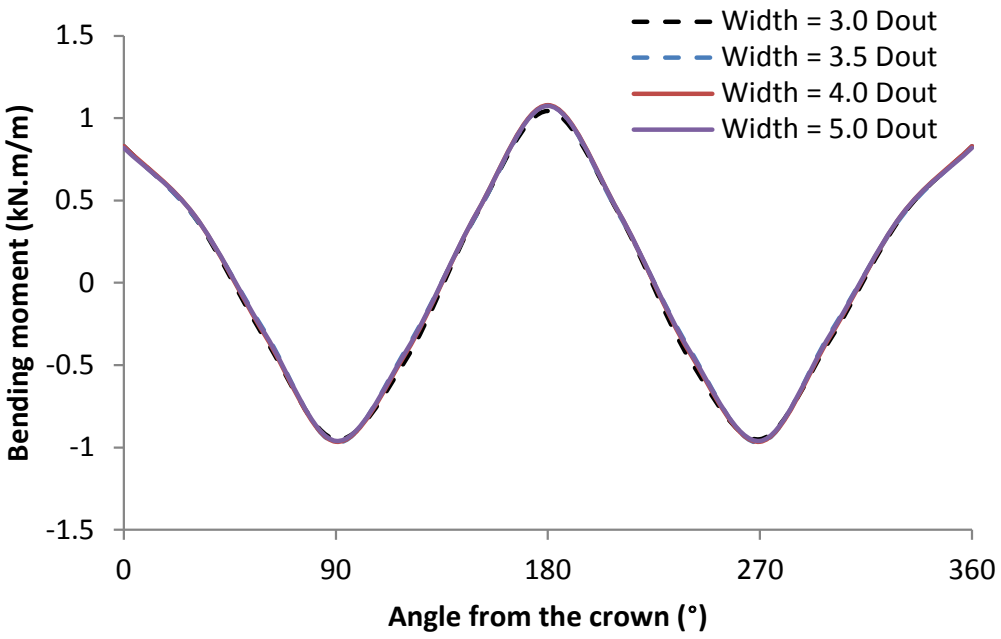

Figure 3.2: Effect of the finite element model width on the bending moment around the pipe for a buried concrete pipe under soil load only

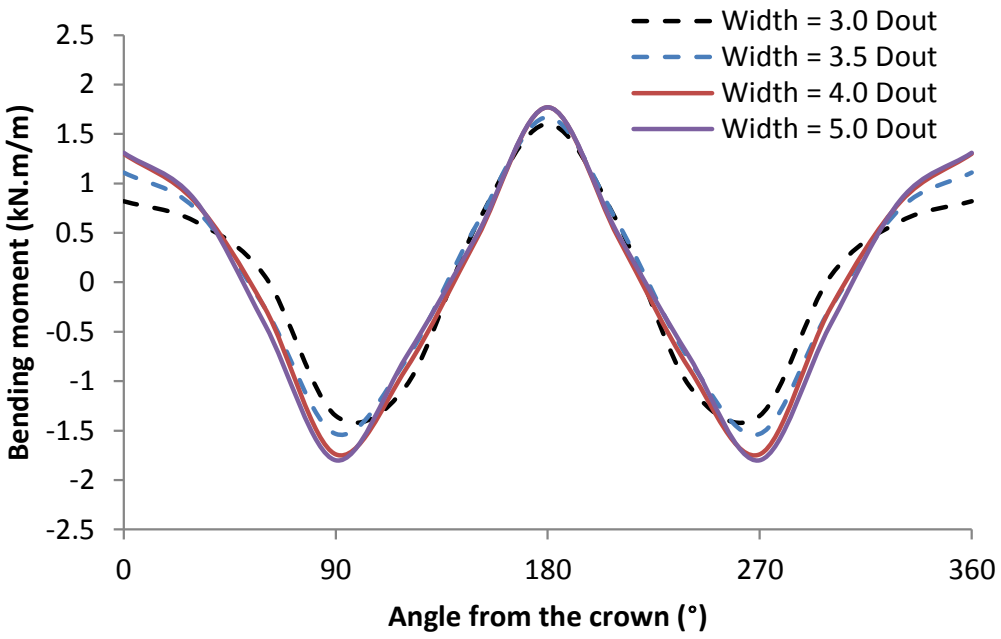

Figure 3.3: Effect of the finite element model width on the bending moment around the pipe for a buried concrete pipe under total load

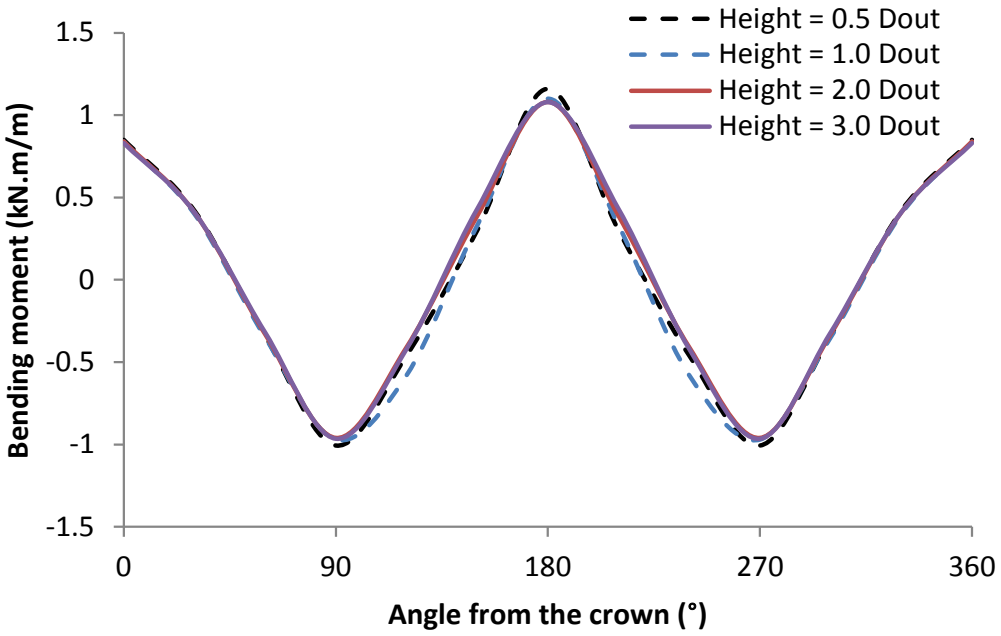

Figure 3.4: Effect of the depth of the soil below the pipe on the developed bending moment for a buried concrete pipe under soil load only

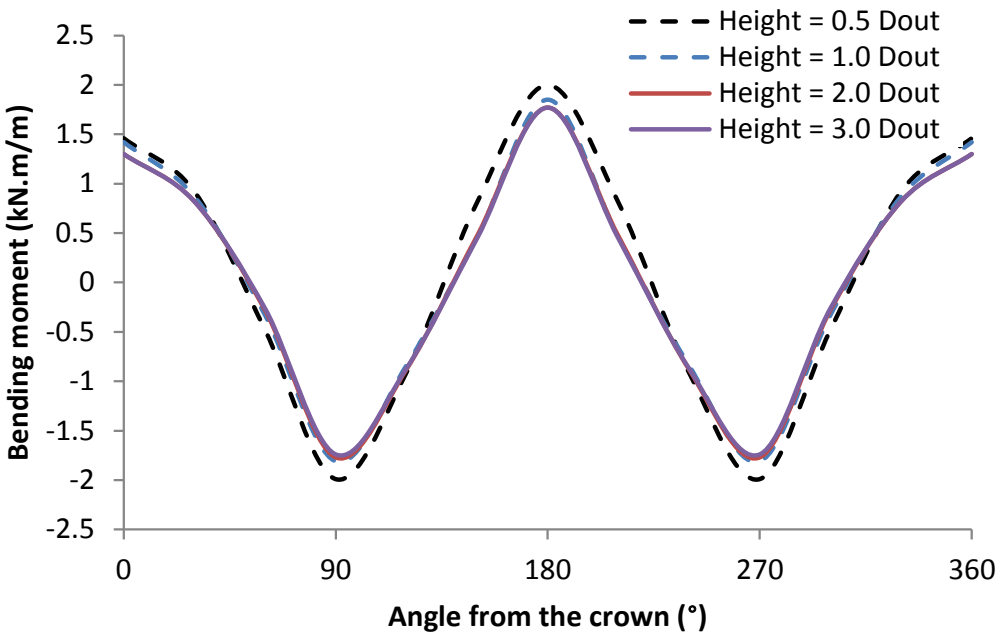

Figure 3.5: Effect of the depth of the soil below the pipe on the developed bending moment for a buried concrete pipe under total load

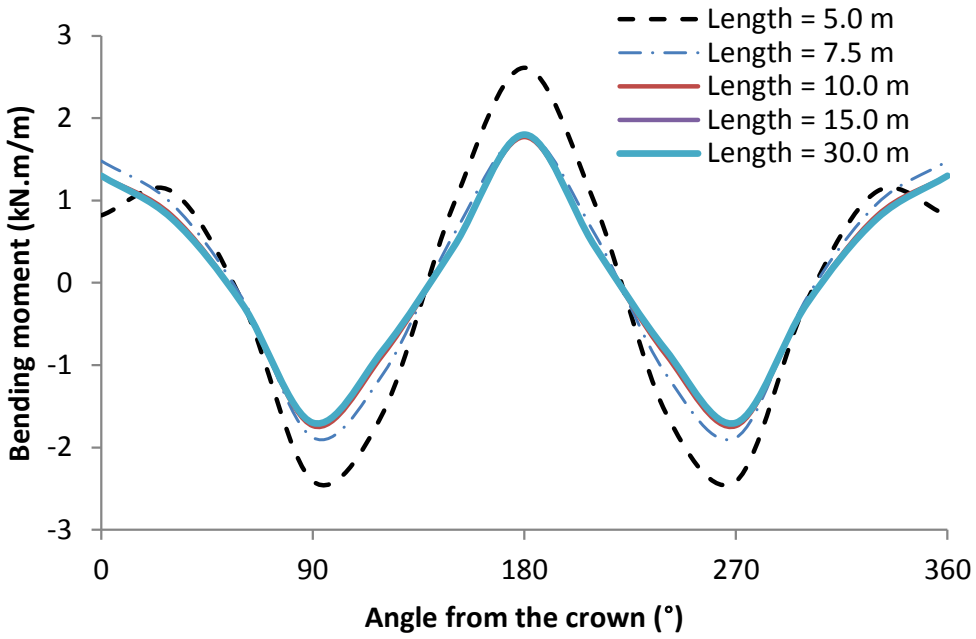

Figure 3.6: Effect of the finite element model length on the developed bending moment for a buried concrete pipe with an outside diameter of 1.0 m

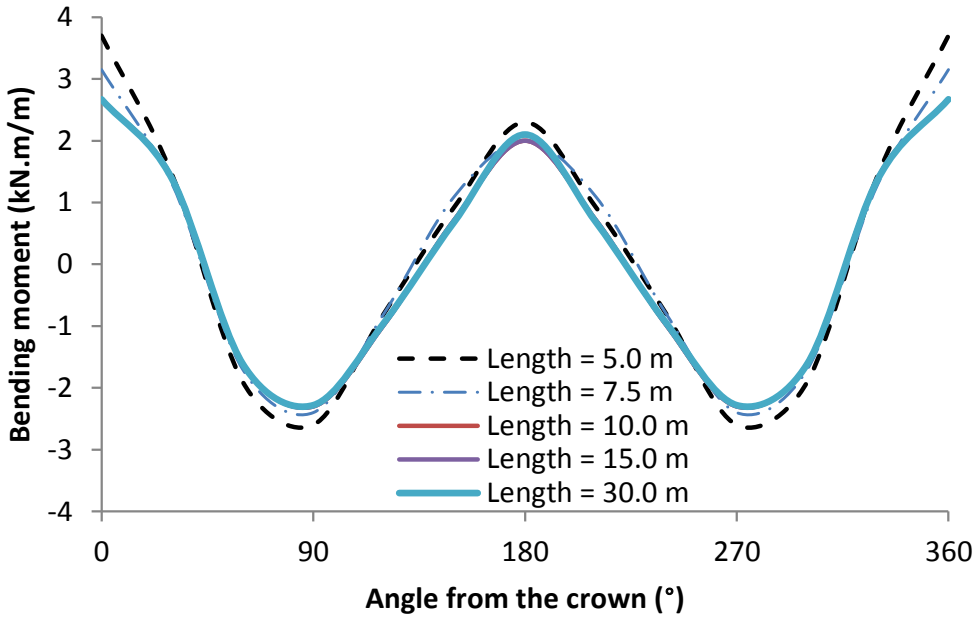

Figure 3.7: Effect of the finite element model length on the developed bending moment for a buried concrete pipe with an outside diameter of 3.0 m

3.2.2.2. Effect of the soil constitutive model

The effect of the soil constitutive model on the finite element predictions was investigated by comparing the results from three different constitutive models for the case of a buried concrete pipe under the effect of the BS main road traffic load. The considered soil models were the linear elastic model (LE), the Mohr-Coulomb elastic-perfectly plastic model (MC) and the Duncan-Chang hyperbolic soil model (DC).

A finite element model was built for this purpose. The finite element model had a length of 10.0 m, a width of 4.0 m and a height of 5.0 m. The buried pipe had an outside diameter of 1.0 m and a wall thickness of 0.076 m. The backfill height was considered to be equal to 1.0 m. SW90 soil was used as a backfill soil, similar to the soil used in the previous section (Section 3.2.2.1). The modulus of elasticity of the soil (E) for the LE and the MC models was calculated using Equation 3.1 (Janbu, 1963) using the parameters adopted from Boscardin et al. (1990) (shown in Table 3.2). A lateral stress (S_3) of 21.00 kPa was used in the equation (Equation 3.1) to calculate the modulus of elasticity. This lateral stress was calculated by taking the average height from the top surface of the model to the pipe invert (i.e. = outside diameter of the pipe + backfill height = 1.0 m +1.0 m) using a coefficient of lateral earth pressure of 1.0 for the compacted backfill soil (Brown and Selig, 1991), and hence the average lateral stress is equal to 21.00 kPa (i.e.$(1 \times 2 \times 21)/2$). Table 3.3 shows the material properties used for the LE and the MC analyses.

Figure 3.8 shows the bending moment developed in the pipe wall for the buried pipe under the total load predicted using the LE, MC and DC models. It can be seen from the figure that the LE and MC models give the same bending moment, illustrating the

insignificant effect of including the soil plasticity on the results (i.e. pipe behaviour). This occurred because the soil in the haunch zone did not reach the condition of failure due to the applied surface pressure. Hence, the support condition provided to the pipe in the MC analysis was similar to that provided with the LE analysis. However, the bending moment predicted using the LE and MC models was higher than that predicted using the DC model by 15% at the pipe crown and 18% at the pipe invert. This is because the difference in the stiffness of the soil surrounding the pipe results in a difference in the support condition. The stiffness of the surrounding soil in the hyperbolic soil model depends on the stress level and changes with every load step. However, the stiffness of the soil is constant for the LE and MC models. These results confirm the observation of Robert et al. (2016) and Katona (2017) on the insignificant effect of the soil plasticity. Hence, robust numerical modelling can be achieved using the DC model, as this model is able to simulate the effect of the stress level on the soil stiffness.

$$E = K \times P_a \times \left(\frac{S_3}{P_a}\right)^n \tag{3.1}$$

Where, E is the modulus of elasticity of the soil; K is the modulus number; n is the modulus exponent; P_a is the atmospheric pressure (100 kPa); and S_3 is the lateral stress.

Table 3.3: The linear elastic model and Mohr-Coulomb elastic-perfectly plastic model material properties of the SW90 soil used in the analysis

Property	SW90
γ (kN/m^3)	20.99
υ	0.30
c'(kPa)	1
ϕ'(°)	42
E (kPa)	32,714

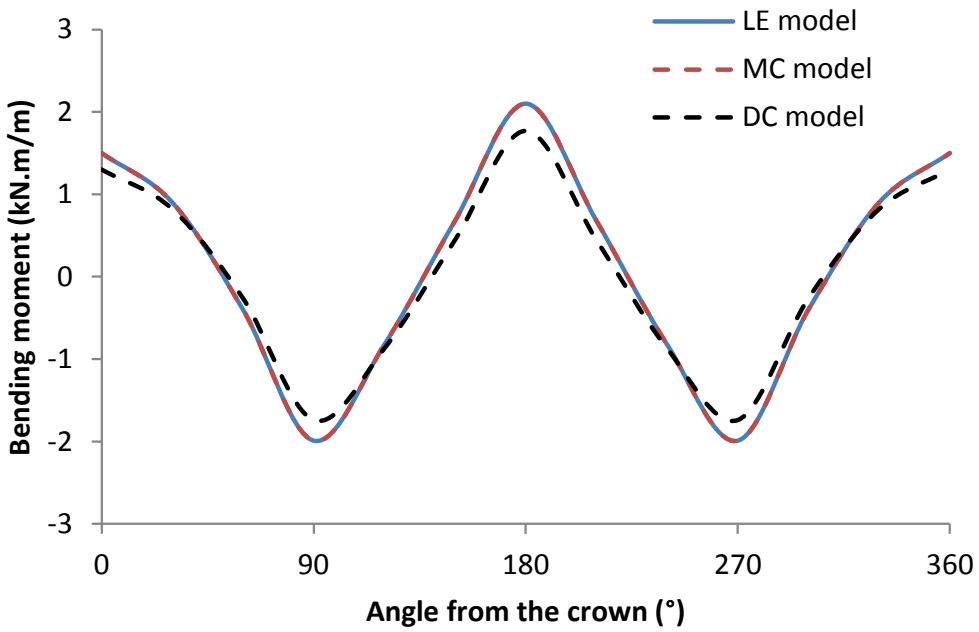

Figure 3.8: Effect of soil constitutive model type on the developed bending moment around a buried concrete pipe under total load

3.2.2.3. Summary

Based on the thorough literature review (Section 3.2.1.) and the sensitivity analyses conducted using MIDAS GTS/NX (Sections 3.2.2.1 and 3.2.2.2), the following can be concluded:

1- Three-dimensional finite element analysis is required to model the soil-pipe interaction under the effect of the traffic loading, to avoid the empiricism associated with the use of the spreading factor in the two-dimensional finite element analysis.
2- Regarding the finite element model extent for studying the behaviour of the buried pipes under the soil load only: the width of the finite element model should be not less than three times the outside diameter of the pipe and the depth of the soil below the pipe should be not less than the outside diameter of the pipe.
3- Regarding the finite element model extent for studying the behaviour of the buried pipes under the BS main road loading configuration: the width of the finite element model should be not less than four times the outside diameter of the pipe, the depth of the soil below the pipe should be not less than twice the outside diameter of the pipe and the length of the model should be not less than 10.0 m.
4- Including the soil plasticity does not affect the accuracy of the finite element analysis. Hence, the finite element analysis can be carried out using either the linear elastic model or the non-linear elastic model. However, the non-linear

elastic model provides a better prediction as it is capable of modelling the dependency of the soil stiffness on the stress level.

5- The interface friction between the soil and the pipe has an insignificant effect on the quality of the finite element results.
6- The deep soil fill can be simulated by applying an equivalent overburden pressure to the top surface of the finite element model, without the need to model the whole soil depth.

The next section discusses the validity of MIDAS GTS/NX, the finite element software used in this research and the finite element approach adopted. It compares the results from the finite element modelling with the laboratory and the field results selected from an extensive literature review.

3.2.3. Validation of the finite element modelling

The purpose of this section is to validate the finite element approach adopted in this research against a number of bench mark problems. Validation problem 1 aimed to validate the linear and non-linear algorithms of MIDAS GTS/NX, by comparing the results from the program with the results of stress-strain relationships obtained from triaxial tests. Validation problems 2 to 5 illustrate the robustness of the methodology of the numerical modelling adopted in this research, by comparing the results of the numerical models with the problems of real (laboratory and field tests) buried pipes tested under static surface loading.

Validation problems 6 and 7 discuss the development of a finite element model to predict the behaviour of buried infrastructures under the effect of the moving loads.

Two field problems were used in the development of the model. The first concerned a large culvert under moving train loads; while the second problem involved a buried metal pipe under moving truck loads. The second problem finished with a comparison between the effect of the static and dynamic moving loads, to illustrate the need to consider the static loads instead of the dynamic moving loads to simulate the stringent loading conditions for buried pipes under traffic loading.

3.2.3.1. Validation problem 1 (validation of MIDAS GTS/NX software)

The numerical analysis reported in this research has been built and conducted using MIDAS GTS/NX, commercial finite element software. This software was used because it has a comprehensive soil constitutive models' library, including simple and advanced complex models. Furthermore, it has the ability to model the moving load and the dynamic soil-structure interaction together. However, a simple validation has been conducted before using this program to make sure that the linear and non-linear algorithms of the program are working properly. This validation involved comparing the results of a developed finite element model using this software (MIDAS GTS/NX) with the results of consolidated-drained triaxial tests reported by Boscardin et al. (1990) for a well-graded sandy soil compacted with a degree of compaction of 85% of the maximum dry standard Proctor density (SW85). The triaxial tests were conducted with a confining pressure of 35 kPa, 105 kPa, 208 kPa and 310 kPa, respectively. The triaxial test results were considered because it can clearly illustrate the ability of the program to model the initial elastic and the complex non-linear behaviour of the soil.

A quarter of the triaxial specimen was modelled taking advantage of the symmetry of the triaxial test. The considered quarter was built with a length, width and height of 1.0 m as shown in the finite element mesh in Figure 3.9; although these dimensions do not affect the prediction accuracy as all of the soil sample is loaded in the test and hence in the model (Surarak et al., 2012). In addition, the idea of the finite element modelling of the triaxial test is to simulate the stress condition applied on the soil sample, meaning that the model shape does not affect the prediction accuracy (i.e. cylinder or cube). Hence, this modelling approach was considered appropriate as it is also used in other finite element packages (PLAXIS and ABAQUS) to validate the finite element algorithms. The bottom of the model was fixed against movement in the lateral and vertical directions similar to the triaxial test. In addition, two of the four sides of the models (see Figure 3.9) were fixed against movement in the lateral directions to simulate the conditions of symmetry.

Two loading stages were considered in the developed model. In the first stage, a uniform pressure equivalent to the confining pressure was applied on the unrestrained faces of the model to simulate the consolidation stage. In the second stage, stress was applied to the top surface of the model as can be seen in Figure 3.9 to model the application of the deviatoric stress. This problem was simulated with the linear elastic model (LE), the Mohr-Coulomb elastic-perfectly plastic model (MC) and the non-linear elastic Duncan-Chang hyperbolic soil model (DC) (Duncan and Chang, 1970) to investigate the accuracy of the algorithms of the program. The hyperbolic soil model parameters of the SW85 soil were taken from Boscardin et al. (1990) and are shown in Table 3.4. The modulus of elasticity of the soil (E) for the LE

and MC models was calculated using Equation 3.1 (Janbu, 1963). The calculated E values are also shown in Table 3.4.

Figures 3.10 to 3.13 show the experimental and predicted stress-strain relationship for a confining pressure of 35 kPa, 104 kPa, 208 kPa and 350 kPa, respectively. The figures clearly illustrate that these models predict the stress-strain relationship as expected for the type of constitutive model used. The relationship stays linear for the LE model and for the MC model it remains linear until it reaches failure where it remains constant. However, the DC model follows the non-linear trend of the experimental relationship as the stiffness changes with the stress level. Hence, it can be concluded that these models are working properly in MIDAS GTS/NX. Therefore, the software can be used with confidence in this research.

It can also be seen from the figures that the DC model deviates from the experimental results at higher strains and particularly at higher deviatoric stresses (Figures 3.12 and 3.13). However, this deviation does not affect the accuracy of the soil-pipe interaction modelling conducted in this research. This is because the soil under such a high stress level (i.e. 208 kPa and 350 kPa) is far away from the effect of the traffic load (the equivalent height for 208 kPa is 10.5 m and the equivalent height for 350 kPa is 17.7 m), as the effect of the traffic load ends at a backfill height of more than 4.0 m, as will be discussed in **Chapters 5 and 6**. Hence, the soil with such a high confining pressure will not reach such high strain values in the analyses conducted during the present study. In addition, the DC model has demonstrated its capability in modelling the soil-pipe interaction, as will be discussed in validation problems 2 to 5.

Table 3.4: The soil parameters used in the triaxial analysis problem

Property	SW85
γ (kN/m^3)	19.82
υ	0.30
c'(kPa)	1
ϕ'(°)	38
K	450
R_f	0.80
n	0.35
$E_{(35)}$ (kPa)	31,163
$E_{(104)}$ (kPa)	45,622
$E_{(208)}$ (kPa)	58,148
$E_{(350)}$ (kPa)	69,765

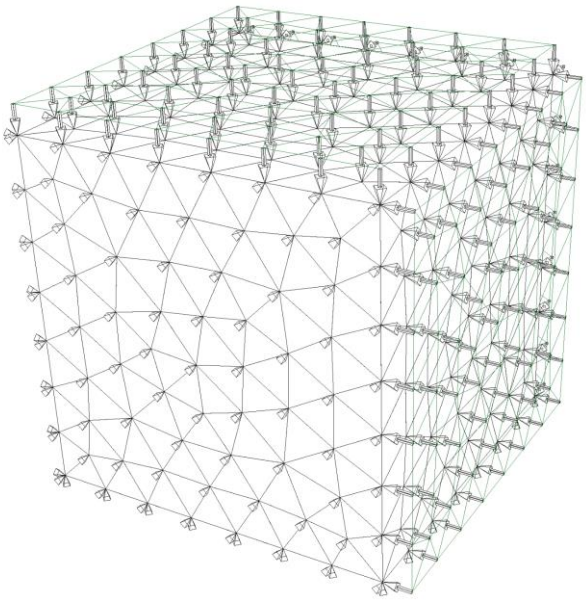

Figure 3.9: Finite element model used for the triaxial problem

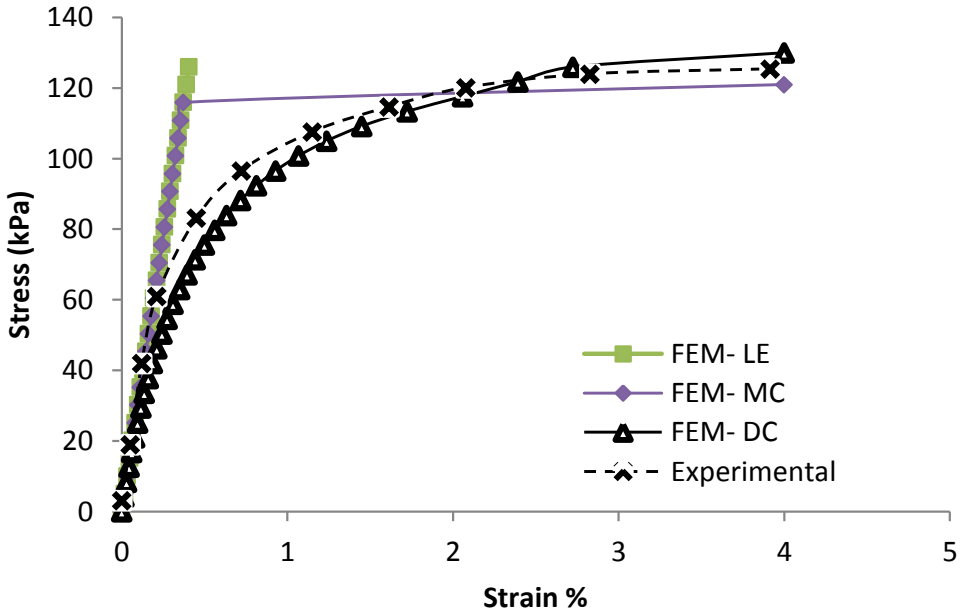

Figure 3.10: Comparison of the numerical and experimental triaxial stress-strain relationship of the SW85 soil with a confining pressure of 35 kPa

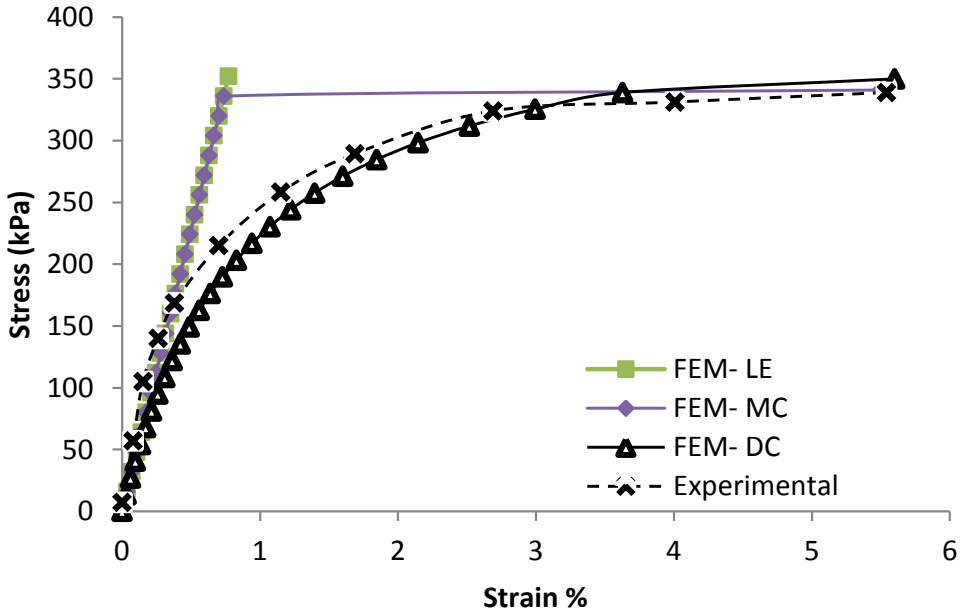

Figure 3.11: Comparison of the numerical and experimental triaxial stress-strain relationship of the SW85 soil with a confining pressure of 104 kPa

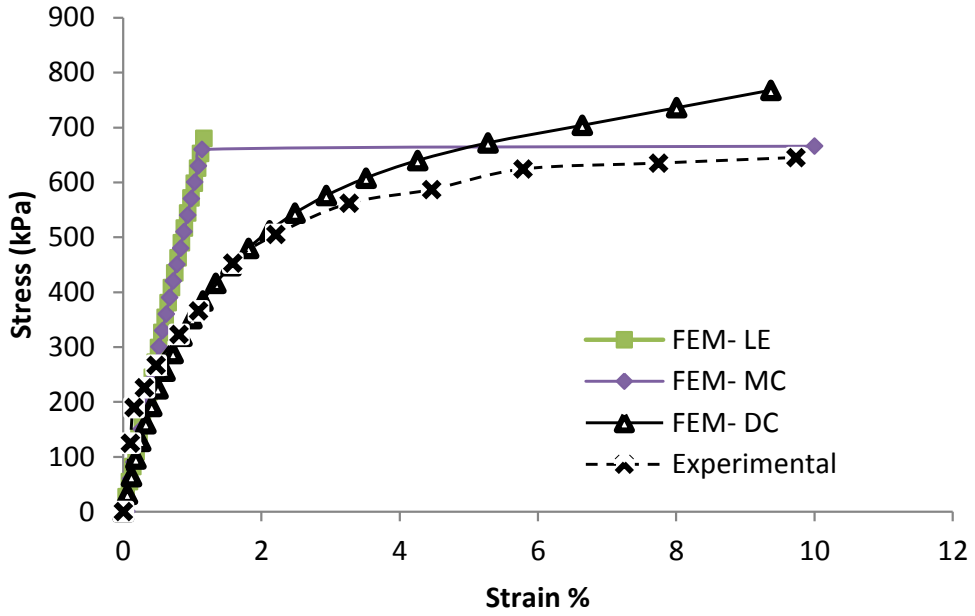

Figure 3.12: Comparison of the numerical and experimental triaxial stress-strain relationship of the SW85 soil with a confining pressure of 208 kPa

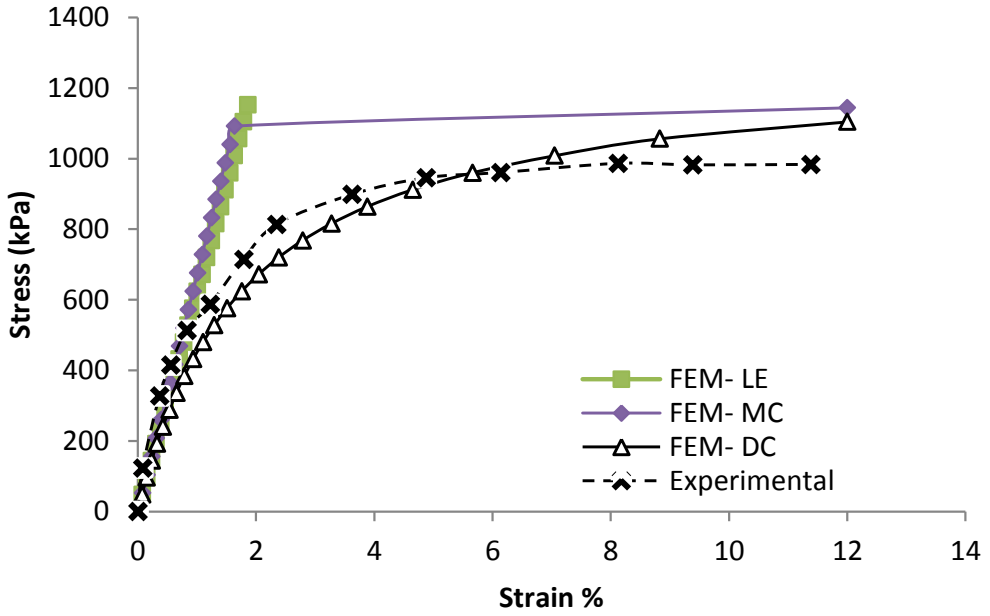

Figure 3.13: Comparison of the numerical and experimental triaxial stress-strain relationship of the SW85 soil with a confining pressure of 350 kPa

3.2.3.2. Validation problem 2

MacDougall (2014) reported on the bending moments associated with a reinforced concrete pipe buried under different backfill heights (0.3 m, 0.6 m and 0.9 m) and loaded at the ground surface with an AASHTO tyre load of 100 kN with a tyre footprint area of 0.25 m x 0.50 m. The inside diameter of the pipe was 0.6 m with a wall thickness of 0.094 m. The compressive strength of the concrete (f_c') was 66,000 kPa (9572.5 psi). The pipe was tested in the test pit at the GeoEngineering laboratory at Queen's University, Canada. The thickness of the bedding soil beneath the pipe was 0.96 m to avoid the influence of the rigid boundary of the test pit base. This bedding soil was followed by a 0.08 m layer of loose bedding soil to provide a uniform support for the pipe in the haunch zone. The soil surrounding the pipe and the backfill soil was added with thin layers (0.2 to 0.3 m) and compacted with a vibrating plate compacter. The surrounding and backfill soils were poorly-graded sandy gravel with a minimum degree of compaction of 90% of the standard Proctor dry density. The pipe was instrumented with strain gauges and the results from these gauges were used to calculate the bending moments.

A numerical model has been built to simulate these laboratory tests. This numerical model was used to provide confidence in the modelling approach, including the constitutive models used and the element types used for modelling the soil and the pipe. The length, width and height of the model was 5.0 m, 5.0 m and 5.0 m respectively. The model width ($\geq$ 4.0 D_{out}) and the soil depth below the pipe ($\geq$ 2.0 D_{out}) satisfy the requirements to avoid the influence of the model boundaries, as discussed in Section 3.2.2.1. A trench with a width of 2.0 m was simulated in one

direction across the model. The height of the trench was changed based on the backfill height, being equal to the backfill height plus the outer diameter of the pipe. The average element size of the pipe, trench and surrounding soil was 0.15 m, 0.15 m and 0.50 m. Four noded tetrahedron soil elements were used to model the trench and surrounding soil; while three noded shell elements were used to model the pipe. The base of the model was restrained against movement in all directions; while the sides of the model were restrained against movement in the horizontal directions. The finite element mesh is shown in Figure 3.14.

A linear elastic model was used to simulate the behaviour of the pipe. This model was considered appropriate because the pipe did not experience any cracking and its response remained in the elastic zone under the full load of 100 kN (MacDougall, 2014). The soil was modelled using the Duncan-Chang hyperbolic soil model (Duncan and Chang, 1970). The backfill height and the surrounding soil was simulated using poorly-graded gravelly sand with a minimum degree of compaction of 90% of the standard Proctor density (GP90); while the soil in the haunch zone was simulated using sandy silt with a compaction degree of 90% (ML90). The hyperbolic material properties of the GP90 and ML90 soils were adopted from Boscardin et al. (1990) and are shown in Table 3.5. The modulus of elasticity (E) and the Poisson's ratio (υ) of the concrete were 38,450,896 kPa and 0.20, respectively. The elastic modulus of the concrete was calculated using Equation 3.2 (ACI, 2014).

$$E = 57000 \times \sqrt{f_c'} \tag{3.2}$$

Three steps were performed to model the installation of the pipe and the loading:

Step 1: the initial stresses of the compacted soil beneath the pipe were calculated using a coefficient of lateral soil pressure of 1.0 (Brown and Selig, 1991).

Step 2: the bedding soil, pipe and soil above the pipe were added in stages, and the lateral soil stresses were calculated using a coefficient of lateral soil pressure of 1.0 (Brown and Selig, 1991). This horizontal soil pressure coefficient (i.e. 1.0) was considered to simulate the effect of compaction (Brown and Selig, 1991; Taleb and Moore, 1999).

Step 3: the traffic load was applied in 25 equal loading increments to reduce the number of iterations required to achieve the convergence.

Figures 3.15, 3.16 and 3.17 compare the calculated and measured bending moment in the pipe wall due to the total load (the backfill soil weight and traffic load) with a backfill height of 0.3 m, 0.6 m and 0.9 m, respectively. It can be seen that the model predicts the bending moment with good accuracy for all of the backfill heights. The percentage difference between the maximum calculated and measured bending moment is 25%, 10% and 15% for backfill heights of 0.3 m, 0.6 m and 0.9 m, respectively. Furthermore, the numerical model is able to predict the trend of the bending moment around the pipe.

It should be noted that it may seem that the obtained percentage difference is high (25%) for the first model, but it was less than that for the other two models (10% and 15%). This difference in the percentage differences indicates a potential variability in the test results, which is expected for such complicated laboratory tests. In addition, the present analysis adopted a thin shell theory, which gives a higher estimation to

the bending moment at the pipe crown as discussed in Section 3.2.1.4.2. Furthermore, comparing these percentages with the results of previous studies which have modelled laboratory and field tests of soil-pipe interaction indicted that the developed model is good. The percentages difference between the experimental and numerical results of previous studies ranged from 0% to 404% (additional details are explained in Section 3.2.3.8). Hence, the model is considered valid bearing in mind the assumptions made in the modelling and the potential variability in the results of such complex tests.

Table 3.5: The material properties of the soil for the validation problem 2 (Boscardin et al., 1990)

Property	GP90	ML90
γ (kN/m^3)	20.99	18.84
υ	0.30	0.30
c'(kPa)	1	24
ϕ'(°)	42	32
K	640	200
R_f	0.75	0.89
n	0.43	0.26

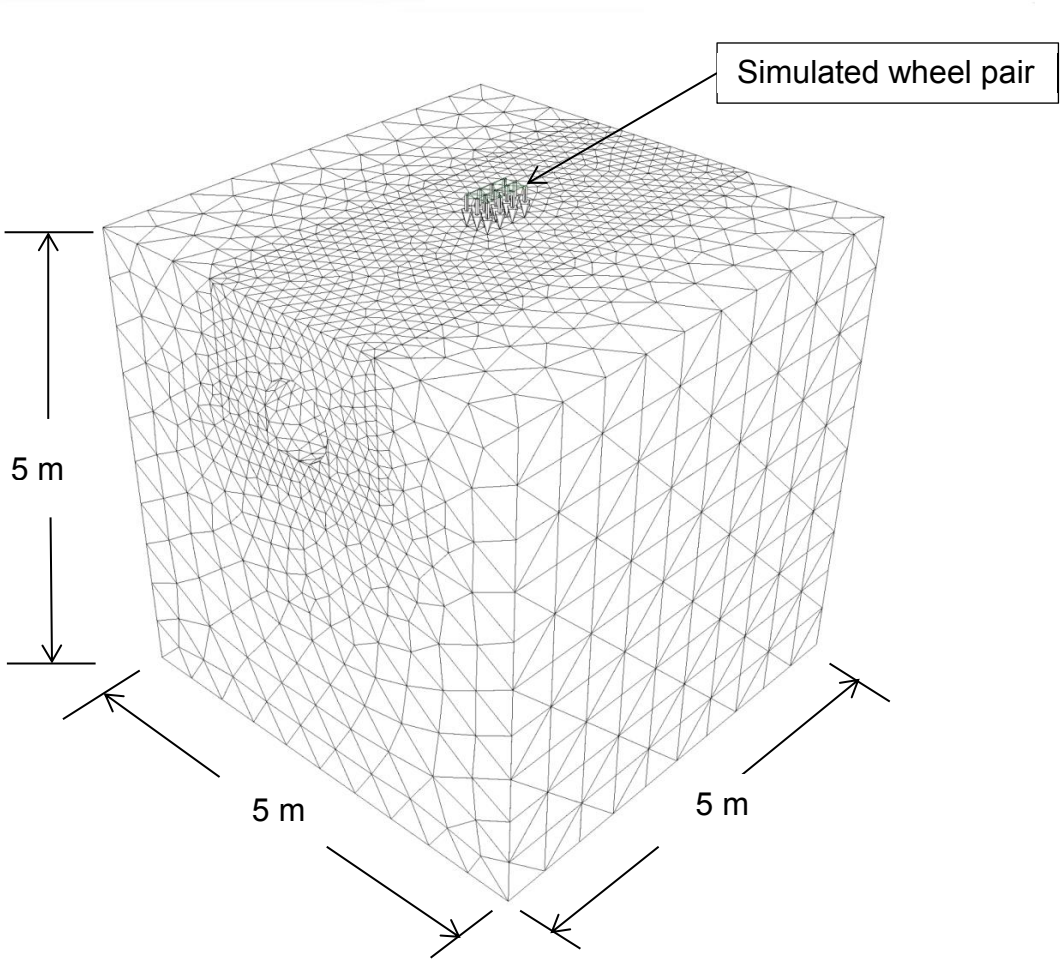

Figure 3.14: Finite element mesh used for validation problem 2

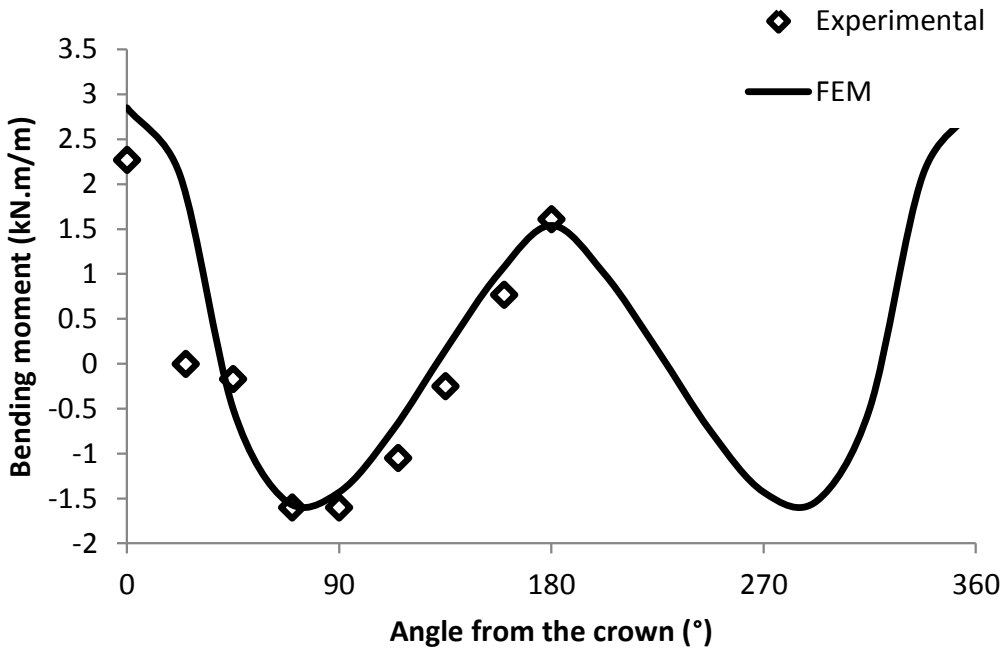

Figure 3.15: Bending moment in the concrete pipe under a total load (soil weight and traffic load) with a backfill height of 0.3 m

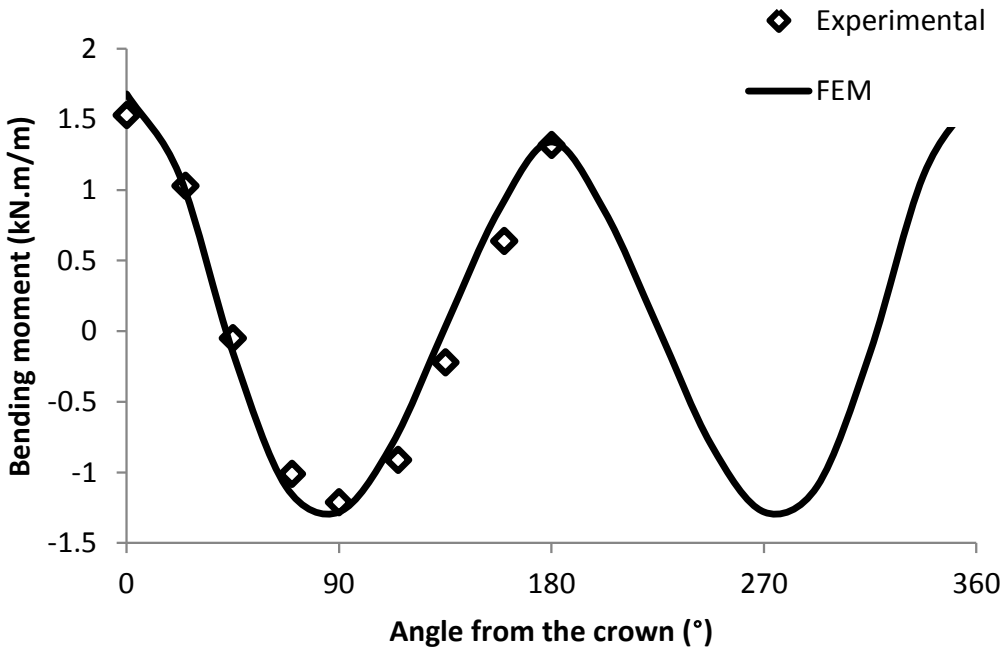

Figure 3.16: Bending moment in the concrete pipe under a total load (soil weight and traffic load) with a backfill height of 0.6 m

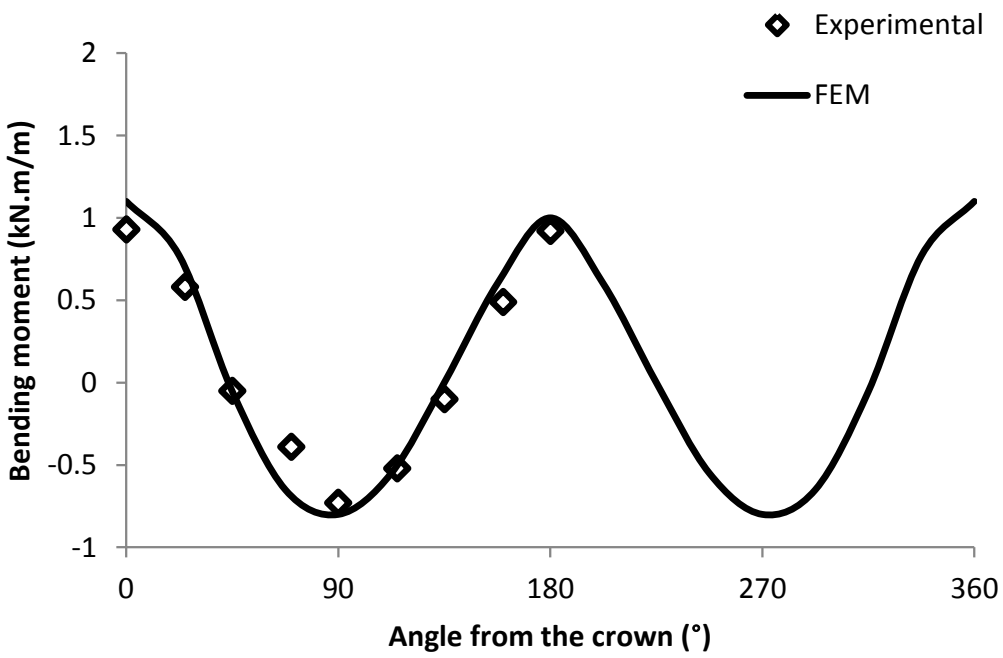

Figure 3.17: Bending moment in the concrete pipe under a total load (soil weight and traffic load) with a backfill height of 0.9 m

3.2.3.3. Validation problem 3

Robert et al. (2016) reported the results of a field study conducted to investigate the hoop wall stress for a buried cast iron pipe subjected to traffic loading. The pipe had an outside diameter of 0.7 m and a wall thickness of 0.025 m. The backfill cover above the pipe was 1.1 m, including a layer of asphalt material. The pipe was tested under a tyre load of 49 kN over a tyre foot print of 0.30 m x 0.30 m.

This field test has been modelled using MIDAS GTS/NX to verify the ability of the finite element model to predict the pipe wall stress. The finite element model was built with a length of 5.0 m, height of 5.0 m and a width of 5.0 m. These dimensions satisfy the requirement to avoid the influence of the finite element model boundaries as discussed in Section 3.2.2.1. A trench with a width of 1.30 m and a height of 1.65

m was simulated in one direction across the model to simulate the excavation and backfilling process. The average element size of the pipe, trench and surrounding soil was 0.15 m, 0.15 m and 0.50 m. The base of the model was restrained against movement in all directions; while the sides of the model were restrained against movement in the horizontal direction. The finite element mesh is shown in Figure 3.18.

A linear elastic model has been used to simulate the behaviour of the pipe and asphalt material. The asphalt layer was modelled using a linear elastic model because the traffic load was relatively low compared to the strength of the asphalt material. Therefore, the behaviour of the asphalt was expected to be in the elastic zone (Robert et al., 2016). The Duncan-Chang hyperbolic soil model (Duncan and Chang, 1970) was used to model the behaviour of the soil. The material properties of the pipe, asphalt and soil are taken from Robert et al. (2016) and Boscardin et al. (1990) and are shown in Table 3.6. Four steps were performed in the finite element analyses to simulate the conditions of the field test:

Step 1: the initial stresses of the soil were calculated. The coefficient of the lateral earth pressure of the natural soil was taken to be equal to 1.0 (Brown and Selig, 1991).

Step 2: the trench was excavated in stages.

Step 3: the bedding soil, pipe, backfill soil, base soil and asphalt soil were added to the model in stages. The coefficient of the lateral earth pressure of the compacted

backfill was taken as equal to 1.0 to simulate compaction process (Brown and Selig, 1991; Taleb and Moore, 1999).

Step 4: the traffic load was applied using 25 equal loading increments.

Figure 3.19 shows the experimental and numerical modelling results of the hoop stress measured at the outside surface of the pipe, due to the total load (the backfill soil weight and traffic load). It can be seen that the model predicted the trend in the stress, where the maximum stress was at the crown of the pipe for both the experimental and finite element modelling results. Furthermore, the model predicted the maximum stress with good accuracy, where the percentage difference between the maximum stress predicted using the developed finite element model and the experimental result was 10%.

Table 3.6: The material properties of the pipe and the soil used in the validation problem 3

Property	Pipe*	Asphalt*	Soil**
γ (kN/m^3)	78.50	22.30	23.30
υ	0.30	0.30	0.30
E (kPa)	120,000,000	175,000	---
c'(kPa)	---	---	1
ϕ'(°)	---	---	54
K	---	---	1300
Rf	---	---	0.65
n	---	---	0.90

* taken from Robert et al. (2016)

** taken from Boscardin et al. (1990)

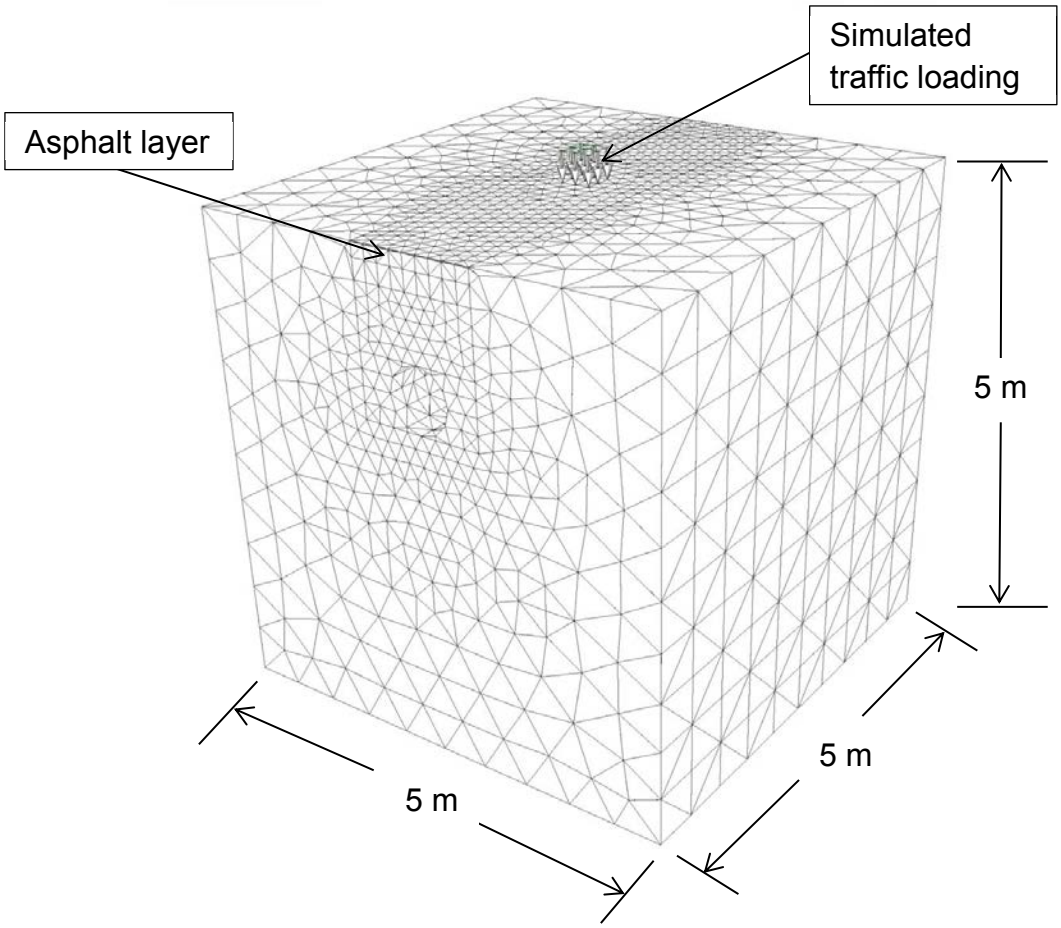

Figure 3.18: The finite element mesh used for validation problem 3

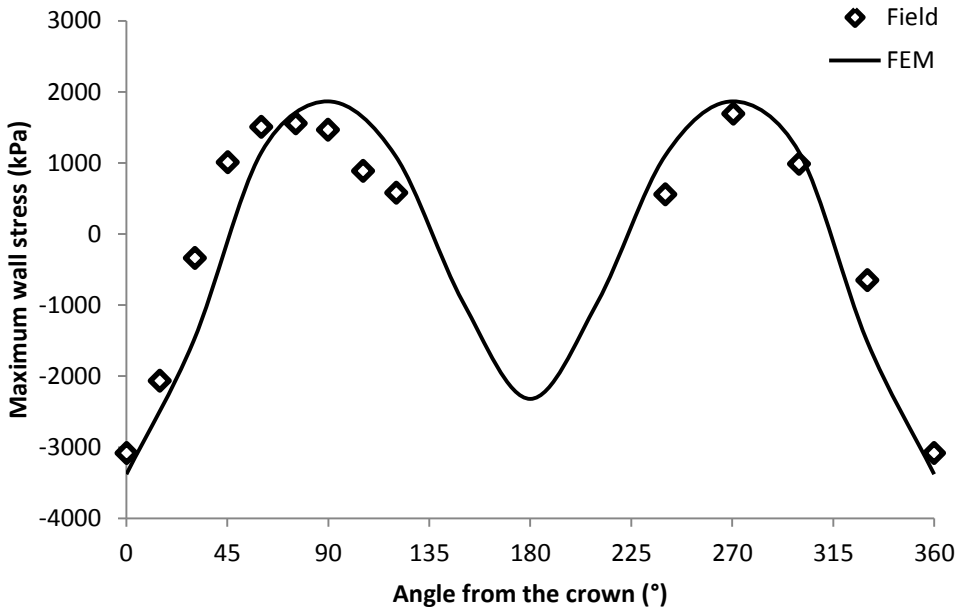

Figure 3.19: Hoop stress within the pipe due to the combined effect of the backfill soil weight and tyre load measured in the outside surface of the pipe

3.2.3.4. Validation problem 4

A field test involving a corrugated HDPE pipe with a nominal diameter of 0.9 m tested under two AASHTO trucks was reported by Arockiasamy et al. (2006). The pipe in this test was buried in a trench with a minimum width of 1.66 m. The backfill height was 0.5 m. Crushed limestone was used for the 0.152 m bedding layer and poorly-graded sand with silt with a degree of compaction of 95% of the standard Proctor maximum dry density was used as the backfill material. The pipe was subjected to surface traffic loads from two axles of two trucks with a maximum axle load of 181 kN. The axle load value simulated an AASHTO HS20 truck with a dynamic allowance factor calculated using the equation from AASHTO (1998). The space between the two trucks was 0.91 m.

A numerical model was developed for this problem, with a length, width and height of 15.0 m, 12.0 m and 10.0 m, respectively. The model width ($\geq$ 4.0 D_{out}) and the soil height below the pipe ($\geq$ 2.0 D_{out}) satisfy the requirements to avoid the influence of the model boundaries, as discussed in Section 3.2.2.1.

Four noded tetrahedron solid elements were used to model the surrounding soil and the trench; while three noded triangular shell elements were used to model the pipe. The finite element mesh is shown in Figure 3.20. The truck load for each tyre was modelled as surface pressure over a tyre foot print area of approximately 0.23 m x 0.31 m (Arockiasamy et al., 2006). A linear elastic model was used to model the pipe. The Duncan-Chang hyperbolic soil model (Duncan and Chang, 1970) was used to represent the behaviour of the soil. The mechanical properties of the bedding soil, backfill soil and natural soil were adopted from the literature (Boscardin et al., 1990) and are shown in Table 3.7. The modulus of elasticity of the pipe (E) and the Poisson's ratio of the pipe (υ) were taken equal to 760,000 kPa and 0.40, respectively (Arockiasamy et al., 2006).

The base of the model was restrained against movement in all directions; while the sides of the model were restrained against movement in the horizontal directions. Four steps were performed in the finite element analyses to simulate the stages of the construction conducted in the field test:

Step 1: the initial earth pressures for the *in-situ* soil were calculated. The coefficient of the lateral earth pressure of the natural soil was taken as equal to 1.0.

Step 2: the trench was excavated.

Step 3: the bedding soil, pipe and backfill soil were added to the model. The coefficient of the lateral earth pressure of the compacted backfill was taken as equal to 1.0 to simulate compaction process (Brown and Selig, 1991; Taleb and Moore, 1999).

Step 4: the traffic load was applied using 25 equal loading increments.

This field test has also been modelled in the literature using two-dimensional finite element analysis and three-dimensional finite element analysis with a linear elastic model for both the soil and the pipe (Arockiasamy et al., 2006); and two-dimensional finite element analysis using a linear elastic model for the pipe and non-linear elastic hyperbolic soil model for the soil (Kang et al., 2014).

Figure 3.21 compares the maximum vertical (at the pipe crown) and horizontal (at the pipe springline) displacements of the pipe obtained from the field results (Arockiasamy et al., 2006), the present model, two- and three-dimensional finite element elastic models (Arockiasamy et al., 2006) and a two-dimensional analysis using the hyperbolic soil model (Kang et al., 2014). Figure 3.22 compares the results of the soil pressure around the pipe obtained from the field test and the same numerical studies.

From Figure 3.21, it can be seen that the present model predicted the displacement of the pipe better than the previous models with a difference of 14% for the vertical displacement (3.50 mm from the field test and 4.00 mm from the developed model) and 13% for the horizontal displacement (1.50 mm from the field test and 1.30 mm from the developed model).

Figure 3.22 shows that the present model predicted the trend of soil pressure around the pipe. It can be seen that the two-dimensional model also predicted the soil pressure reasonably well. However, Kang et al. (2014) did not report the value of the spread factor which was used in their analysis. The difference between the actual and predicted results can be justified by the complexity and variability of the soil density pattern around the pipe and the difference between the real and the assumed soils' properties as the behaviour of the flexible pipe is significantly affect by the soil around the pipe (Rogers et al., 1996; Dhar et al., 2004; Chapman et al., 2007).

Table 3.7: The material properties of the soil for validation problem 4 (Boscardin et al., 1990)

Property	Backfill	Bedding	Natural soil
γ (kN/m^3)	19.91	22.07	22.07
υ	0.30	0.30	0.30
c'(kPa)	28	0	0
ϕ'(°)	34	48	48
K	440	950	950
Rf	0.95	0.70	0.70
n	0.40	0.60	0.60

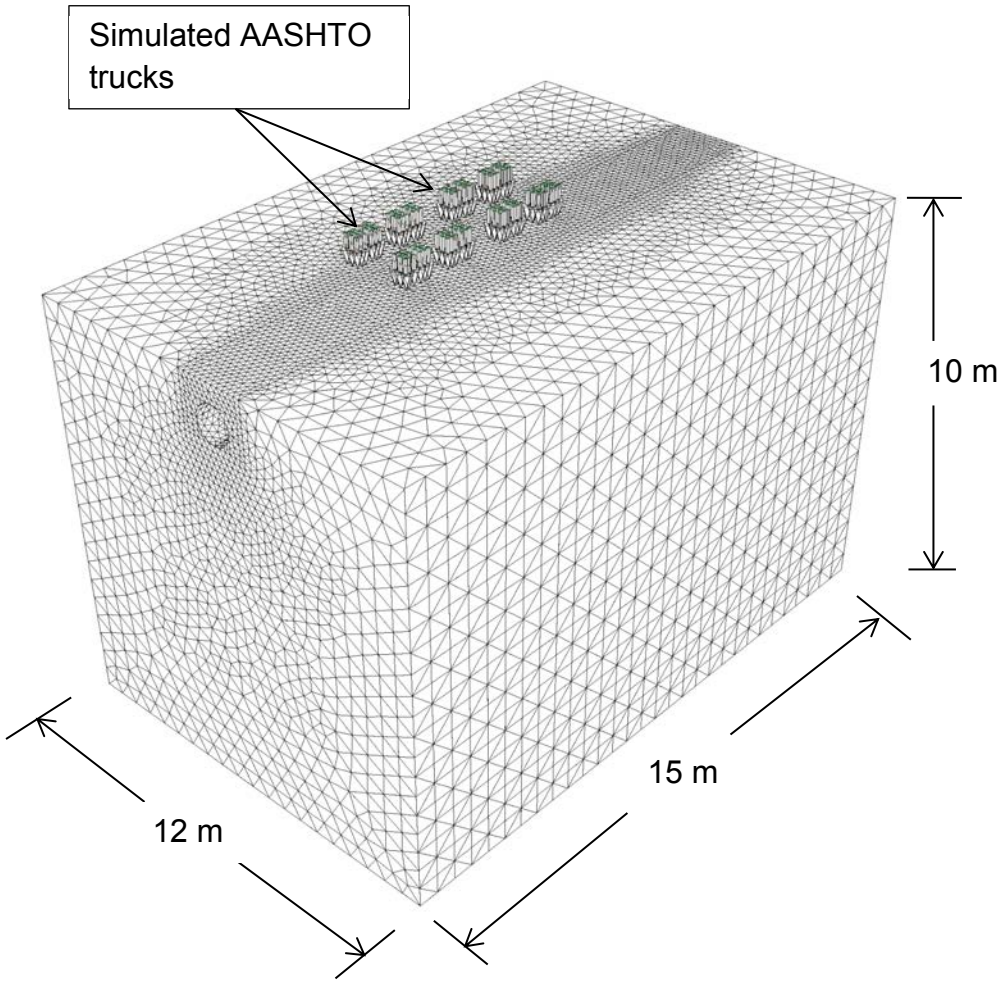

Figure 3.20: Finite element model used for validation problem 4

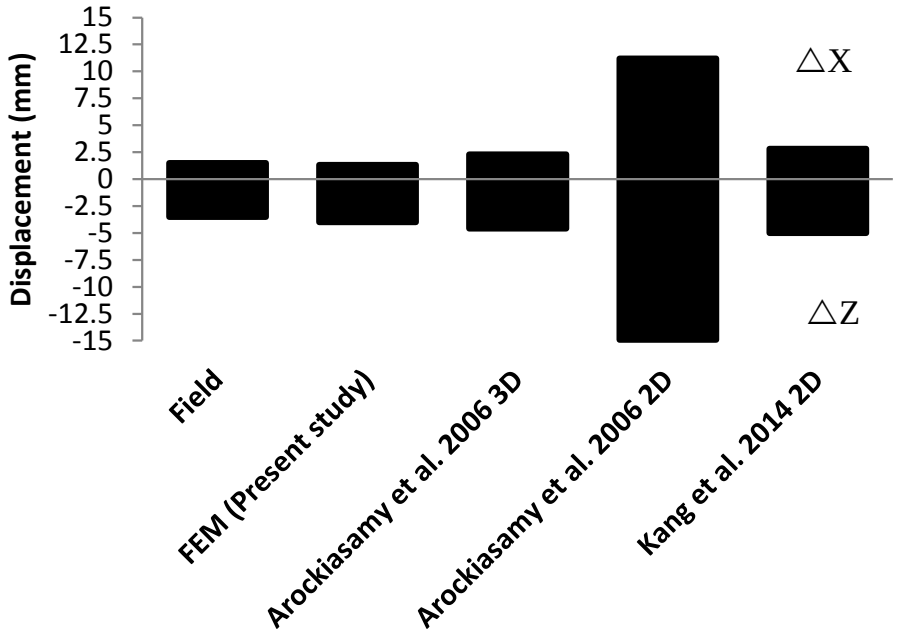

Figure 3.21: Comparison of the vertical (at the pipe crown) and horizontal (at the pipe springline) displacement of the HDPE pipe under traffic load

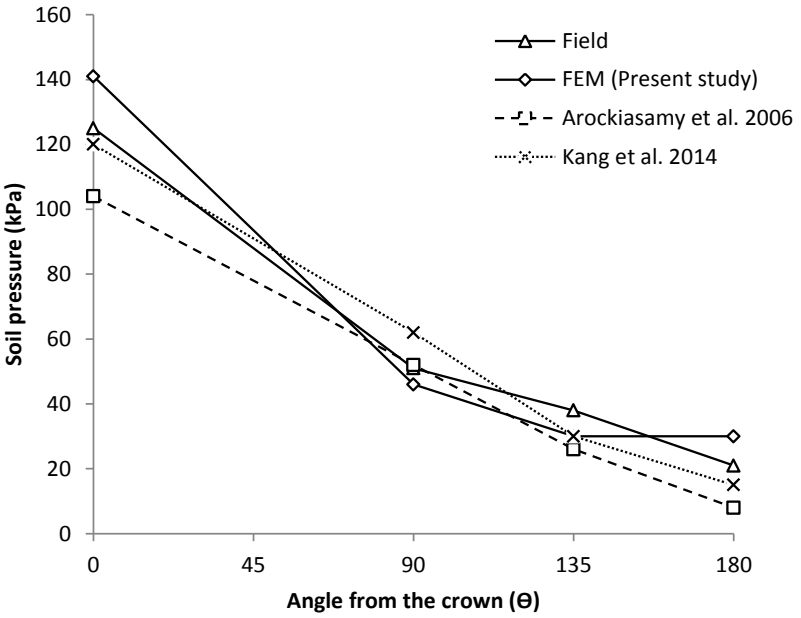

Figure 3.22: Comparison of the soil pressure around the HDPE pipe under total load

3.2.3.5. Validation problem 5

The crown vertical displacement of a buried PVCu pipe with an external diameter of 0.5 m and a wall thickness of 0.013 m has been reported by Kraus et al. (2014). This pipe was tested in a laboratory test box with a length, width and height of 3.1 m, 2.4 m and 2.6 m, respectively. A surface load of 107 kN was applied over a plate with an area of 0.90 m x 0.90 m. The backfill height in this test was 0.5 m. A gravelly soil with a degree of compaction of 95% of the standard Proctor maximum dry density was used as the bedding material, and a sandy soil with a degree of compaction of 95% of the standard Proctor maximum dry density was used as the backfill and the natural soil.

This test was modelled numerically using 0.15 m size elements for the pipe and the soil. The length, width and height of the numerical model was 3.1 m, 2.4 m and 2.6 m, respectively. The model width ($\geq$ 4.0 $\mathrm{D_{out}}$) and the soil depth below the pipe ($\geq$ 2.0 D_{out}) satisfy the requirements to avoid the influence of the model boundaries. A linear elastic model was used to model the pipe. The Duncan-Chang hyperbolic soil model (Duncan and Chang, 1970) was used to represent the behaviour of the soil. The material properties of the soils were adopted from the literature (Boscardin et al., 1990) and are shown in Table 3.8. The modulus of elasticity (E) and the Poisson's ratio (υ) of the pipe were taken as 689,000 kPa and 0.35, respectively (Kraus et al., 2014). The base of the model was restrained against movement in all directions; while the sides of the model were restrained against movement in the horizontal directions only. Three steps were performed to model the installation of the pipe and the loading:

Step 1: the initial earth pressures of the compacted soil beneath the pipe were calculated using a coefficient of lateral earth pressure of 1.0 (Brown and Selig, 1991).

Step 2: the bedding soil, pipe, and soil above the pipe were added in stages. The lateral earth pressures were calculated using a coefficient of lateral earth pressure of 1.0 to simulate compaction effect (Brown and Selig, 1991; Taleb and Moore, 1999).

Step 3: the surface load was applied in 25 equal loading increments.

The predicted and recorded vertical displacement of the PVCu pipe crown is shown in Figure 3.23. It can be seen that a good estimation is obtained from the numerical model, where the percentage difference between the maximum predicted and measured vertical displacement is equal to 7%. It can be also be seen that the difference between the results is less than that for validation problem 4; which is expected as the laboratory tests for small flexible pipe diameters are usually more controlled, with less uncertainties regarding the compaction of the soil, the recorded results and the uniformity of the support around the pipe.

Table 3.8: The material properties of the soil for validation problem 5 (Boscardin et al., 1990)

Property	Backfill, bedding and surrounding soil
γ (kN/m3)	22.07
υ	0.30
c'(kPa)	1
ϕ'(°)	48
K	950
Rf	0.70
n	0.60

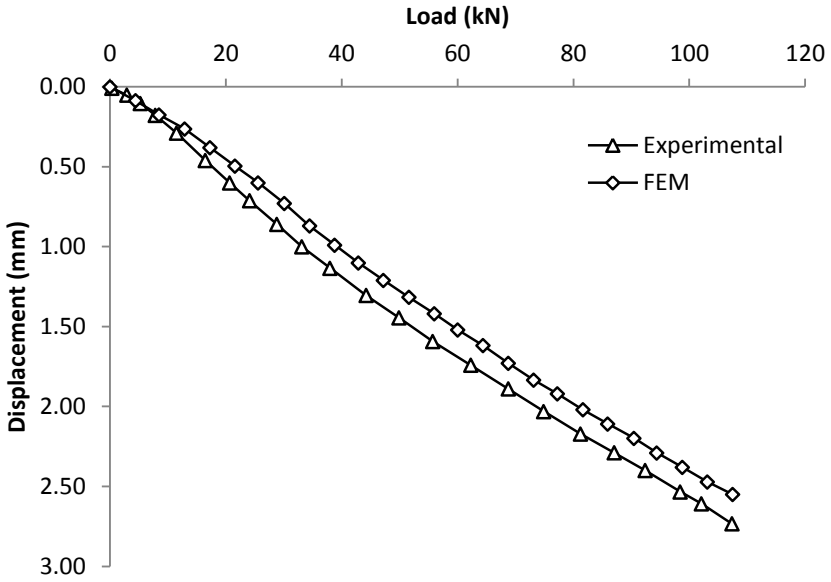

Figure 3.23: Predicted and measured vertical displacement of the PVCu pipe crown

3.2.3.6. Validation problem 6

Mellat et al. (2014) investigated the crown vertical displacement of a buried, in-service, large diameter, corrugated culvert under moving train loads using field and

finite element studies. An X52 commuter train with a speed of 180 km/h was used in the field test. The culvert had an elliptical cross section. The horizontal diameter of the culvert was 3.8 m, while the vertical diameter was 4.2 m. The total length of the train was 54 m and consisted of two coaches. Each coach had four axles with a total axle load of 185 kN. The distance between the axles is shown in Figure 3.24. The finite element analysis involved modelling the field test using ABAQUS software, where linear elastic modelling was considered in the finite element analysis.

This study was considered to test the capabilities of MIDAS GTS/NX in modelling the response of the buried pipes and culverts under the effect of dynamic moving loads. This study was taken into account because all of the information required for conducting correct modelling (i.e. material properties of the culvert and the soil, culvert dimensions and loading configurations) is available in the paper of Mellat et al. (2014). In addition, the test was also modelled by Mellat et al. (2014) using ABAQUS software, as mentioned in the previous paragraph; hence, this allows a direct comparison between the numerical modelling results of MIDAS GTS/NX and ABAQUS.

The problem was modelled with dimensions similar to the field dimensions. The corrugated culvert was simulated by using shell elements with an equivalent thickness of 0.061 m as proposed by Mellat et al. (2014). Four noded tetrahedron solid elements were used to model the ballast and the backfill layers; while three noded triangular shell elements were used to model the culvert. The base of the model was restrained against movement in all directions; while the sides of the model were restrained against movement in the horizontal direction. Ground surface spring

elements (viscous dampers) were used in the sides and the bottom of the model to simulate the infinite boundary conditions. This technique is used to eliminate the effect of S and P wave reflection (Sayeed and Shahin, 2016). Wave reflection is a phenomenon that happens in dynamic finite element analyses if standard static finite element boundary conditions are used. These standard boundaries will create a wave reflection, which in turn will lead to superimpose of these waves with the progressing waves (Liu and Quek Jerry, 2003). Hence, special treatment is required for the model boundaries in dynamic finite element analyses. The model was developed with an average element size of 0.70 m, 0.70 m and 1.00 m for the ballast layer, culvert, and the backfill and surrounding soil, respectively. The mesh of the developed three-dimensional finite element model is shown in Figure 3.25.

The moving wheels were modelled using a train dynamic load table available in MIDAS GTS/NX. This modelling technique allows the user to model the moving loads by specifying the nodes of the loading path and arranging a table for the wheels' loads, the offset distance between the wheels, and the train speed. By using this technique, the program automatically changes the loads on the mesh as the time increases, depending on the speed of the train. It should be noted that the moving wheels were modelled as concentrated loads because the wheel load concentrates below the rail seat and does not distribute equally on the whole sleeper area due to the issues associated with the contact area between the sleeper and the ballast layer as noted by Shenton (1978) and Abadi et al., (2015). Hence, using point loads to model the moving train loads does not affect the accuracy of the finite element model predictions. A time step of 0.01 sec was considered in the analysis based on the finite element mesh size and the speed of the train following the Courant-Friedrichs-

Lewy condition (Galavi and Brinkgreve, 2014). The time step was calculated based on the mesh size to avoid the model instability caused by the wave progress in the dynamic finite element analysis (Vivek, 2011). The material properties of the ballast, backfill and culvert are taken from Mellat et al. (2014) and are shown in Table 3.9.

The measured (field) results, numerical results using ABAQUS (Mellat et al. 2014) and numerical results from the present analysis (using MIDAS GTS/NX) of the crown vertical displacement induced due to a moving X52 train with a speed of 180 km/h are shown in Figure 3.26. It is worth mentioning here that Mellat et al. (2014) did not model all of the train loads in the finite element analysis; they considered only the two middle bogie loads of the train to reduce the computational time. It can be seen from Figure 3.26 that the developed model predicts the crown vertical displacement with good accuracy compared to the field data and ABAQUS software. The percentage difference between the maximum calculated and measured crown vertical displacement is 15%. Furthermore, the developed model is able to predict the trend of the displacement time relationship, as can be clearly seen in Figure 3.26. Hence, these results give confidence in the methodology adopted for modelling this complex problem. Therefore, the developed model can be taken forward to investigate other scenarios of buried culverts under traffic loading.

Table 3.9: Material properties for the soil and the culvert (Mellat et al. 2014)

Part	E (kPa)	υ	γ (kN/m^3)
Ballast	200,000	0.30	17.65
Backfill and surrounding soil	100,000	0.30	15.70
Culvert	23,700,000	0.30	76.52

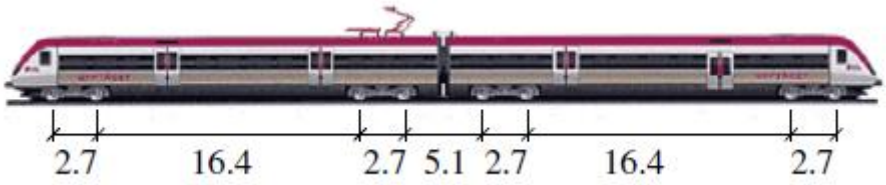

Figure 3.24: The distances of the axles of the X52 train (Mellat et al. 2014) (dimensions are in m)

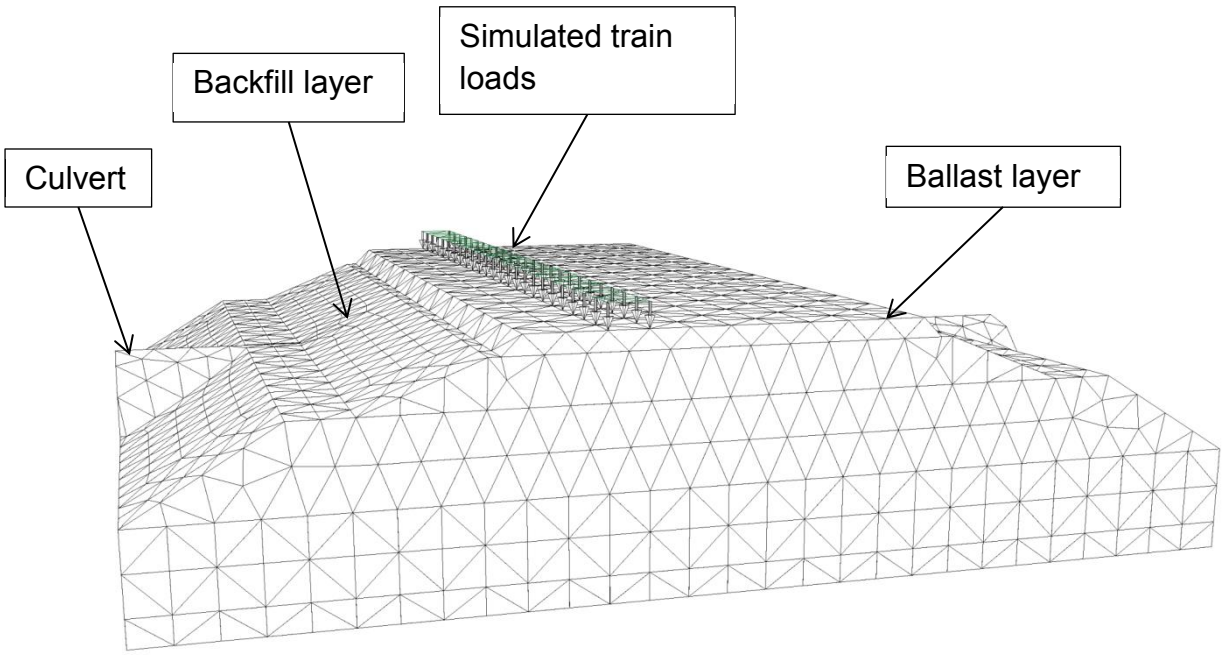

Figure 3.25: The finite element mesh used for validation problem 6

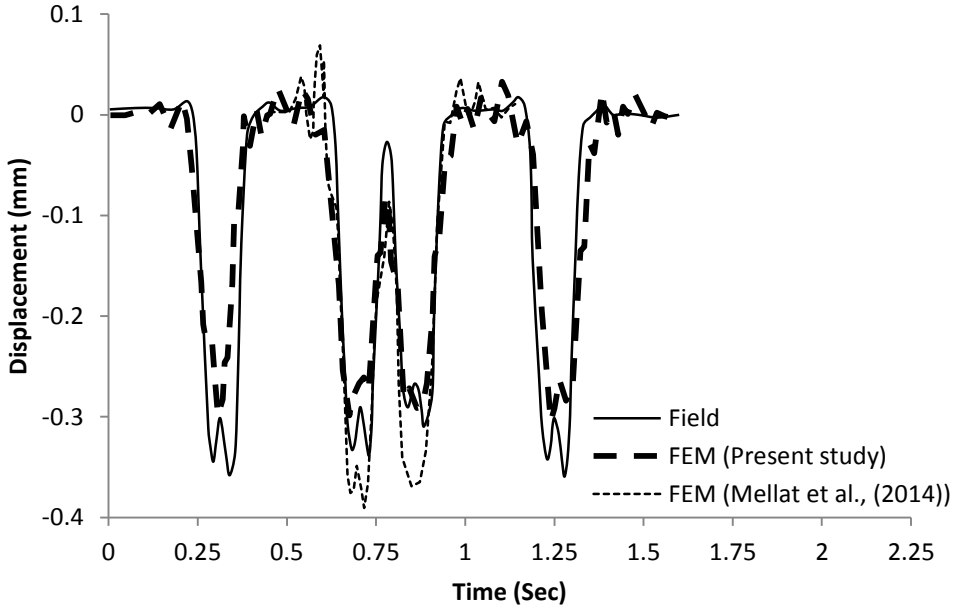

Figure 3.26: Crown vertical displacement time response due to the effect of moving train loads

3.2.3.7. Validation problem 7

Sheldon et al. (2015) reported the crown displacement of a buried, in-service, metal pipe under the effect of static and moving truck loads. The moving truck tests were carried out with four different speeds (8 km/h, 16 km/h, 32 km/h and 48 km/h). The pipe had an inner diameter of 1.2 m and was buried with a backfill height of 0.5 m. Linear displacement sensors were used to measure the crown displacement. These sensors were installed in the upstream and downstream sides of the pipe joint. The upstream sensor recorded the vertical displacement of the pipe crown and the downstream sensor recorded the vertical displacement of the pipe joint. The test truck had a steering axle load of 59 kN and rear axle load of 133 kN. The axles were spaced by 4.3 m. The distance between the rear wheel pairs was equal to 1.4 m.

These tests have been modelled using MIDAS GTS/NX and have been considered to test the capabilities of the developed finite element model. Further, the author wished to compare the behaviour of the buried pipe under static and moving loads to do a blind check on the conclusions of Sheldon et al.'s (2015) study, hence, illustrating the robustness of the present research.

Four noded tetrahedron solid elements were used to model the soil and the asphalt layer; while three noded triangular shell elements were used to model the pipe. The joint was not considered in the finite element model as this model was used as a first approximation to the problem. Hence, the problem was simplified as the aim was to compare the behaviour of the buried pipes under static and moving loads to find the critical loading condition and compare the findings with the conclusions of Sheldon et al. (2015). The developed model had a width, length and height of 5.0 m, 15.0 m and 10.0 m, respectively. A trench with a width of 2.4 m, a height of 2.1 m and a length of 15.0 m was considered in the model to use finer elements around the pipe to improve the prediction ability. The model was built with an average element size of 0.15 m for the culvert, 0.15 m for the trench, 0.25 m for the road and 0.50 m for the natural soil. The three-dimensional finite element model is shown in Figure 3.27. The base of the model was restrained against movement in all directions; while the sides of the model were restrained against movement in the horizontal direction. Ground surface spring elements with damping constants were used in the sides and the bottom of the model to reduce the effect of the wave's reflection, due to the dynamic analysis of the moving load problem.

A well-graded sandy soil with a degree of compaction of 90% (SW90) was considered in the developed model as a backfill soil, followed by an asphalt layer with a thickness of 0.1 m. A linear elastic model was used to simulate the behaviour of the pavement, soil and pipe. The soil was modelled using the linear elastic model to reduce the computational time required for this time-dependent complex three-dimensional finite element analysis. The modulus of elasticity (E) of the SW90 soil was calculated using Equation 3.1 (Janbu, 1963) and the hyperbolic soil model parameters published by Boscardin et al. (1990) (shown in Table 3.2). A lateral stress (S_3) of 19.32 kPa was used in Equation 3.1 to calculate the modulus of elasticity. This lateral stress was calculated by taking the average height from the top surface of the model to the pipe invert using a coefficient of lateral earth pressure of 1.0 for the compacted backfill soil (Brown and Selig, 1991). The natural soil was assumed to be stronger than the backfill soil. The material properties of the SW90 soil and the natural soil are shown in Table 3.10. The material properties of the asphalt layer and the culvert are taken from the literature (Kang et al., 2014; Sheldon et al., 2015) and are shown in Table 3.10. The culvert was modelled using an effective thickness of 2.0×10^{-5} m (Sheldon, 2011).

The moving truck loads were modelled, assuming concentrated moving loads, with the aid of the dynamic train table available in MIDAS GTS/NX software. The truck tyres were modelled as concentrated moving loads to avoid the complexity associated with the non-uniform distribution of the tyre pressure due to the moving of the truck, which was noticed by De Beer et al. (1997). In addition, the actual pressure distribution of the moving tyres was not measured during the tests. Furthermore, this simplification was found to provide a reasonable estimation for the displacement of

the pipe, as will be discussed in the results. The space between the concentrated loads was considered equal to 1.4 m, similar to that reported in the field tests. The time step was calculated based on the mesh size and the velocity of the truck following the Courant-Friedrichs-Lewy condition (Galavi and Brinkgreve, 2014).

The measured and predicted pipe crown vertical displacement time response of the pipe under a moving truck with a speed of 8 km/h, 16 km/h, 32 km/h and 48 km/h is shown in Figures 3.28, 3.29, 3.30 and 3.31, respectively. It can be seen that the developed model is able to predict the trend behaviour of the displacement time response for all of the considered speeds. In addition, the developed model predicted the maximum displacement with good accuracy: where the percentage difference of the field and numerical maximum crown vertical displacement is equal to 3%, 5%, 22% and 20% for truck speeds of 8 km/h, 16 km/h, 32 km/h and 48 km/h, respectively. However, Figures 3.28 and 3.29 show a shift in the results of the finite element simulation in comparison with the field tests. This might be due to issues related to a change in the truck speed during the tests.

The difference in the results can be justified by the use of the linear elastic model to simulate the behaviour of the pipe. This model (as discussed in Section 3.2.1.3) is not able to simulate the dependency of the soil stiffness on the stress level. Hence, the support condition provided to the pipe is not captured accurately by using this model. Moreover, the assumption of concentrated moving loads also affected the accuracy of the developed model, as it is difficult to assume a correct tyre stress distribution due to the moving action (unless it has been measured during the tests), which has been demonstrated by De Beer et al. (1997). In addition, the difference

between the soil in the field and the soil used in the modelling may also have affected the prediction accuracy of the developed model. Furthermore, the potential variability in the test results, especially for such complicated field tests, might also have contributed to the high percentage difference noted for the tests with truck speeds of 32 km/h and 48 km/h.

A static finite element analysis was also conducted by considering the case of the rear axle load being directly on the top of the pipe, similar to the loading condition of the real static test conducted by Sheldon et al. (2015). The tyre load was modelled as a surface pressure over a tyre foot print area of approximately 0.25 m x 0.50 m (Sheldon, 2011); as this technique was found to provide a good prediction to the response of the buried pipe under static loading, as discussed in the validation problems 2 to 5. The maximum vertical static displacement at the crown of the buried pipe was equal to 1.28 mm, compared to an experimental value of 1.49 mm, indicating a reasonable predictive ability for the developed model (i.e. percentage difference of 14%). This difference is due to the use of the linear elastic model as discussed in the previous paragraph.

Figure 3.32 shows the ratio of the maximum static crown displacement to the maximum dynamic crown displacement for different truck speeds (obtained from Figures 3.28, 3.29, 3.30 and 3.31). It can be clearly seen from the figure that the static displacement is higher than the dynamic displacement for all of the truck speeds; where the ratio ranges from 1.36 to 1.42 depending on the truck speed. Hence, it can be concluded that the static loading condition simulates the worst-case scenario. This observation confirms the observations of Sheldon et al. (2015) and

Robert et al. (2016). Therefore, the static loading condition was used in all of the subsequent analyses conducted in this research (reported in **Chapters 5 and 6**).

Table 3.10: Material properties used in the finite element analysis

Part	E (kPa)	υ	γ (kN/m^3)
Natural soil	49,685	0.30	22.00
Backfill soil	30,813	0.30	21.00
Pipe	200,000,000	0.20	78.00
Asphalt	4,500,000	0.30	23.23

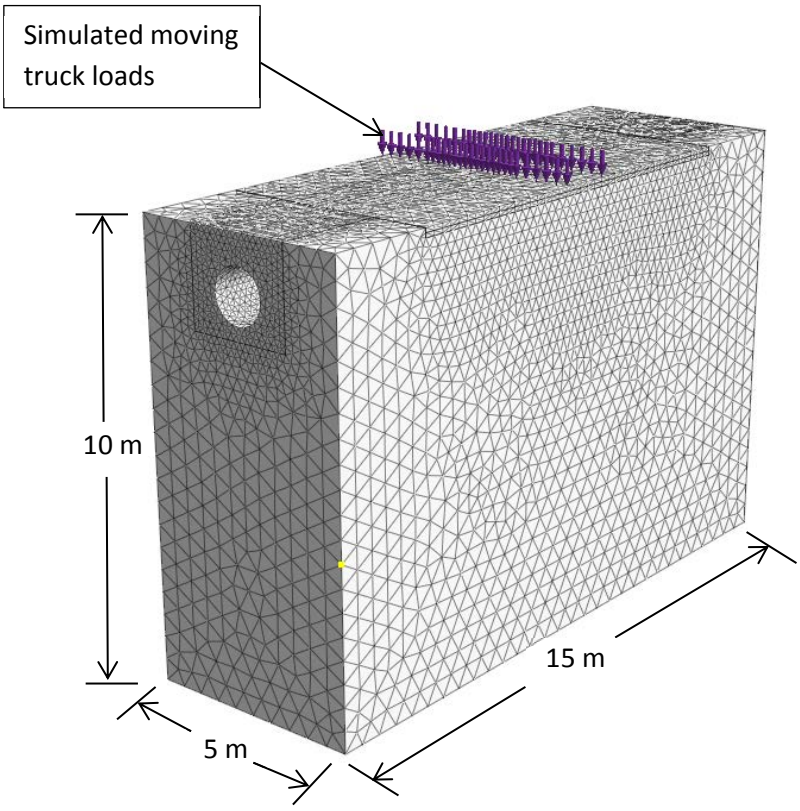

Figure 3.27: The finite element mesh used for validation problem 7

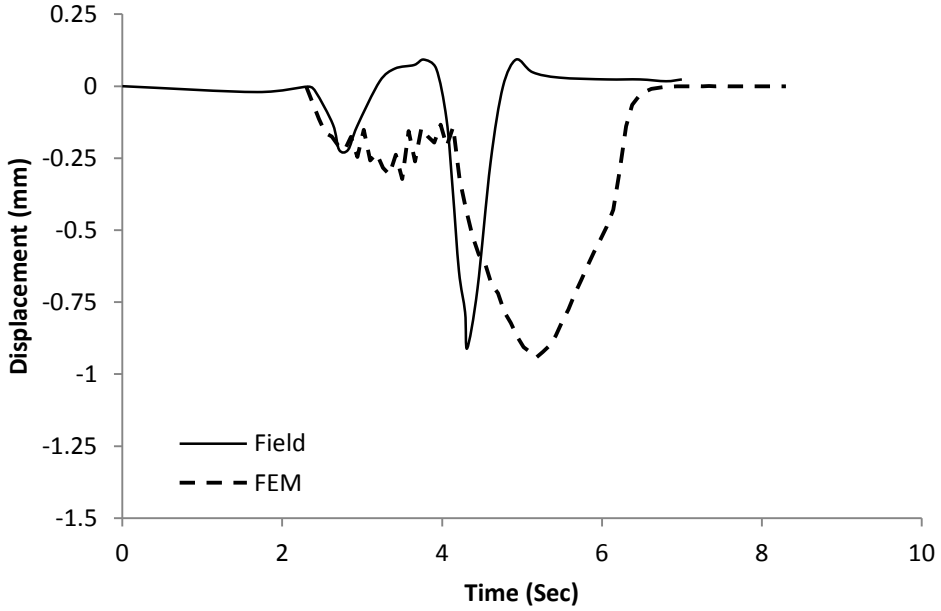

Figure 3.28: Crown vertical displacement time response under a moving truck with a speed of 8 km/h

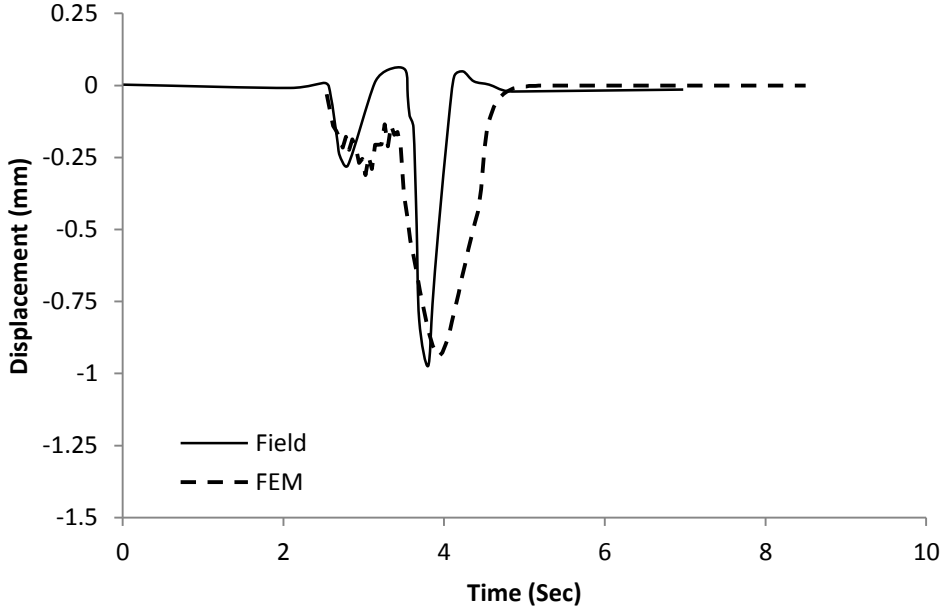

Figure 3.29: Crown vertical displacement time response under a moving truck with a speed of 16 km/h

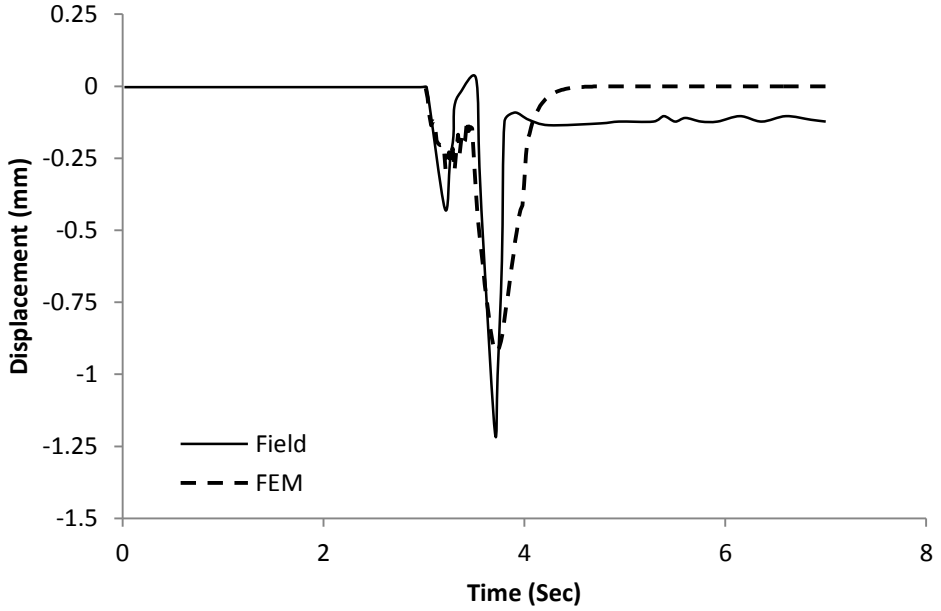

Figure 3.30: Crown vertical displacement time response under a moving truck with a speed of 32 km/h

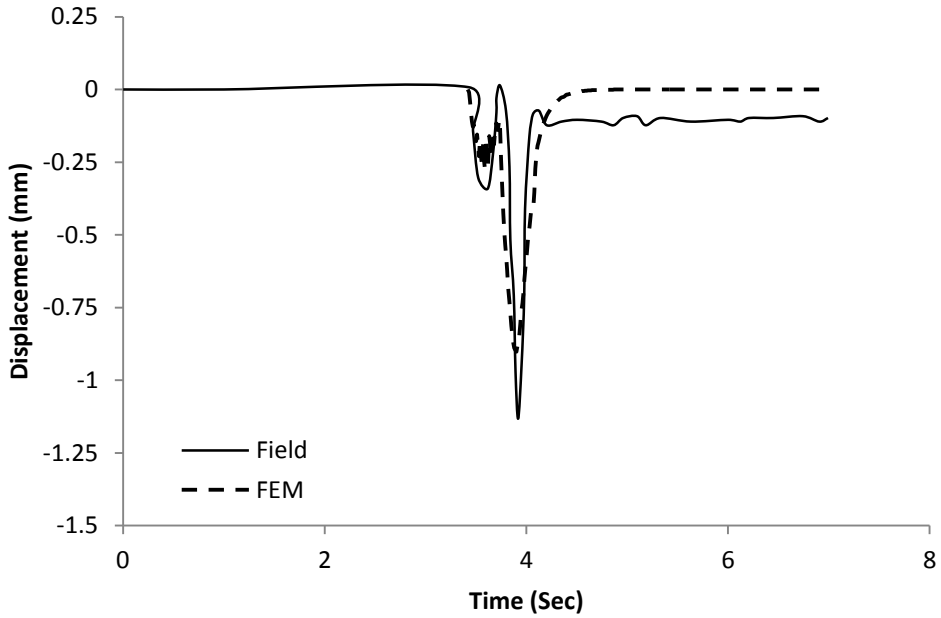

Figure 3.31: Crown vertical displacement time response under a moving truck with a speed of 48 km/h

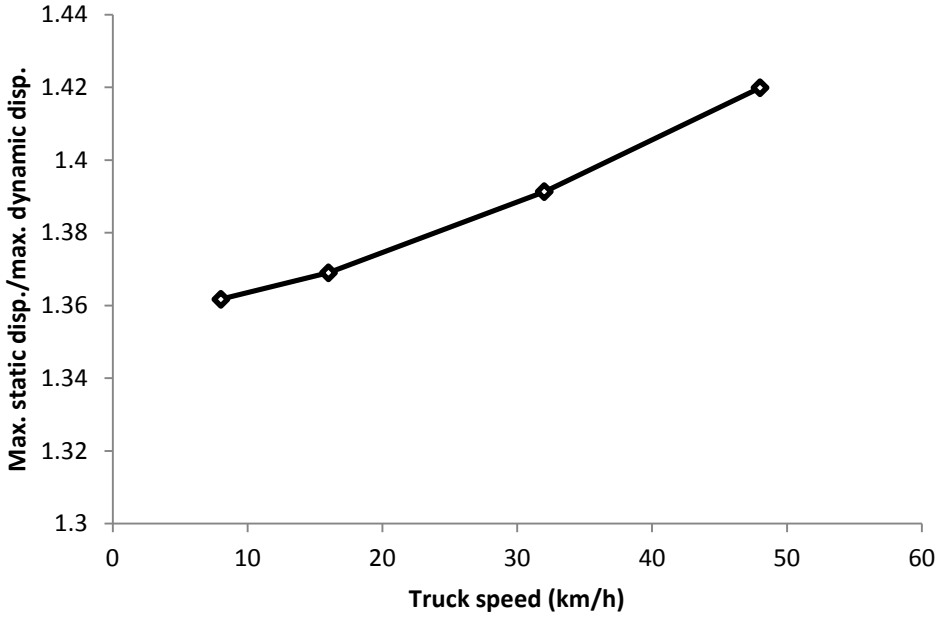

Figure 3.32: Ratio of the maximum static displacement to the maximum dynamic displacement for different truck speeds

3.2.3.8. Summary

In conclusion, the results from the validation problems (validation problems 1 to 5) have demonstrated the robustness of the methodology of the numerical modelling. The validation problems showed that the developed model is able to predict the bending moment in the pipe wall, pipe wall stress, pipe displacement and soil pressure around the pipe. In addition, the differences noted between the obtained and numerical results were expected, as the laboratory and field tests are not as perfect as the assumptions in the numerical modelling, where the density of the soil around the pipe might be affected by the installation quality. Moreover, as discussed in validation problem 2, there is a potential variability in the results of such complex tests. Importantly, the obtained percentage differences of this study (7%- 25%) lie

within the percentage differences obtained by previous studies as shown in Table 3.11, bearing in mind that the problems considered in this study were for both controlled laboratory tests and field tests. Also, the uncertainties associated with pipe installation, pipe testing, data recording and data processing should be taken into consideration when judging the accuracy of the numerical methodology.

Therefore, this methodology can be taken forward to investigate other scenarios of pipes with different diameters and thicknesses, under shallow and deep burial conditions through extensive parametric studies, and so achieve the aim of this research.

Table 3.11: Percentage differences of previous studies and the present study

No.	Reference	Type of experimental study	Absolute percentage error between numerical and experimental results (%)
1	Yoo et al. (1999)	Laboratory (1-g)	1-128
2	Dhar et al. (2004)	Laboratory (1-g)	0-2
3	Arockiasamy et al. (2006)	Field	2-404
4	Petersen et al. (2010)	Field	7-192
5	García (2012)	Laboratory (1-g)	25
6	Kang et al. (2013a)	Laboratory (1-g)	1
7	Turan et al. (2013)	Field	0-20
8	Kang et al. (2014)	Field	4-281
9	Meguid and Kamel (2014)	Field	40-62
10	Chaallal et al. (2015b)	Field	16-46
11	Robert et al. (2016)	Field	5-111
12	**Present study****	**Laboratory (1-g) and field**	**7-25**

** Range of percentage difference was calculated based on validation problems 2 to 5 only, as these problems were modelled using the hyperbolic soil model.

3.3. Evolutionary polynomial regression (EPR) analysis

Evolutionary polynomial regression (EPR) is a data mining method that combines the least square fitting technique with the genetic algorithm optimisation to find the best mathematical expression that describes the relationship between the input and output data (Giustolisi and Savic, 2006). This technique was used in this research because it has been successfully used by other researchers to model complex relationships (Savic et al., 2006; Faramarzi et al., 2012; Javadi et al., 2012a, b; Faramarzi et al., 2013; Ahangar-Asr et al., 2014; Alani et al., 2014; Faramarzi et al., 2014; Ahangar Asr and Javadi, 2016). The EPR methodology and the EPR modelling steps are described in the following subsections.

3.3.1. EPR methodology

The EPR methodology is based on forming a number of candidate relationships between the input and output data, by an evolutionary process using a genetic algorithm. The development of the candidate relationships depends on the number of data used in the analysis, the proposed type of the relationships between the input and output data, the proposed range of exponents for the developed relationships and the proposed number of terms for the developed relationships. The typical formulation of the EPR is shown in Equation 3.3 (Giustolisi and Savic, 2006).

$$Y = \sum_{j=1}^{m} F\left(\mathbf{X}, f(\mathbf{X}), a_j\right) + a_0 \qquad (3.3)$$

Where, Y is the predicted dependent input value from the EPR model; a_j is a constant value; F is a function evolved during the process depending on the input

and output data; $\mathbf{X}$ is the matrix of the input independent variables; $f(\mathbf{X})$ is the type of function defined by the user; and m is the number of terms in the proposed model excluding the bias term a_0.

A genetic algorithm is used in the construction and evolution of Equation 3.3. However, the type of function $\left(f(\mathbf{X})\right)$ and the number of the terms (m) are defined by the user depending on the understanding of the physical phenomenon of the input and output data (Alani and Faramarzi, 2014), or based on a trial and error process.

The first step to find the relationship between the input and output data is to re-write Equation 3.3 in a vector form as shown in Equation 3.4 (Giustolisi and Savic, 2006).

$$\mathbf{Y}_{N\times 1}\,(\boldsymbol{\Theta},\mathbf{Z}) = \left[\mathbf{I}_{N\times 1}\;\mathbf{Z}^{j}_{N\times m}\right] \times [a_0\; a_1 \ldots a_m]^T = \mathbf{Z}_{N\times d} \times \boldsymbol{\Theta}^{T}_{d\times 1} \tag{3.4}$$

Where, $\mathbf{Y}_{N\times 1}\,(\boldsymbol{\Theta},\mathbf{Z})$ is the vector of the least square estimate of N target values; $\boldsymbol{\Theta}_{d\times 1}$ is the vector of $d = m + 1$ parameters aj and a_0($\boldsymbol{\Theta}^T$ is the transposed vector); and $\mathbf{Z}_{N\times d}$ is a matrix formed by unity vector ($\mathbf{I}$) for bias a_0 and m vectors of variables $\mathbf{Z}^j$. For a fixed j, the variables $\mathbf{Z}^j$ are a product of the independent predictor vectors of inputs, $\mathbf{X} = \langle \mathbf{X_1}\; \mathbf{X_2} \ldots \mathbf{X_k} \rangle$ (Alani and Faramarzi, 2014).

The search for the best fit relationship starts from Equation 3.4. The matrix of the input data $\mathbf{X}$ is shown in Equation 3.5 (Giustolisi and Savic, 2006).

$$\mathbf{X} = \begin{bmatrix} \mathrm{X}_{11} & \cdots & \mathrm{X}_{1\mathrm{k}} \\ \cdots & \cdots & \cdots \\ \mathrm{X}_{\mathrm{N}1} & \cdots & \mathrm{X}_{\mathrm{Nk}} \end{bmatrix} = [\mathbf{X_1} \quad \ldots \quad \mathbf{X_k}] \tag{3.5}$$

Where, the kth column of $\mathbf{X}$ represents the candidate variable for the jth term of Equation 3.4. Hence, the $\mathbf{Z}_{N\times m}^{j}$ in Equation 3.4 can be written as shown in Equation 3.6 (Alani and Faramarzi, 2014).

$$\mathbf{Z}_{N\times 1}^{j} = \left[(\mathbf{X}_1)^{\mathrm{ES}(j,1)} \ (\mathbf{X}_2)^{\mathrm{ES}(j,2)} \ \ldots \ (\mathbf{X}_k)^{\mathrm{ES}(j,k)}\right] \tag{3.6}$$

Where, $\mathbf{Z}^{j}$ is the vector of the jth column in which the elements are a product of candidate independent inputs; $\mathbf{ES}$ is the exponents matrix used in the relationship evolution; and k is the number of independent variables.

To illustrate the final equation, assuming that the vector of the exponents specified by the user was $\mathbf{EX} = [0, 1, 2]$, the number of terms specified by the user (m) (excluding bias) was 4 and the number of independent variables used in the analysis (k) was 3, then the number of columns of the $\mathbf{ES}$ matrix will be 3 (equal to the number of the independent variables) and the number of rows will be 4 (equal to the number of the terms specified by the user). Then, the matrix of the Exponent $\mathbf{ES}$ will be (as an example):

$$\mathbf{ES} = \begin{bmatrix} 0 & 1 & 2 \\ 0 & 1 & 1 \\ 1 & 2 & 0 \\ 1 & 1 & 0 \end{bmatrix} \tag{3.7}$$

Applying the matrix shown in Equation 3.7 to Equation 3.6 produces four mathematical equations as shown in Equations 3.8 to 3.11.

$$\mathbf{Z_1} = (\mathbf{X}_1)^0.(\mathbf{X}_2)^1.(\mathbf{X}_3)^2 = \mathbf{X}_2.\mathbf{X}_3^2 \tag{3.8}$$

$$\mathbf{Z_2} = (\mathbf{X}_1)^0.(\mathbf{X}_2)^1.(\mathbf{X}_3)^1 = \mathbf{X}_2.\mathbf{X}_3 \quad (3.9)$$

$$\mathbf{Z_3} = (\mathbf{X}_1)^1.(\mathbf{X}_2)^2.(\mathbf{X}_3)^0 = \mathbf{X}_1.\mathbf{X}_2^2 \quad (3.10)$$

$$\mathbf{Z_4} = (\mathbf{X}_1)^1.(\mathbf{X}_2)^1.(\mathbf{X}_3)^0 = \mathbf{X}_1.\mathbf{X}_2 \quad (3.11)$$

Hence, the expression of Equation 3.4 will be:

$$Y = a_0 + a_1.\mathbf{Z_1} + a_2.\mathbf{Z_2} + a_3.\mathbf{Z_3} + a_4.\mathbf{Z_4}$$
$$= a_0 + a_1.\mathbf{X}_2.\mathbf{X}_3^2 + a_2.\mathbf{X}_2.\mathbf{X}_3 + a_3.\mathbf{X}_1.\mathbf{X}_2^2 + a_4.\mathbf{X}_1.\mathbf{X}_2 \quad (3.12)$$

The least square fitting technique is used to solve the overdetermined system in Equation 3.12 (Giustolisi and Savic, 2006). The coefficient of determination (CD) is calculated for each relationship as shown in Equation 3.13.

$$CD = 1 - \frac{\sum_N (Y_a - Y)^2}{\sum_{NP} (Y_a - \frac{1}{N}\sum_N Y_p)^2} \quad (3.13)$$

Where, Y_a is the dependent input value; Y is the predicted dependent input value from the EPR model; and NP is the number of data points.

After calculating the coefficient of determination, the analysis is then repeated by changing the order of the exponents based on the range specified initially (further details can be found in Giustolisi and Savic, 2006). The change in order of the exponents is based on the genetic algorithm. The use of the genetic algorithm improves the search for the best fit relationship (Giustolisi and Savic, 2006). Again, the equation is solved for the new arrangement using the least square technique and

the coefficient of determination (CD) is calculated. This process is repeated until the total number of iterations is met. The relationship which achieves the highest CD value is selected (Alani et al., 2014; Faramarzi et al., 2014).

Giustolisi and Savic (2006) developed the original EPR procedure with a single objective; where the fitness of the mathematical expression was selected based on the best fit model with a penalisation technique to avoid overfitting the problem (Giustolisi and Savic, 2006). However, Giustolisi and Savic (2009) improved this technique and developed a multi-objective EPR (EPR-MOGA) because the single objective EPR had a number of disadvantages. The improvement involved utilising one objective to control the fitness of the model; while the complexity of the model is controlled by using one or two functions. Therefore, this research utilises the multi-objective EPR, which is available in the EPR MOGA software. Further details about the EPR-MOGA technique can be found in Giustolisi and Savic (2009).

It should be noted that in addition to the relationship structure shown in Equation 3.12, there are four additional types of functions ($f(\mathbf{X})$) available in the EPR MOGA-XL software. These functions are logarithmic, exponential, tangent hyperbolic and secant hyperbolic. In addition, the EPR MOGA-XL software allows other structures of polynomial relationships as shown in Equations 3.14 to 3.16.

$$\mathbf{Y} = a_0 + \sum_{j=1}^{m} a_j . (\mathbf{X_1})^{ES(j,1)} \dots (\mathbf{X_k})^{ES(j,k)} . f\left((\mathbf{X_1})^{ES(j,k+1)}\right) \dots f\left((\mathbf{X_1})^{ES(j,2k)}\right) \quad (3.14)$$

$$\mathbf{Y} = a_0 + \sum_{j=1}^{m} a_j . f\left((\mathbf{X_1})^{ES(j,1)} \dots (\mathbf{X_k})^{ES(j,k)}\right) \quad (3.15)$$

$$\mathbf{Y} = g\left(a_0 + \sum_{j=1}^{m} a_j . (\mathbf{X_1})^{ES(j,1)} \dots (\mathbf{X_k})^{ES(j,k)}\right) \quad (3.16)$$

3.3.2. EPR modelling procedure

Based on a thorough literature review of the previous studies which have successfully used the EPR analysis (Savic et al., 2006; Faramarzi et al., 2012; Javadi et al., 2012a,b; Faramarzi et al., 2013; Alani et al., 2014; Faramarzi et al., 2014), two steps are required for robust EPR modelling:

Preparation step: the dataset is prepared in this step by dividing it into training (80%) and validation (20%). This process is used in the EPR modelling technique to ensure the generalisation capability and robustness of the developed model. EPR is not a simple curve fitting method. It searches for the best model using an evolutionary pattern recognition methodology, as discussed in Section 3.3.1. Therefore, the developed model should be tested using unseen data to ensure that the model is reliable and able to predict the overall trend behaviour. Thus, the general statistical characteristics (the standard deviation ($STDV$), maximum (Max), minimum (Min) and mean ($mean$) values) of the training and validation data should be similar to avoid model extrapolation (Alani et al., 2014).

Testing step: the developed model is tested in this step by using a sensitivity analysis to make sure that the model is capable of capturing the trend behaviour of the data used in the modelling. This step is necessary to increase the confidence in the prediction abilities of the developed model.

3.4. General summary

This chapter has thoroughly discussed the methodology of the finite element analysis and the evolutionary polynomial regression analysis (EPR) in two separate sections.

Section 3.2 focused on the finite element analysis, where the key elements required to model the complex soil-pipe interaction in the finite element simulation have been identified, based on a thorough literature review together with a sensitivity analysis using MIDAS GTS/NX. A thorough literature review discussed the two-dimensional and the three-dimensional finite element analysis, the size of the finite element model in terms of boundary effects, the soil and pipe constitutive models, the interaction zone between the soil and the pipe and the simulation of the external load applied on the pipe. In addition, a sensitivity analysis was conducted to study the effect of the model extent, soil non-linearity and soil plasticity. Furthermore, the methodology of the finite element modelling was tested using laboratory and field results collected from the literature, for buried pipes tested under static and moving surface loads. This methodology will be used in the following chapters to achieve the aim of this research.

The methodology of the EPR analysis has been discussed in Section 3.3. In addition, the steps required to model the data using the EPR analysis have also been identified in this section. These steps will be followed in the following chapters for robust and representative EPR modelling.

Chapter 4
BEHAVIOUR OF BURIED CONCRETE PIPES UNDER SOIL LOAD ONLY

4.1. Introduction

This chapter discusses the behaviour of buried concrete pipes under the effect of the backfill soil load only. The chapter aimed to address the gaps in the knowledge related to the behaviour and design of buried concrete pipes under backfill soil load only (detailed in Section 2.2.4) by discussing the following questions:

1- What are the parameters affecting the behaviour of buried concrete pipes under backfill soil load only?
2- Is the current design methodology of both the BS and AASHTO robust and economical?
3- Is it possible to enhance the design methodology of buried concrete pipes to enable a more economical and robust design?

The chapter starts with a brief description of the numerical model used in the analysis (Section 4.2). The model is then used in a comprehensive parametric study to investigate the behaviour of buried concrete pipes under backfill soil load only and the robustness of the BS and AASHTO soil load bedding factors (Section 4.3). The chapter finishes with the development of new soil load bedding factor models (Section 4.4) and a general summary (Section 4.5). It is important to mention that the analysis time for the models considered in this chapter ranged from 10 to 30 minutes, depending on the pipe diameter.

4.2. Numerical modelling details

The finite element model was developed using MIDAS GTS/NX. The width and length of the model was equal to 4.0 $Dout$ m and 5.0 m, respectively. The backfill height above the pipe was fixed at 1.0 m for all of the models used in this chapter; while the soil height below the pipe was equal to 1.7 $Dout$ m. These dimensions satisfy the requirements to avoid the influence of the finite element model extent (detailed in Section 3.2.2.1). A trench with a width of 2.7 $Dout$ m and a height equal to the backfill height plus the outside diameter of the pipe was considered in the modelling, to use finer elements around the pipe to enhance the accuracy of the numerical modelling (i.e. similar to validation problem 2 (Section 3.2.3.2)). The boundary conditions, the elements' types, the constitutive models for the soil and the pipe, and the elements' sizes were the same as for the validation problems. The numerical model is shown in Figure 4.1. Three steps were performed to model the installation of the pipe and the deep soil fill:

Step 1: the initial earth pressure of the soil beneath the pipe was calculated using a coefficient of lateral earth pressure of 1.0 (Brown and Selig, 1991).

Step 2: the bedding soil, pipe and surrounding and backfill soil were added in steps. The horizontal earth pressure for these soil layers was calculated using a coefficient of lateral earth pressure of 1.0 (Brown and Selig, 1991).

Step 3: a uniformly distributed load was applied on the top of the model to simulate the deep soil fill. This technique was used to reduce the computational time as discussed in Section 3.2.1.7.

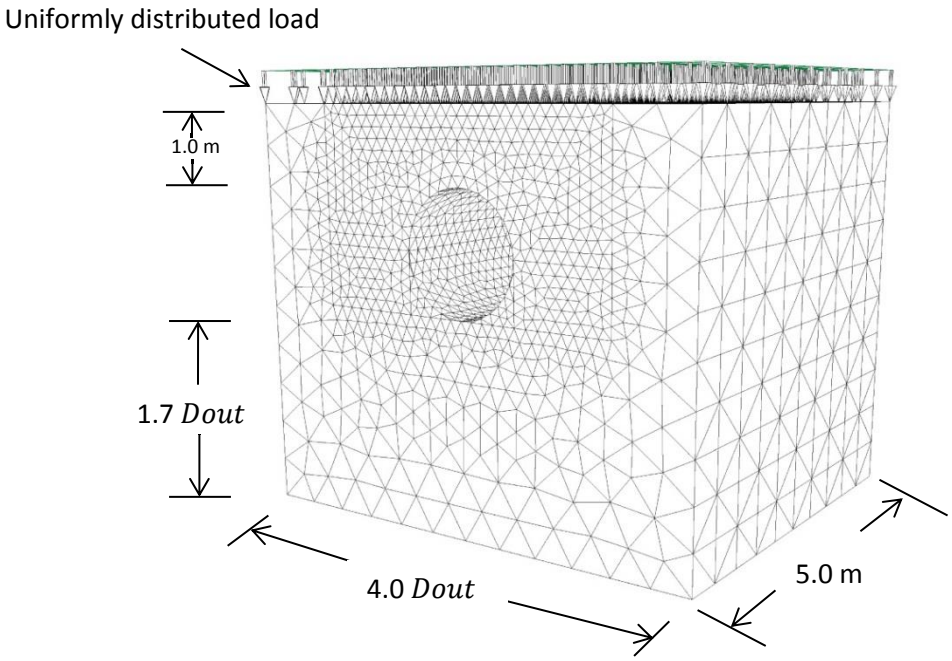

Figure 4.1: Finite element mesh of the problem

4.3. Parametric study

A parametric study has been carried out to investigate the effect of backfill height, pipe diameter and pipe wall thickness on the bending moments developed in the pipe wall under soil loads, and hence the associated soil load bedding factor. The pipe diameters considered are shown in Table 4.1. These diameters were considered to investigate the impact of the pipe diameter on the bedding factor and hence, implicitly the soil arching.

A maximum backfill height of 40.0 m has been considered in the finite element analyses. This backfill height was considered necessary to provide a greater understanding of the effect of backfill height on the bending moment and the associated soil load bedding factor. This also implicitly provides greater understanding of the soil arching effect, as previous studies have shown that vertical

arching is significantly affected by the backfill height (Kang et al., 2007; Allard and El Naggar, 2016) as discussed previously in Section 2.2.2. It should be noted that the backfill height has been taken down to a minimum of 1.0 m, although it is recognised at these lower backfill heights traffic loading will be dominant in this region when the pipes are buried under trafficked areas. However, there are instances where pipes are laid under soil load only and the surface is not trafficked. Hence, it was felt that it is important to provide analyses, and hence the ability to determine soil load bedding factors, for the full range of backfill heights (i.e. 1.0 m to 40.0 m). In addition, the effect of the traffic load on the behaviour of buried concrete pipes is discussed in the next chapter (**Chapter 5**).

The four AASHTO installation types (Type 1, Type 2, Type 3 and Type 4) have been considered in the analysis by changing the degree of compaction and the type of soil in the haunch zone based on the AASHTO recommendation (detailed in Section 1.6.1). It is worth mentioning here that in the AASHTO Type 1 installation, the pipe is fully supported and hence it is equivalent to class S in the BS. In addition, in class F the pipe is partially supported in the haunch zone, which is similar to Type 3. Furthermore, in class N and DD the pipe is directly installed on stiff soil, hence it is similar to AASHTO Type 4 installation. Finally, the minimum support condition of class B (i.e. BF = 1.9) can be considered similar to Type 2, where the pipe is well supported but not quite as well supported as for class S. Therefore, the cases considered in this chapter are also similar to the BS classes and hence the results are equally applicable to the BS classes.

It should be noted that the bedding soil beneath the pipe in these analyses has been modelled using a compacted well-graded sandy soil (SW) with a degree of compaction of 90% of the standard Proctor maximum dry density for all of the installation types (SW90). The assumption of stiff bedding was made to simulate the worst-case scenario since excavating the native soil under the pipe is a time consuming process and increases the installation cost by approximately 15% (Wong et al., 2006). Hence, it is expected that the pipe is laid directly on the stiff soil in practice (over-consolidated natural soil) and the AASHTO standard of loose soil beneath the pipe for Type 1, Type 2 and Type 3 installation conditions is not followed. However, the full haunch zone has been modelled following the AASHTO recommendation with a SW95 soil for Type 1, SW90 soil for Type 2, ML90 soil for Type 3 and ML49 soil (uncompacted soil) for Type 4 (Figure 1.3). The backfill soil was modelled using a SW90 soil for all of the cases. The soil parameters used in the analyses are shown in Table 4.2.

As discussed previously in Section 3.2.1.4.2, it is important to mention that the assumption of thin shell theory has been employed (i.e. using shell elements to model the pipe) to add additional conservatism to the analysis, as the thin shell theory provides a higher bending moment than the thick ring theory, with a percentage range from 2% to 10% (Moore et al., 2014). Hence, the bedding factor derived using this theory will be less than that derived following the thick shell theory.

The soil load bedding factor (BF) has been calculated by dividing the maximum positive bending moment developed in the pipe wall during the three-edge bearing test, based on the force calculated using the AASHTO arching factors (Equation 1.6),

by the maximum positive bending moment developed in the buried pipe (obtained from the numerical modelling), as shown in Equation 4.1 (Young and O'Reilly, 1987; Petersen et al., 2010). This approach has been adopted because the development of the crack in the concrete pipe wall is related to the development of the bending moment in the pipe wall, as the bending moment controls the design of the buried pipes (i.e. it controls the tensile stresses in the pipe wall) (Tan and Moore, 2007).

$$BF = \frac{0.318 \times W_t \times r}{M} \tag{4.1}$$

Where, W_t is the calculated total force applied on the pipe; r is the radius of the pipe measured to the centre of the pipe wall; and M is the bending moment of the buried pipe calculated from the finite element modelling.

Table 4.1: Pipe diameters and wall thicknesses

Inside diameter (D) (m)	Wall thickness (t) (m)
0.3	0.055
0.6	0.094
1.2	0.144
2.4	0.229

Table 4.2: Material properties used in the parametric finite element analysis (Boscardin et al., 1990)

Property	SW95	SW90	ML90	ML49
γ (kN/m^3)	22.07	20.99	18.84	10.40
υ	0.30	0.30	0.30	0.30
c'(kPa)	1	1	24	1
ϕ'(°)	48	42	32	23
K	950	640	200	16
R_f	0.70	0.75	0.89	0.55
n	0.60	0.43	0.26	0.95

4.3.1. Effect of installation condition and backfill height

Figures 4.2(a) and (b) show the effect of the installation type on the bending moment developed around a concrete pipe with an inside diameter of 1.2 m buried for backfill heights of 10.0 m (Figure 4.2(a)) and 39.0 m (Figure 4.2(b)), respectively. It can be seen that the bending moment at the invert of the pipe increases as the installation quality decreases, for example changing the installation type from 1 to 4 increases the bending moment at the invert zone by 82% for backfill heights of 10.0 m (Figure 4.2(a)) and 39.0 m (Figure 4.2(b)). This is due to the concentration of the reaction forces at the invert of the pipe as the quality of the soil in the haunch zone decreases (Pettibone and Howard, 1967; Wong et al., 2006). However, it can be seen that there is no significant increase in the bending moment at the invert of the pipe as the installation type changes from Type 1 to Type 2, where the percentage increase is

equal to 6% and 9% for the 10.0 m and 39.0 m soil fill, respectively. The figures also show that the installation type does not significantly affect the bending moment developed at the crown of the pipe (the maximum percentage difference is 18%).

Figure 4.3 shows the effect of backfill height on the maximum bending moment developed in a pipe with an inside diameter of 0.3 m. As expected, increasing the backfill height increases the maximum bending moment due to the increase of the soil pressure. In addition, it can also be seen that changing the bedding type (i.e. the soil in the haunch zone) has a significant effect on the developed bending moment. For example, changing the bedding type from Type 1 to Type 2 increases the maximum bending moment by 19%; while changing the bedding type from Type 1 to Type 4 increases the bending moment by 62%. This increase is due to the concentration of the forces in the invert zone, which increases the maximum bending moment as discussed in the previous paragraph.

Figure 4.4 shows the calculated soil load bedding factor using Equation 4.1 for a pipe diameter of 0.3 m with different backfill heights and installation types. It can be seen that increasing the backfill height non-linearly increases the bedding factor. The non-linear behaviour is due to the decrease of the negative arching as the backfill height increases and the use of a constant arching factor in the AASHTO equation to calculate the laboratory force (i.e. Equation 1.6). This is in agreement with the conclusions of Kang et al. (2007) and Allard and El Naggar (2016), where they also found that the negative vertical arching decreases as the backfill height increases. Furthermore, it can be seen that as the installation quality decreases, the bedding factor also decreases due to the significant increase in the bending moment.

However, the bedding factors for installation Type 1 are almost the same as for Type 2, with an average percentage difference of 1%. This is due to the use of a higher vertical arching factor in the laboratory force calculation for Type 2 installations (i.e. VAF = 1.4). This has eliminated the difference in the bending moment between Types 1 and 2 (i.e. 19%) and produced very similar values for the bedding factor.

It is also noted that after a backfill height of approximately 10.0 m, the bedding factors do not change significantly. This means that the negative soil arching does not significantly decrease after a backfill height of 10.0 m. In addition, Figure 4.4 shows that the support of the pipe has an effect on the soil arching, since the rate of increase in the bedding factor for Types 1 and 2 was higher than that for Types 3 and 4, after a backfill height of 10.0 m.

Figures 4.5 and 4.6 show the ratio of the soil load bedding factor obtained from the present study to the design bedding factors adopted in the AASHTO standard and BS, respectively. The AASHTO soil load bedding factors were calculated from Table 1.1 depending on the diameter of the pipe and the installation condition. Similarly, for the BS, the bedding factors were calculated from Table 1.2 depending on the installation condition. However, the minimum values (2.2 for class S, 1.9 for class B, 1.5 for class F and 1.1 for class N) were used as the numerical modelling simulated the worst-case scenario. It can be seen that for both standards the bedding factors adopted are conservative except for the AASHTO standard for Type 1 installation, where the ratio is less than 1.00. Furthermore, it can be seen that the degree of conservatism of both design standards increases as the backfill height increases, or

as the installation quality decreases. However, for Type 3 and 4 installations, the ratio stabilises after approximately 15.0 m of backfill height.

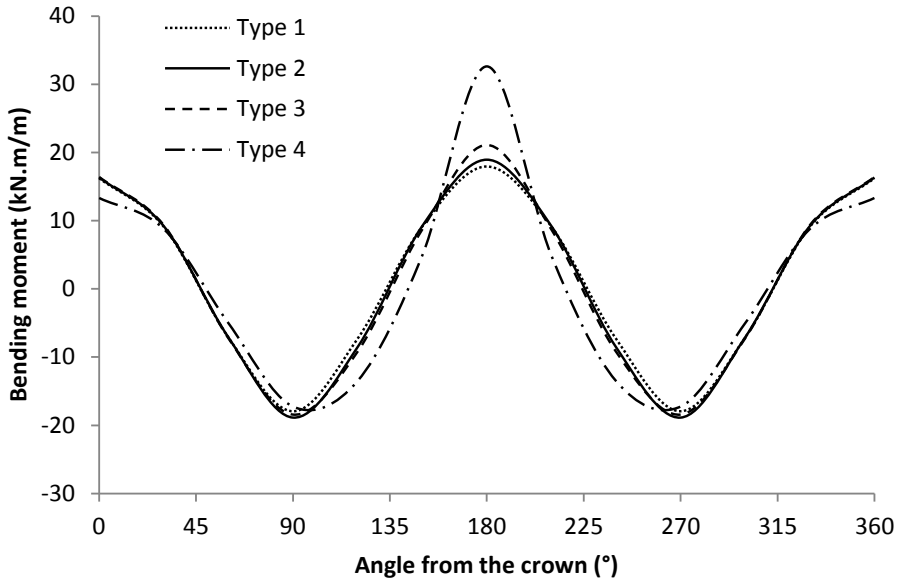

(a)

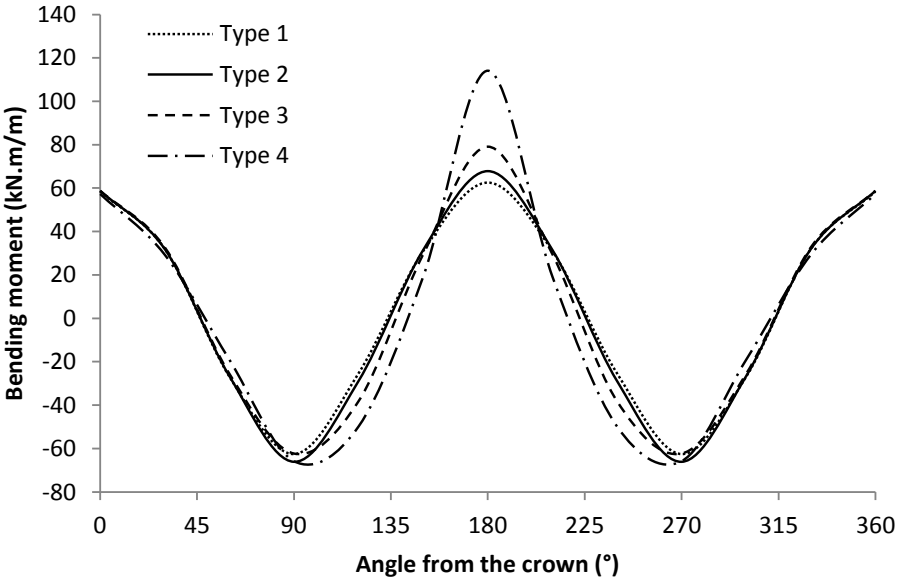

(b)

Figure 4.2: Effect of backfill height on the bending moment around the pipe: (a) H = 10.0 m; (b) H = 39.0 m

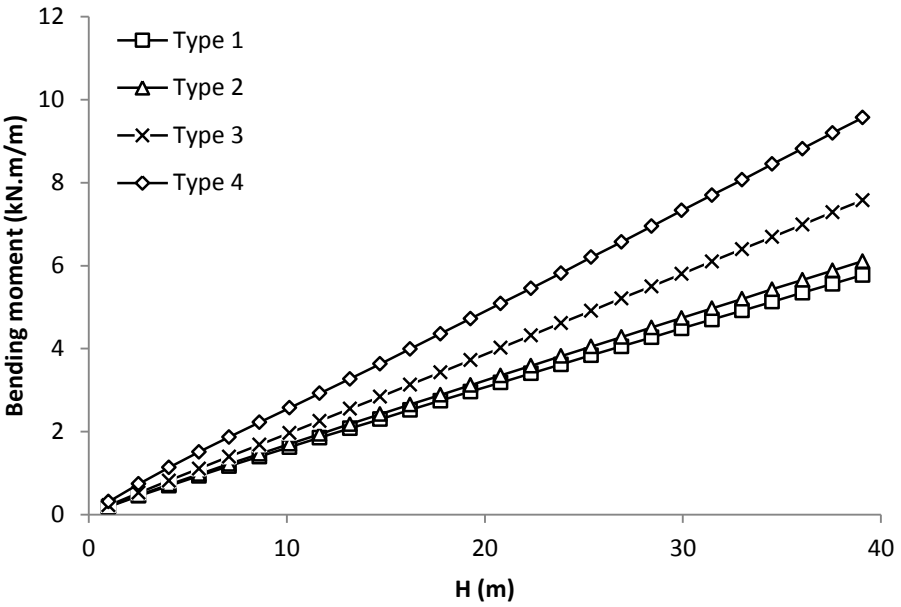

Figure 4.3: Effect of backfill height on the developed maximum bending moment for a pipe with a diameter of 0.3 m buried in different installation conditions

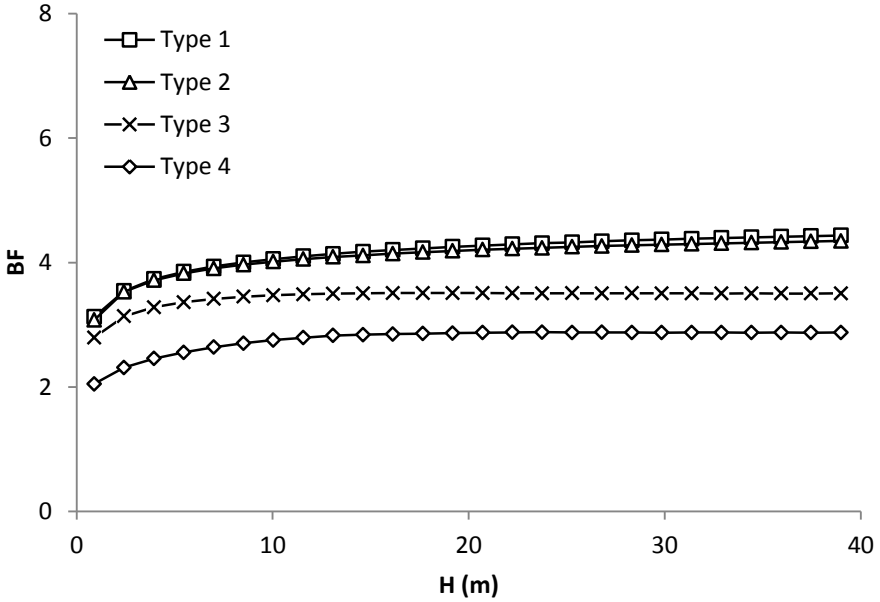

Figure 4.4: Effect of backfill height on the soil load bedding factor for a pipe diameter of 0.3 m buried in different installation conditions

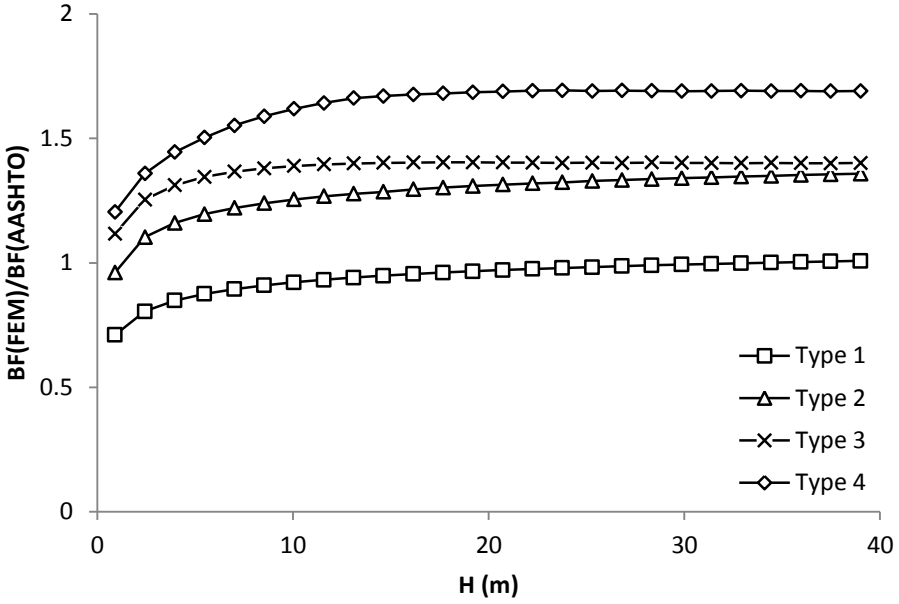

Figure 4.5: Ratio of bedding factors obtained from the numerical modelling and the AASHTO standard values (pipe diameter 0.3 m)

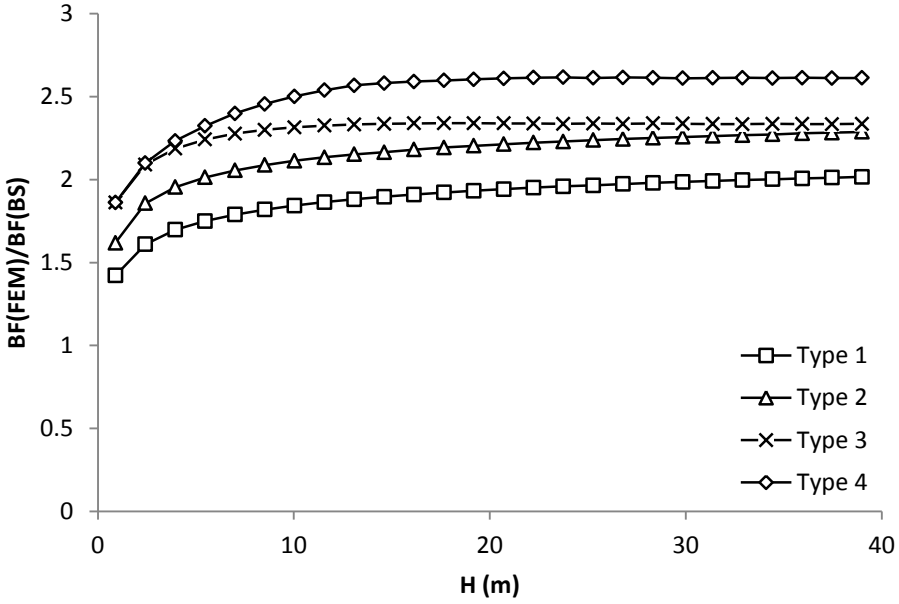

Figure 4.6: Ratio of bedding factors obtained from the numerical modelling and the BS values (pipe diameter 0.3 m)

4.3.2. Effect of pipe diameter

Figure 4.7 shows the effect of the pipe diameter on the maximum bending moment developed for the buried pipes installed using a Type 1 installation condition. As expected, increasing the diameter of the pipe significantly increases the bending moment. The average percentage increase in the maximum bending moment is equal to 240%, 1013% and 4237% as the diameter changes from 0.3 m to 0.6 m, 1.2 m and 2.4 m, respectively. This is because of the increase in the soil pressure at the invert of the pipe as the diameter of the pipe increases, due to the increase of the backfill height above the invert; and hence due to the larger span (pipe diameter), the bending moment increases (Wong et al., 2006).

Figure 4.8 shows the effect of the pipe diameter on the calculated soil load bedding factor. It can be seen that there is a complex interaction between bedding factor and diameter and backfill height over the first 16.0 m, after which the relationships stabilize. This behaviour is due to the over simplification in the analytical method adopted in the design standards for calculating the soil force applied on the pipe. The method takes the horizontal projection of the pipe and assumes that the pipe is a rectangular culvert and uses a constant vertical arching factor derived from the pipe thrust at the springline. As a result, the force applied on the pipe calculated in the laboratory and used to calculate the laboratory bending moment term in Equation 4.1 (i.e. $0.318 \times W_t \times r$) increases significantly as the diameter of the pipe increases. Taking this into account, together with the change in arching and the increase in the soil pressure as the backfill height and the diameter increase, produces these complex relationships.

Figures 4.9 and 4.10 show the ratio of the soil load bedding factor obtained from the present study to the design bedding factor adopted in the AASHTO standard and BS for pipes buried using a Type 2 installation, respectively. It can be seen from Figure 4.9 that the AASHTO bedding factors are conservative, except for a pipe with an inside diameter of 2.4 m buried with a backfill height less than 2.0 m. Figure 4.10 shows that the BS bedding factors are conservative for all cases. Furthermore, it can also be seen from both figures that increasing the backfill height increases the degree of conservatism (although for the smaller diameter pipes the value does not increase significantly after approximately 15.0 m of backfill height). This is due to the independency of the bedding factors adopted in both standards on the backfill height. In addition, Figure 4.9 shows that the ratio between the bedding factor obtained from the numerical modelling to the AASHTO bedding factor is equal to 1.71 for a pipe with an inside diameter of 0.6 m and a backfill height of 20.3 m. This is in good agreement with the ratio (experimental bedding factor to the AASHTO bedding factor) reported by MacDougall et al. (2016) from their experimental study (reported previously in Section 2.2.2) on a pipe with the same dimensions (diameter and wall thickness) and backfill height, where the calculated ratio was 1.77 (i.e. percentage difference 3%). This gives additional validation to the robustness of the methodology of the numerical analysis used in this research.

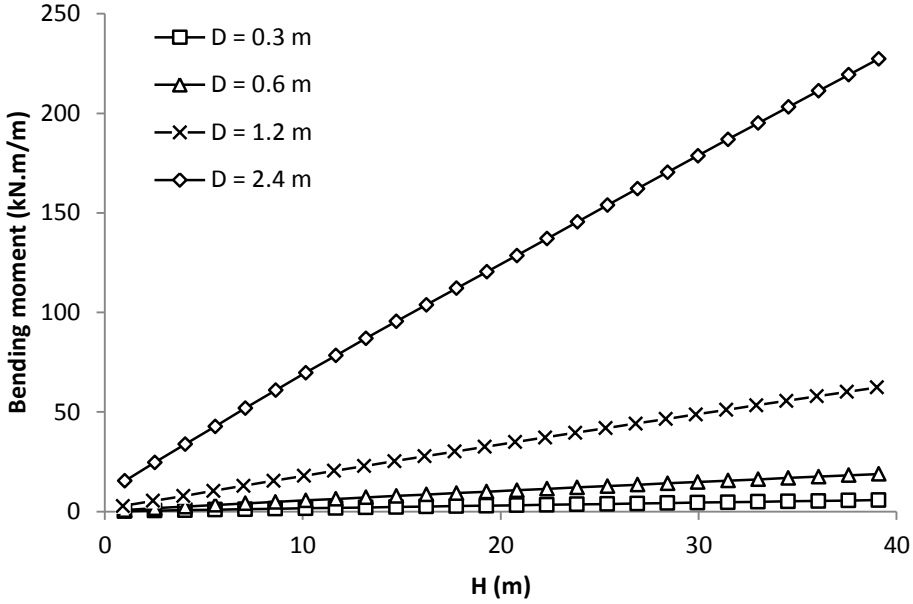

Figure 4.7: Effect of pipe diameter on the maximum bending moment developed in the buried pipes installed using the AASHTO Type 1 installation

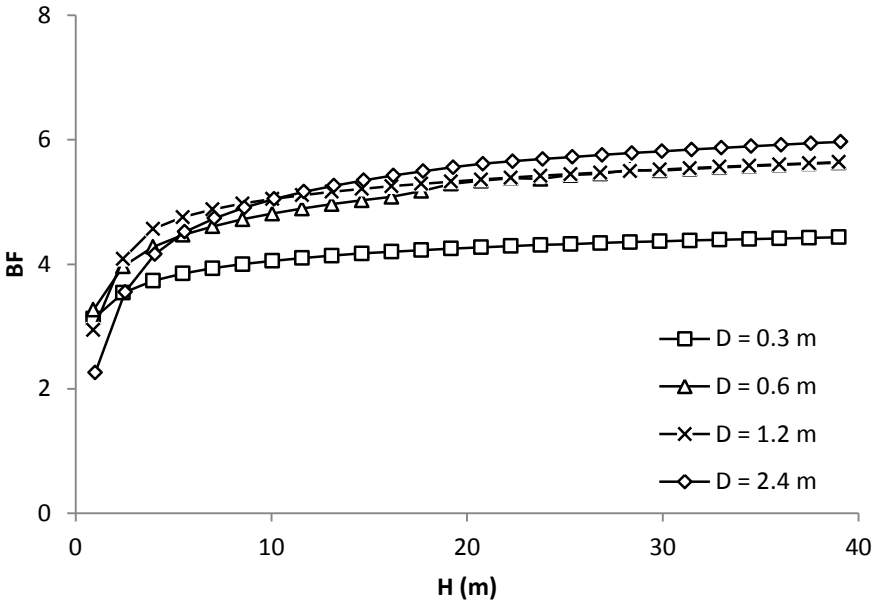

Figure 4.8: Effect of pipe diameter on the calculated soil load bedding factor for buried pipes installed using the AASHTO Type 1 installation

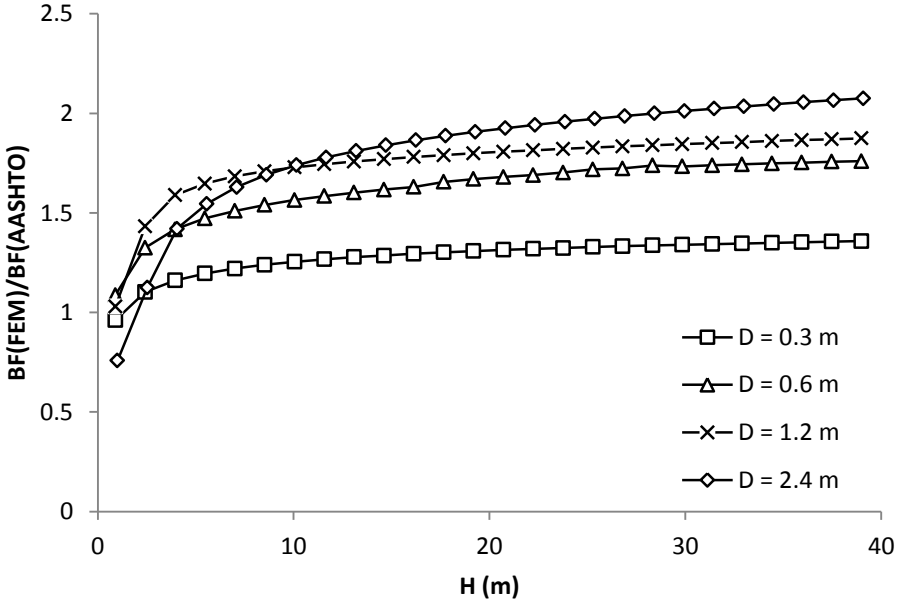

Figure 4.9: Ratio of bedding factor obtained from the numerical modelling and the bedding factor from the AASHTO for pipes buried using a Type 2 installation

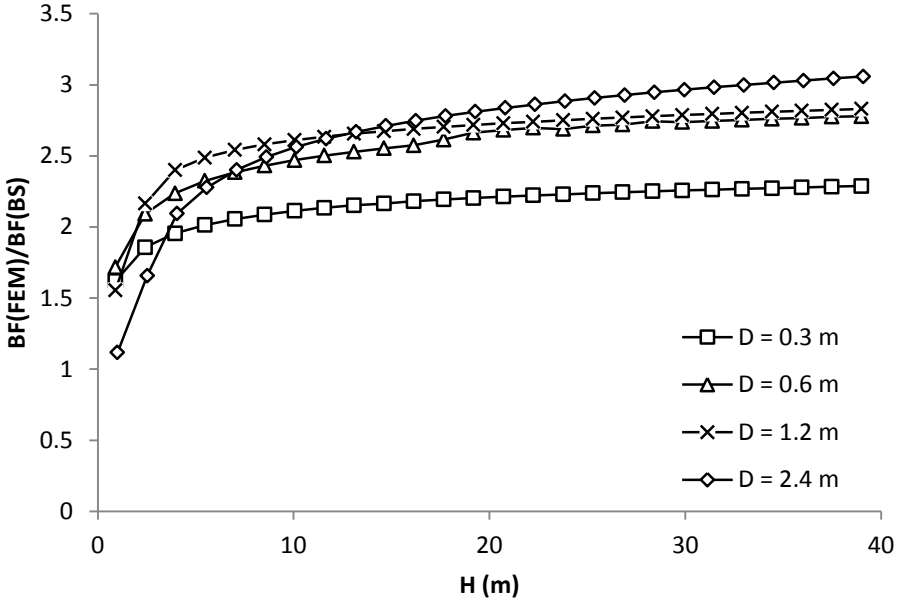

Figure 4.10: Ratio of bedding factor obtained from the numerical modelling and the bedding factor from the BS for pipes buried using a Type 2 installation

4.3.3. Effect of pipe thickness

To investigate the effect of the pipe wall thickness, additional finite element models were built with two additional wall thicknesses, one was equal to half of the original thickness (shown in Table 4.1) and the other was assumed to be double the original thickness. This was done to provide a general understanding of the bending moments and also to demonstrate the dependency of the calculated bedding factor on changes in wall thickness. Figure 4.11 shows the maximum bending moment for a 2.4 m diameter pipe with different wall thicknesses buried using a Type 1 installation condition. It can be seen that doubling the wall thickness of the pipe increases the maximum bending moment by 73%; while decreasing the pipe wall thickness by half decreases the maximum bending moment by 61%. The increase in the bending moment can be explained by the concept of soil arching, where increasing the wall thickness of the pipe increases the pipe stiffness; this consequently increases the negative arching meaning that the soil pressure attracted by the pipe will be increased (Moore, 2001; Kang et al., 2007), and hence this induces a larger bending moment.

Figure 4.12 shows the soil load bedding factor calculated from the maximum bending moment values. The figure shows that the bedding factor values are affected by the wall thickness of the pipe, whereby increasing the wall thickness decreases the bedding factor, due to an increase in the field bending moment (i.e. the bending moment from the finite element modelling). This figure also indicates that the design standards should consider the pipe thickness when calculating the bedding factor to ensure a robust design.

In summary, the parametric study has shown that the BS bedding factors are very conservative and the ratio of the bedding factors obtained from the finite element modelling to the design standard bedding factors ranged from 1.03 to 3.08. For the AASHTO standard, the bedding factors are not safe for shallow depths, but become increasingly more conservative as the backfill height increases; the ratio of the bedding factors obtained from the numerical modelling to the design standard bedding factors ranged from 0.61 to 2.08. Furthermore, the results have shown that the bedding factor is significantly affected by the diameter of the pipe, the backfill height and the wall thickness of the pipe. Therefore, to achieve a robust design, all of these parameters should be considered.

To make the results from this study more useful for pipe designers, an advanced data mining technique (evolutionary polynomial regression) has been employed to derive explicit and concise models for the bedding factors for each installation type. The decision to use this technique was made because of the highly complex behaviour of the bedding factor and its interaction with the parameters discussed earlier. Furthermore, an attempt was made to use classical non-linear regression analysis to obtain correlations, however this resulted in poor accuracy. Details of the evolutionary polynomial regression modelling are described in detail in the following section.

It should be noted that only limited results for selected cases were presented in this section to show the effect of the backfill height, pipe diameter and pipe wall thickness. The full results of the parametric study for all of the pipes and the installation conditions can be found in **Appendix A**.

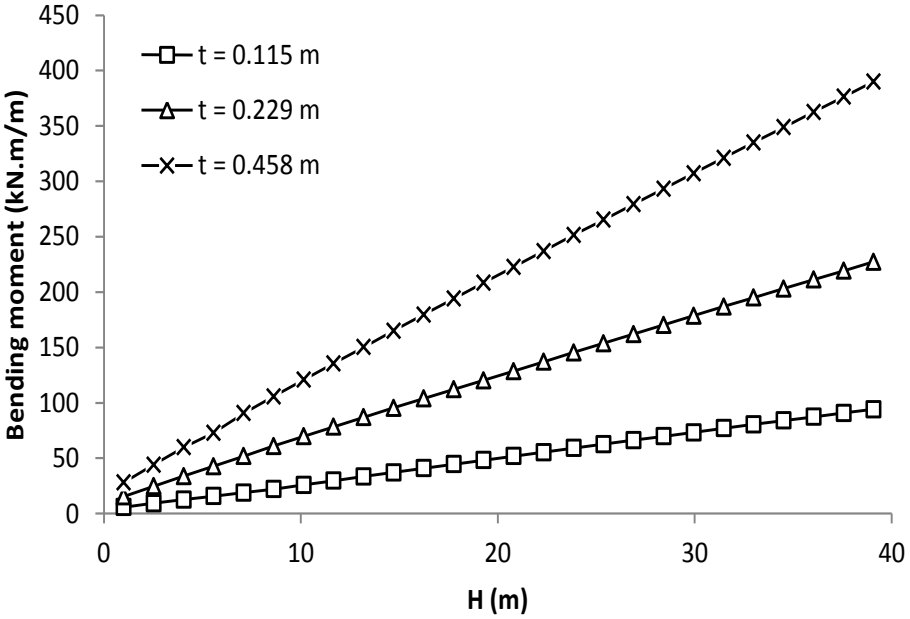

Figure 4.11: Effect of pipe wall thickness on the maximum bending moment developed for buried pipes installed using the AASHTO Type 1 installation

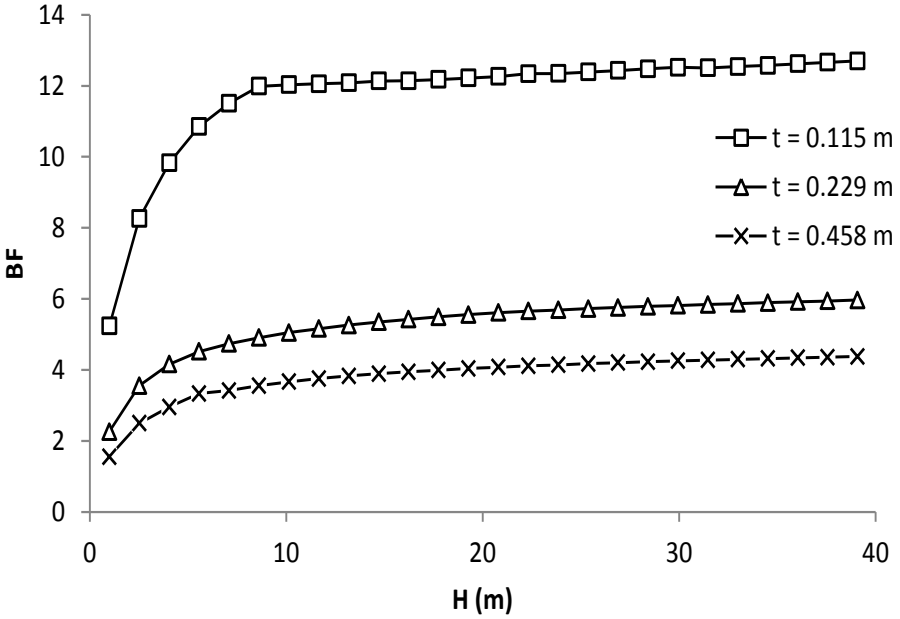

Figure 4.12: Effect of pipe wall thickness on the calculated soil load bedding factor for buried pipes installed using the AASHTO Type 1 installation

4.4. Development of the soil load bedding factor model

4.4.1. Modelling the soil load bedding factor

As demonstrated in Section 4.3, the calculated soil load bedding factor is significantly affected by the wall thickness of the pipe (t), the inside diameter of the pipe (D) and the backfill height (H) for all the installation types considered. This means that incorporating all of these parameters into the resulting model is necessary to achieve a robust and economical concrete pipe design.

For each installation type, a total number of 312 points was obtained from the finite element modelling for different diameters, backfill heights and wall thicknesses. All of these data were used in the training and testing of the models. It is common in artificial intelligent techniques to divide the data into two sets. One set is used for training the model and the other set is used for validating the capabilities of the developed model (Alani et al., 2014) as discussed in Section 3.3.2. Hence, the general statistical characteristics of the training and validation data should be similar to avoid model extrapolation (Alani et al., 2014). Therefore, the data were randomly shuffled and divided into a training set with 80% of the data and a validation set with 20% of the data. A statistical analysis was conducted after completing the random shuffle to make sure that the training and validation data were comparable, which in turn provided a robust and representative model. Table 4.3 shows the minimum (Min), maximum (Max), mean ($mean$) and the standard deviation ($STDV$) values for the training, the validation and all the data sets used in the EPR modelling for each installation type.

The EPR analysis was started after completing the preparation of the training and validation data. In order to find the best mathematical expression, different exponent ranges, function types and numbers of terms were tested. As mentioned previously in Section 3.3.1, the EPR searches for the best mathematical expression by changing the exponent of the parameters used and then solves the overdetermined system using the least squares method. The accuracy of the mathematical expression at each step was measured by calculating the CD (Equation 3.13). As the number of evolutions increased, the EPR learnt the best arrangement of the exponents and selected the best solution based on the calculated CD value. At the end of the analysis, the EPR provided different models with different numbers of terms.

Figures 4.13 to 4.18 show the effect of the number of terms on the accuracy of the developed EPR model for the case of a 0.6 m inside diameter concrete pipe buried in a Type 3 standard installation. Table 4.4 shows the EPR models of Figures 4.13 to 4.18 and the CD values (for training and validation data) for each model. It can be seen from the figures and the table that increasing the number of terms increases the accuracy of the developed model. However, the accuracy is not affected significantly when the number of terms increases more than five. In addition, increasing the number of terms increases the model complexity and the risk of overfitting. Also, providing a simple model is better from a practical point of view. Therefore, an effort was made to select the simplest model which captures the trend behaviour with the minimum percentage error for all of the considered diameters without significantly affecting the accuracy. This has been done by comparing the results of the EPR model with 2 terms, 3 terms, 5 terms, 6 terms and 7 terms and the finite element results, and applying the aforementioned criteria (i.e. model simplicity, trend

behaviour and percentage error). Equations 4.2 to 4.5 show the chosen models from the EPR analysis for installation Type 1, Type 2, Type 3 and Type 4, respectively.

$$BF = -11.72 \times \frac{t^2}{D^2} - 0.0037 \times \frac{D}{t^2} - 1.05 \times \frac{D}{\sqrt{t} \times \sqrt{H}} + 0.0206 \times \frac{D^2}{t^2} + 5.14 \quad (4.2)$$

$$BF = -11.72 \times \frac{t^2}{D^2} - 0.0037 \times \frac{D}{t^2} - 1.05 \times \frac{D}{\sqrt{t} \times \sqrt{H}} + 0.0202 \times \frac{D^2}{t^2} + 5.14 \quad (4.3)$$

$$BF = -2.82 \times \frac{t}{D \times \sqrt{H}} - 0.003 \times \frac{D}{t^2} + 0.0195 \times \frac{D^2}{t^2} - 0.13 \frac{D^2}{t \times \sqrt{H}} + 3.4 \quad (4.4)$$

$$BF = -1.09 \times \frac{1}{\sqrt{H}} + 0.0077 \times \frac{D^2}{t^2} - 0.059 \times \frac{D^2}{t \times \sqrt{H}} + 2.74 \quad (4.5)$$

Figures 4.19, 4.20, 4.21 and 4.22 show the EPR prediction (i.e. Equations 4.2, 4.3, 4.4 and 4.5) for the training and validation data in comparison with the finite element results. In addition, the coefficient of determination (CD) values obtained for the training and validation data are shown in Table 4.5. It can be seen from Figures 4.19, 4.20, 4.21 and 4.22 and Table 4.5 that the EPR predicts the bedding factor with very good accuracy for all of the installation types. It should be noted here that the models were trained and tested with the data range provided from the finite element analysis (i.e. an inside diameter ranging from 0.3 m to 2.4 m and a backfill height ranging from 1.0 m to 40.0 m). Therefore, these models are only applicable to pipes with similar diameters and backfill heights used in the current study and without the effect of the traffic load. Any attempts to use the model outside this range may result in a significant error.

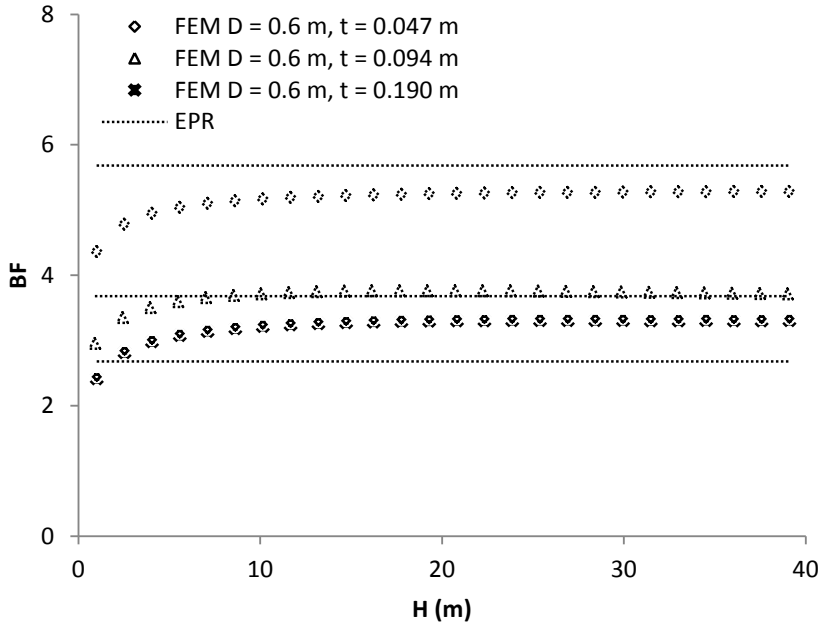

Figure 4.13: EPR calculated soil load bedding factors compared to the finite element results (EPR model consists of two terms as shown in Table 4.4)

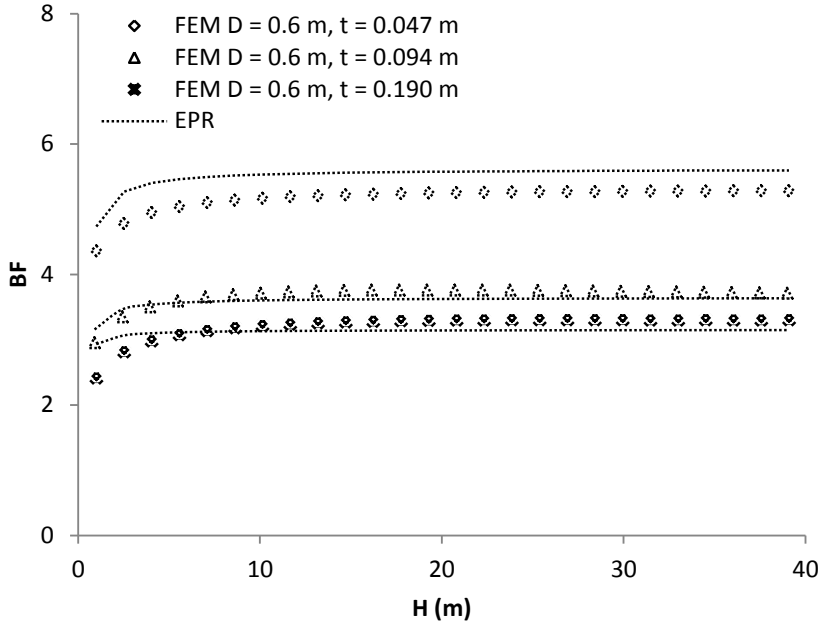

Figure 4.14: EPR calculated soil load bedding factors compared to the finite element results (EPR model consists of three terms as shown in Table 4.4)

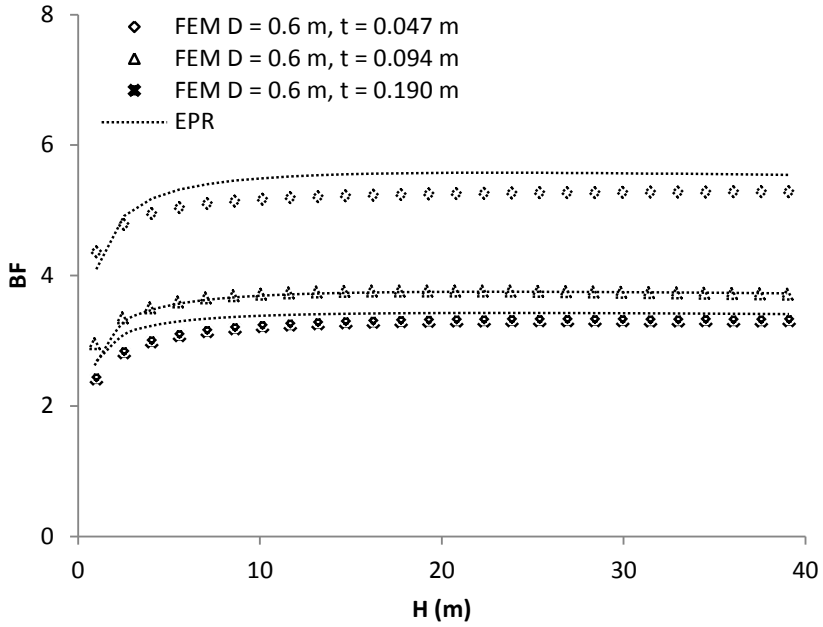

Figure 4.15: EPR calculated soil load bedding factors compared to the finite element results (EPR model consists of four terms as shown in Table 4.4)

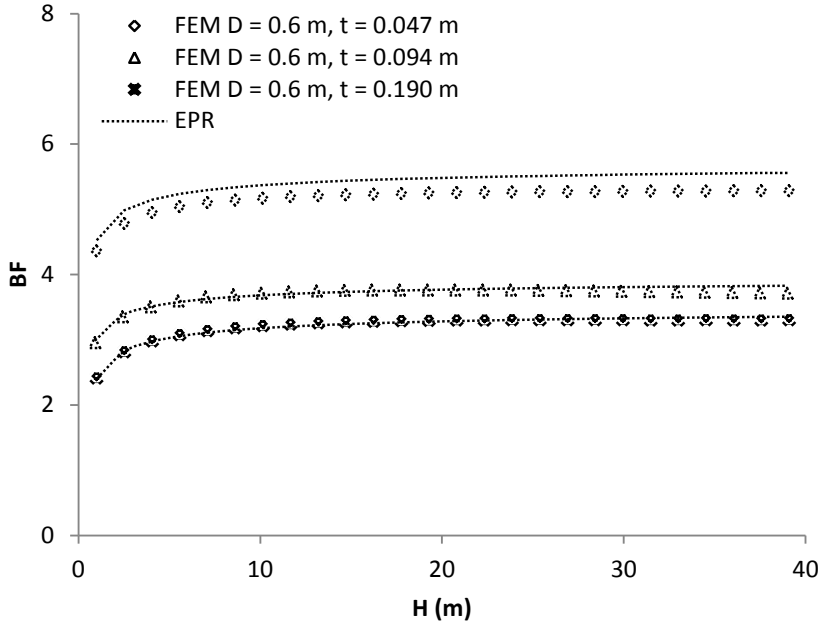

Figure 4.16: EPR calculated soil load bedding factors compared to the finite element results (EPR model consists of five terms as shown in Table 4.4)

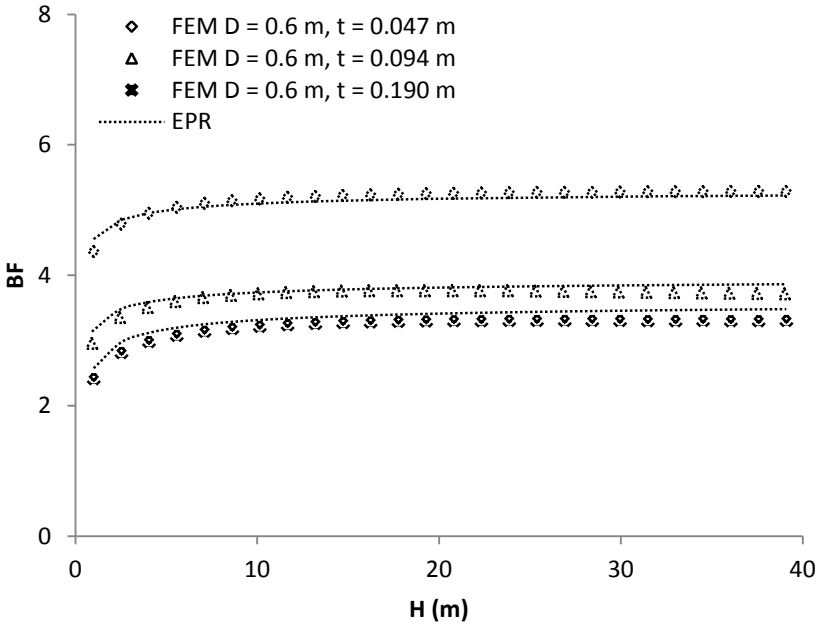

Figure 4.17: EPR calculated soil load bedding factors compared to the finite element results (EPR model consists of six terms as shown in Table 4.4)

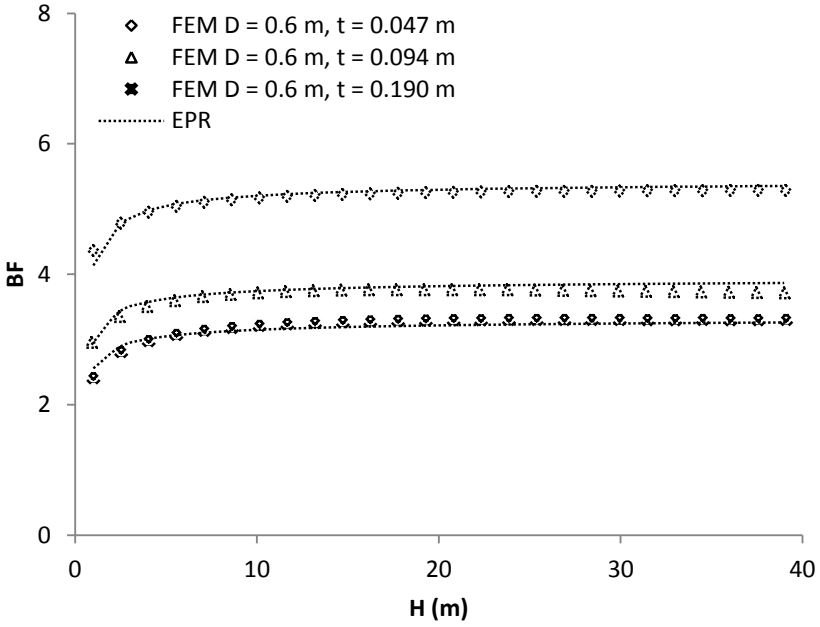

Figure 4.18: EPR calculated soil load bedding factors compared to the finite element results (EPR model consists of seven terms as shown in Table 4.4)

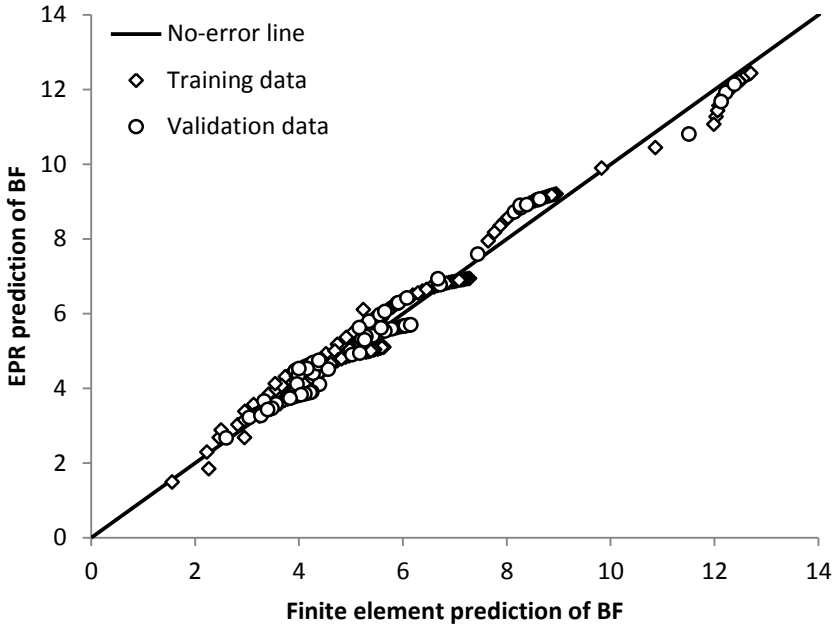

Figure 4.19: EPR calculated soil load bedding factors compared to the finite element results for installation Type 1

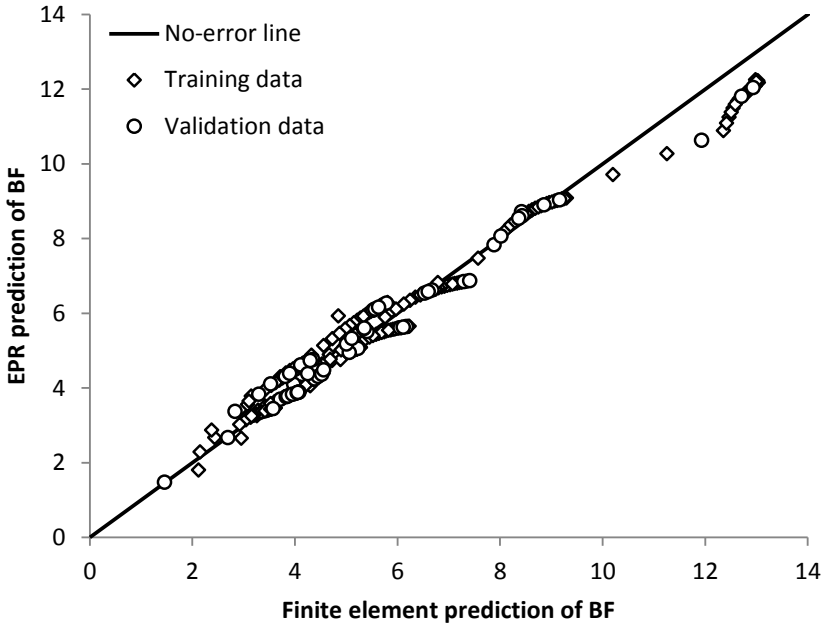

Figure 4.20: EPR calculated soil load bedding factors compared to the finite element results for installation Type 2

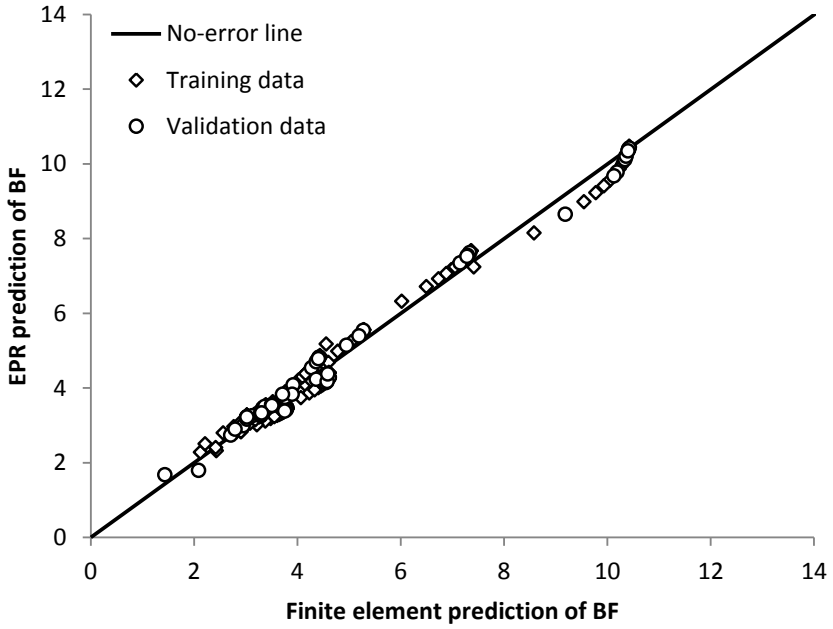

Figure 4.21: EPR calculated soil load bedding factors compared to the finite element results for installation Type 3

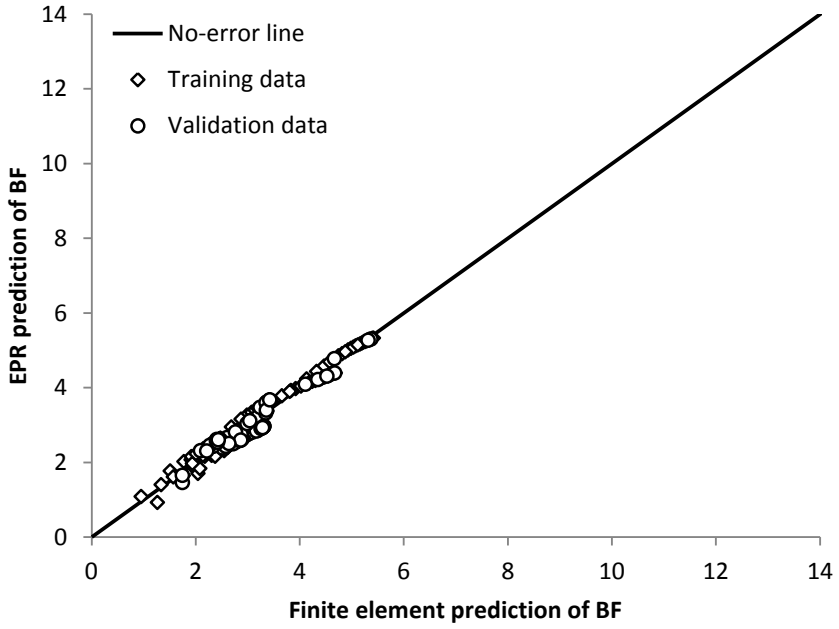

Figure 4.22: EPR calculated soil load bedding factors compared to the finite element results for installation Type 4

Table 4.3: Statistics for the data used in the EPR analysis

		Type 1				Type 2				Type 3				Type 4			
		D (m)	t (m)	H (m)	BF	D (m)	t (m)	H (m)	BF	D (m)	t (m)	H (m)	BF	D (m)	t (m)	H (m)	BF
Training data	$Mean$	1.2	0.150	20.56	5.67	1.1	0.150	19.76	5.58	1.2	0.150	19.40	4.77	1.1	0.150	20.16	3.02
	Min	0.3	0.028	0.90	1.55	0.3	0.028	0.90	1.46	0.3	0.028	0.90	1.44	0.3	0.028	0.90	0.96
	Max	2.4	0.458	39.10	12.70	2.4	0.458	39.10	13.04	2.4	0.458	39.10	10.43	2.4	0.458	39.10	5.42
	$STDV$	0.8	0.120	11.30	2.35	0.8	0.120	11.37	2.46	0.8	0.120	11.54	1.87	0.8	0.120	11.40	0.79
Validation data	$Mean$	1.1	0.150	17.77	5.32	1.1	0.150	20.98	5.70	1.1	0.140	22.43	4.53	1.2	0.160	19.36	2.99
	Min	0.3	0.028	0.90	2.22	0.3	0.028	0.90	2.12	0.3	0.028	1.00	2.12	0.3	0.028	1.00	1.27
	Max	2.4	0.458	39.09	12.34	2.4	0.458	39.10	12.99	2.4	0.458	39.09	10.43	2.4	0.458	39.10	5.37
	$STDV$	0.8	0.120	11.87	2.26	0.8	0.120	11.81	2.57	0.8	0.110	10.83	2.08	0.8	0.130	11.70	0.73
All data	$Mean$	1.1	0.150	20.01	5.56	1.1	0.150	20.01	5.60	1.1	0.150	20.01	4.60	1.1	0.150	20.01	3.01
	Min	0.3	0.028	0.90	1.55	0.3	0.028	0.90	1.46	0.3	0.028	0.90	1.44	0.3	0.028	0.90	0.96
	Max	2.4	0.458	39.10	12.70	2.4	0.458	39.10	13.04	2.4	0.458	39.10	10.42	2.4	0.458	39.10	5.42
	$STDV$	0.8	0.120	11.45	2.33	0.8	0.120	11.45	2.48	0.8	0.120	11.45	1.92	0.8	0.120	11.45	0.78

Table 4.4: Effect of number of terms on the CD for Type 3 installation

Number of terms	EPR model	CD training (%)	CD validation (%)
2	$BF = 0.31 \times \frac{t}{D \times \sqrt{H}} - 0.003$	78.92	82.92
3	$BF = 0.016 \times \frac{D^2}{t^2} - 0.11\frac{D^2}{t \times H} + 2.99$	96.67	97.93
4	$BF = -0.017 \times \frac{\sqrt{H}}{\sqrt{D \times}\sqrt{t}} - 0.85 \times \frac{D}{\sqrt{t \times}\sqrt{H}} + 0.017 \times \frac{D^2}{t^2} + 3.74$	97.40	98.49
5	$BF = -2.82 \times \frac{t}{D \times \sqrt{H}} - 0.003 \times \frac{D}{t^2} + 0.0195 \times \frac{D^2}{t^2} - 0.13 \times \frac{D^2}{t \times \sqrt{H}} + 3.4$	97.68	98.56
6	$BF = -1.49 \times \frac{t}{D^2 \times \sqrt{H}} + 0.00027 \times \frac{1}{D \times t^2} - 0.006 \times \frac{D}{t^2} + 0.02 \times \frac{D^2}{t^2} - 0.36 \times \frac{D^2}{\sqrt{t} \times \sqrt{H}} + 3.54$	98.47	98.89
7	$BF = -0.82 \times \frac{\sqrt{D}}{\sqrt{H}} + 0.155 \times \frac{D}{t} + 16.63 \times D \times t^2 - 0.091 \times \frac{D^2}{t \times H} + 0.134 \times \frac{D^2}{t} - 3.67 \times D^2 \times t + 2.51$	99.66	99.62

Table 4.5: Coefficient of determination (CD) for the training and validation data (%)

Data set	Type 1	Type 2	Type 3	Type 4
Training	97.81	97.70	97.68	96.00
Validation	97.40	97.90	98.56	96.32

4.4.2. Sensitivity analysis

As discussed in Section 3.3.2, the developed model using the EPR should be tested using a sensitivity analysis to increase confidence in its predictive ability. Therefore, the results of a sensitivity analysis are presented in this section to show the performance of the developed models. The aim is to illustrate that these models are able to predict the complex trend behaviour of the soil load bedding factor which has been presented and discussed in the parametric study section (Section 4.3).

Figure 4.23 shows the effect of the backfill height and installation condition on the calculated bedding factor, using the developed models for the case of a pipe with an inside diameter of 1.2 m and a thickness of 0.144 m. It can be seen that the models are able to show the effect of the backfill height and the installation condition on the bedding factor, which has been discussed in Section 4.3.1.

Figure 4.24 ((a), (b), (c) and (d)) shows the effect of the pipe diameter on the bedding factor. Again, the results show that the developed models can capture the complex interaction of the bedding factor values as the diameter changes for all of the installation conditions.

Figure 4.25 ((a), (b), (c) and (d)) shows the effect of the pipe wall thickness on the calculated bedding factor values for all of the installation conditions. The results clearly illustrate the ability of the developed model to capture the trend behaviour of the bedding factor as the thickness of the pipe changes.

In summary, these results give additional confidence in the validity of the models and hence these models can be recommended for use in the design practice within the range of pipe size used to develop them.

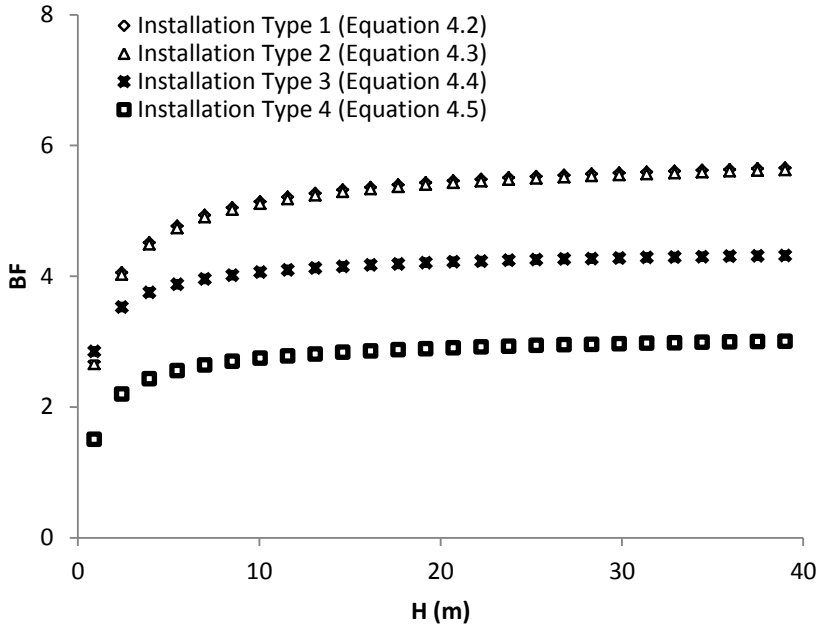

Figure 4.23: Effect of the backfill height and installation condition on the calculated bedding factor

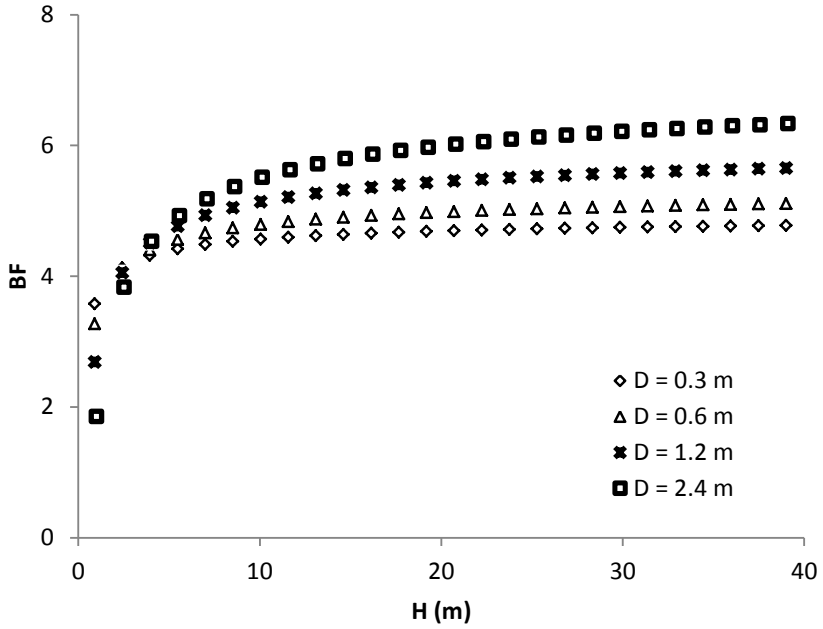
8
6
4
2
0
BF
0
10
20
30
40
H (m)
D = 0.3 m
D = 0.6 m
D = 1.2 m
D = 2.4 m

(a)

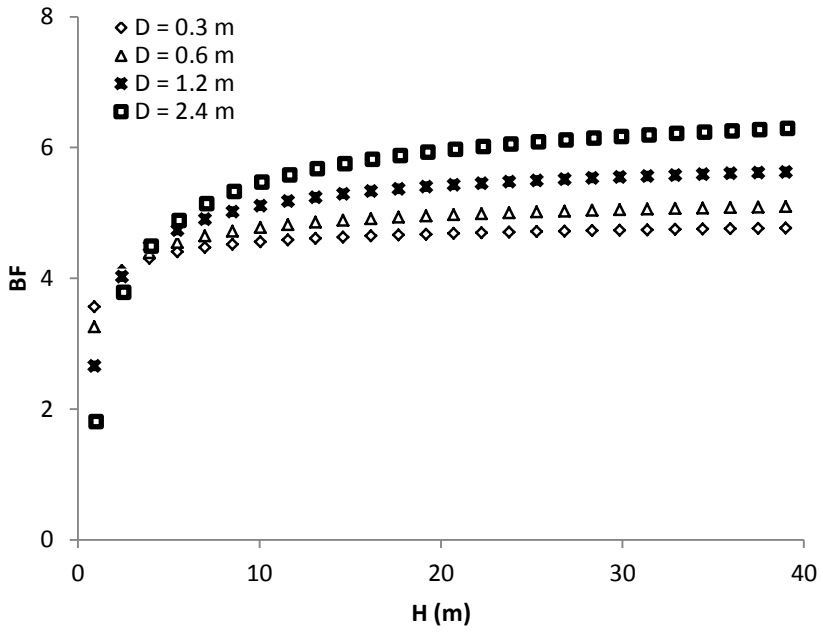
8
6
4
2
0
BF
0
10
20
30
40
H (m)
D = 0.3 m
D = 0.6 m
D = 1.2 m
D = 2.4 m

(b)

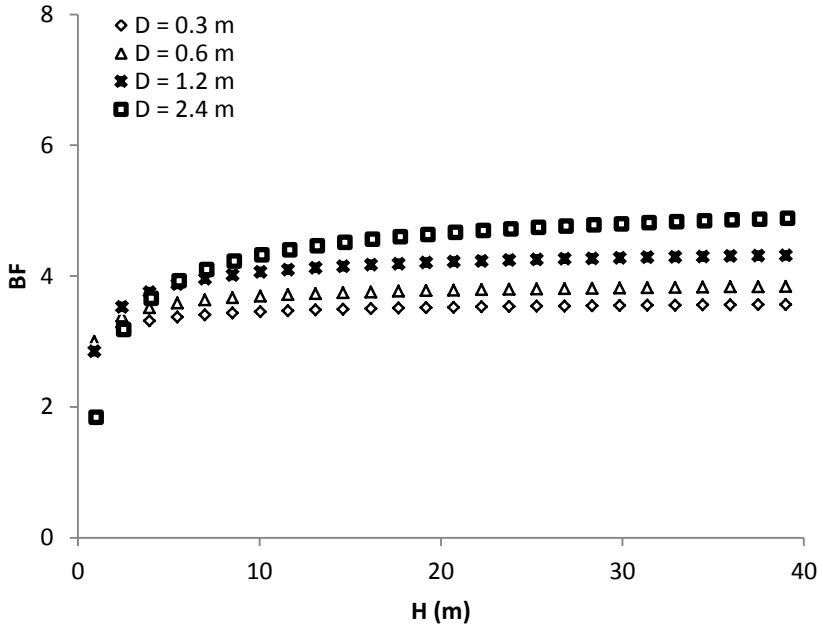

(c)

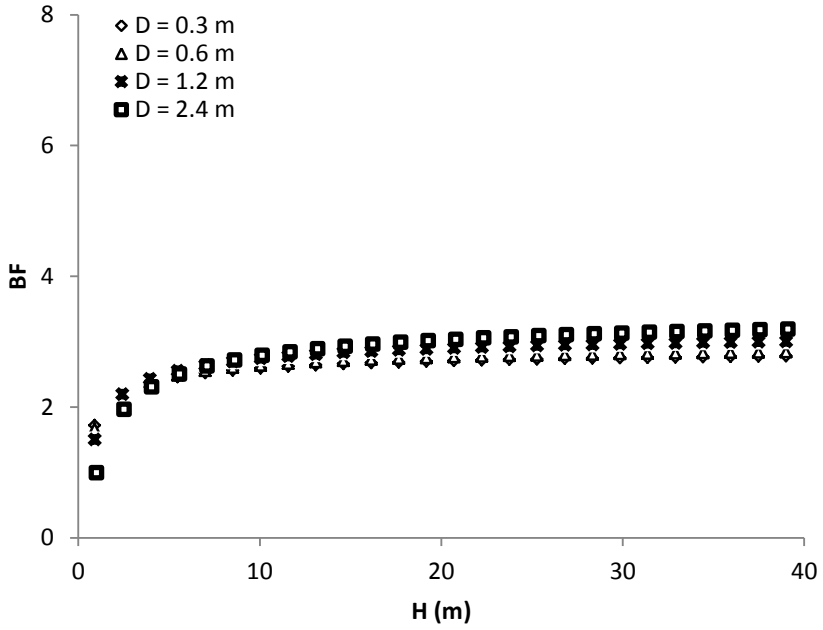

(d)

Figure 4.24: Effect of pipe diameter on the calculated soil load bedding factor: (a) Type 1 (Equation 4.2); (b) Type 2 (Equation 4.3); (c) Type 3 (Equation 4.4); (d) Type 4 (Equation 4.5)

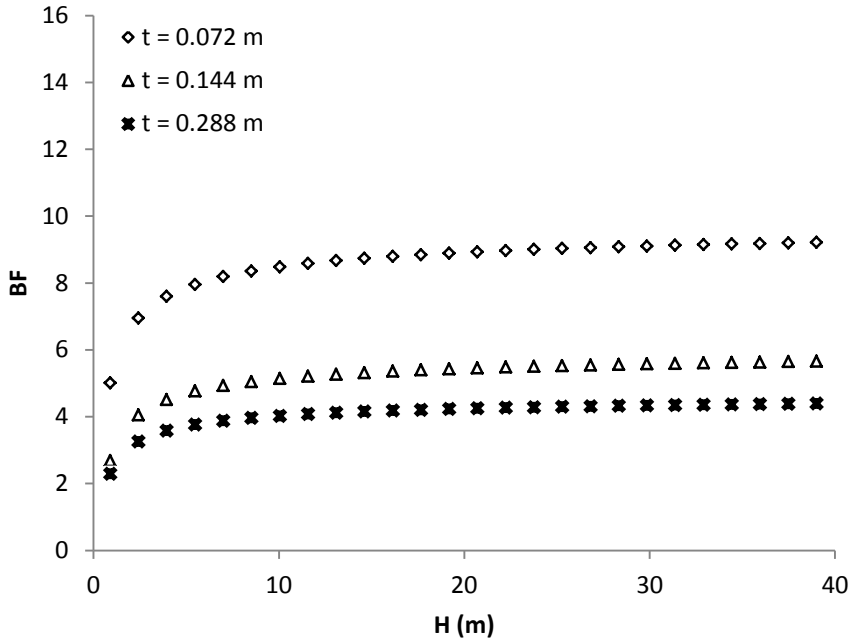
t = 0.072 m
t = 0.144 m
t = 0.288 m
BF
H (m)
0
2
4
6
8
10
12
14
16
0
10
20
30
40

(a)

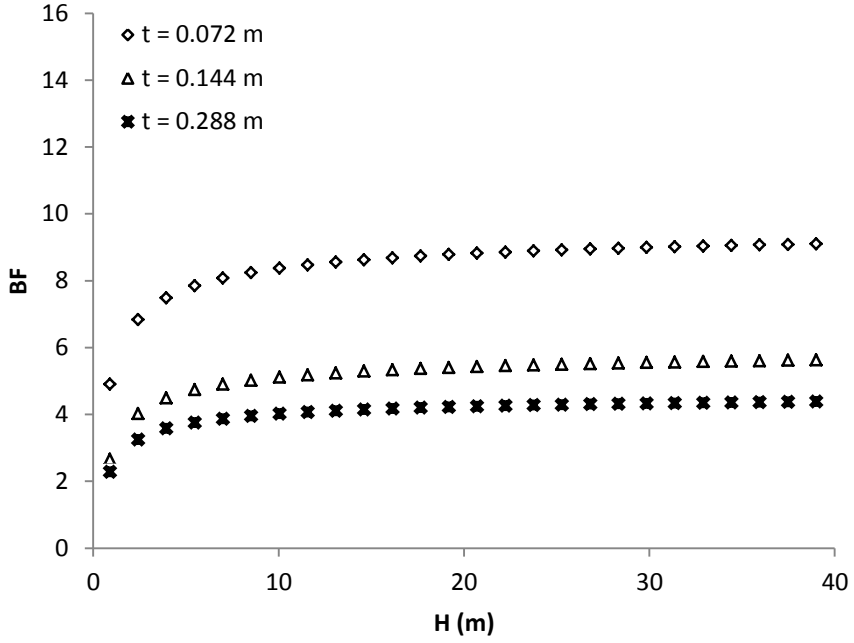
t = 0.072 m
t = 0.144 m
t = 0.288 m
BF
H (m)
0
2
4
6
8
10
12
14
16
0
10
20
30
40

(b)

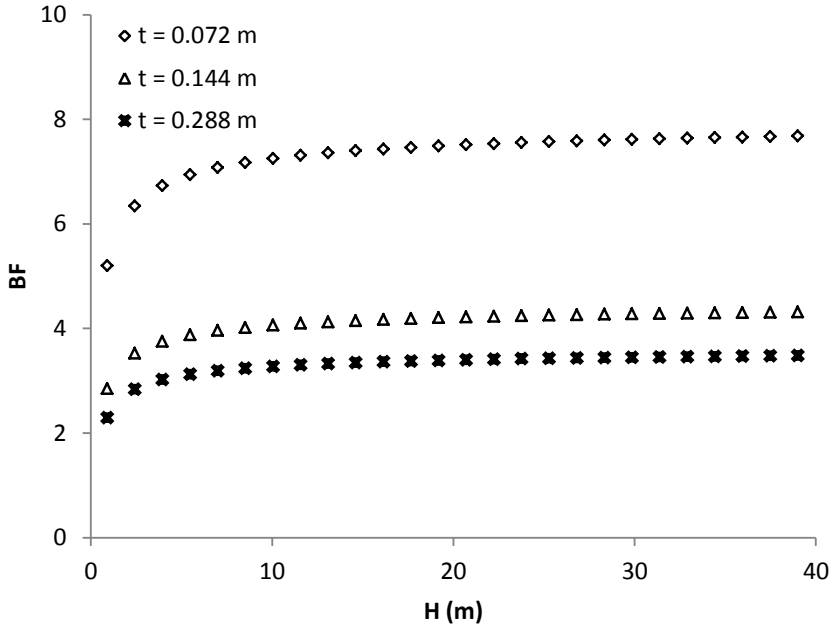

(c)

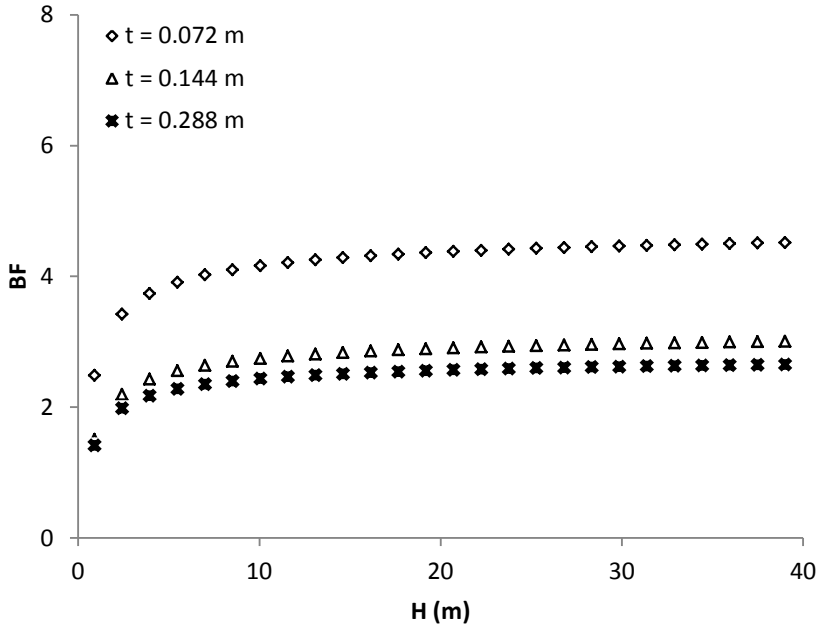

(d)

Figure 4.25: Effect of pipe wall thickness on the calculated soil load bedding factor: (a) Type 1 (Equation 4.2); (b) Type 2 (Equation 4.3); (c) Type 3 (Equation 4.4); (d) Type 4 (Equation 4.5)

4.4.3. Comparison with previous studies

As mentioned in Section 2.4, only one experimental study has reported the soil load bedding factor of a concrete pipe buried under deep soil fill (MacDougall et al., 2016). MacDougall et al. (2016) tested a buried concrete pipe under deep soil fill using a biaxial test cell. The pipe used had an inside diameter of 0.6 m and a wall thickness of 0.094 m. They tested the pipe by applying a uniformly distributed load to simulate the deep soil fill in the biaxial cell. The pipe was installed using a Type 2 installation. The strain in the pipe and the developing crack width in the pipe wall were monitored during the test and the pipe was tested until it reached the failure limit (i.e. a crack width of 0.254 mm). The bedding factor was found to be 5.3 at a backfill height of 20.3 m.

In this section, the capabilities of the model developed for the bedding factor corresponding to a Type 2 installation (Equation 4.3) were tested by comparing the model prediction with the experimental bedding factor reported by MacDougall et al. (2016). The pipe geometric properties and backfill height reported by MacDougall et al. (2016) were used in the prediction. The calculated bedding factor using Equation 4.3 was equal to 5.0. Hence, the result from the model is in excellent agreement with the experimental bedding factor with a percentage difference of 6%. This comparison gives additional validation for the methodology adopted in this chapter. The proposed models for the bedding factor can therefore be used with confidence in practice for achieving an economic pipe design, relative to the conservative values obtained from the current design AASHTO standard and the BS. In addition, the models proposed here can easily be applied to any pipe wall thickness. This is very useful if the

designer wants to use a pipe with a non-standard thickness (i.e. different from the AASHTO recommended thicknesses for different pipe classes).

4.5. Summary

This chapter has investigated the behaviour of buried concrete pipes under backfill soil load only using three-dimensional finite element modelling. The effect of the backfill height, pipe diameter, installation condition and pipe wall thickness were considered. The robustness of the BS and AASHTO bedding factors was also investigated. The bedding factor was derived using the maximum bending moment obtained from the finite element analysis.

The results from this chapter clearly demonstrated the issues in the current BS and AASHTO design bedding factors for the case of the backfill soil load only. In addition, the results clearly showed the need to include the effect of the backfill height, installation condition, pipe diameter and pipe wall thickness in calculating the bedding factor for a robust, safe and economical design. As a result, new bedding factor models were derived using the EPR analysis. The developed bedding factor models were robustly tested via a sensitivity analysis and a comparison with the experimental study of MacDougall et al. (2016) to increase confidence in these models. The ability of the developed models to capture the trend behaviour noticed in the parametric study and the very good agreement (percentage difference 6%) with the experimental bedding factor value reported by MacDougall et al. (2016) demonstrated the accuracy and the robustness of the derived bedding factor models. Hence, it was concluded that the developed models can be used with confidence for the design of the buried concrete pipes under backfill soil load only.

It should be noted that this chapter has focused on the soil load only. Hence, the next chapter (**Chapter 5**) discusses the behaviour of the buried pipes under traffic loading and investigates the robustness of the BS design methodology for buried concrete pipes under the combined effect of the backfill soil load and traffic loading.

Chapter 5
RESPONSE OF BURIED CONCRETE PIPES UNDER TRAFFIC LOADING

5.1. Introduction

Concrete pipes are likely to be buried shallowly under roads to transport waste water and/or storm water. Therefore, these pipes need to resist the applied load from the traffic. This chapter studies the behaviour of buried concrete pipes under the effect of the total load (the backfill soil load and the BS traffic loading). The chapter also investigates the robustness of the BS bedding factors for the case of the buried pipes under total load. It aims to address the gaps in the knowledge of the behaviour of buried concrete pipes under total load (detailed in Section 2.2.4) by discussing the following questions:

1- What are the parameters affecting the behaviour of buried concrete pipes under total load?
2- What is the backfill height limit to the effect of traffic loading?
3- Does changing the pipe diameter affect the backfill height limit?
4- Is the BS design methodology of buried concrete pipes under total load robust and economical?
5- Is it possible to enhance the BS design methodology and make it more economical and robust?

The effect of the main road traffic load configuration position and direction with respect to the buried concrete pipe is investigated firstly to find the critical loading condition. The critical loading condition is then used in a comprehensive parametric

study to investigate the behaviour of buried concrete pipes. The results of the maximum bending moment are used to calculate the bedding factor and to investigate the robustness of the total load BS design bedding factors. The development of new bedding factor models is then discussed and the robustness of these models is illustrated. Lastly, the chapter finishes with a summary of the main findings of the study. It is important to mention that the analysis time for the models considered in this chapter ranged from 20 to 60 minutes, depending on the pipe diameter and the backfill height.

5.2. Load configuration and critical load condition

As stated in **Chapters 1 and 2**, one of the objectives of this research was to investigate the behaviour and the design of buried concrete pipes under the main road traffic load configuration recommended by the BS (BSI, 2010), as it represents the worst-case scenario compared to other BS loading configurations (refer to Section 1.6.3 for more details). The loading configuration for main road (hereafter referred to as the MR-BSI traffic load) is comprised of two axles with four wheels on each axle as shown in Figure 5.1(a). The centre to centre spacing between the wheels is 1.0 m and the centre to centre spacing between the axles is 1.8 m (Figure 5.1 (b)). The total load of each wheel is 113 kN including a dynamic allowance factor of 1.3. This load is modelled as a surface pressure in the present analysis with a wheel foot print area of 0.50 m $\times$ 0.25 m (Petersen et al., 2010; Sheldon, 2011; Kang et al., 2013a; Kang et al., 2014); as this technique was found to provide a good prediction to the response of buried pipes under static loading as discussed in the validation problems 2 to 5 and validation problem 7.

To find the critical loading condition, the effect of the truck position with respect to the buried concrete pipe has been investigated. The cases of a truck travelling parallel and perpendicular to the pipeline axis were investigated at different $\boldsymbol{S}$ values; where $\boldsymbol{S}$ is the horizontal distance between the centreline of the pipe and the first set of wheels for the truck travelling parallel to the pipe (Figure 5.1(b)) or the distance between the centreline of the pipe and the right-hand truck axle for the case of a truck travelling perpendicular to the pipe (Figure 5.1(c)).

A sandy soil with a degree of compaction of 95% of the standard Proctor maximum dry density (SW95) was used as the backfill and the natural soil. The hyperbolic soil model was used to model the soil. The material properties of the soil are shown in Table 4.2. The buried concrete pipe was modelled using a linear elastic model. The modulus of elasticity (E) and the Poisson's ratio (υ) of the concrete pipe were taken as 24,856,000 kPa and 0.20, respectively (Petersen et al., 2010). The backfill height of 0.5 m was considered in the analysis. The model boundaries and the modelling steps were similar to those used in validation problem 4.

Figure 5.2 shows the maximum bending moment of the pipe for different $\boldsymbol{S}$ values for the case of a truck moving parallel to the pipeline axis. It can be seen that the maximum bending moment is equal to 2.9 kN.m/m when $\boldsymbol{S}$ = 0.00 m.

Figure 5.3 shows the maximum bending moment of the buried concrete pipe for different $\boldsymbol{S}$ values for the case of a truck moving perpendicular to the pipeline axis. It can be seen from this figure that the maximum bending moment was obtained when the centre of the right-hand axle was above the crown ($\boldsymbol{S}$ = 0.00 m) and is equal to 4.0 kN.m/m.

It can be concluded from these figures (Figures 5.2 and 5.3) that the highest bending moment in the pipe wall is obtained when the truck is moving perpendicular to the pipeline axis and the critical case is obtained when the centre of the right-hand axle is above the crown of the pipe. This is because the stress level on the crown of the pipe is larger when the axle load is directly above the pipe; which is in agreement with the experimental finding of Rakitin and Xu (2014) (detailed in Section 2.2.3), who noticed that the highest bending moment in the buried pipe wall was recorded when the heaviest axle of the vehicle was directly above the pipe. Hence, this loading condition will be used in the parametric study to simulate the worst-case scenario of the MR-BSI traffic load.

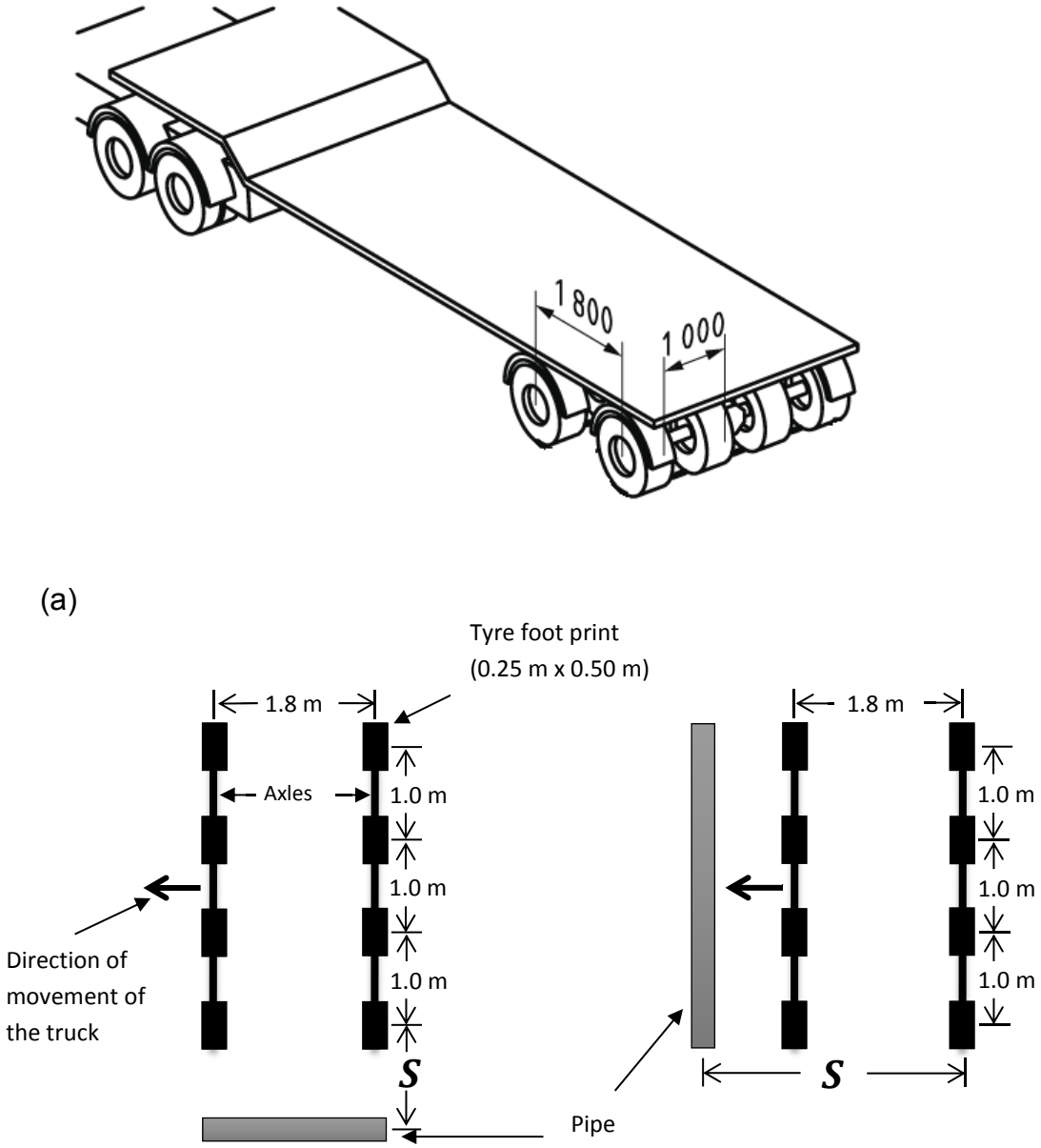

Figure 5.1: (a) Illustration of the main road British standard design truck (BSI, 2010); (b) the first load case (the axles perpendicular to pipe, but the truck moving parallel to the pipe); (c) the second load case (axles parallel to the pipe, but the truck moving perpendicular to the pipe)

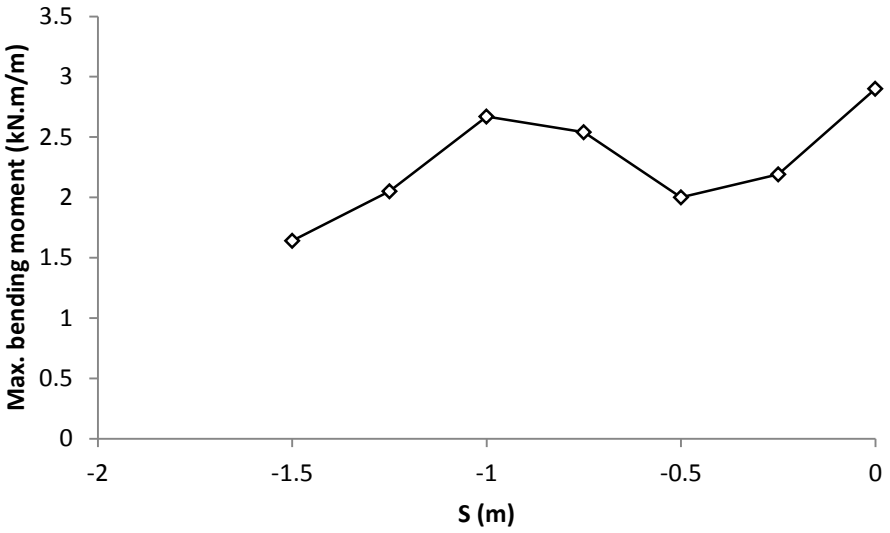

Figure 5.2: Results of the maximum bending moment from the analysis of the buried concrete pipe for the case of the MR-BSI traffic load travelling parallel to the pipeline axis with different S values (Note: S = 0.00 when the first set of wheels are directly above the pipeline axis, as shown in Figure 5.1(b))

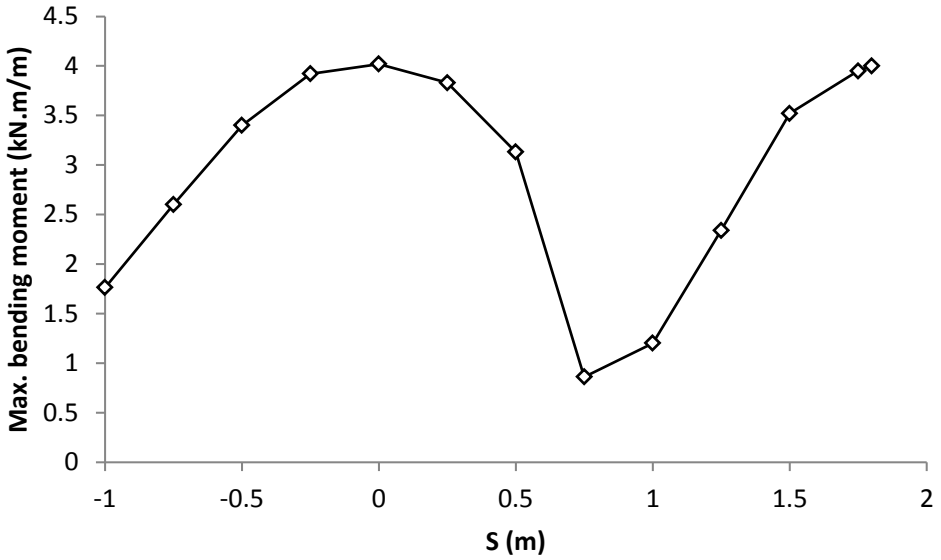

Figure 5.3: Results of the maximum bending moment from the analysis of the buried concrete pipe for the case of the MR-BSI traffic load travelling perpendicular to the pipeline axis with different S values (Note: As shown in Figure 5(c), S = -1.00 m when the right-hand axle is 1.00 m to the left of the pipeline axis; S = 0.00 when the right-hand truck axle is directly above the pipeline axis and the other axle is 1.80 m to the left of the pipeline axis; S = 1.80 m means the left-hand truck axle is directly above the pipeline axis and the other axle is 1.80 m to the right of the pipeline axis.)

5.3. Parametric study

A parametric study has been conducted to thoroughly investigate the effect of the MR-BSI traffic load on the bending moment developed in the buried concrete pipe wall, and hence enable a comprehensive understanding of the behaviour of the buried concrete pipes under traffic load. The effect of pipe wall thickness, pipe diameter, backfill height and support condition have been considered in these

analyses. Table 5.1 shows the diameters and the wall thicknesses considered in the analysis.

A minimum backfill height of 1.0 m has been considered because it is the minimum backfill height allowed in the UK for the buried pipe under the MR-BSI traffic load (HA, 2001). Four different installation conditions have been investigated covering the range of a very good quality installation (Type 1 in AASHTO) to a poor quality installation (Type 4 in AASHTO). The quality of the installation has been investigated by changing the soil in the haunch zone. The soils considered, similar to that considered in **Chapter 4**, were SW95 (to simulate a very good quality installation (Type 1 according to AASHTO)); SW90 (to simulate a good quality installation (Type 2 according to AASHTO)); ML90 (to simulate a reasonable quality installation (Type 3 according to AASHTO)); and ML49 (to simulate a poor quality installation (Type 4 according to AASHTO)). The backfill soil above the pipe was simulated with the SW90 soil in all of the cases. The natural soil was assumed to be stiffer than the backfill soil to simulate the case of an over-consolidated soil, which is usually the case for a pavement soil due to the cyclic action of the moving traffic. Furthermore, the bedding soil was simulated using the SW90 soil, similar to that considered in **Chapter 4**. The bedding soil was simulated with a well compacted soil to investigate the worst-case scenario of a pipe directly installed on a stiff soil, as discussed earlier in **Chapter 4**.

The hyperbolic soil model parameters for the SW95, SW90, ML90 and ML49 soils were taken from the literature (Boscardin et al., 1990) and are shown in Table 4.2. The material properties of the surrounding soil are shown in Table 5.2. The modulus

of elasticity (E) and the Poisson's ratio (υ) of the concrete pipe were taken as 24,856,000 kPa and 0.20, respectively (Petersen et al., 2010).

The finite element model used in the analysis had a width of 12.0 m, a length of 15.0 m and a height of 10.0 m (similar to validation problem 4). The model satisfies the boundary requirements for the width, the height of the soil below the pipe and the length for all of the considered pipes (refer to Section 3.2.2.1 for details). However, the height of the model increased slightly for the largest pipe for the case of a backfill height of 1.5 m, to avoid the influence of the model extent. The boundary conditions, the element types, the element sizes and the modelling steps were the same as for validation problem 4. Figure 5.4 shows the finite element mesh used in the analysis. The following subsections discuss the results of the parametric study.

Table 5.1: Pipe diameters and wall thicknesses (Petersen et al., 2010)

Inside diameter (D) (m)	Wall thickness (t) (m)
0.3	0.051
0.6	0.076
1.2	0.127
2.4	0.229

Table 5.2: Material properties of the natural soil used in the parametric finite element analysis

Property	Natural soil
γ (kN/m3)	21.00
υ	0.30
c'(kPa)	30
ϕ'(°)	36
K	1500
Rf	0.90
n	0.65

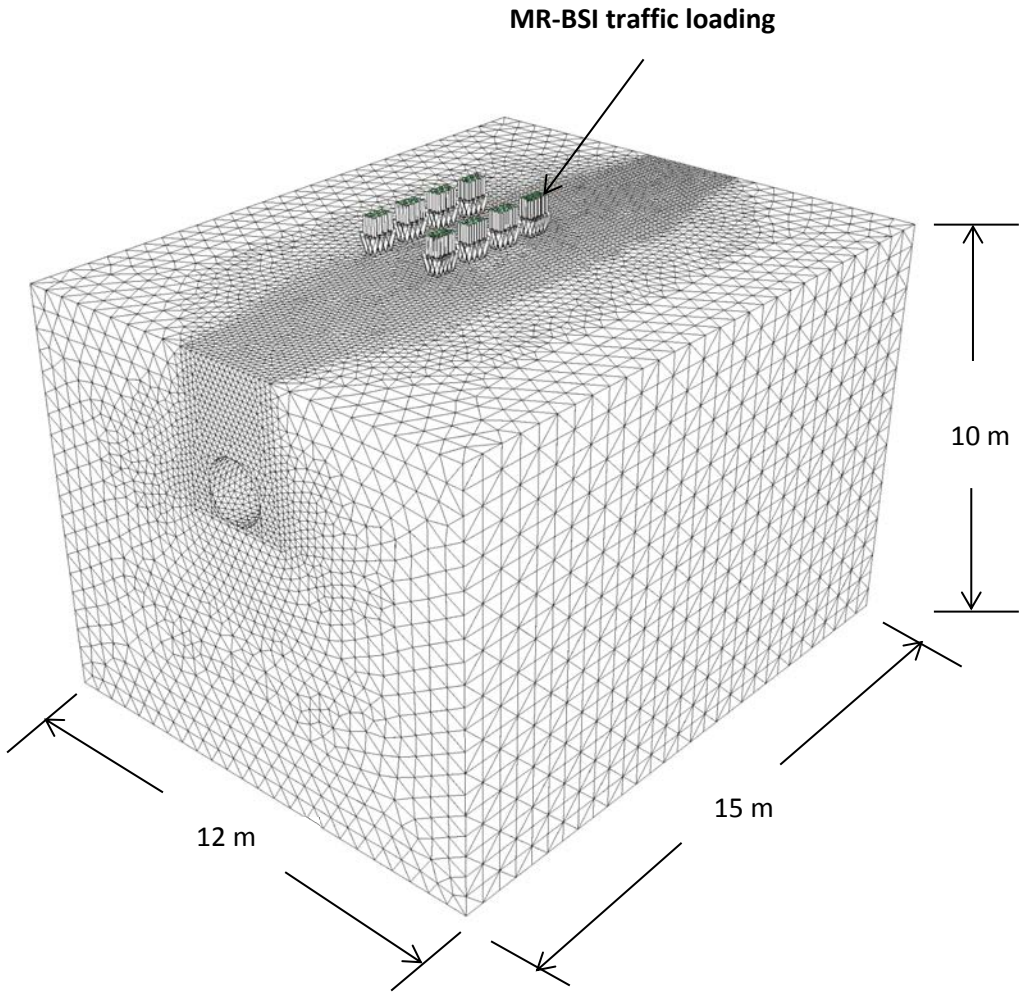

Figure 5.4: The finite element mesh used

5.3.1. Effect of backfill height and pipe diameter

The bending moment due to the soil weight only and total load (combined soil weight and traffic load) have been investigated in this section. This was undertaken to study the reduction in the effect of the traffic load as the backfill height (H) increases for all of the considered diameters, and also to find the backfill height limit for the effect of the traffic load.

Figure 5.5 shows the bending moment due to the soil weight only and the total load for a pipe with an inside diameter of 0.3 m. It can be clearly seen that the presence of the traffic load significantly increases the bending moment in the pipe wall. However, the effect of the traffic load considerably decreases as the backfill height increases; where the percentage increase in the maximum bending moment due to traffic load is 353% for a backfill height of 1.0 m and decreases to 22% for a backfill height of 2.5 m. It can also be seen that the traffic load did not affect the maximum bending moment for a pipe buried with a backfill height of 3.0 m.

Figures 5.6, 5.7 and 5.8 show the effect of the traffic load on the bending moment for pipes with an inside diameter of 0.6 m, 1.2 m and 2.4 m, respectively. Generally, these figures show a similar trend to that shown in Figure 5.5, where the traffic load increases the bending moment in the pipe wall. However, it can be clearly seen that increasing the diameter of the pipe decreases the influence of the traffic load. For a backfill height of 1.0 m, the percentage increase in the bending moment is 205%, 119% and 12% for pipes with an inside diameter of 0.6 m, 1.2 m and 2.4 m, respectively. Importantly, Figure 5.7 shows that the influence of the traffic load for a 1.2 m pipe becomes very small at a backfill height of 2.5 m, where the percentage

increase is less than 7%. Furthermore, Figure 5.8 shows that the traffic load has no effect on the maximum bending moment for a 2.4 m pipe with a backfill height of 1.5 m. This behaviour is different from that observed for pipes with diameters of 0.3 m, 0.6 m and 1.2 m (Figures 5.5, 5.6 and 5.7). This is due to the insignificant effect of the traffic load on the soil pressure developed at the invert of the 2.4 m pipe with a backfill height of 1.5 m, as shown in Figure 5.9(d) when compared with the other diameters (Figures 5.9(a), (b) and (c)). Figure 5.9(d) shows that the mean soil pressure at the invert of the 2.4 m pipe does not increase due to the application of the traffic load, which is different from other diameters shown in Figures 5.9(a), (b) and (c). In addition, the initial soil pressure at the invert of the 2.4 m pipe (due to soil weight only) is higher than the crown soil pressure, even after the application of the traffic load. Therefore, there was no increase in the maximum bending moment. These results are in general agreement with the ACPA recommendation on the influence of traffic load, where the ACPA suggests that the traffic load is not significant for a backfill height equal to or greater than 3.0 m (ACPA, 2011). However, the present study has shown that although the ACPA recommendation is valid, it is conservative for large diameter pipes, where the effect of the traffic load becomes insignificant when the backfill height is equal to or greater 1.5 m for the 2.4 m diameter pipe. Therefore, the BS should include a backfill height limit for the influence of traffic load depending on the pipe diameter.

Finally, comparing the results of Figures 5.5, 5.6, 5.7 and 5.8 shows that increasing the diameter of the pipe increases the bending moment at the shoulder, springline and invert of the pipe. This is due to the increase in backfill height above the pipe in

these zones as the diameter increases, which means that the soil weight above these locations will increase; hence, leading to a larger induced bending moment.

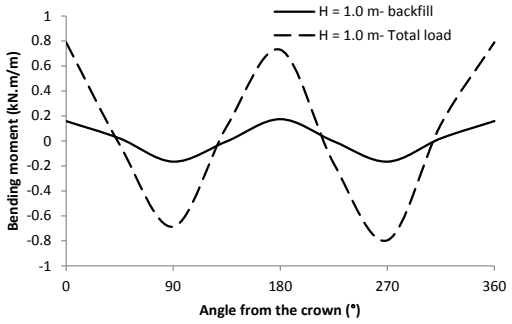

(a)

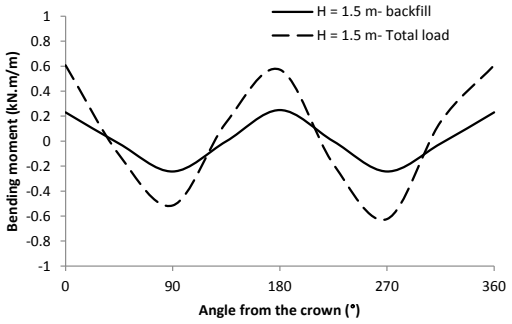

(b)

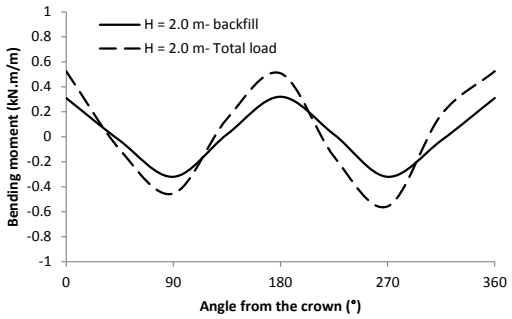

(c)

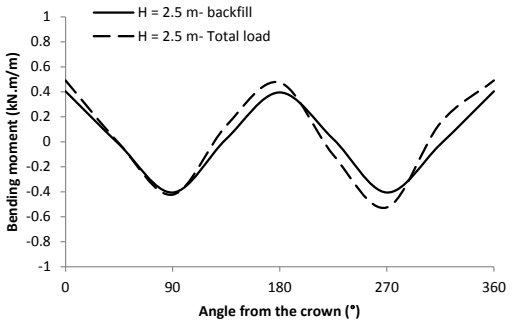

(d)

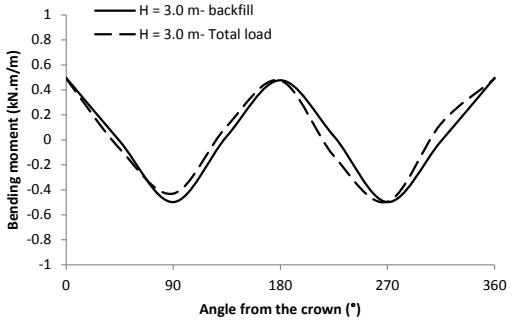

(e)

Figure 5.5: Bending moment around a pipe with an inside diameter of 0.3 m for different backfill heights: (a) H = 1.0 m; (b) H= 1.5 m; (c) H= 2.0 m; (d) H= 2.5 m; (e) H= 3.0 m

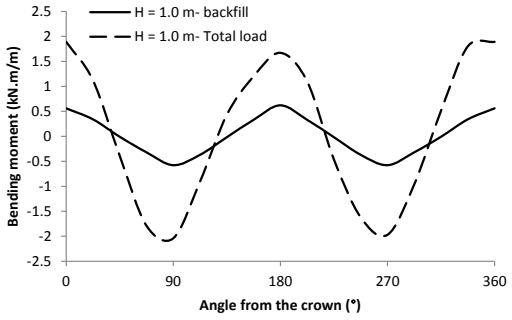

(a)

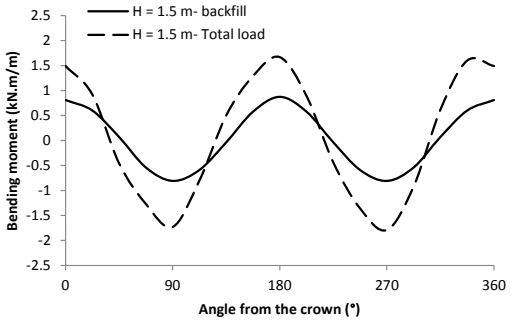

(b)

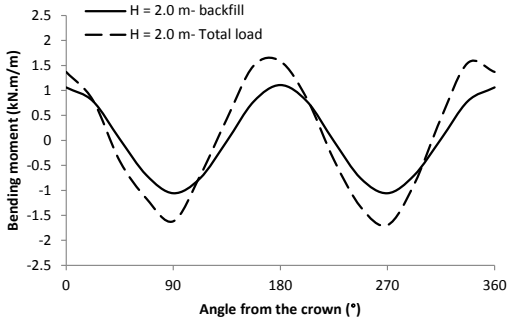

(c)

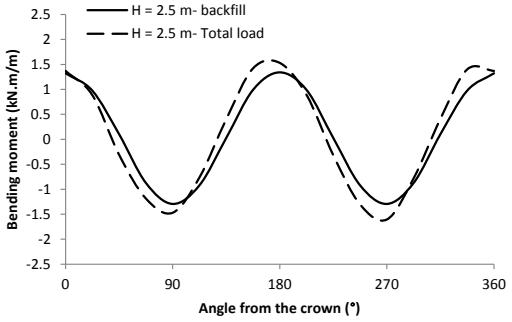

(d)

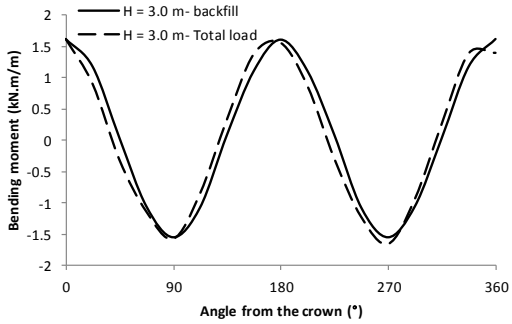

(e)

Figure 5.6: Bending moment around a pipe with an inside diameter of 0.6 m for different backfill heights: (a) H= 1.0 m; (b) H= 1.5 m; (c) H= 2.0 m; (d) H= 2.5 m; (e) H= 3.0 m

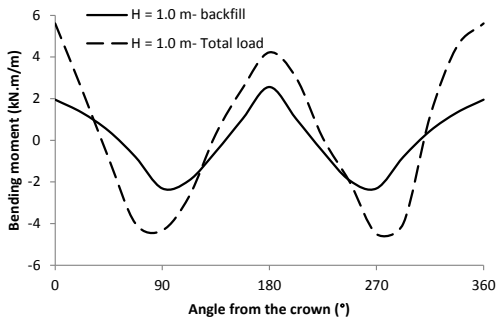

(a)

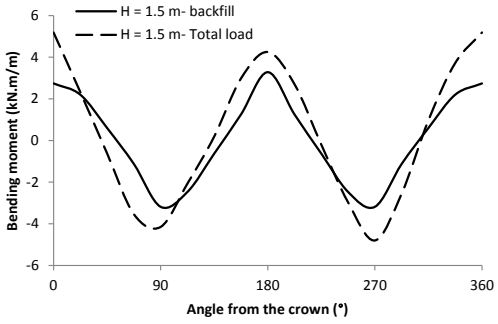

(b)

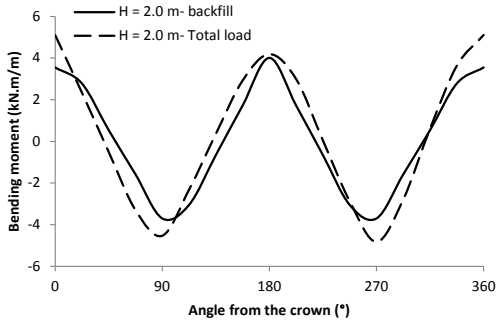

(c)

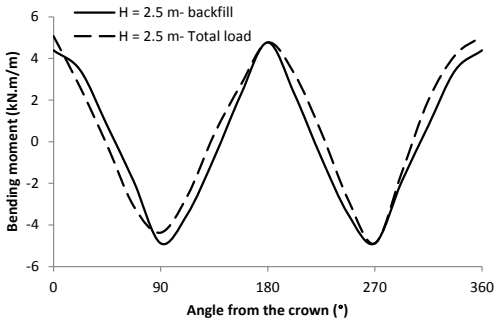

(d)

Figure 5.7: Bending moment around a pipe with an inside diameter of 1.2 m for different backfill heights: (a) H= 1.0 m; (b) H= 1.5 m; (c) H= 2.0 m; (d) H= 2.5 m

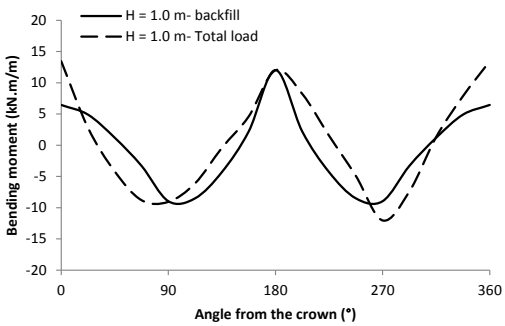

(a)

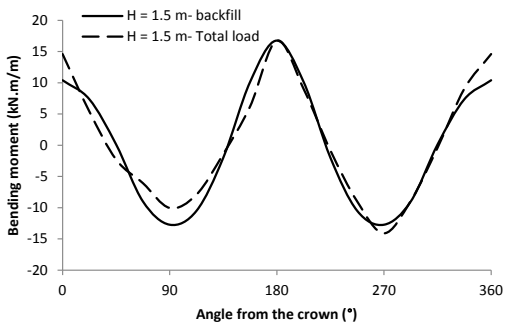

(b)

Figure 5.8: Bending moment around a pipe with an inside diameter of 2.4 m for different backfill heights: (a) H= 1.0 m; (b) H= 1.5 m

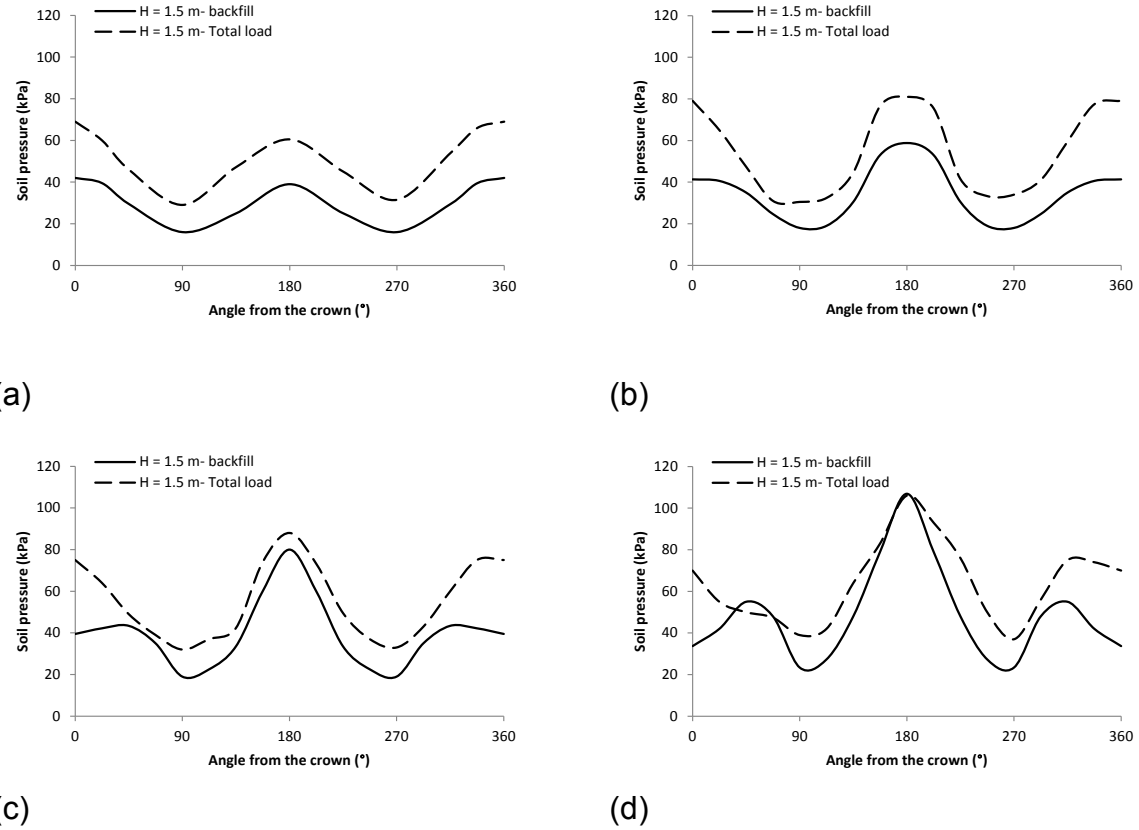

Figure 5.9: Mean soil pressure around the pipe: (a) D= 0.3 m; (b) D= 0.6 m; (c) D= 1.2 m; (d) D = 2.4 m

5.3.2. Effect of soil support (installation type)

The effect of the installation quality has been investigated by changing the soil type at the haunch zone. This has been considered because changing the quality of the haunch soil affects the soil pressure developed at the invert zone (Pettibone and Howard, 1967; Wong et al., 2006). Hence, this is expected to impact on the induced bending moment in the pipe wall similar to the behaviour observed under soil load only (detailed in Section 4.3.1).

Figure 5.10 shows the effect of the installation quality on the induced bending moment for a pipe with an inside diameter of 0.3 m and a backfill height of 1.0 m

under the total load. It can be seen from this figure that the bending moment does not significantly increase when the haunch soil changes from SW95 (very good installation) to SW90 (good installation) or ML90 (reasonable installation), where the percentage increase is equal to 1% and 4%, respectively. This behaviour is different from that observed under soil load only (discussed in Section 4.3.1). This difference in the behaviour is due to the higher soil pressure developed at the crown of the pipe as a result of the application of the traffic load, compared to the case of the soil load only. The increase in the soil pressure at the invert reduces the impact of the concentration of the reaction forces at the invert zone as the installation quality decreases. However, the figure shows that changing the haunch soil from SW95 (very good installation) to ML49 (poor installation) noticeably increases the bending moment (percentage increase 36%) and changes the zone of the maximum bending moment from the crown to the invert of the pipe.

It can also be seen that changing the installation quality does not significantly impact on the bending moment developed at the crown or the springline, similar to the behaviour observed under soil load only.

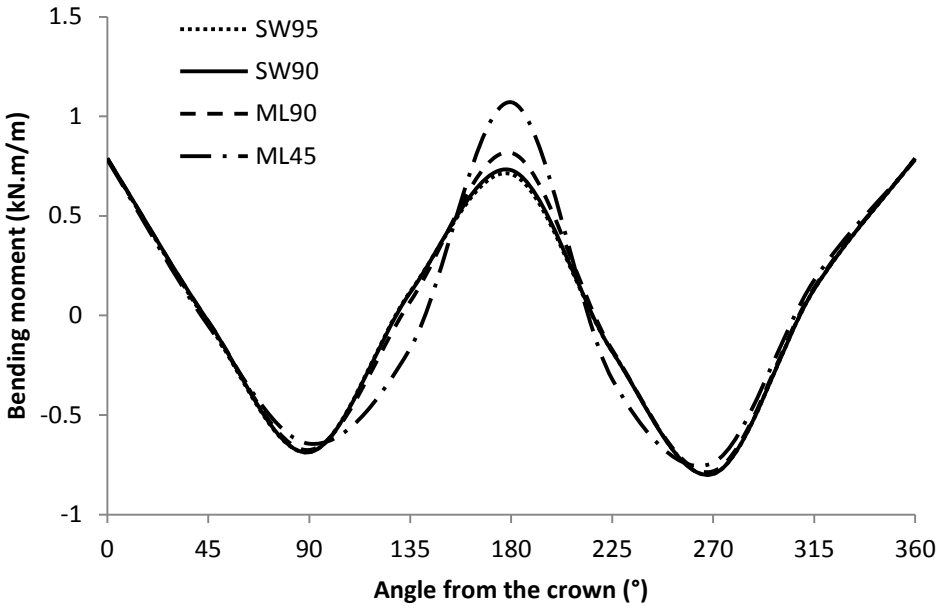

Figure 5.10: Effect of installation quality on the bending moment of a pipe with an inside diameter of 0.3 m and a backfill height of 1.0 m

5.3.3. Effect of pipe wall thickness

To investigate the effect of the pipe wall thickness, additional models were considered with two thicknesses: one was equal to half of the original thicknesses shown in Table 5.1 and the second was double the original thicknesses, similar to that conducted in **Chapter 4** (Section 4.3.3). This was done for all of the pipes with all of the considered backfill heights. The aim was to study the impact of the pipe wall thickness on the bending moment developed in the pipe wall and quantify the percentage change in the bending moment for buried pipes under total load. It should be noted that the finite element model's width and height was increased to 15.0 m and 12.0 m respectively, for the largest pipe diameter (D = 2.4 m) with the double wall thickness, to avoid the influence of the finite element model's extent.

Figure 5.11 shows the effect of the pipe wall thickness on the bending moment due to total load on a pipe with an inside diameter of 1.2 m and a backfill height of 1.0 m. It can be clearly seen that the bending moment is significantly affected by changing the pipe wall thickness; decreasing the pipe thickness by half decreases the maximum bending moment by 48%, while doubling the pipe thickness increases the bending moment by 36%. This as a result of the increase of the soil pressure attracted by the pipe, as the stiffness increases because of the increase in the pipe thickness and vice versa, as discussed earlier in Section 4.3.3.

From this parametric study it can be concluded that the bending moment induced in the pipe wall due to the total load, for the pipe diameters considered in this study, is affected by the backfill height (up to 2.5 m), the installation condition and the pipe wall thickness. Hence, all of these parameters should be considered when testing and improving the current design total load bedding factors, as the bedding factor is dependent on the bending moment (Young and O'Reilly, 1987; Petersen et al., 2010). The next section discusses the calculation of the total load bedding factors and the robustness of the BS bedding factors.

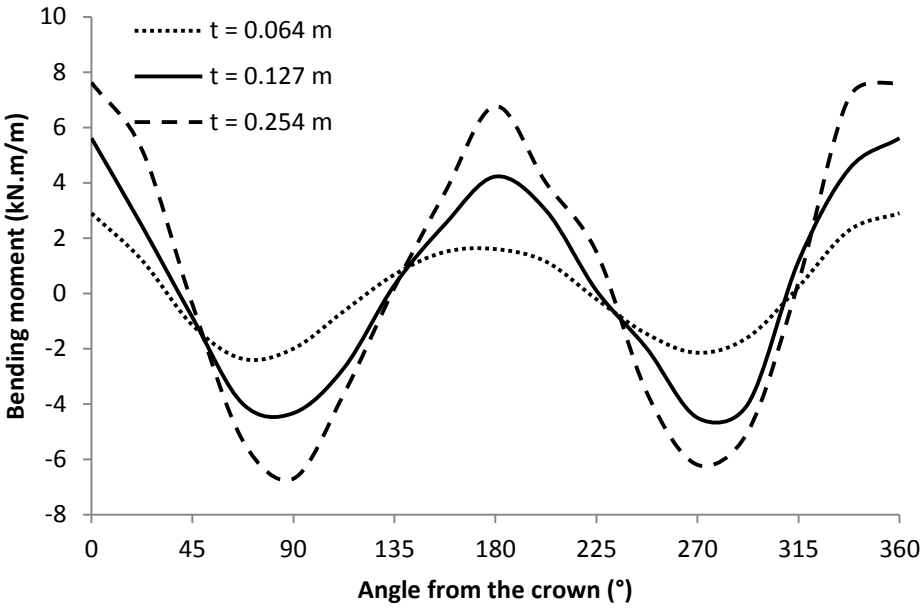

Figure 5.11: Effect of pipe wall thickness on the induced bending moment in the pipe wall for a pipe with an inside diameter of 1.2 m and a backfill height of 1.0 m under the total load

5.4. Total load bedding factor

The maximum bending moment obtained from the finite element modelling for each case was used to calculate the total load bedding factor; as the bedding factor can be obtained by taking the ratio of the maximum positive bending moment in the laboratory condition (i.e. under the three-edge loading condition) to the maximum positive bending moment in the field condition (obtained from the finite element modelling), as discussed earlier in Section 4.3 (Equation 4.1) (Young and O'Reilly, 1987; Petersen et al., 2010). The total force applied on the pipe (W_t) is calculated based on the BS using Equation 1.1. The details of the total force calculation are shown in **Appendix B**.

Figures 5.12 and 5.13 show the total load bedding factors obtained for the cases of good installation (SW90 soil in the haunch zone) and poor installation (ML49 soil in the haunch zone), respectively. Other installation conditions (haunch support with SW95 and ML90) have not been considered, as the results of the parametric study showed an insignificant effect from these installation conditions on the bending moment compared with the good installation (SW90 in the haunch zone) for the buried concrete pipes under total load. This means that these conditions will not significantly affect the total load bedding factor values.

It can be seen from Figure 5.12 that for the good installation condition, increasing the backfill height increases the total load bedding factor; whereas the relationship of the bedding factor with the backfill height for the poor installation condition (Figure 5.13) depends on the pipe diameter. The difference in the trend behaviour of the bedding factor between the poor and good installation conditions is due to the independency of the laboratory force calculated following the BS method (Equation 1.1) on the installation condition, where Equation 1.1 assumes that the maximum force will always be at the pipe crown. Therefore, the laboratory bending moment will be the same for both installation conditions; while the field bending moment (obtained from the finite element modelling) is significantly affected by the support condition.

It can also be seen for both installation conditions that increasing the diameter of the pipe increases the total load bedding factor. This is due to the oversimplification in the design force calculation (Equation 1.1); where in Equation 1.1 the maximum vertical soil pressure at the pipe crown is multiplied by the pipe diameter to convert the soil pressure into a line load. This oversimplification leads to a very high value of

the laboratory bending moment (M_{lab}) ($M_{lab} = 0.318 \times W_t \times r$), as the diameter of the pipe increases and hence provides a higher total load bedding factor value because of the significant increase of the laboratory bending moment term in the bedding factor equation (Equation 4.1).

The total load bedding factors obtained in this study were used to investigate the robustness of the design standard by calculating the ratio of the obtained total load bedding factor (BF(FEM)) to the design bedding factor (BF(BS)). The BS bedding factors were calculated using Table 1.2. A value of 1.9 was considered for the good installation condition, as it is similar to a class B installation, and a value of 1.1 was considered for the poor installation condition, as the poor installation modelled in this chapter is similar to classes N and DD (i.e. where the pipe is installed directly on a stiff soil with poor support in the haunch zone).

Figures 5.14 and 5.15 show the calculated ratio for pipes with wall thicknesses from Table 5.1, for good installation and poor installation conditions, respectively. It can be seen from the figures that the BS bedding factors are overly conservative for both installation conditions, where the ratio of the obtained to design bedding factor ranges from 1.63 to 4.92 for the good installation and from 2.45 to 4.68 for the poor installation conditions. This is resulting from the oversimplification in the method used in the BS for calculating the force applied on the pipe, as mentioned previously, where the BS method estimates the design force by multiplying the maximum soil pressure at the crown of the pipe by the diameter of the pipe. This means that the BS method assumes the vertical soil pressure over the top half of the pipe will be equal to the maximum soil pressure at the pipe crown. However, the maximum vertical soil

pressure over the top half of the pipe is significantly affected by the angle from the crown, as shown in Figures 5.16, 5.17, 5.18 and 5.19. These figures show the total vertical pressure applied over the top half of pipes with a backfill height of 1.0 m buried in a good installation condition, calculated using the BS method and the finite element analyses for pipes with an internal diameter of 0.3 m, 0.6 m, 1.2 m and 2.4 m, respectively. It can be seen from these figures that although the BS method underestimates the maximum vertical soil pressure for all of the considered diameters, it also assumes a uniform soil pressure over the top half of the buried pipe. This assumption produces a very high design force and hence very high bending moments in the laboratory test. Furthermore, converting the force applied over the top half of the pipe to a line load and using this force in the laboratory test is not correct, especially for the good installation condition, because this assumption concentrates all of the force in the pipe crown. However, the soil pressure in reality is applied over the entire top half of the pipe, including the crown and the shoulders of the pipe. Hence, it will affect the entire top half of the pipe and not only the crown. Therefore, it can be concluded that this methodology does not truly simulate the actual scenario and leads to an over conservative design.

As a result, a solution to these significant issues in the methodology of the load calculation is required to make sure that the design of the rigid buried pipes is robust and economic. However, any modified solution needs to be practical and related to the three-edge bearing test, as this is the only available method to test the quality of the pipe. Thus, proposing new total load bedding factors based on the results of this study would improve the design methodology and implicitly account for the issues demonstrated previously; hence, a robust and economical design of concrete pipes

would be possible. The EPR was therefore employed to derive explicit and concise mathematical models for the total load bedding factor, as the relationships of the calculated total load bedding factor are complicated and significantly affected by the pipe diameter, backfill height, pipe thickness and installation conditions, as discussed previously. The development of the bedding factor models are discussed in the next section.

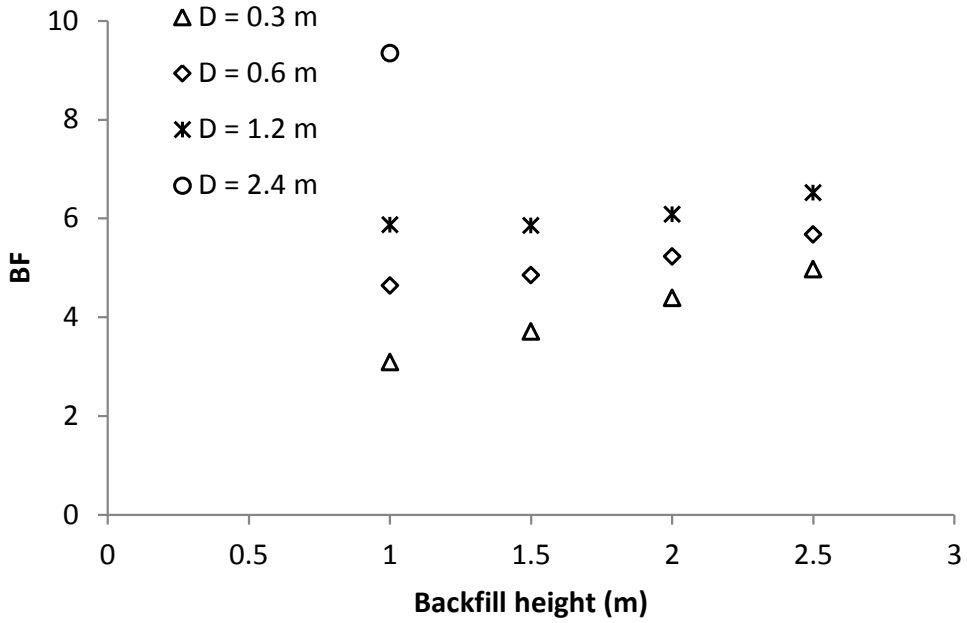

Figure 5.12: Calculated total load bedding factor for pipes with sizes as in Table 5.1 for the good installation (SW90 in the haunch zone)

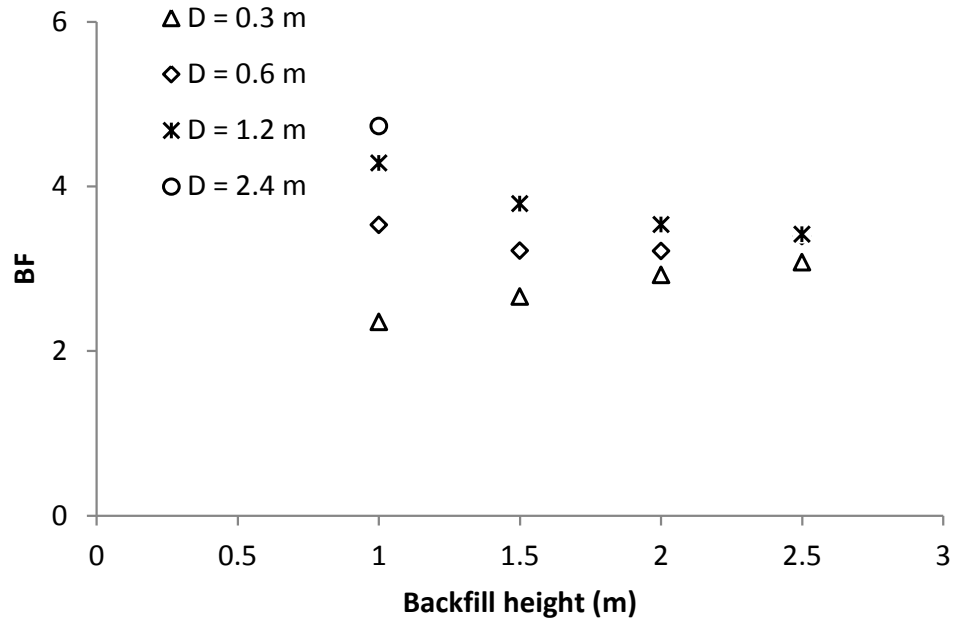

Figure 5.13: Calculated total load bedding factor for pipes with sizes as in Table 5.1 for the poor installation (ML49 soil in the haunch zone)

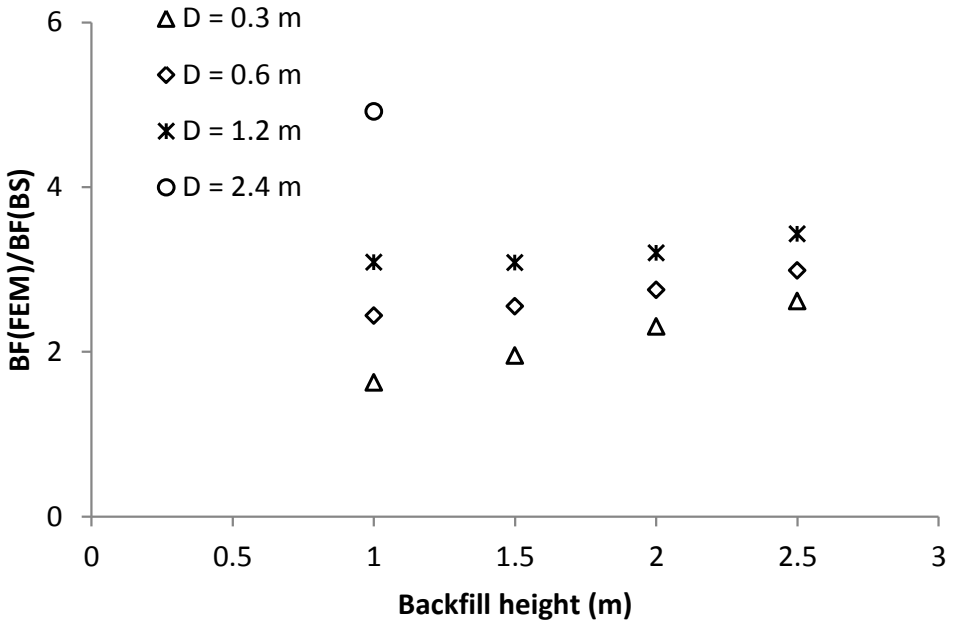

Figure 5.14: Ratio of total load bedding factors obtained from the numerical modelling and the BS values for the good installation

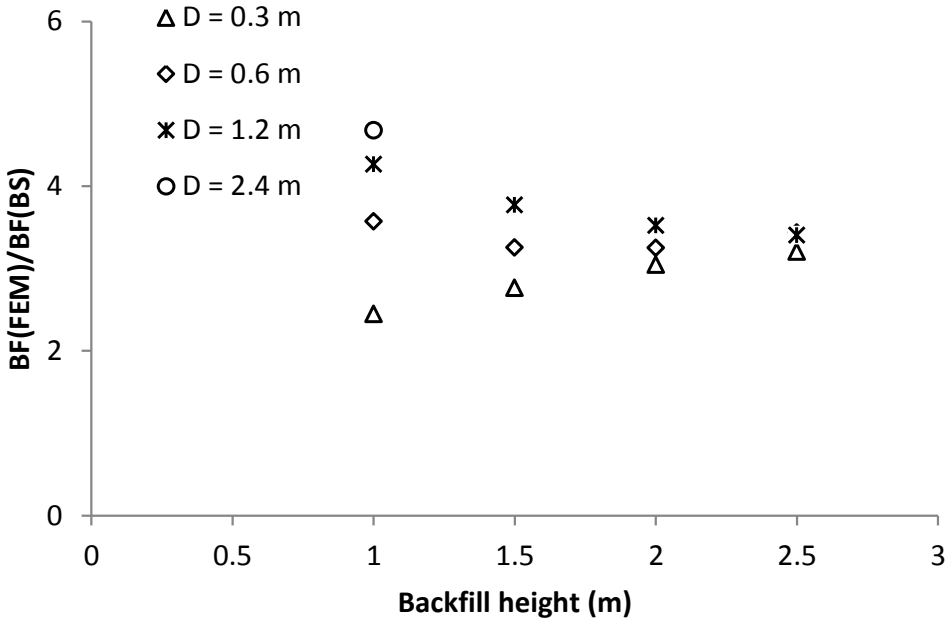

Figure 5.15: Ratio of total load bedding factors obtained from the numerical modelling and the BS values for the poor installation

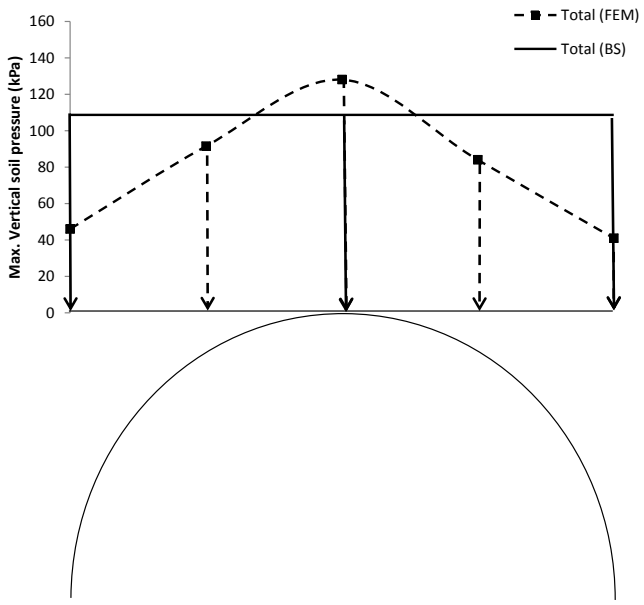

Figure 5.16: The BS and finite element analysis results of the total maximum vertical soil pressure applied over the top half of the pipes buried in the good installation condition with a backfill height of 1.0 m for an inside diameter of 0.3 m

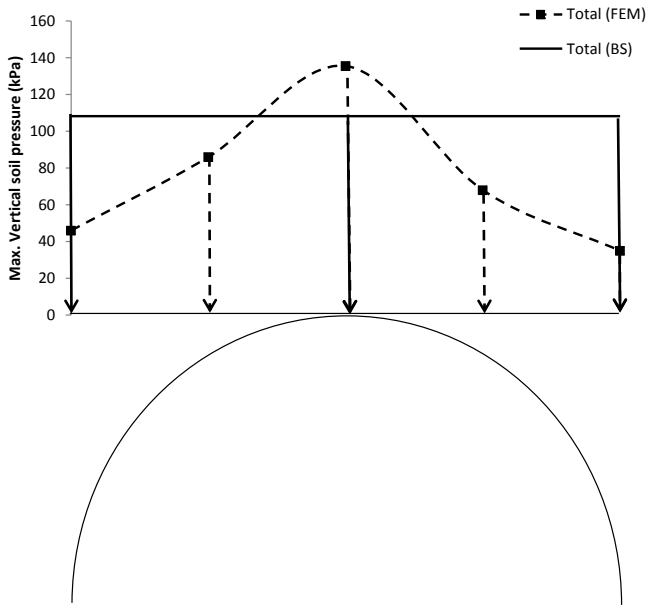

Figure 5.17: The BS and finite element analysis results of the total maximum vertical soil pressure applied over the top half of the pipes buried in the good installation condition with a backfill height of 1.0 m for an inside diameter of 0.6 m

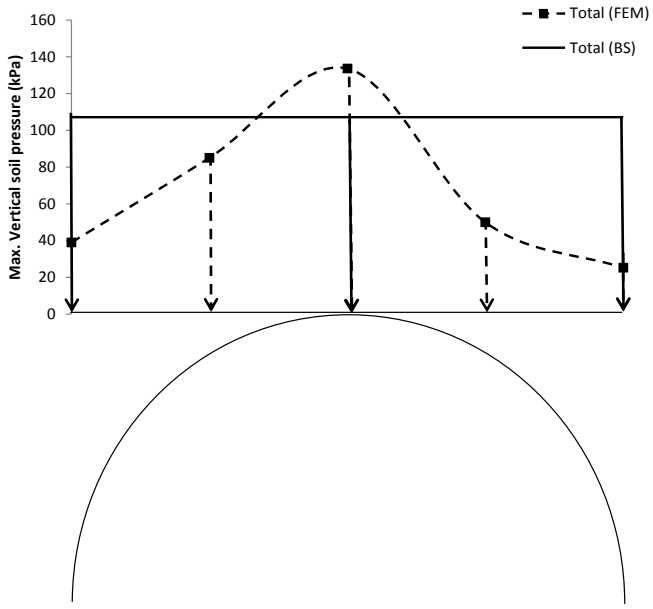

Figure 5.18: The BS and finite element analysis results of the total maximum vertical soil pressure applied over the top half of the pipes buried in the good installation condition with a backfill height of 1.0 m for an inside diameter of 1.2 m

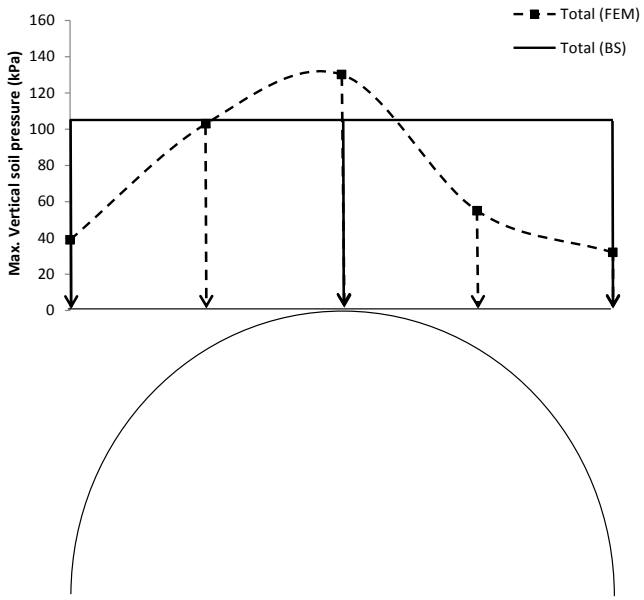

Figure 5.19: The BS and finite element analysis results of the total maximum vertical soil pressure applied over the top half of the pipes buried in the good installation condition with a backfill height of 1.0 m for an inside diameter of 2.4 m

5.5. Development of the total load bedding factor model

5.5.1. Modelling the total load bedding factor

The results of the parametric study showed that the total load bedding factor is significantly affected by the pipe diameter, pipe wall thickness and backfill height. Therefore, incorporating all of these parameters is necessary to ensure that the developed models are robust and representative. Hence, all of the bedding factor data were used to develop the bedding factor model for each installation condition (i.e. good and poor installation conditions). The data are divided into training data (80%) and validation data (20%). An effort was made to carefully divide the data into training and validation data sets with comparable general statistical characteristics. Table 5.3 shows the standard deviation ($STDV$), maximum (max), minimum (min)

and mean ($mean$) values for the data used for the training, validation and all the data used in the modelling for both the good and poor installation conditions.

Several attempts were made to obtain a mathematical expression with a very high accuracy by trying different exponents for the developed mathematical expression, different function types and different number of terms. In every attempt, the EPR changes the exponent of the independent parameters based on the genetic algorithm and the range specified initially; solves the mathematical system using the least squares method; and finally calculates the coefficient of determination (CD) (Equation 3.13). As the number of iterations increases, the EPR learns the best exponent arrangement. Subsequently, the EPR increases the number of terms and repeats the aforementioned procedure until it reaches the maximum number of terms. Ultimately, the EPR reports the final models with the CD value for the training and validation data.

It was found that as the number of terms increases, the CD value also increases. This observation is similar to that noticed in the EPR modelling of the soil load bedding factor reported previously in Section 4.4.1. However, increasing the number of terms increases the model complexity and increases the possibility of overfitting. Therefore, the selection of the models was done based on the model simplicity and the ability of the model to represent the trend behaviour of the input data. The ability to replicate the trend behaviour was checked by carefully comparing the results of the developed models with the original data. The simplest model, which was able to reasonably replicate the trend, was selected for each installation condition. Equations 5.1 and

5.2 show the selected models for the good and poor installation conditions, respectively.

$$BF = -0.21 \times \frac{1}{\sqrt{D} \times \sqrt{t}} + 6.15 \times \frac{\sqrt{t} \times \sqrt{H}}{\sqrt{D}} + 0.017 \times \frac{D^2 \times \sqrt{H}}{t^2} + 0.35 \times \frac{D^2}{\sqrt{t} \times H^2} + 1.52 \quad (5.1)$$

$$BF = -0.13 \times \frac{1}{\sqrt{t} \times D \times H^2} + 9 \times \frac{t}{D} + 0.15 \times \frac{D}{t \times H^2} + 0.007 \times \frac{D^2}{t^2} + 1.55 \quad (5.2)$$

Figures 5.20 and 5.21 compare the finite element results with the EPR model results for both the training and validation data for the good installation and poor installation, respectively. Furthermore, Table 5.4 presents the CD value for the training and validation data for both models. Figures 5.20 and 5.21, together with Table 5.4, illustrate that the models developed using this procedure are able to predict the bedding factor with a very high accuracy.

Table 5.3: Statistics for the data used in the EPR analysis

		Good installation				Poor installation			
		D (m)	t (m)	H (m)	BF	D (m)	t (m)	H (m)	BF
Training data	$Mean$	0.8	0.11	1.66	6.63	0.8	0.100	1.72	4.07
	Min	0.3	0.026	1.00	3.09	0.3	0.026	1.00	2.35
	Max	2.4	0.458	2.50	16.38	2.4	0.458	2.50	8.06
	$STDV$	0.6	0.090	0.58	2.77	0.6	0.090	0.59	1.17
Validation data	$Mean$	0.9	0.120	1.81	6.50	0.9	0.150	1.57	3.49
	Min	0.3	0.026	1.00	3.36	0.3	0.026	1.00	2.44
	Max	2.4	0.254	2.50	13.07	2.4	0.254	2.50	4.73
	$STDV$	0.7	0.090	0.59	3.21	0.7	0.100	0.53	0.80
All data	$Mean$	0.8	0.110	1.69	6.60	0.8	0.110	1.69	3.96
	Min	0.3	0.026	1.00	3.09	0.3	0.026	1.00	2.35
	Max	2.4	0.458	2.50	16.38	2.4	0.458	2.50	8.06
	$STDV$	0.6	0.090	0.58	2.82	0.6	0.090	0.58	1.13

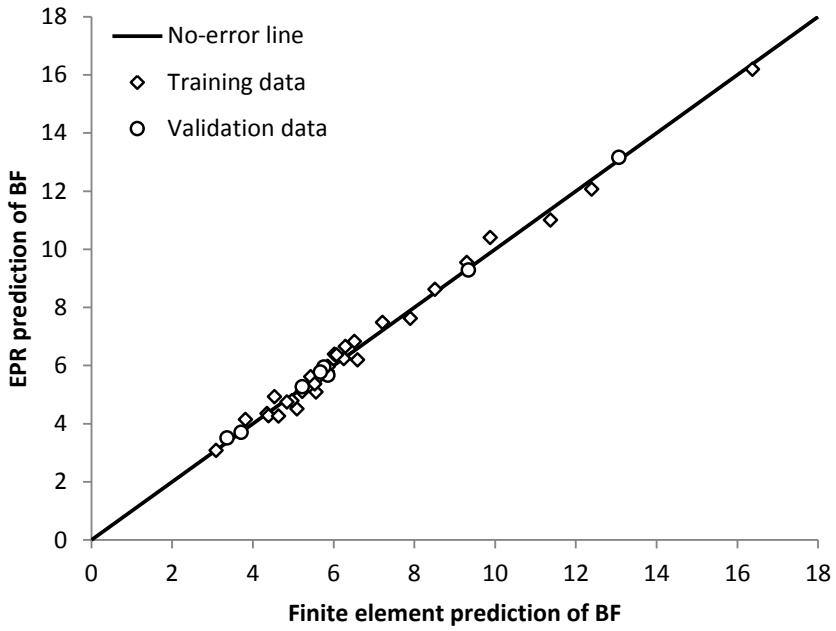

Figure 5.20: EPR predicted total load bedding factors compared to the finite element results for the good installation

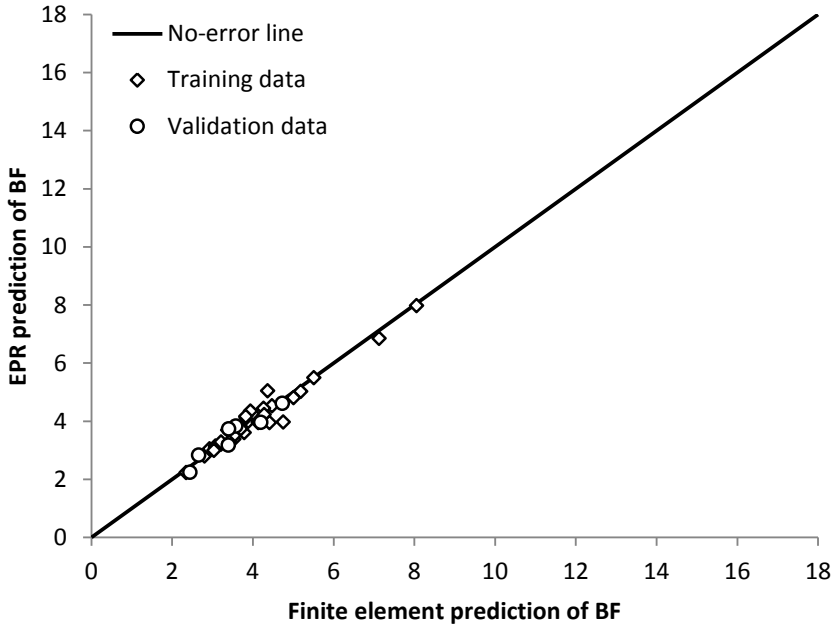

Figure 5.21: EPR predicted total load bedding factors compared to the finite element results for the poor installation

Table 5.4: Coefficient of determination (CD) for the training and validation data (%)

Data set	Good installation	Poor installation
Training	98.97	94.41
Validation	99.41	89.64

5.5.2. Sensitivity analysis

A sensitivity analysis has been conducted by comparing the trend behaviour of the developed models with that discussed in Section 5.4, in order to develop additional confidence in the predictive ability of these models.

Figures 5.22 and 5.23 show the results of the comparison of the calculated (using finite element modelling) and predicted (using EPR) total load bedding factor values

for all of the considered diameters and backfill heights for both the good and poor installation conditions, respectively. It can be seen from Figure 5.22 that the developed model for the good installation is able to predict the trend behaviour observed and discussed in Section 5.4, where increasing the pipe diameter and the backfill height increases the total load bedding factor. Figure 5.23 shows that the developed model for the poor installation is able to model the dependency of the total load bedding factor-backfill height relationship on the pipe diameter. Hence, these models can be used with confidence to overcome the oversimplifications in the design standard and ensure robust and economical designs. It should be noted, however, that these models have been derived and tested using pipes with an inside diameter range of 0.3 m to 2.4 m. Therefore, the use of these models for predicting the total load bedding factor of pipes outside this diameter range is not recommended and may cause significant errors.

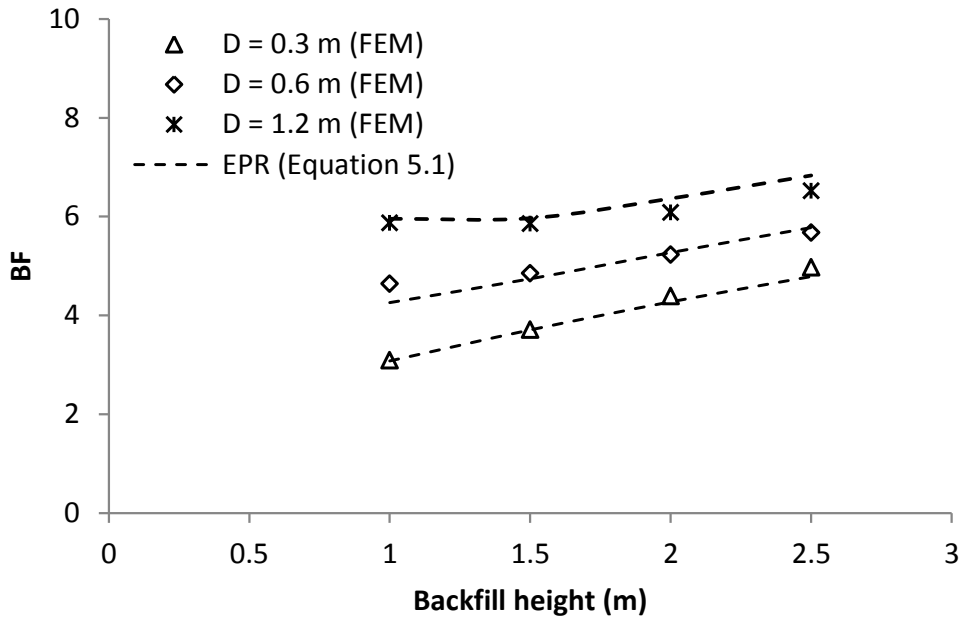

Figure 5.22: The results of the sensitivity analysis for the good installation

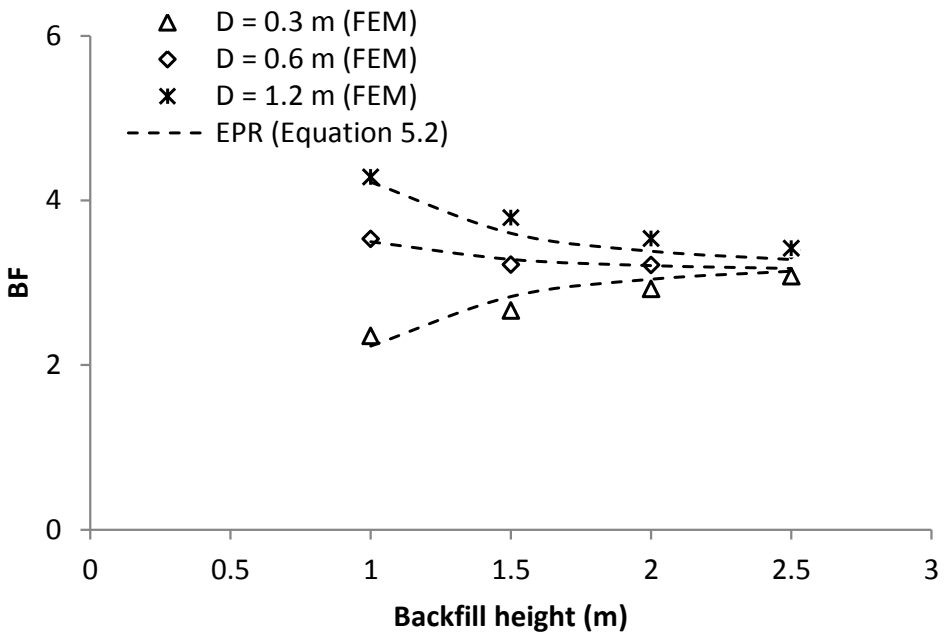

Figure 5.23: The results of the sensitivity analysis for the poor installation

5.6. Summary

This chapter has investigated the effect of the MR-BSI traffic loading on the behaviour and the design of buried concrete pipes. A detailed parametric study has been conducted to investigate the response of buried concrete pipes under traffic loading using robust three-dimensional finite element analysis.

The results of the parametric study illustrated the direct relationship between the pipe diameter and the effect of the traffic load. In addition, the backfill height limit to the effect of the traffic loading was found to be significantly affected by the pipe diameter. Furthermore, the results showed the significant effect of the installation condition and pipe wall thickness on the response of the buried concrete pipe. Hence, the results illustrated the need to consider the effect of the pipe diameter, backfill height, pipe wall thickness and installation condition in the analysis and design of buried pipes.

Lastly, the design methodology of the BS was investigated, where the issues with the current BS design methodology have been demonstrated. As a result, new total load bedding factor models have been developed to overcome the issues in the BS design methodology. The new models enable a more economical and robust design of buried concrete pipes within the ranges used to develop these models.

Chapter 6
RESPONSE OF BURIED PVCu PIPES UNDER TRAFFIC LOADING

6.1. Introduction

Flexible pipes are widely used for transporting potable water, storm water and waste water (Balkaya et al., 2012a; Chaallal et al., 2015b; Mohamedzein and Al-Aghbari, 2016). Hence, these pipes are likely to be subjected to loads if buried at shallow depth due to the backfill soil weight and traffic activities. Thus, a comprehensive understanding of the behaviour of these pipes with good and poor installation conditions is very important to achieve a robust design. This chapter therefore focuses on improving the current state of the art of buried flexible pipes, based on the gaps in the knowledge discussed in Section 2.3.4, by investigating the following aspects:

1- The effect of pipe diameter, backfill height and traffic load on the behaviour of the buried polyvinyl chloride (PVCu) pipes with good installation.
2- The impact of the poor installation (poor haunch support) on the behaviour of the PVCu pipes under traffic load.
3- Compare the results of both good and poor haunch support with the design limits specified in the BS (BSI, 1997; BSI, 2010) to investigate the performance of pipes according to the BS design standard, and hence make the results from this research useful in practice for designing buried flexible pipes.
4- Improve the design methodology of the BS to account for the effect of poor haunch support and ensure more robust and safe designs, as the poor haunch

support is expected in practice (Boschert and Howard, 2014; Turney et al., 2015). Hence, the effect of the poor haunch support should be accounted for when designing buried flexible pipes.

Firstly, the effect of the truck position and direction with respect to the buried flexible pipe is studied. The critical loading condition is then used in a comprehensive parametric study to investigate the behaviour of the buried pipes and the performance of the pipes based on the BS for good installation (good haunch support) and poor installation (poor haunch support). The results are then used to incorporate the effect of the poor haunch support in the BS design methodology. Finally, the chapter ends with a summary of the key findings of this study. It is important to mention that the analysis time for the models considered in this chapter ranged from 20 to 60 minutes, depending on the pipe diameter and the backfill height.

6.2. Load configuration and critical load condition

The critical load condition of the main road BS (MR-BSI) traffic load for the buried flexible pipes was investigated firstly to make sure that the subsequent analyses consider the worst-case scenario. It was felt necessary to study the effect of the truck position and distance with respect to the buried flexible pipe and to not depend on the critical load condition obtained for the buried concrete pipe (detailed in Section 5.2), because the behaviour of the buried flexible pipe is different from that of the concrete pipe, as discussed previously in Section 1.3.

The cases of a truck travelling parallel and perpendicular to the pipeline axis were investigated at different S values, similar to that conducted in Section 5.2, as shown in Figure 5.1 (refer to Section 5.2 for more details).

The material properties of the surrounding soil, bedding soil, backfill soil and pipe, which are mentioned in validation problem 4, are used in this analysis with a backfill height of 0.5 m. This was considered in order to allow a direct comparison with the behaviour of the buried flexible pipe under two AASHTO trucks, which was investigated in validation problem 4. For each case, the maximum principal stress and maximum horizontal (at the pipe springline) and vertical (at the pipe crown) displacement of the pipe were recorded.

Figure 6.1 shows the maximum horizontal (at the pipe springline) and vertical displacement (at the pipe crown) and maximum principal stress of the pipe for different S values for the case of a truck moving parallel to the pipeline axis (Figure 5.1(b)). It can be seen that the maximum horizontal and vertical displacement are equal to 2.18 mm and 6.78 mm when S = 0.00 m. In addition, the maximum principal stress was also obtained when S = 0.00 m and is equal to 3,707 kN/m^2.

Figure 6.2 shows the maximum horizontal (at the pipe springline) and vertical displacement (at the pipe crown) and the maximum principal stress of the pipe for different S values for the case of a truck moving perpendicular to the pipeline axis (Figure 5.1(c)). It can be seen that the maximum vertical displacement and principal stress in the pipe were obtained when the centre of the right-hand axle was above the crown (S = 0.00 m) and are equal to 10.10 mm and 4,743 kN/m^2, respectively. However, the maximum horizontal displacement of 3.90 mm was recorded when the

centre of the right-hand axle was 0.25 m away from the crown of the pipe ($\boldsymbol{S}$ = 0.25 m).

It can be concluded from these figures that the highest vertical and horizontal displacements in the pipe are obtained when the truck is moving perpendicular to the pipeline axis and the critical case is obtained when the centre of the right-hand axle is above the crown of the pipe. This is because of the dependency of the pipe behaviour on the surrounding soil stiffness (Rogers 1987; Rogers et al., 1996; Chapman et al., 2007) and the dependency of the soil stiffness on the stress level. The confining pressure in the soil adjacent to the sides of the pipe is larger for the cases where the pipe is between the two axle loads because of an increase in the stress level, which increases the stiffness of the soil adjacent to the sides of the pipe. Increasing the soil stiffness increases the side support on the pipe and hence, the settlement and the pipe wall stress will be smaller. However, for the case where one axle is directly above the pipe, the stress level will not distribute equally around the pipe and the soil stiffness will be smaller. Furthermore, the stress level on the crown of the pipe will be larger when the axle load is directly above the pipe.

These results are in agreement with the findings from Chaallal et al. (2015a), who observed from a field test involving a flexible pipe under two axle loads that the worst-case for the pipe was when one of the axles was directly above the pipe.

Comparing the results of the critical case of the MR-BSI traffic load and the case of the two axles of the two HS20 design trucks (from validation problem 4) shows that the MR-BSI traffic load is much more stringent with the calculated horizontal and

vertical displacements under the MR-BSI traffic load, being 195% and 153% higher, respectively.

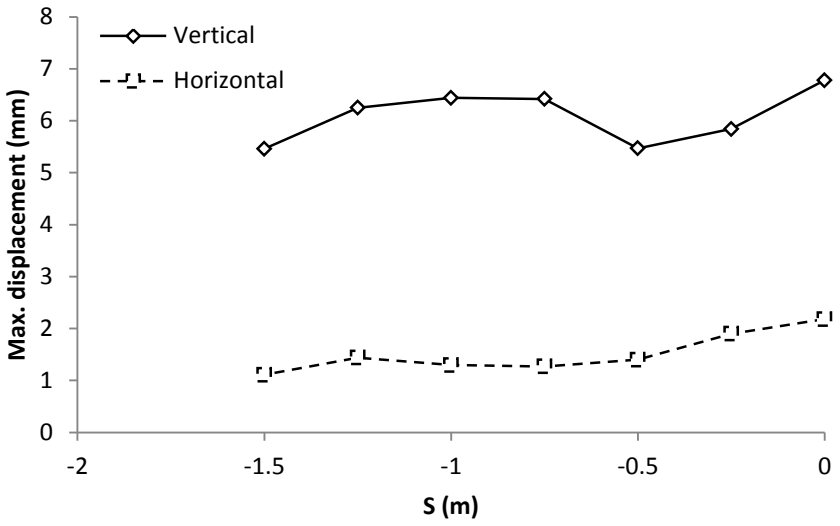

(a)

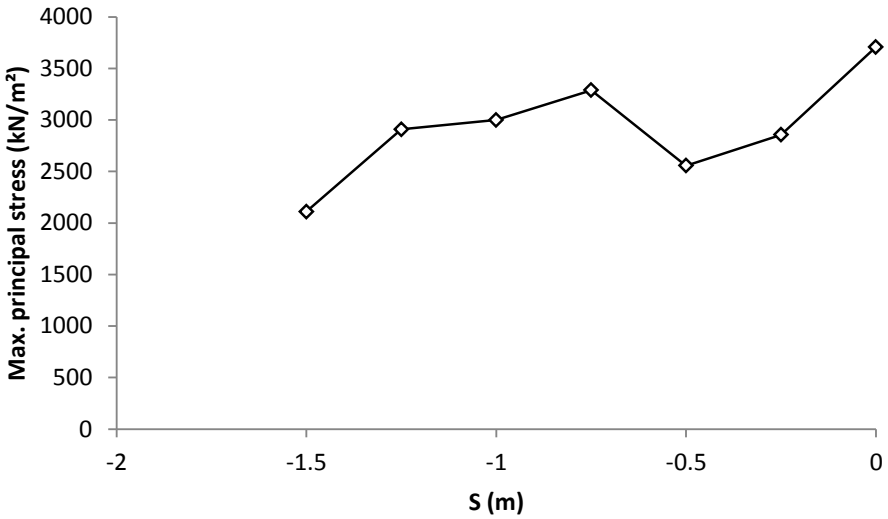

(b)

Figure 6.1: Results from the analysis of the pipe for the case of the MR-BSI traffic load travelling parallel to the pipeline axis with different S values: (a) maximum vertical (at the pipe crown) and horizontal (at the pipe springline) displacement; (b) maximum principal stress

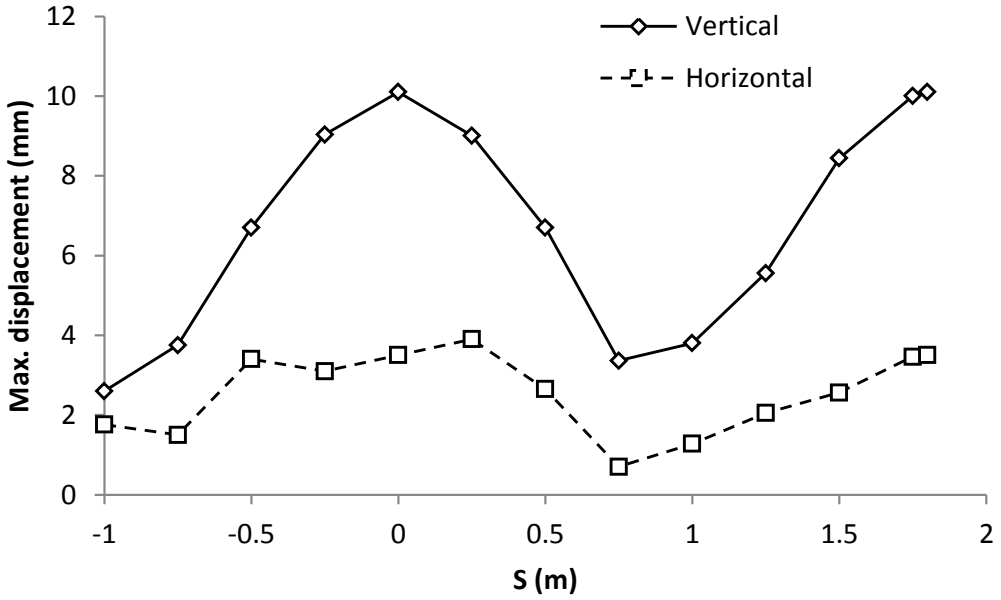

(a)

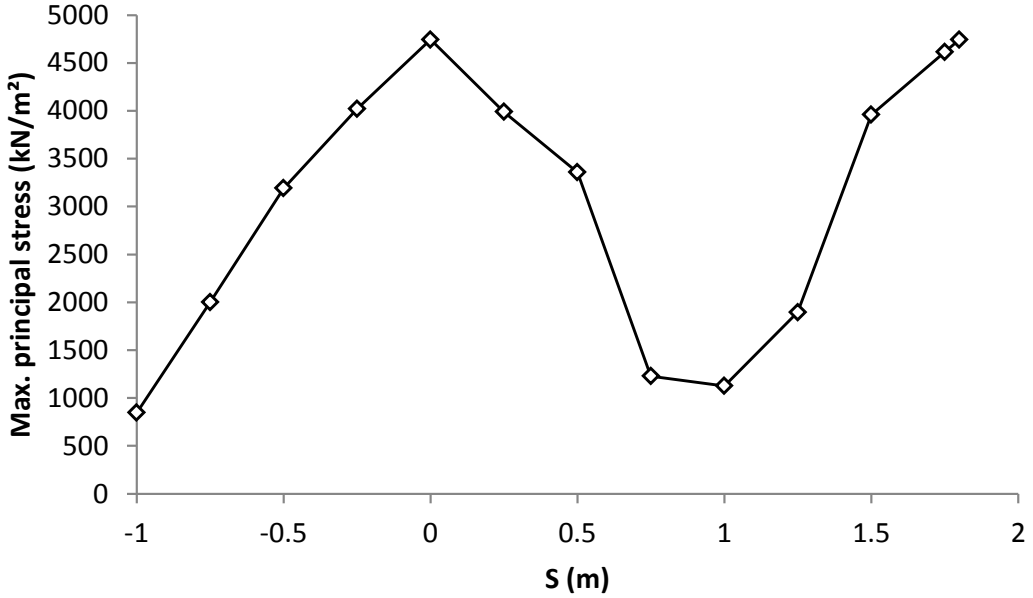

(b)

Figure 6.2: Results from the analysis of the pipe for the case of the MR-BSI traffic load travelling perpendicular to the pipeline axis with different S values: (a) maximum vertical (at the pipe crown) and horizontal (at the pipe springline) displacement; (b) maximum principal stress

6.3. Material properties of the soil and pipe and the pipes' diameters

The SW90 was considered for the backfill, haunch zone (for the models with good installation) and bedding soils. This soil type was chosen to simulate a pipe buried in a good quality backfill material (Chaallal et al., 2015a). The assumption of a stiff bedding layer was made to simulate the expected worst-case scenario where the pipeline is laid directly on to a native over-consolidated soil (similar to the assumption made in **Chapter 5**). The poor installation has been simulated by using the ML49 in the haunch zone. The material properties of the trench soils (SW90 and ML49) are taken from the literature (Boscardin et al., 1990), while the *in situ* soil was assumed to be stronger than the backfill soil (similar to the assumption made in **Chapter 5**). The material properties of the SW90 and ML49 soils can be found in Table 4.2.

The long-term material properties of the PVCu material were considered in this study as these properties represent the worst-case scenario (i.e. lower yield stress and critical buckling pressure). The PVCu material properties (modulus of elasticity (E), Poisson's ratio (υ) and tensile yield stress), pipe diameters and pipe wall thicknesses were adopted from the literature (Petersen et al., 2010; AASHTO, 2013) and are shown in Table 6.1. The tensile yield stress of the PVCu material (shown in Table 6.1) is usually considered as the yield stress for both tension and compression when calculating the factor of safety in the design practice of flexible pipes (Katona, 1990; AASHTO, 2013); although, the compressive strength of the PVCu material is higher (Ognedal et al., 2012; Mohamedzein and Al-Aghbari, 2016). This consideration is accepted in the pipeline industry to add additional conservatism to the design of flexible pipes (Katona, 1990). Therefore, the tensile yield stress has also been

considered as the yield stress for both tension and compression. The critical buckling pressure for each pipe was calculated using Equation 1.11 as recommended by the BS (i.e. assuming the condition of an unsupported pipe) and is also shown in Table 6.1.

The boundary conditions, the elements' types, the element sizes and the modelling steps were the same as for validation problem 4. The following sections discuss the results of the parametric study.

Table 6.1: Diameters, thicknesses and material properties of the pipes used in this study

Inside diameter (D) (m)*	Wall thickness (t) (m)*	Critical buckling pressure (kPa)**	E (kPa)*	υ*	Yield stress (kPa)***
0.3	0.036	1726	689,000	0.35	17,237
0.6	0.061	916			
0.9	0.070	588			
1.3	0.089	369			

* adopted from Petersen et al., (2010)

** calculated using Equation 1.11

*** adopted from AASHTO (2013)

6.4. Results of good installation

The behaviour of the pipe with good installation was considered first to understand the impact of the pipe diameter, backfill height and traffic load on the response of the PVCu pipe; and hence provide a comprehensive understanding before studying the effect of the poor installation. A minimum backfill height of 1.0 m was considered as it

is the minimum accepted backfill height for the buried pipes under the MR-BSI traffic loading condition (HA, 2001). The results of this section are divided into three subsections covering the maximum soil pressure, the vertical displacement of the pipe crown and the pipe wall stress.

6.4.1. Maximum soil pressure

Figure 6.3 shows the maximum vertical soil pressure applied at the pipe crown due to the backfill soil weight only. It can be clearly seen from the figure that increasing the backfill height linearly increases the maximum soil pressure due to the increase of the soil weight above the pipe. It can also be observed that increasing the diameter of the pipe decreases the maximum soil pressure. This is due to the decrease in the pipe stiffness as the diameter of the pipe increases; which in turn reduces the percentage of load attracted by the pipe as a result of soil arching (Moore, 2001; Kang et al., 2007).

Figure 6.4 shows the maximum soil pressure at the crown of the pipe due to the MR-BSI traffic load only. The soil pressure for each case has been obtained by subtracting the maximum soil pressure due to backfill soil weight only at the pipe crown from the maximum soil pressure due to total load (combined backfill soil weight and traffic load). The predicted maximum soil pressure from the BS equation (BSI, 2010) (Equation 1.13) is also shown in this figure. It can be seen that the maximum soil pressure due to the effect of traffic load only decreases nonlinearly as the backfill height increases. The percentage decrease in the tyre stress (i.e. 904 kPa) for a backfill height of 1.0 m is equal to 91%, 89%, 88% and 88% for pipe inside diameters of 0.3 m, 0.6 m, 0.9 m and 1.3 m, respectively. This reveals that approximately 90%

of the tyre stress is reduced at a backfill height of 1.0 m. For a backfill height of 3.0 m, the percentage decrease is equal to 99%, 98%, 98% and 97% for pipe diameters of 0.3 m, 0.6 m, 0.9 m and 1.3 m, respectively. It can also be seen that the effect of the traffic load ends at a backfill height of 4.5 m. Similar observations were also found by Bian et al. (2012) from a full-scale study on the effect of truck loads on an arched concrete culvert (width of 3.5 m and height of 2.5 m) buried in a poorly-graded gravel with a backfill height ranging from 0.5 m to 3.5 m. Bian et al. (2012) noticed that the tyre stress decreased by 91% at a depth of 1.0 m below the ground surface.

Comparing the results of the maximum soil pressure under traffic load only with the BS equation (Equation 1.13) shows in general, that the equation underestimates the soil pressure at a backfill height of 1.0 m and overestimates the soil pressure at a backfill height equal to or greater than 2.0 m. The ratio between the soil pressure predicted from the numerical modelling and the soil pressure calculated from Equation 1.13 varies between 1.05 and 0.24 for the 0.3 m diameter pipe, 1.33 and 0.34 for the 0.6 m diameter pipe, 1.35 and 0.37 for the 0.9 m diameter pipe and 1.37 and 0.40 for the 1.3 m diameter pipe.

Figure 6.5 shows the maximum vertical soil pressure applied at the pipe crown due to total load. The figure shows that the maximum vertical soil pressure decreases nonlinearly then increases approximately linearly. This is because of the interaction of both the weight of the backfill above the pipe and the traffic load; where the traffic load significantly influences the maximum soil pressure. However, as the backfill height increases, the influence of the traffic load significantly decrease; which in turn impacts on the maximum soil pressure.

Figure 6.6 shows the factor of safety against buckling obtained by dividing the critical buckling pressure (shown in Table 6.1) by the maximum soil pressure at the crown of the pipe obtained from the modelling (Figure 6.5). It can be seen that although the critical buckling pressure for the unsupported pipes was used, the factor of safety is very high for all the cases with a minimum value of 3.10. This indicates that the pipes are safe against buckling for the good installation conditions, as the obtained factor of safety is higher than the BS minimum requirement (i.e. higher than 2).

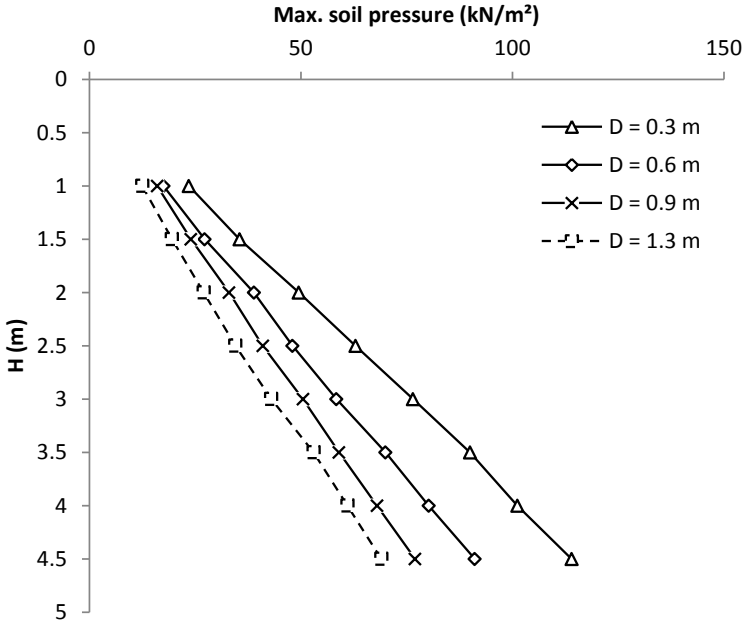

Figure 6.3: Maximum soil pressure at the crown of the pipe under the backfill soil weight only

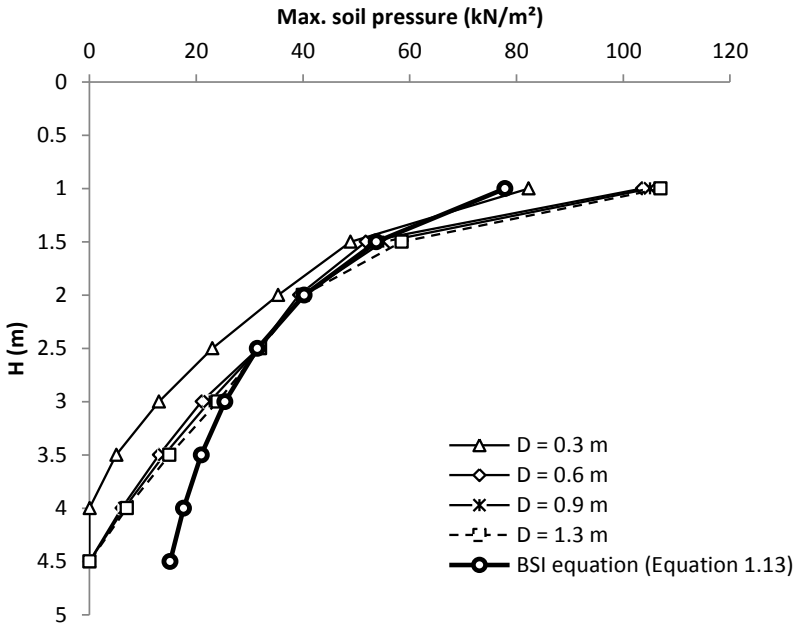

Figure 6.4: Maximum soil pressure at the crown of the pipe under the MR-BSI traffic load only

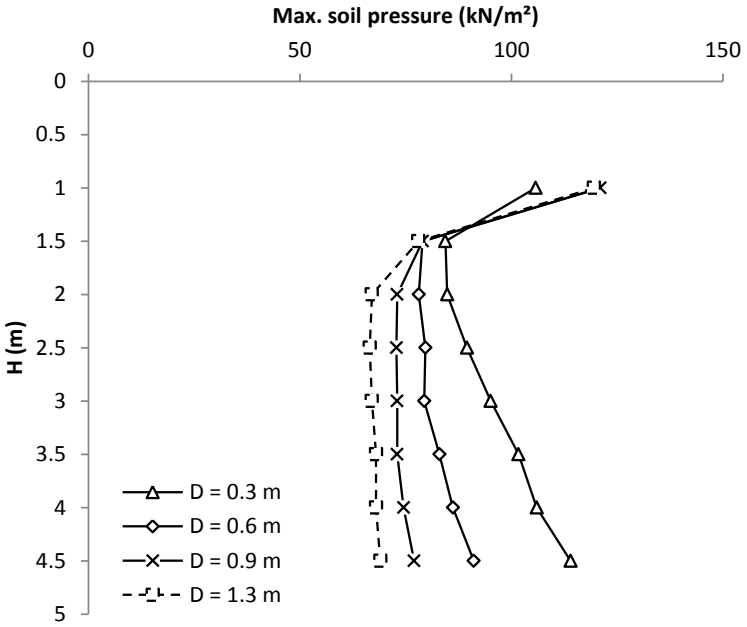

Figure 6.5: Maximum soil pressure at the crown of the pipe under the total load

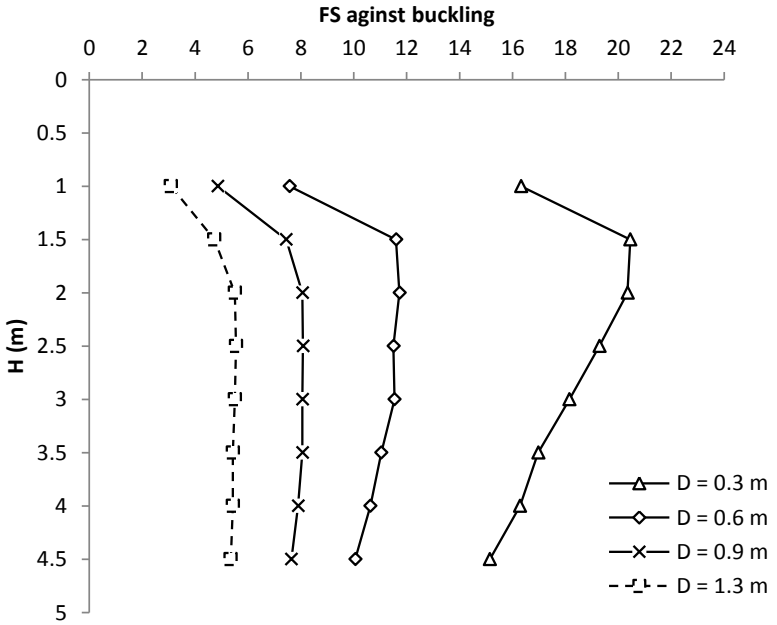

Figure 6.6: Factor of safety against buckling for buried PVCu pipes with good haunch support and subjected to the total load

6.4.2. Pipe crown vertical displacement

Figure 6.7 shows an example of the deformed shape of the pipe due to the application of the total load for the case of a pipe with an inside diameter of 1.3 m, buried with a backfill height of 1.0 m. It can be seen that the pipe is deformed into a heart shape. This heart shape has been formed due to the significant increase in the soil pressure at the crown of the pipe as a result of the application of the traffic load. However, it can also be seen that the deformed shape is not symmetric. This is due to the non-uniformity of the traffic load applied on the surface, where the critical loading condition was used, as mentioned previously. This gives additional confidence in the validity of the numerical methodology adopted in this research, where other experimental studies have also reported the same deformed shape for

plastic pipes under the surface load effect (Chapman et al., 2007; Chaallal 2015a). This observation is also in agreement with the hypothesis proposed by Rogers (1988) for the behaviour of buried flexible pipes under applied loads (discussed in Section 2.3.3).

Figure 6.8 shows the crown vertical displacement for all of the considered cases due to the application of the total load. It can be seen that the crown vertical displacement follows the same trend observed for the maximum soil pressure, where the vertical displacement decreases nonlinearly as the backfill height increases and then increases. Again, this is due to the interaction effect of the backfill weight and traffic load and the decrease in the effect of the traffic load as the backfill height increases. It can also be noticed that increasing the diameter of the pipe increases the crown vertical displacement. This is due to the significant decrease in the pipe stiffness as the diameter increases, where the pipe becomes more responsive to the applied load as the stiffness decreases. These results are in agreement with the experimental finding reported by Sargand et al. (2001a), where they found that increasing the diameter of the flexible pipe increases the crown vertical displacement.

Figure 6.9 presents the normalized vertical displacement (i.e. ratio of the maximum pipe displacement to the pipe inside diameter) for all of the considered scenarios. It is shown that the normalized vertical displacement is less than 5.00% for all of the considered cases; where the maximum normalized vertical displacement is 1.05%, recorded for the smallest pipe diameter (D = 0.3 m) with a backfill height of 1.0 m. This gives a minimum factor of safety of 4.76 (i.e. 5.00%/1.05%) for the pipe

displacement limitation based on the minimum BS requirements (5.00%) for safe performance of buried flexible pipes.

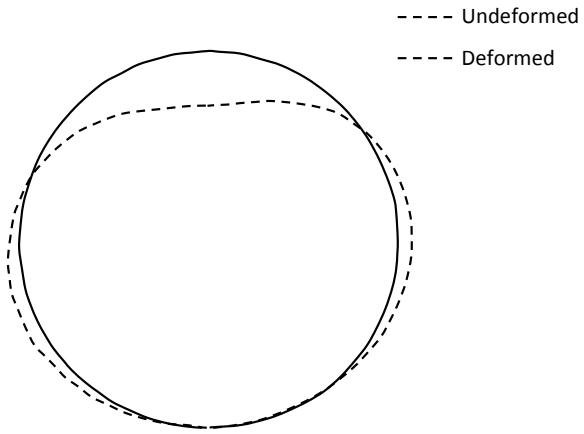

Figure 6.7: Deformed shape of the PVCu pipe due to the total load (pipe with an inside diameter of 1.3 m and a backfill height of 1.0 m) (Note: the deformed shape is magnified by a factor of 47)

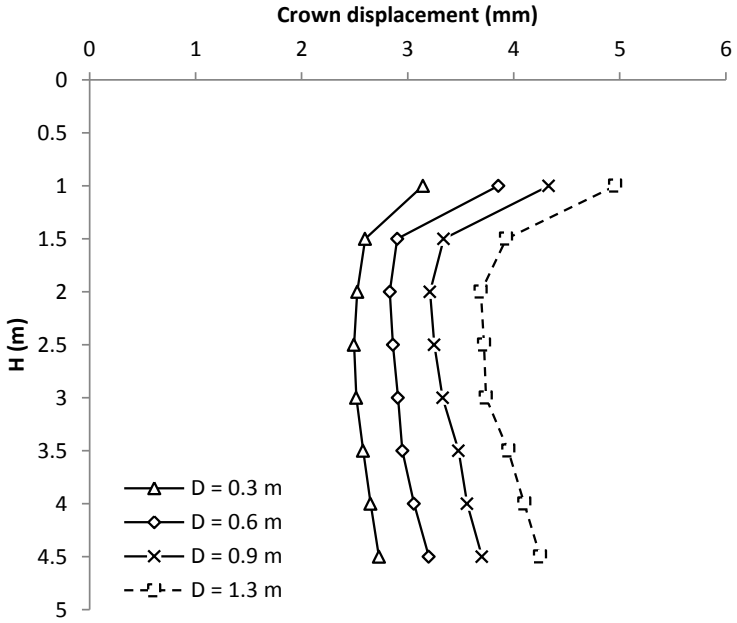

Figure 6.8: PVCu pipe crown vertical displacement under the total load

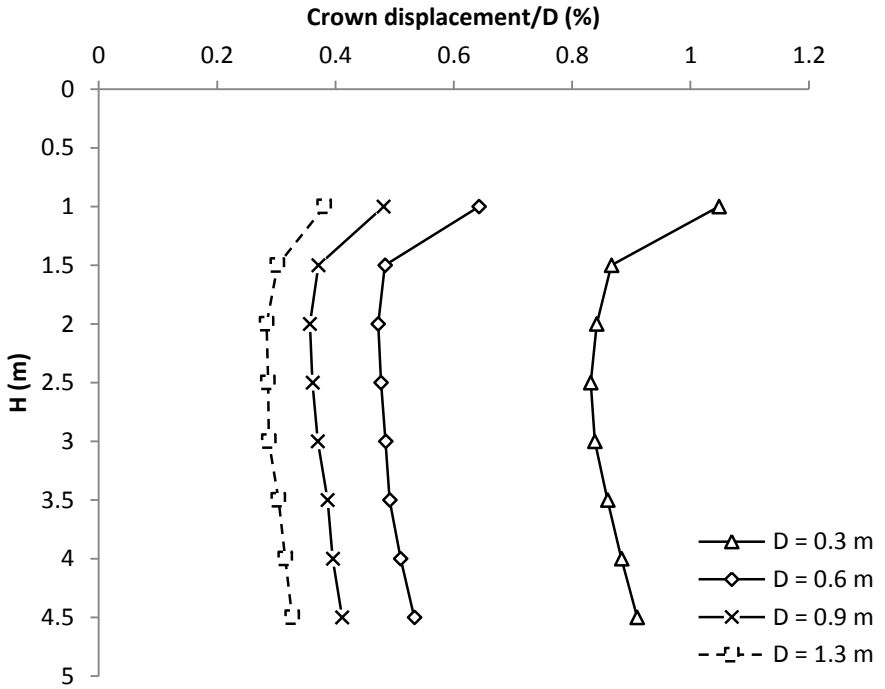

Figure 6.9: Normalized displacement (crown vertical displacement/D) under the total load

6.4.3. Pipe wall stress

It is important to investigate the pipe wall stress to estimate the factor of safety of the pipe against material failure. Some studies have investigated the failure of PVCu pipes using the maximum hoop stresses (Zhan and Rajani, 1997; Kang et al., 2013a, b, 2014). However, Balkaya et al. (2012a, b, 2013) mentioned that the principal wall stress represents the critical stress condition for PVCu pipes. Hence, they used the maximum principal stress to study the factor of safety of the pipe under the effect of erosion voids. Therefore, because of this difference of opinion in the literature, both the maximum hoop stresses and principal stresses have been investigated to find the critical stress condition. Figure 6.10 shows a comparison of the hoop and principal

stress around the pipe for the case of a pipe with an inside diameter of 0.9 m buried with a backfill height of 1.5 m under the effect of the total load. It can be clearly seen from the figure that both the maximum hoop and principal stresses occur at the pipe springline and on the compressive side. However, the maximum principal stress (977 kPa) is higher than the maximum hoop stress (722 kPa), with a percentage difference of 35%. This confirms the finding of Balkaya et al. (2012a, b, 2013). Thus, the principal stress has been used to study the pipe wall stress and the factor of safety of the pipes against material failure.

Figures 6.11 and 6.12 present the maximum principal stress (compressive stress) for all of the considered pipes under the soil weight only and the total load, respectively. Figure 6.11 shows that, as expected, increasing the backfill height linearly increases the maximum principal stress, which is due to the increase in the soil pressure. However, the figure indicates that increasing the diameter of the pipe increases the wall stress. This is due to the increase of the soil pressure applied at the pipe shoulders as the diameter increases and hence resulting in a higher stress at the springline.

Figure 6.12 shows that the wall stress nonlinearly decreases for all of the diameters up to a backfill height of 1.5 m. After this the wall stress increases for the pipes with an inside diameter ranging from 0.6 m to 1.3 m; while the stress decreases for the smallest diameter pipe as the backfill height increases from 1.5 m to 2.0 m. This complex behaviour is due to the interaction of the effect of the backfill weight and traffic load, as discussed previously in Section 6.4.1. It can also be seen that increasing the diameter of the pipe increases the maximum wall stress.

Figure 6.13 displays the factor of safety against the pipe material failure for all of the considered cases. This factor of safety has been calculated by dividing the yield stress of the pipe material (Table 6.1) by the maximum wall stress (Figure 6.12). It can be clearly seen that the pipes are safe against failure with a minimum factor of safety of 11.55.

In summary, the results of the robust three-dimensional finite element modelling have shown that PVCu pipes are safe based on the BS criteria if a good support has been provided for the pipe during the installation.

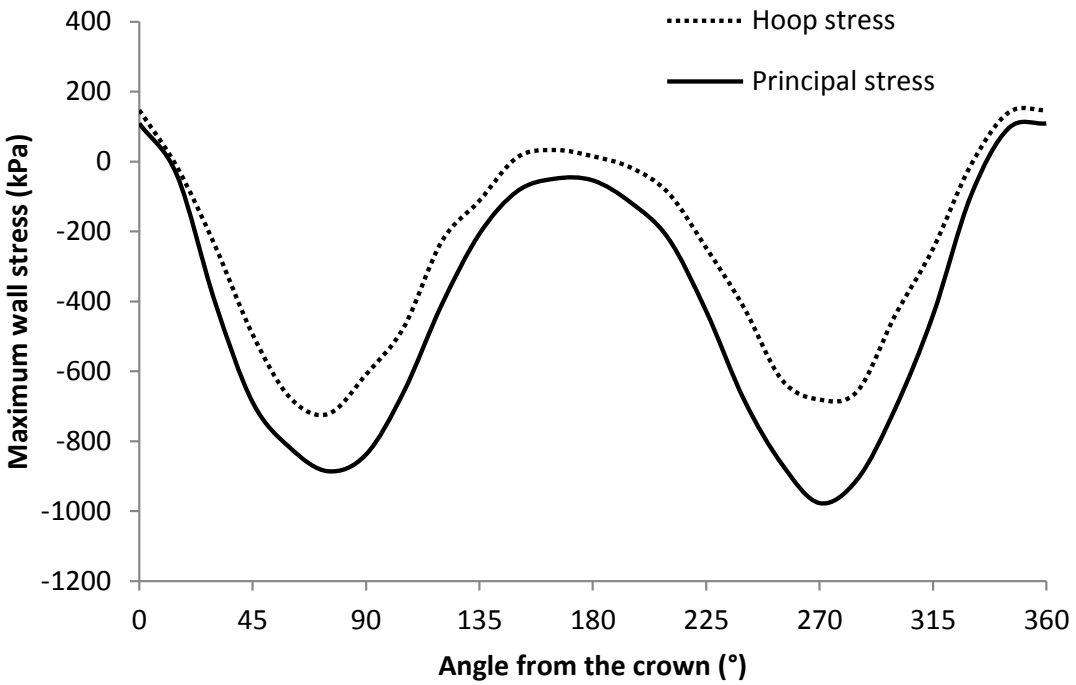

Figure 6.10: Comparison of the hoop and principal wall stresses induced due to the application of the total load for a pipe with an inside diameter of 0.9 m buried with a backfill height of 1.5 m

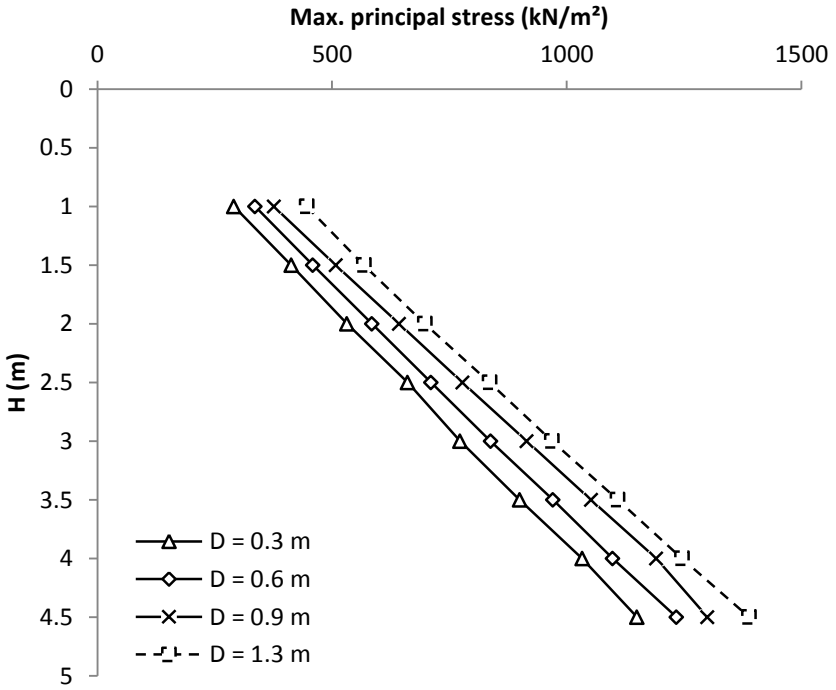

Figure 6.11: Maximum principal stress in the pipe wall under the backfill soil only

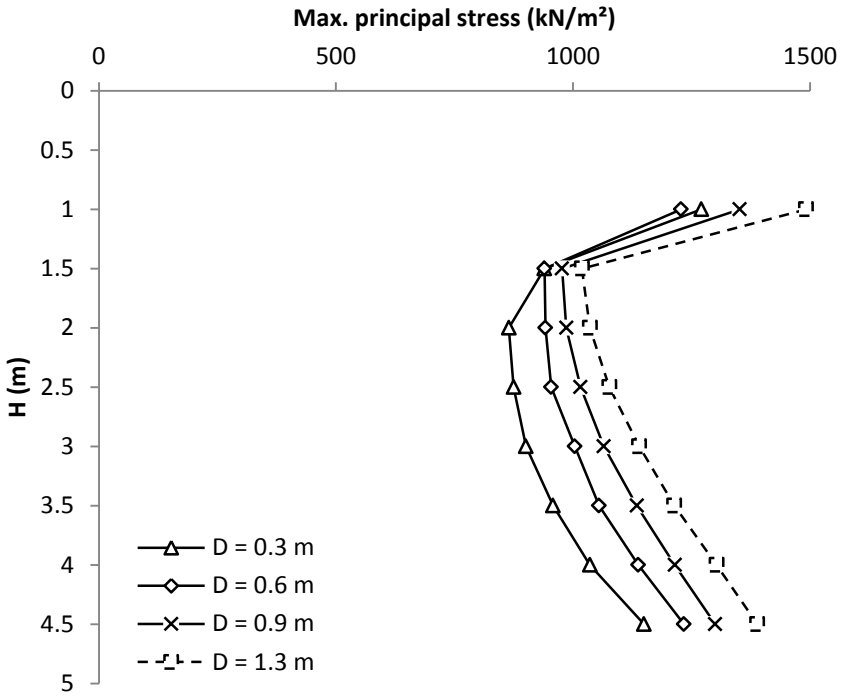

Figure 6.12: Maximum principal stress in the pipe wall under the total load

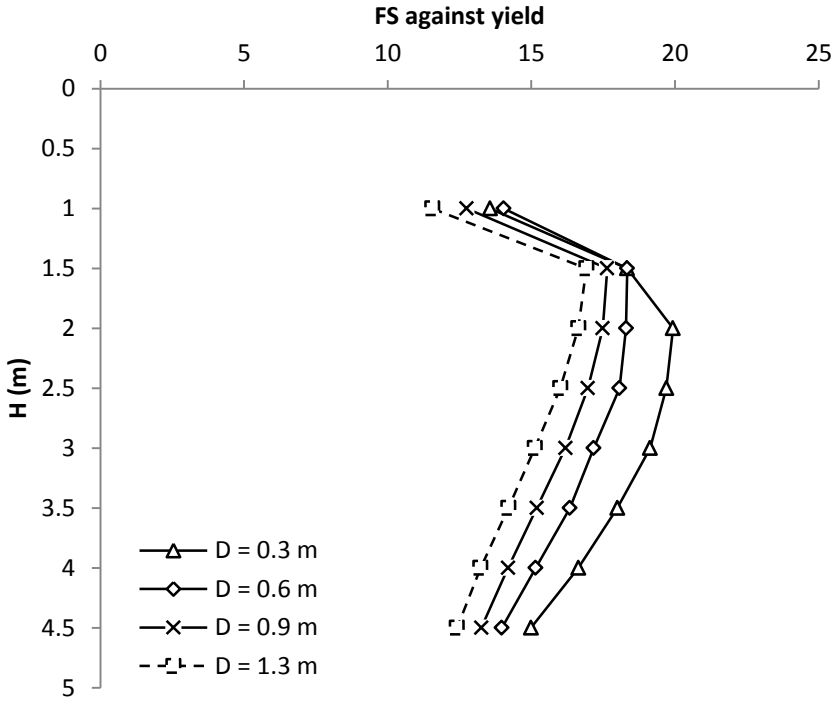

Figure 6.13: Factor of safety of PVCu pipes against material yield (pipes buried with good installation)

6.5. Results of poor installation

The results for the poor installation are presented in terms of ratios or percentage differences based on the results for the good installation. This has been considered to provide an in-depth understanding of the impact of poor installation (poor haunch support) in comparison with good installation. The following subsections present in detail the effect of poor installation on the maximum soil pressure, crown vertical displacement and pipe wall stress.

6.5.1. Maximum soil pressure

Figure 6.14 shows a comparison between the maximum vertical soil pressure for a good installation and a poor installation condition for a pipe with an inside diameter of 1.3 m and a backfill height of 1.0 m. It can be seen that the soil pressure significantly increases at the pipe invert due to the poor installation. This increase is due to the concentration of the reaction pressure in the invert zone. This means the soil in the invert zone has to react to most of the pressure developed above the pipe in order to satisfy equilibrium conditions, as a result of the lack of mobilization of the haunch support. The figure also indicates that poor installation does not significantly affect the maximum soil pressure at the crown of the pipe, where the percentage difference is 2%. However, the soil pressure in the shoulders, springline and haunch zones significantly decreases due to this poor installation.

Figure 6.15 displays the soil pressure ratio (the ratio of the maximum vertical soil pressure for the poor installation condition to the maximum soil pressure for the good installation condition) for all of the considered cases. It can be seen that the maximum soil pressure ratio significantly increases for all of these considered scenarios. It can also be noticed that increasing the pipe diameter or backfill height increases the soil pressure ratio due to the increase in the soil weight above the invert, as the backfill height or diameter increases. Hence, the reaction pressure at the invert will be increased because of the lack of support in the haunch zone. However, this increase is not linear, where the ratio approximately stabilizes after a backfill height of 3.0 m for all of the considered diameters. This behaviour is due to the significant decrease of the traffic load effect as the backfill height increases.

Figure 6.16 shows the factor of safety against buckling for the poor installation condition calculated using the maximum soil pressure. The factor of safety for the pipes with an inside diameter of 1.3 m significantly decreases compared to the full haunch support, where the minimum factor of safety becomes 2.05 compared to a minimum value of 3.10 (Figure 6.6) for the good installation (a percentage decrease of 34%). However, comparing the factor of safety for all of the cases with the BS factor of safety requirement (i.e. 2.00), shows that the pipes are safe against buckling even with the increase in soil pressure due to a lack of good support.

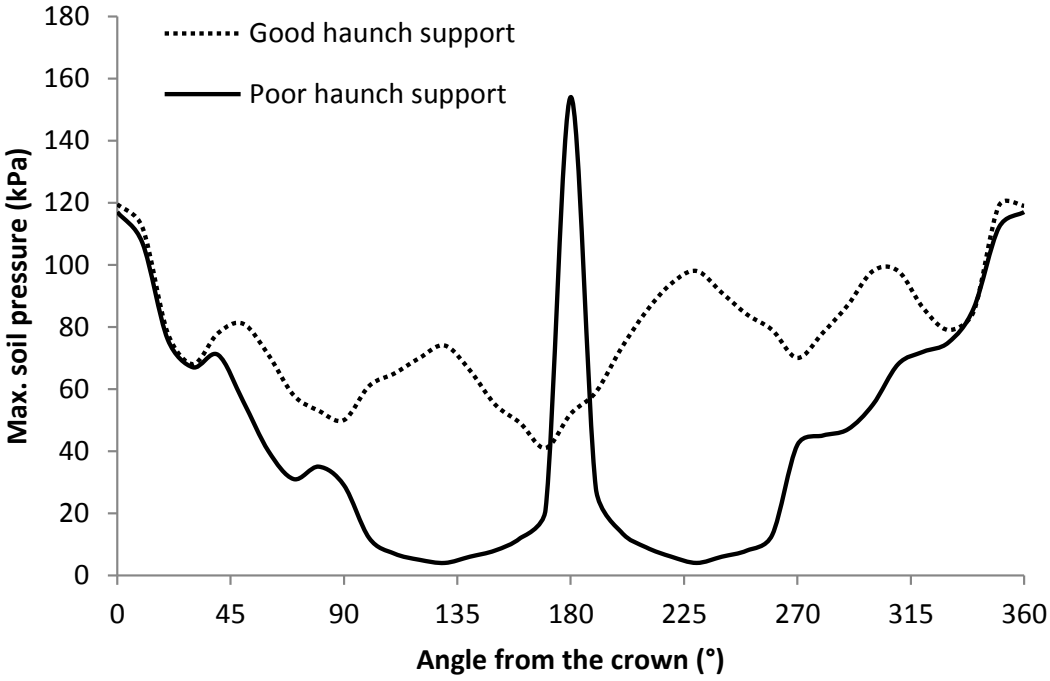

Figure 6.14: Effect of poor haunch support on the developed vertical maximum soil pressure around a pipe with an inside diameter of 1.3 m and a backfill height of 1.0 m

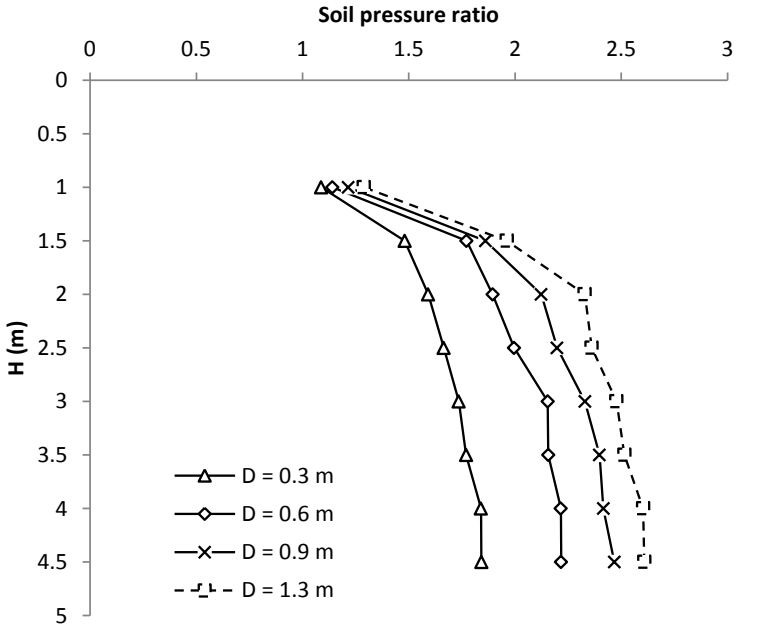

Figure 6.15: The ratio of the maximum vertical soil pressure for the poor installation condition to the maximum soil pressure for the good installation condition

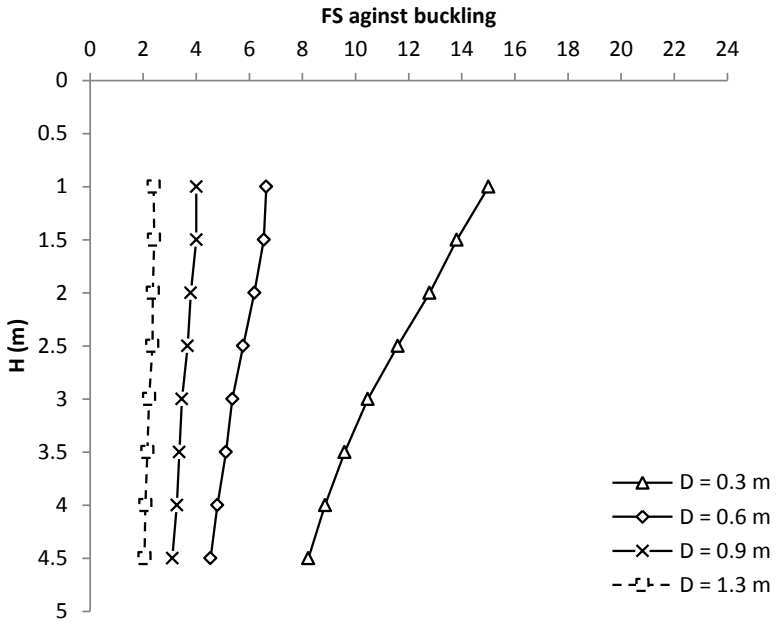

Figure 6.16: Factor of safety against buckling for buried PVCu pipes with poor haunch support under the total load

6.5.2. Pipe crown vertical displacement

The effect of poor installation on the deformed shape and the maximum pipe vertical displacement has been investigated. Figure 6.17 shows a comparison of the deformed shape of a buried pipe under the effect of the total load with both good and poor installation conditions. It can be seen that poor installation changes the deformed shape of the pipe from a heart shape into an inverted heart shape. This is due to the lack of good support at the haunch zone, which makes the pipe deflect more easily in this zone as a reaction to the applied load. This observation is consistent with that reported by Dhar et al. (2004) and Chapman et al. (2007) and the hypothesis proposed by Rogers (1988) for the behaviour of buried flexible pipes under applied loads. Furthermore, it can be seen that the crown vertical displacement is also increased due to this poor installation.

Figure 6.18 displays the percentage increase in the crown vertical displacement calculated based on the good installation results for all of the considered cases. The figure shows that increasing the pipe diameter significantly increases the crown vertical displacement, indicating that increasing the pipe diameter increases the dependency of the developed crown vertical displacement on the haunch support. The percentage increase ranged from 6% to 62% depending on the pipe diameter and backfill height. The figure also shows that the percentage increase decreases nonlinearly as the backfill height increases, followed by a nonlinear increase. This is due to the interaction of the soil weight and the traffic load and the dependency of the crown vertical displacement on the haunch support and the applied load.

Figure 6.19 presents the normalized crown vertical displacement with respect to the pipe's inside diameter. It can be seen from the figure that, although there was a significant increase in the pipe's vertical displacement due to the poor installation, the maximum displacement is lower than the 5.00% limitation with a minimum factor of safety of 4.24 (i.e. 5.00%/1.18%).

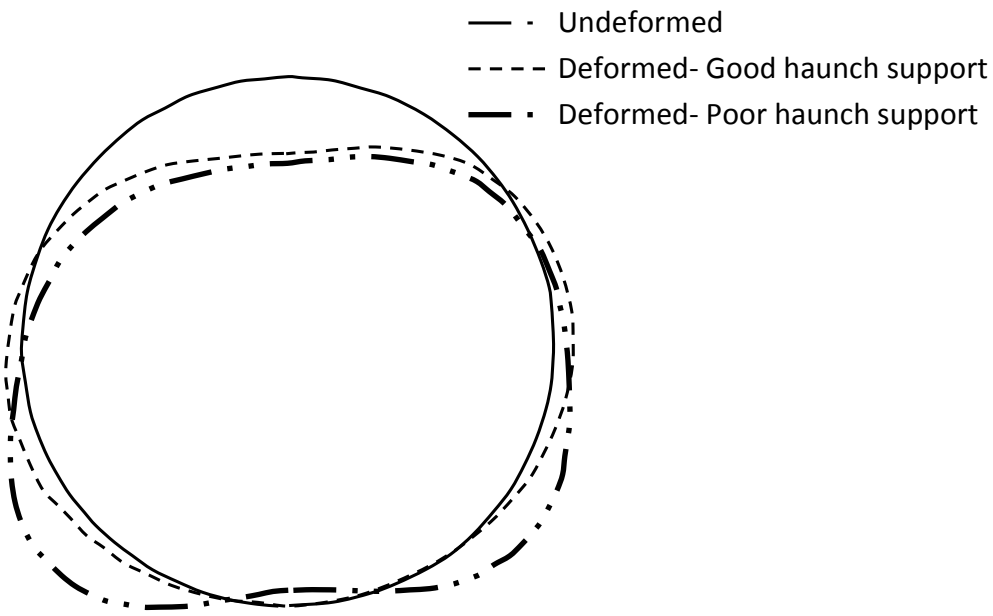

Figure 6.17: Comparison of the deformed shape for the good and poor installation conditions for a pipe with an inside diameter of 1.3 m and a backfill height of 1.0 m (Note: the deformed shape is magnified by a factor of 47)

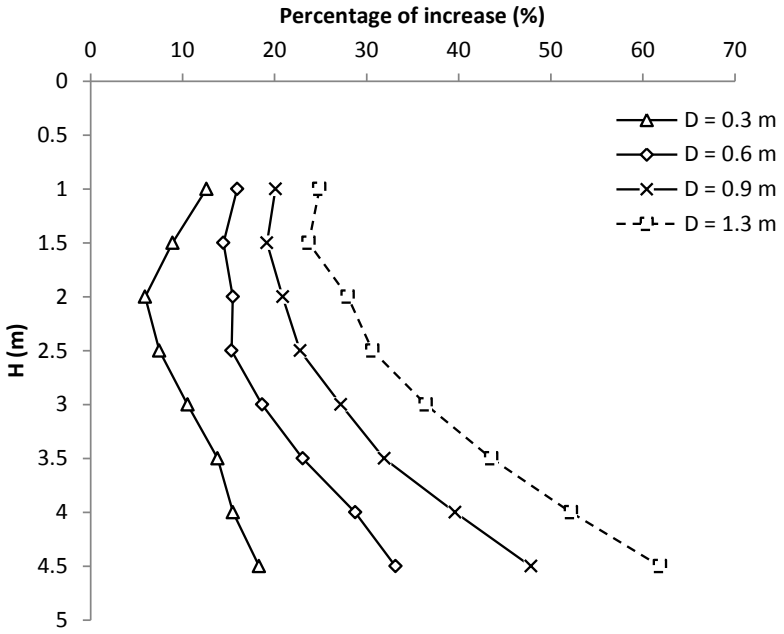

Figure 6.18: Percentage increase in the pipe crown vertical displacement due to a poor installation

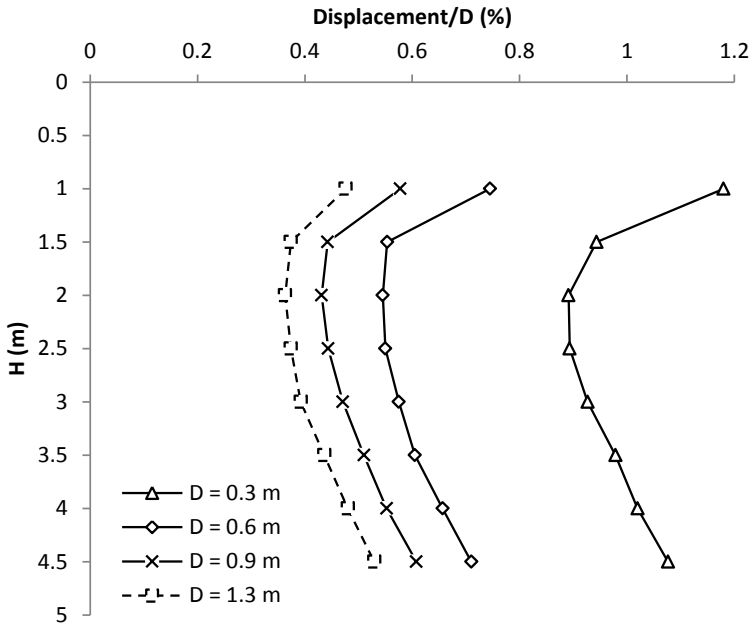

Figure 6.19: Normalized displacement (crown vertical displacement/D) under the total load

6.5.3. Pipe wall stress

Figure 6.20 shows the effect of the poor installation on the developed principal stress in comparison with the good installation, for a pipe with an inside diameter of 0.6 m buried with a backfill height of 2.0 m under the effect of the total load. It can be seen that the zone of the maximum principal stress changes from the pipe crown to the pipe invert due to the poor installation. This is as a result of the significant increase in soil pressure at the pipe invert because of the poor installation, as discussed in Section 6.5.1.

To investigate the percentage increase in the maximum pipe wall stress for all of the considered cases, the ratio of the maximum wall stress for the poor installation condition (T) to the maximum wall stress for the good installation condition (To) has been calculated and presented in Figure 6.21. From this figure, it can be seen that the maximum pipe wall stress significantly increases due to the poor haunch support, where the ratio ranges from 1.46 to 2.23. It can also be noticed that the ratio increases as the diameter of the pipe increases, due to the increase of the soil weight above the pipe invert as the diameter increases. Hence, the reaction pressure at the pipe invert significantly increases. Moreover, increasing the backfill height to 3.0 m increases the maximum wall stress ratio. Again, this is also as a result of the increase in the stress at the pipe invert as the backfill height increases. However, the increase in the invert stress is affected by the traffic load reduction as the backfill height increases. Hence, the ratio decreased slightly after a backfill height of 3.0 m.

Figure 6.22 shows the factor of safety against pipe material failure obtained using the maximum pipe wall stress. It can be seen from this figure that although the pipe wall

stress has significantly increased for all of the considered cases, the pipes are still far away from failure, with a factor of safety ranging from 5.83 to 11.51. This means that the PVCu pipes are safe against material failure even with the poor installation condition.

In summary, the results for both poor and good installation conditions demonstrated that the design of buried PVCu pipes is governed by the critical buckling (Figures 6.6 and 6.16) as the pipe wall stress is far away from failure (Figures 6.13 and 6.22) and the pipe's vertical displacement is also far away from the 5.00% limit (Figures 6.9 and 6.19). In addition, the results of the poor installation showed significant changes in the behaviour of the pipes because of poor haunch support. However, the comparisons with the BS limitations indicated that the PVCu pipes were performing very well even if poor haunch support is provided during installation. This indicates that the pipe wall thicknesses considered in this research (i.e. the wall thicknesses adopted from Petersen et al., 2010) provide a very conservative and uneconomic design. Hence, it is important to find the minimum pipe wall thickness which can be used safely for buried PVCu pipes under the most stringent conditions (i.e. under traffic loading and with poor installation) to achieve a robust and economic design. In addition, an update to the design methodology of the BS is required to account for poor installation with other grades of PVCu pipe, as the current BS design methodology assumes good installation (i.e. good haunch support) (BSI, 1997; BSI, 2010). The next section therefore discusses the derivation of safe and economic wall thicknesses and an update of the BS methodology to account for the effect of poor installation (i.e. poor haunch support).

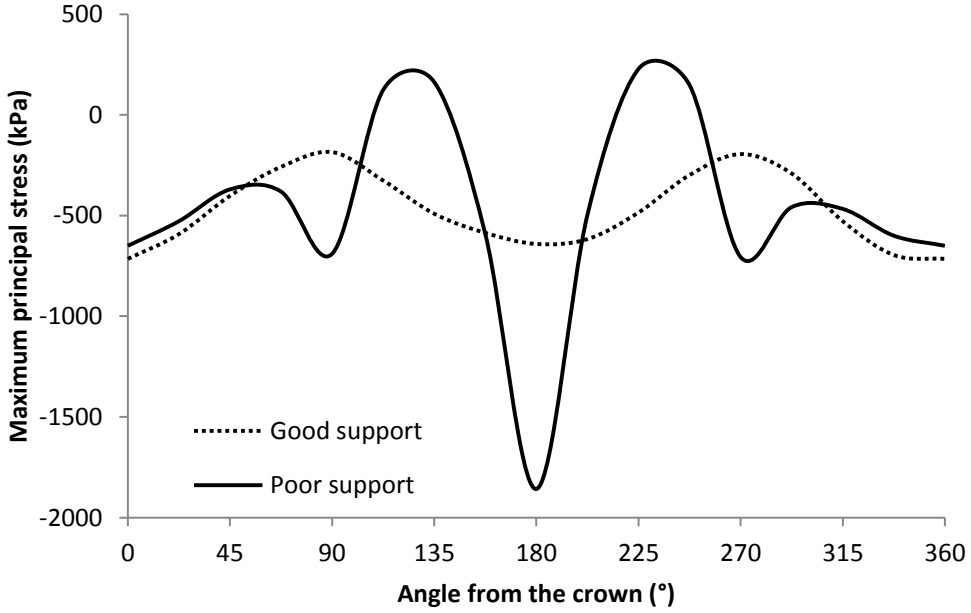

Figure 6.20: Comparison of the principal wall stress for a good and poor haunch supported pipe under total load (pipe internal diameter of 0.6 m and backfill height of 2.0 m)

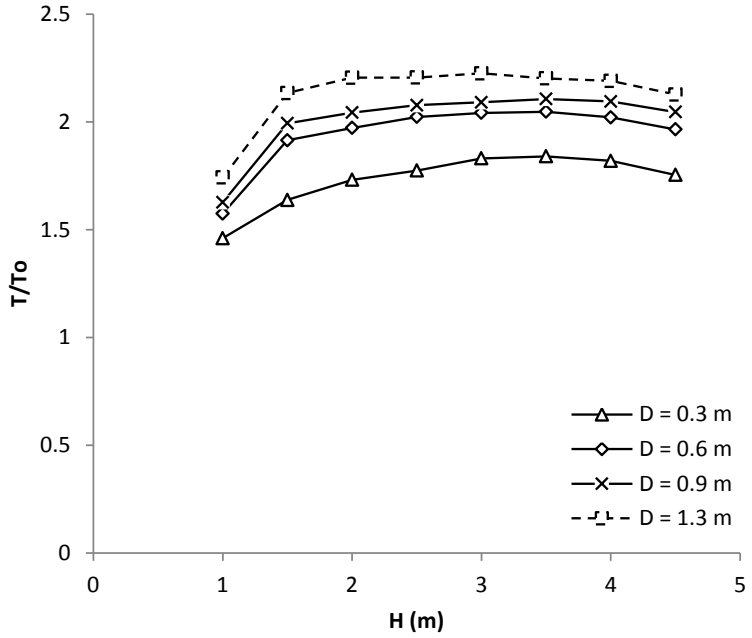

Figure 6.21: The ratio of maximum wall stress for the poor installation (T) to the maximum wall stress for the good installation (To)

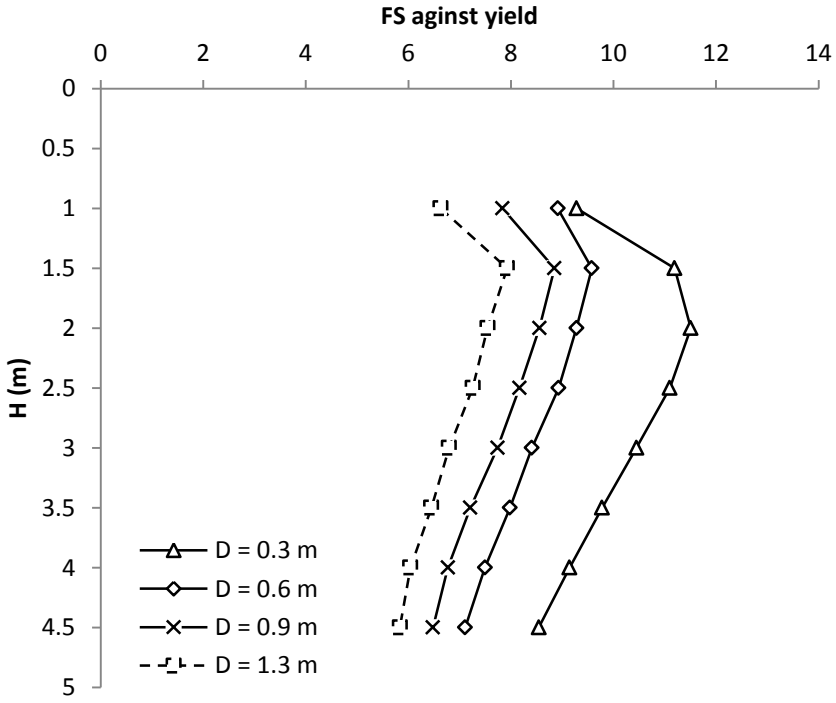

Figure 6.22: Factor of safety of PVCu pipes against material yield (pipes buried with poor installation)

6.6. Practical implications

6.6.1. Minimum safe wall thickness

The minimum pipe wall thickness for all of the cases considered in this study was calculated using the following methodology:

1- The results of the poor installation analyses showed that the buckling pressure governs the design of the buried PVCu pipes under the effect of the total load. Hence, the first step was to make sure that the proposed pipe wall thickness satisfies the limit for the critical buckling pressure. This has been done by calculating the critical buckling pressure for each case, by multiplying the

maximum soil pressure obtained from the poor installation analysis by two (the minimum factor of safety against buckling recommended in the BS (BSI, 1997)). The calculated ultimate buckling pressure was then used in Equation 1.11 to find the required minimum pipe wall thickness for each case by following a trial and error process.

2- The buried pipes with the new wall thicknesses (calculated in step 1) were then evaluated using the finite element model developed in this study to make sure that the pipe's maximum displacement (crown vertical displacement) and pipe wall stress for the new minimum wall thicknesses did not exceed the limits specified in the BS (i.e. the maximum displacement is less than 5.00% and the pipe wall stress is less than the yield stress of the pipe material). The poor installation condition was considered in all of the finite element analyses to make sure that the new wall thicknesses accounted for the worst-case scenario expected in practice, as discussed previously.

Figure 6.23 shows the minimum wall thickness calculated in step 1 for all of the considered cases. Figures 6.24 and 6.25 show the factor of safety against pipe material failure and the normalised vertical displacement of the pipe crown obtained from the finite element analysis for the pipes with the proposed new wall thicknesses, respectively. It can be seen from these figures that as expected, the pipes' wall thickness calculated based on the critical buckling limit satisfy the BS limitations for both the yield stress and the maximum displacement ratio. Hence, the wall thicknesses shown in Figure 6.23 can be easily used for an economic, safe and robust design of buried PVCu pipes under traffic load with poor installation, where only the pipe's inside diameter and backfill height are required.

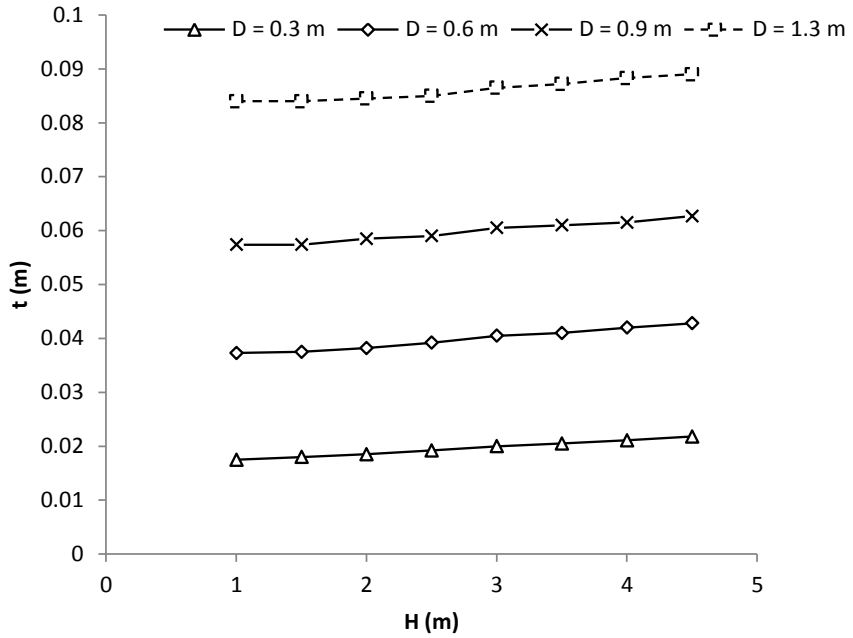

Figure 6.23: Minimum pipe wall thickness required for a safe performance of a buried PVCu pipe with poor installation

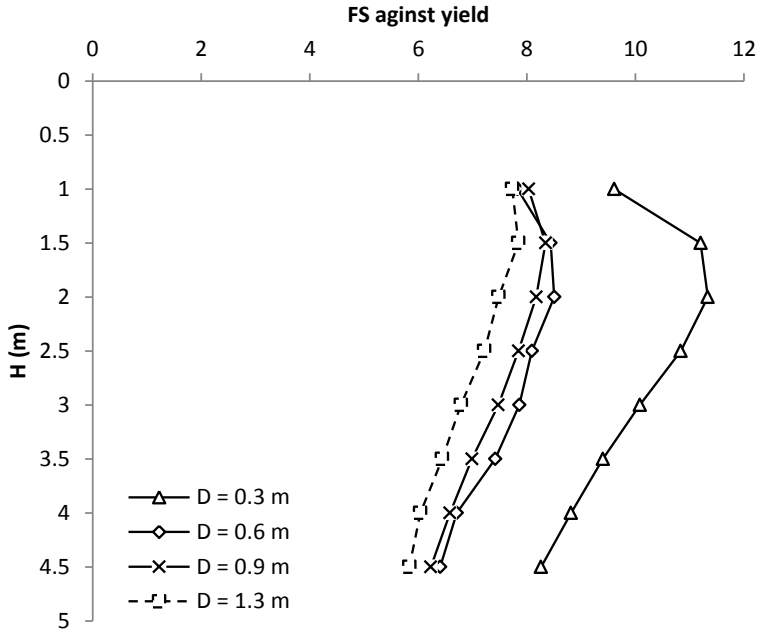

Figure 6.24: Factor of safety against pipe material failure for pipes with the minimum wall thicknesses

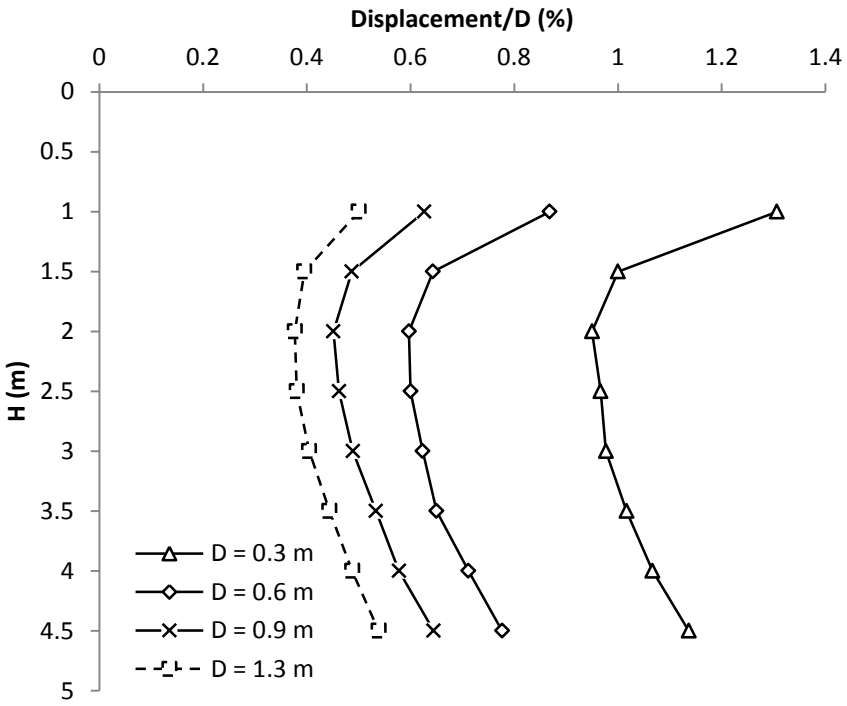

Figure 6.25: Normalized vertical displacement (crown vertical displacement/D) for pipes with the minimum wall thicknesses

6.6.2. Update to the design methodology of the BS

The previous section discussed the derivation of safe minimum wall thicknesses for the PVCu pipes considered in this study. However, the long-term modulus of elasticity of the PVCu material is significantly affected by the grade, and ranges from 689,000 kPa to 1,089,372 kPa (Petersen et al., 2010; AASHTO, 2013; Kraus et al., 2014). In addition, the calculated pipe wall thickness is significantly affected by the pipe's modulus of elasticity, as the pipe design is governed by critical buckling; which directly depends on the pipe's modulus of elasticity, as can be clearly seen in Equation 1.11. This means that the use of the proposed wall thicknesses (Figure 6.23) is limited to pipes with a modulus of elasticity of 689,000 kPa. Hence, a more general solution that can be used for different grades of PVCu pipe is proposed in

this section. The approach magnifies the calculated soil pressure using a correction factor to account for the significant effect of poor installation. This correction factor is obtained, for all of the cases considered in this study, by dividing the maximum soil pressure at the pipe invert for the poor installation condition (obtained from the finite element analysis) by the maximum soil pressure calculated based on the British Standard (Equation 1.9 + Equation 1.13) (BSI, 2010).

The correction factors are shown in Figure 6.26 and these enable designers to incorporate the effect of poor installation into the design of PVCu pipes. Figure 6.26 can cope with pipes of different moduli of elasticity, as it was found from the finite element analysis that the modulus of elasticity of the PVCu pipe does not significantly affect the calculated correction factor (the percentage difference in the correction factor was less than 1% as the modulus of elasticity changed from 689,00 kPa to 1,089,372 kPa). The designer can use Figure 6.26 to find the required correction factor depending on the inside diameter of the pipe and the backfill height, and then multiply this factor by the maximum soil pressure at the pipe crown obtained from the British Standard equations (Equation 1.9 + Equation 1.13), which assumes a good installation (i.e. good haunch support). The designer can then use Equation 1.11 to find the minimum pipe wall thickness (i.e. design the pipe) to satisfy the critical buckling requirements, as demonstrated in step 1 in Section 6.6.1. The calculated thickness already satisfies the displacement and wall stress requirements as has been demonstrated earlier in Section 6.6.1.

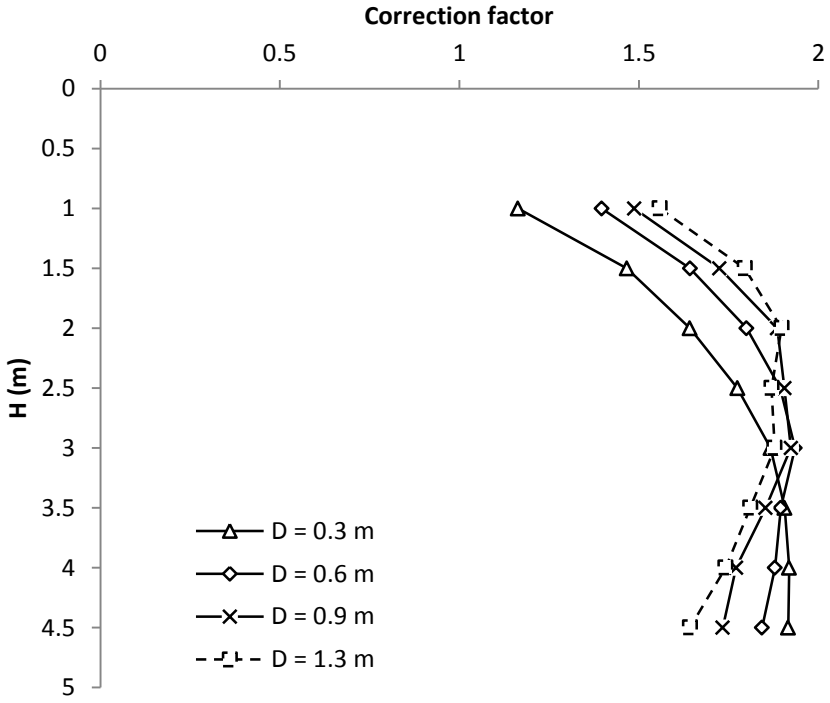

Figure 6.26: Correction factor for the maximum soil pressure on the pipe under the total load for different backfill heights

6.7. Comparisons of the displacement and wall stress

The original idea was to compare the results of the vertical displacement of the pipe crown and pipe wall stress obtained from the finite element analysis with the closed form solutions adopted in the BS to investigate the robustness of the BS design methodology and to use the EPR to improve the robustness of the BS design approach, as discussed in Section 1.7 (**Objectives 12 and 13 of this study**). However, as demonstrated in this chapter, the design of the buried PVCu pipes is controlled by the critical buckling (i.e. soil pressure), and the pipe displacement and the pipe wall stress are far away from critical conditions. Hence, it was felt unnecessary to continue with these objectives. In addition, the proposed correction

factor chart (Figure 6.26) implicitly accounts for the error in the BS maximum soil pressure equation (Equation 1.13) and implicates the effect of the poor installation in the design practice of buried PVCu pipes.

6.8. Summary

This chapter aimed to develop a clear understanding of the response of buried PVCu pipes under the MR-BSI traffic loading using a validated three-dimensional finite element model. The effect of the pipe diameter, backfill height and installation condition were investigated through a detailed parametric study. The results of the good installation illustrated the significant effect of the pipe diameter on the behaviour of the buried PVCu pipe. In addition, the results showed significant issues with the maximum soil pressure equation used in the BS (Equation 1.13). The results of the poor installation and the comparisons with the results of the good installation showed the importance of the installation quality. Furthermore, the necessity to consider the poor haunch support in the design practice of buried flexible pipes is important, as it causes a significant increase in the maximum soil pressure applied on the pipe, pipe crown vertical displacement and pipe wall stress. Notably, a new design methodology was proposed to account for the effect of the poor installation in the design practice of buried PVCu pipes.

Chapter 7
CONCLUSIONS AND SUGGESTIONS FOR FUTURE RESEARCH

7.1. Introduction

In this research, a three-dimensional finite element method and evolutionary polynomial regression analysis were used to improve the understanding and propose improvements in the design methods for buried rigid (concrete) and flexible (polyvinyl chloride (PVCu)) pipes, to aid a more economic and robust design.

A three-dimensional finite element model was developed, validated and used to carry out parametric based studies to investigate the complex behaviour of buried concrete and PVCu pipes under the effect of backfill soil weight and traffic loading, based on the gaps in the knowledge identified from a critical and extensive literature review detailed in **Chapter 2**. This model was developed based on a comprehensive literature review of previous studies of soil-pipe interaction combined with sensitivity analyses. In addition, the results of the developed model were validated against instrumented laboratory and field tests on buried pipes under the effect of backfill soil weight and static and moving traffic loads.

Detailed parametric studies were then conducted to investigate the effect of the pipe diameter, backfill height, installation conditions and pipe wall thickness on the response of concrete and PVCu pipes under the effect of the soil load and combined soil and traffic loads. The results of the parametric studies were discussed carefully to provide an insight into the behaviour of buried concrete and PVCu pipes and to quantify the parameters that affect the response of the pipe.

Importantly, the results of the parametric studies were then used to investigate the robustness of the current design standards (BS, 2010; AASHTO, 2016). Furthermore, novel improvements in the design methodologies of buried concrete and PVCu pipes have been proposed using the data obtained from the three-dimensional finite element analysis utilising an evolutionary polynomial regression analysis (EPR) (for concrete pipes) and the soil pressure design equations used in the BS (for PVCu pipes).

This chapter summarizes the key findings from the studies conducted in this research and provides suggestions for future studies. The chapter has been divided into five sections. The first three sections discuss the key findings from **Chapter 4**, **Chapter 5 and Chapter 6.** The fourth section summarizes **the contributions to the field of knowledge (i.e. the findings which were not known before this research)** and hence shows how **the present study has achieved the aim**. Finally, the chapter finishes with suggestions for future research.

7.2. Conclusions from the study of the behaviour of buried concrete pipes under soil load only (Chapter 4)

The behaviour of buried pipes under backfill soil load only has been thoroughly investigated in this research to address the research needs noted from the extensive literature review conducted in **Chapter 2**. The effect of the pipe diameter, pipe thickness, backfill height and installation conditions on the maximum bending moment of the pipe have been thoroughly investigated and discussed. The results of the maximum bending moment obtained from these analyses have been used to calculate and study the soil load bedding factor. The results of the soil load bedding

factor have been compared with the design bedding factors recommended in the BS and AASHTO standard. The following conclusions can be drawn from this study:

1- The maximum bending moment developed in buried concrete pipes is significantly affected by the pipe diameter, pipe wall thickness and backfill height.
2- The recommended bedding factors in the BS are conservative; where the ratio of the bedding factors obtained from the finite element modelling to the design standard bedding factors ranged from 1.03 to 3.08, depending on the installation type, pipe diameter and backfill height. This means that current design practice is not economic. Furthermore, the BS neglects the effect of the pipe diameter, pipe wall thickness and backfill height, which have been shown to have significant impact on the bedding factor.
3- Regarding the bedding factors recommended by AASHTO, the ratio of the bedding factor calculated from the finite element modelling, to the design standard bedding factor, ranged from 0.61 to 2.08. Furthermore, the AASHTO design standard neglects the effect of the pipe wall thickness and backfill height, which have been shown to significantly affect the bedding factor. Therefore, it is suggested that the AASHTO recommended bedding factors could be improved by considering these other factors.
4- New soil load bedding factor models (Equations 4.2 to 4.5) were developed using an EPR analysis. The models were developed using the bedding factors obtained from the results of the finite element modelling. These models account for the effect of the pipe diameter, pipe wall thickness and backfill

height. Hence, a more economic and robust design can be achieved by using the models from this study.

5- Excellent agreement was obtained when the results of the soil load bedding factor model for a Type 2 installation was compared with the bedding factor obtained from a real pipe test by MacDougall et al. (2016) (percentage difference was 6%), providing confidence in the methodology adopted in this study.

7.3. Conclusions from the study of the behaviour of buried concrete pipes under traffic loading (Chapter 5)

The response of buried concrete pipes under the BS main road traffic load requirements was investigated using a validated three-dimensional finite element model. The study provided an insight into the effect of the pipe diameter, backfill height and pipe wall thickness on both the developed bending moment in the pipe wall and the soil pressure around the pipe. Furthermore, the study has presented for the first time a rigorous investigation into the robustness of the BS methodology for designing buried concrete pipes under traffic loading. The following conclusions can be drawn from the study:

1- The critical loading condition of the BS main road design truck is obtained when the truck is moving perpendicular to the concrete pipeline axis with the centre of the right-hand axle above the crown of the pipe.

2- The effect of traffic load is significantly affected by the pipe diameter, where increasing the diameter of the pipe decreases the influence of the traffic load. However, the traffic load does not affect the developed bending moment in the

pipe wall for a backfill height greater than 2.5 m for pipes with an inside diameter of 0.3 to 1.2 m. Moreover, the effect of traffic load on the maximum bending moment vanishes after a backfill height of 1.0 m for a pipe with an inside diameter of 2.4 m. Therefore, the study suggests including these backfill height limits on the effect of the traffic load in the BS.

3- The developed bending moment in the pipe wall is significantly influenced by the pipe wall thickness, where increasing the pipe thickness increases the bending moment.

4- Changing the support condition from a very good installation (using SW95 soil in the haunch zone) to a reasonable installation (using ML90 soil in the haunch zone) does not significantly affect the developed bending moment. However, providing a poor support condition for the pipe in the haunch zone significantly increases the bending moment. Hence, a better pipe performance can be achieved by providing good support in the haunch zone.

5- The results showed that the BS method to calculate the force applied on the pipe is overly conservative; where the assumption of a uniform vertical soil pressure above the top half of the pipe, with a magnitude equal to the vertical soil pressure at the pipe crown, does not represent real conditions. This assumption leads to a very high design load, and hence an uneconomical design.

6- The calculated bedding factors based on the results of the finite element modelling showed that the bedding factors adopted in the BS are overly conservative, where the ratio of the predicted to the obtained bedding factors ranged from 1.63 to 4.92. The study illustrated that this over-conservatism is

due to the oversimplification in the design force calculation, based on the BS method.

7- New bedding factor models have been proposed using the EPR analysis technique for both the good and poor installation conditions (Equations 5.1 and 5.2). The use of these models ensures an economical and robust design of concrete pipes; as these models implicitly account for the error due to the oversimplification in the force calculation following the BS method.

7.4. Conclusions from the study of the behaviour of buried PVCu pipes under traffic loading (Chapter 6)

This study has presented for the first time a robust comprehensive analysis studying the effect of pipe diameter, backfill height and installation condition on the behaviour of buried flexible pipes subjected to the BS main road traffic load requirements. The results presented in this study have provided details previously missing in the literature and also an insight into the behaviour of flexible pipes with both good and poor installation. The key findings from this study are as follows:

1- Similar to the buried concrete pipes, the critical loading condition of the BS main road design truck is obtained when the truck is moving perpendicular to the PVCu pipeline axis with the centre of the right-hand axle above the crown of the pipe.

2- The BS main road design truck imposes a higher stress and displacement on the pipe compared with two AASHTO HS20 trucks; where the predicted horizontal (at the pipe springline) and vertical (at the pipe crown) displacements under the critical loading condition of the BS main road design

truck are 195% and 153% higher than that predicted under two HS20 design trucks with two axles.

3- The equation recommended by the BS (BSI, 2010) for estimating the maximum soil pressure on a buried pipe (Equation 1.13) has been shown not to be accurate. A new correction factor chart (Figure 6.26) has been proposed based on the results of an extensive numerical study to improve the accuracy of the BS design equation.

4- The effect of the traffic loading on the behaviour of the buried PVCu pipes is negligible for a backfill height greater than 4.0 m for all pipe diameters considered in this research.

5- Increasing the diameter of the pipe for both good and poor installation conditions increases the vertical displacement of the pipe crown and pipe wall stress; although the maximum soil pressure generally decreased with an increase in the pipe diameter. This is due to a decrease in the pipe stiffness and an increase in the soil weight above the pipe's shoulders as the diameter increases.

6- The maximum principal stress is higher than the hoop stress for both good and poor installation conditions. Hence, future studies should consider the maximum principal stress to investigate the factor of safety against failure of the pipe material.

7- Poor installation (poor haunch support) significantly increases the vertical displacement of the pipe crown with the effect increasing as the diameter of the pipe increases. The percentage increase ranged from 6% to 62%, depending on the pipe's diameter and backfill height.

8- Increasing the pipe's diameter increases the dependency of the pipe crown vertical displacement on the haunch support.

9- Poor installation (poor haunch support) changes the zone of the maximum pipe wall stress from the springline to the pipe invert and significantly increases the maximum pipe wall stress, with a percentage increase ranging from 46% to 123%, depending on the pipe's diameter and backfill height. The percentage increase increases as the diameter or the backfill height increases.

10- The critical buckling governs the design of buried PVCu pipes under the effect of traffic loading, for both good and poor installation conditions.

11- A new design chart (Figure 6.23) has been proposed in this study to calculate the required minimum pipe wall thickness for a robust and economic design of buried PVCu pipes under the stringent BS traffic loading condition. The design chart accounts for the effect of poor haunch support and can be used easily by only knowing the pipe's inside diameter and backfill height. In addition, this chart can be used by PVCu pipe manufacturers to produce more economical buried pipes.

12- A new correction factor chart (Figure 6.26) has been proposed in this study to incorporate the effect of poor haunch support in the design methodology of the BS. This chart can be used to correct the BS maximum soil pressure equation for PVCu pipes, and this is insensitive to the long-term modulus of elasticity for the pipe and so can be used for different grades (i.e. different initial modulus of elasticity) of PVCu pipe. The design chart is easy to use as it only requires the pipe's diameter and the backfill height.

7.5. Contributions to the field of knowledge and achievement of the aim

It is clearly evident from Sections 7.2, 7.3 and 7.4 that **the aim of the present study has been addressed**; where an improved understanding of the soil-pipe interaction was achieved and a more robust and economical design is proposed for both concrete and PVCu pipes. The following points provide a focused description of the contributions to the field of knowledge **(i.e. the novelty of this research)** and hence show how the present study has addressed the aim:

1- A critical literature review that identified the issues in the previous studies was presented. This critical review has shown that a lot of studies available in the literature followed a wrong methodology or did not justify the considered research path. It is believed that this review will be of great help to researchers and pipeline engineers who may wish to utilise the conclusions from these studies. To the knowledge of the author, no other study has critically evaluated the buried pipe literature in such detail, nor illustrated the gaps in the knowledge.

2- This research has demonstrated the need to include the effect of the pipe diameter, backfill height and pipe thickness in the design methodology of the buried concrete pipes, under soil load only and under total load (combined backfill soil weight and traffic load). Previous studies have not investigated the effect of the pipe diameter, backfill height and pipe thickness.

3- A new set of robust bedding factor models for designing buried concrete pipes subjected to soil load only was proposed. The proposed bedding factor models enable a robust and economic design of buried pipes. Previous

studies have not suggested bedding factor models nor compared the results of a numerically derived bedding factor with an experimentally calculated bedding factor.

4- This research has illustrated the need to link the pipe diameter with the backfill height to correctly understand the effect of the traffic loading on the behaviour of buried concrete pipes. This finding is new, as previous studies investigated the effect of the traffic load without linking it to the pipe diameter. These previous studies only considered one pipe diameter in their parametric studies.

5- The research has highlighted the issues in the BS method for calculating the design force applied on the buried concrete pipe. It also showed the actual soil pressure distribution on the top half of the pipe. This finding is novel because no previous study has considered the behaviour of buried concrete pipes under the BS traffic loading nor investigated the robustness of the BS design methodology.

6- Innovative bedding factor models for designing buried concrete pipes under total load are proposed. These models enable a robust and economic design of buried pipes under total load. No previous study has proposed a modification to the BS design bedding factors.

7- This research has illustrated the practical implications of the complex interaction of the pipe's diameter, backfill height and installation condition on the design of buried PVCu pipes. This is novel because no previous study has investigated the design implications of these factors.

8- It has been shown that only the critical buckling needs to be considered in the design of buried PVCu pipes under the combined backfill soil weight and traffic loading. This finding is new as previous studies did not consider, nor discuss, pipe buckling. Only the pipe displacement and pipe wall stress were investigated previously.

9- A novel design chart has been proposed for PVCu pipes. This design chart illustrates the effect of the poor haunch support in the design of buried PVCu pipes. Additionally, this design chart implicitly accounts for the error in the BS main road traffic loading soil pressure equation (Equation 1.13). This study is the first to link the effect of the pipe diameter and poor haunch support with the design standards for buried PVCu pipes.

7.6. Limitation of the research

It is important to mention that the studies conducted in this research have considered limited conditions (i.e. very stiff bedding, stiff surrounding soil, very stringent loading condition and compacted backfill soil). Hence, the conclusions obtained from these studies (reported in Sections 7.2, 7.3 and 7.4) and the suggested design improvements are limited to cases similar to those considered in this research. The conclusions and the proposed design models may not be valid for different conditions such as a very soft bedding soil, different traffic loading configuration, pipe buried in a chemically active soil, pipe buried in a loose backfill soil and buried pressurized pipe. Such conditions may change the soil arching, stress distribution around the pipe and maximum soil pressure applied on the pipe, ultimately leading to different behaviours from those discussed in this research. However, this research has demonstrated the

issues associated with the current design standards. Therefore, it is highly recommended to use a validated finite element analysis for designing a buried pipe with conditions different from those considered in this research. Additionally, a complete research programme is required to improve the current BS design methodology for the cases outside the scope of this research, as will be suggested in Section 7.7.

7.7. Suggestions for future research

The following are some of the suggestions for future research to improve the understanding of the behaviour of buried pipes and the design practice:

1- Investigate the robustness of the BS design methodology for buried pipes with different conditions to those considered in this research such as a very soft bedding soil, different traffic loading configuration, pipe buried in chemically active soil, pipes buried in loose backfill and buried pressurized pipes.
2- Investigate the robustness of the BS design methodology for buried, corrugated PVCu and HDPE pipes, as this study focused on PVCu pipes with smooth walls. Such a study is required because corrugated pipes respond differently to the applied load. This has been demonstrated by Elshimi (2011), who showed significant differences in the wall stress of a corrugated wall culvert compared to a smooth wall culvert with an equivalent stiffness.
3- Study the effect of erosion voids on the behaviour and the design of buried concrete pipes under the BS traffic loading. Erosion voids form due to leakage from pipes and change the stress distribution around the pipes. Hence, these voids change the value and the location of the maximum soil pressure, the

maximum bending moment and the maximum pipe wall stress (Kamel and Meguid, 2013; Meguid and Kamel, 2014; Balkaya et al., 2012a, b; 2013). Therefore, a thorough investigation is required to investigate the effect of the erosion voids and their implication for design.

4- This research has shown that the PVCu pipe displacement and PVCu pipe wall stress are far below the design limits and only the critical buckling is controlling the design. However, this conclusion cannot be generalized to PVCu pipes under deeper soil fill (more than 4.5 m), as this study only considered a maximum backfill height of 4.5 m. Hence, this study should be extended to backfill heights of more than 4.5 m to investigate the behaviour, and hence the design implications, of buried PVCu pipes under deep soil fill.

5- Investigate the response of a buried pipes joints with good and poor installation conditions under the effect of the BS traffic loading. A separation of the joint between two pipes may occur due to the applied traffic load (García and Moore, 2015b; Rakitin and Xu, 2015; Sheldon et al., 2015; Xu et al., 2017). This separation may cause water leakage through the joint; which subsequently may create an erosion void, leading ultimately to a loss of support to the pipe. Therefore, a good understanding of the behaviour of the pipes joints is required, and hence design limits for the displacement and rotation of pipes joints should be established in the BS.

Appendix A: Full results of the parametric study of the behaviour of the pipe under soil load

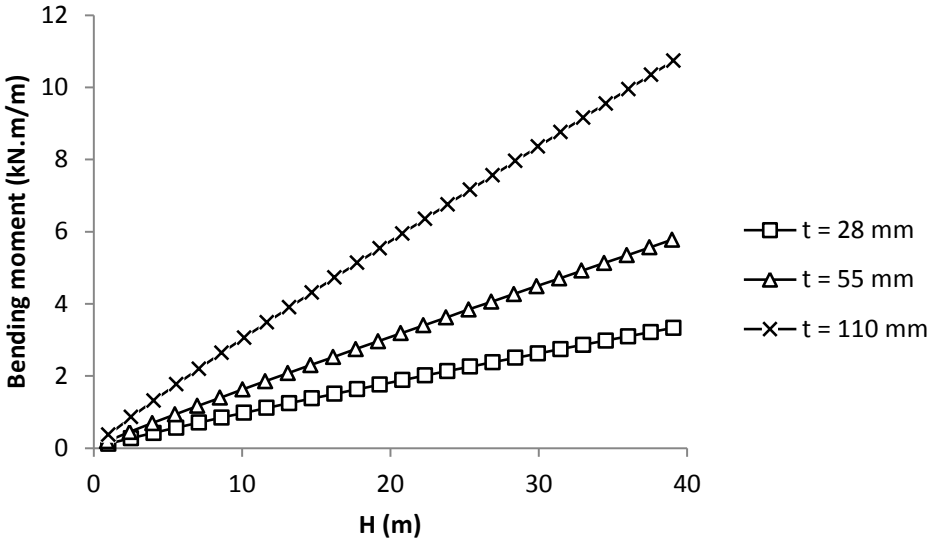

Figure A.1: Effect of backfill height on the developed maximum bending moment for a pipe with a diameter of 0.3 m buried in Type 1 installation

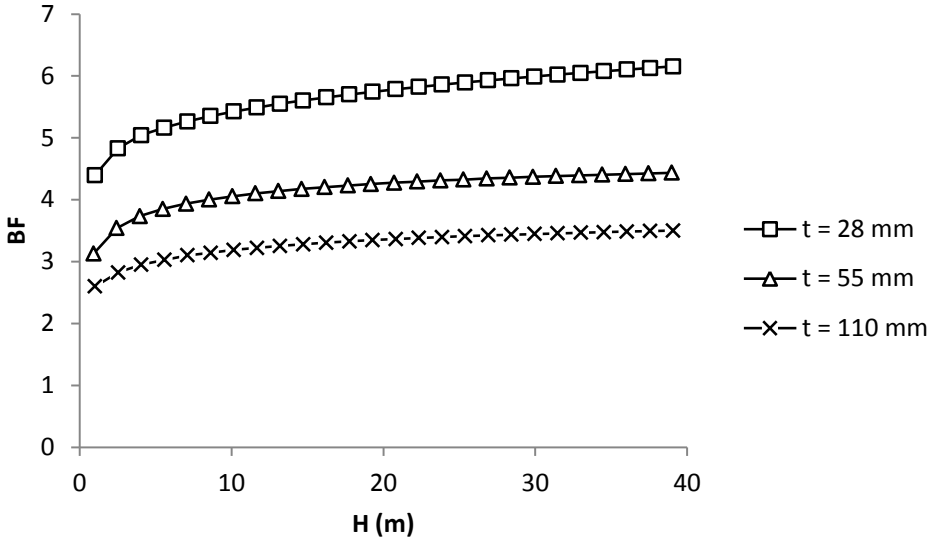

Figure A.2: Effect of backfill height on the soil load bedding factor for a pipe diameter of 0.3 m buried in Type 1 installation

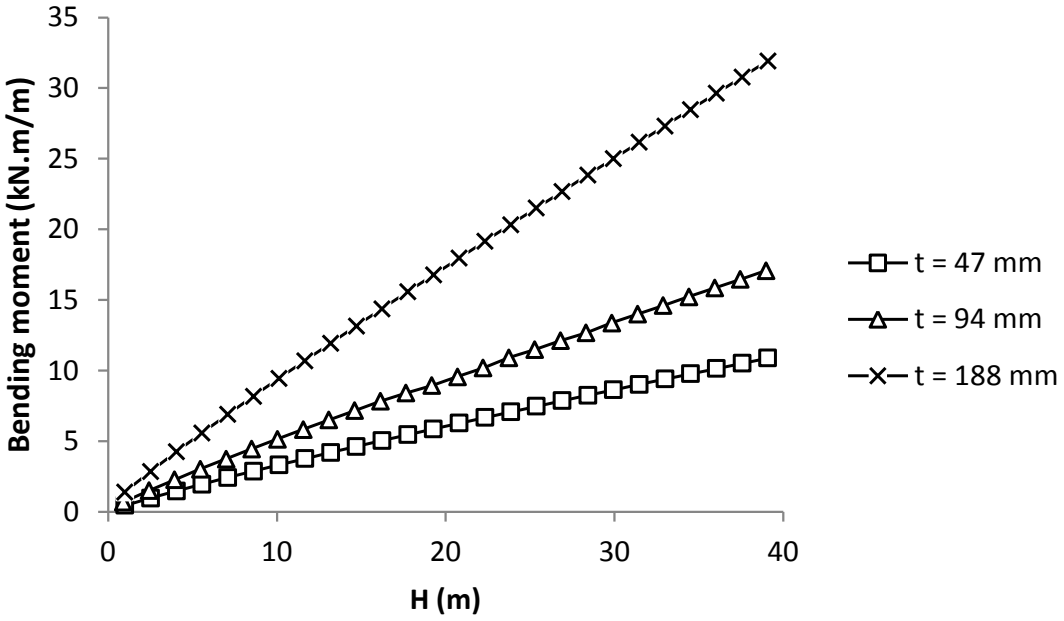

Figure A.3: Effect of backfill height on the developed maximum bending moment for a pipe with a diameter of 0.6 m buried in Type 1 installation

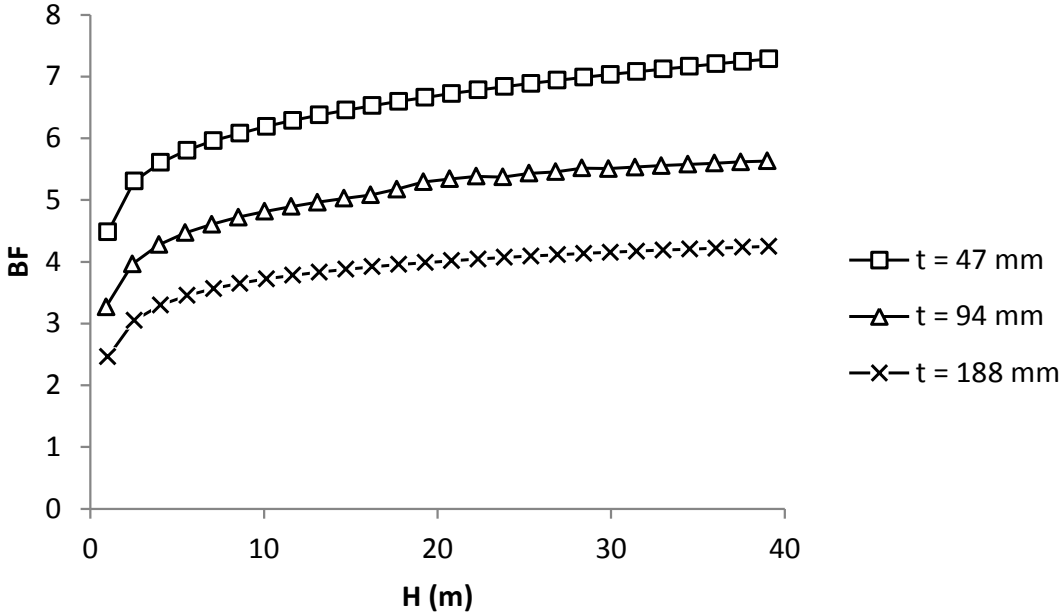

Figure A.4: Effect of backfill height on the soil load bedding factor for a pipe diameter of 0.6 m buried in Type 1 installation

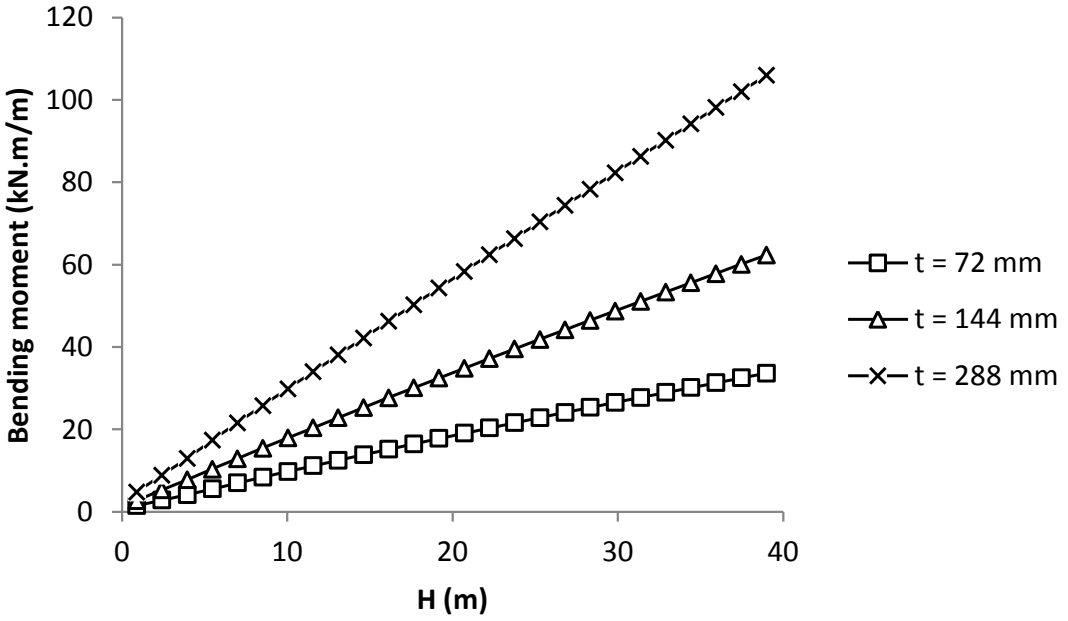

Figure A.5: Effect of backfill height on the developed maximum bending moment for a pipe with a diameter of 1.2 m buried in Type 1 installation

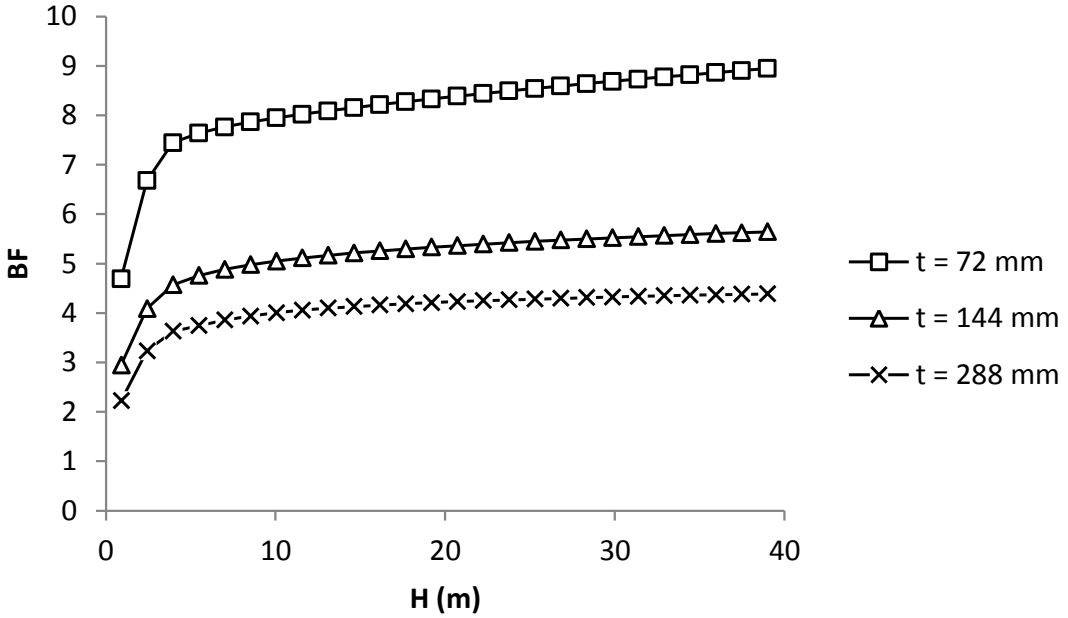

Figure A.6: Effect of backfill height on the soil load bedding factor for a pipe diameter of 1.2 m buried in Type 1 installation

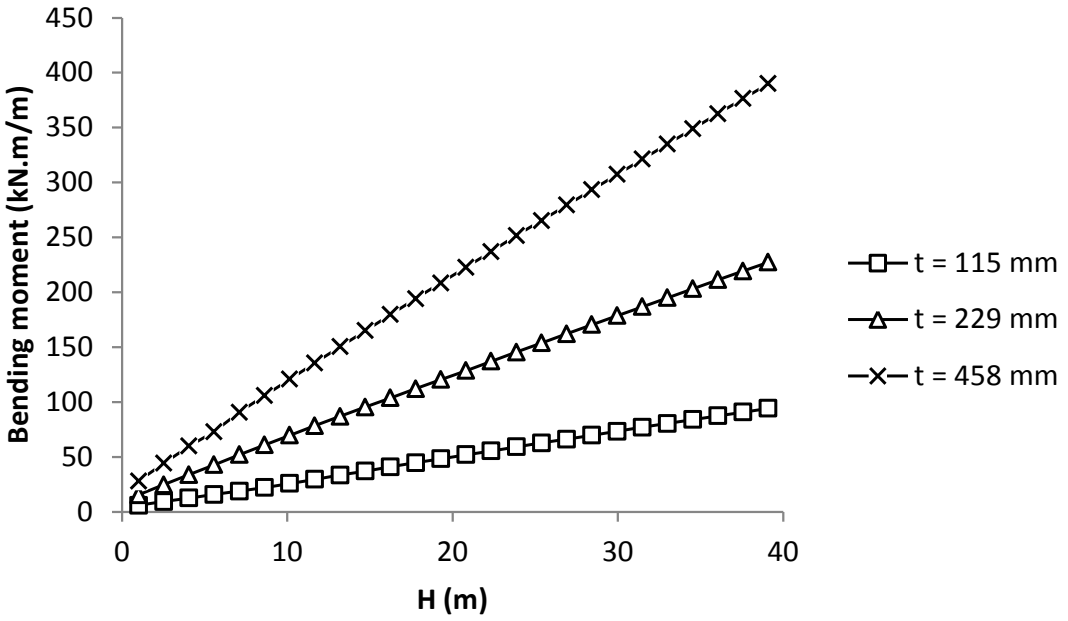

Figure A.7: Effect of backfill height on the developed maximum bending moment for a pipe with a diameter of 2.4 m buried in Type 1 installation

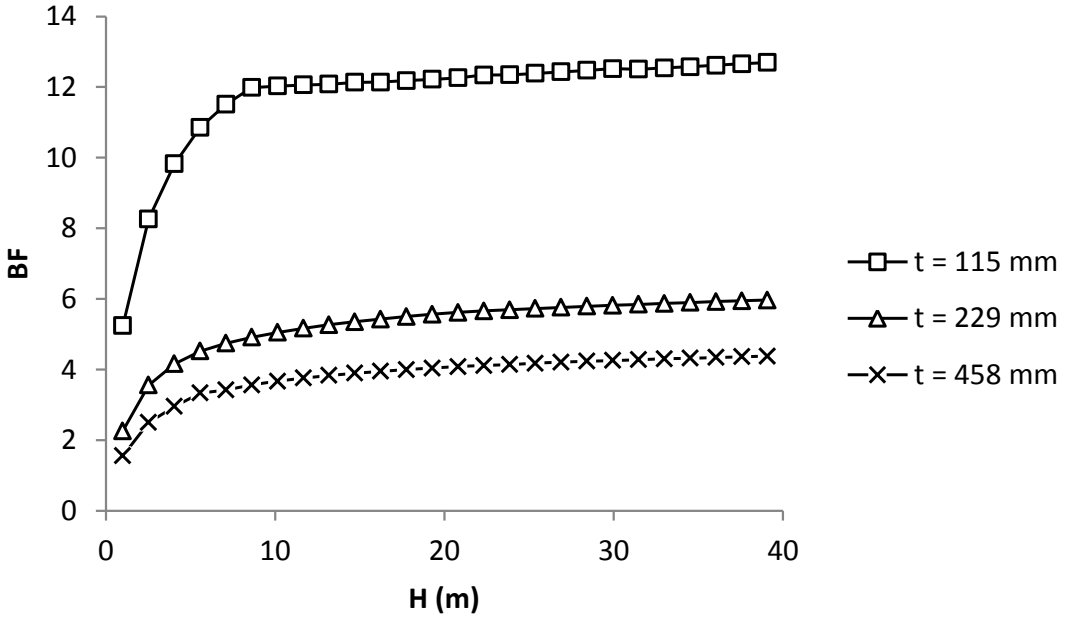

Figure A.8: Effect of backfill height on the soil load bedding factor for a pipe diameter of 2.4 m buried in Type 1 installation

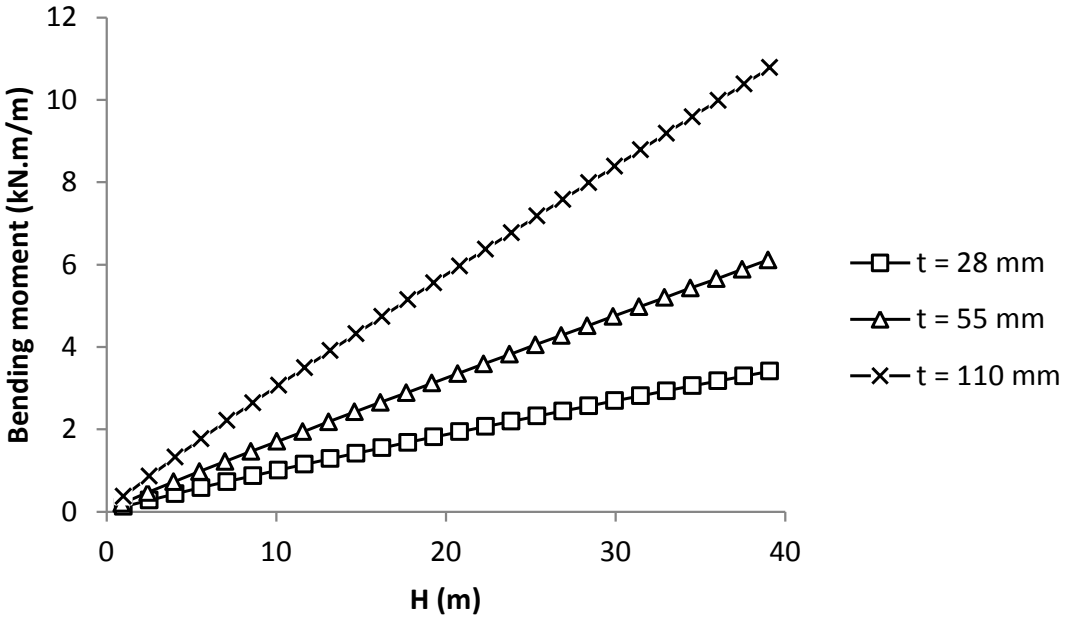

Figure A.9: Effect of backfill height on the developed maximum bending moment for a pipe with a diameter of 0.3 m buried in Type 2 installation

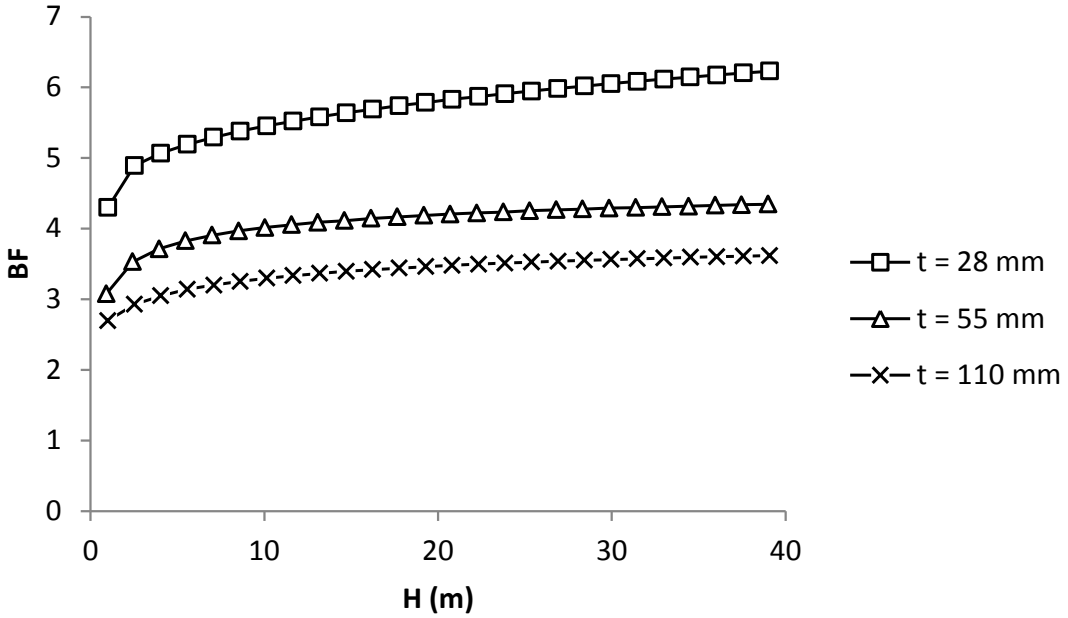

Figure A.10: Effect of backfill height on the soil load bedding factor for a pipe diameter of 0.3 m buried in Type 2 installation

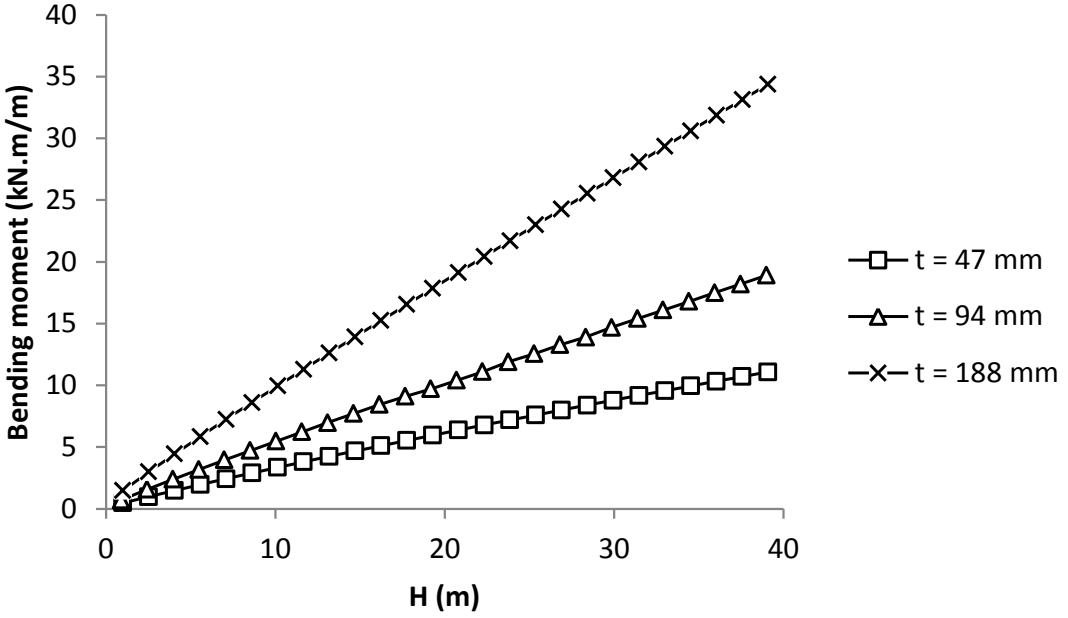

Figure A.11: Effect of backfill height on the developed maximum bending moment for a pipe with a diameter of 0.6 m buried in Type 2 installation

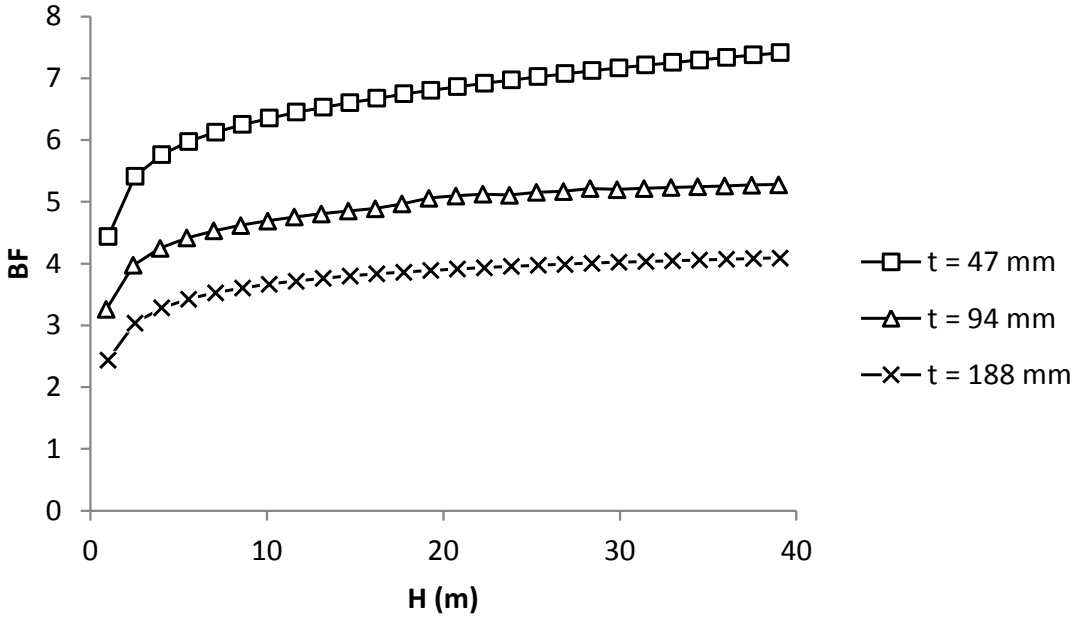

Figure A.12: Effect of backfill height on the soil load bedding factor for a pipe diameter of 0.6 m buried in Type 2 installation

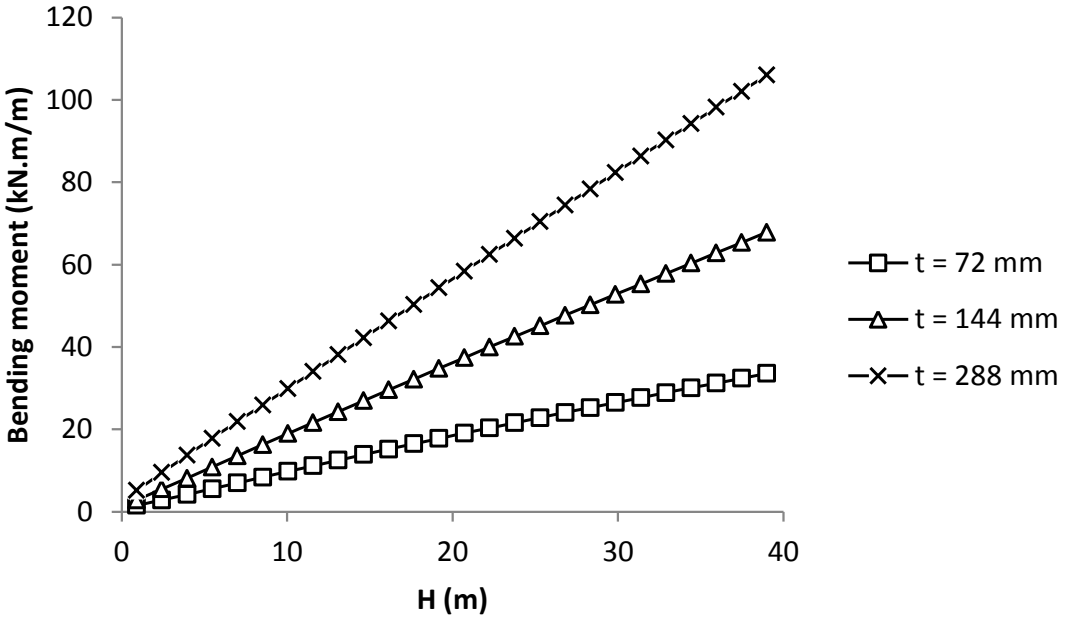

Figure A.13: Effect of backfill height on the developed maximum bending moment for a pipe with a diameter of 1.2 m buried in Type 2 installation

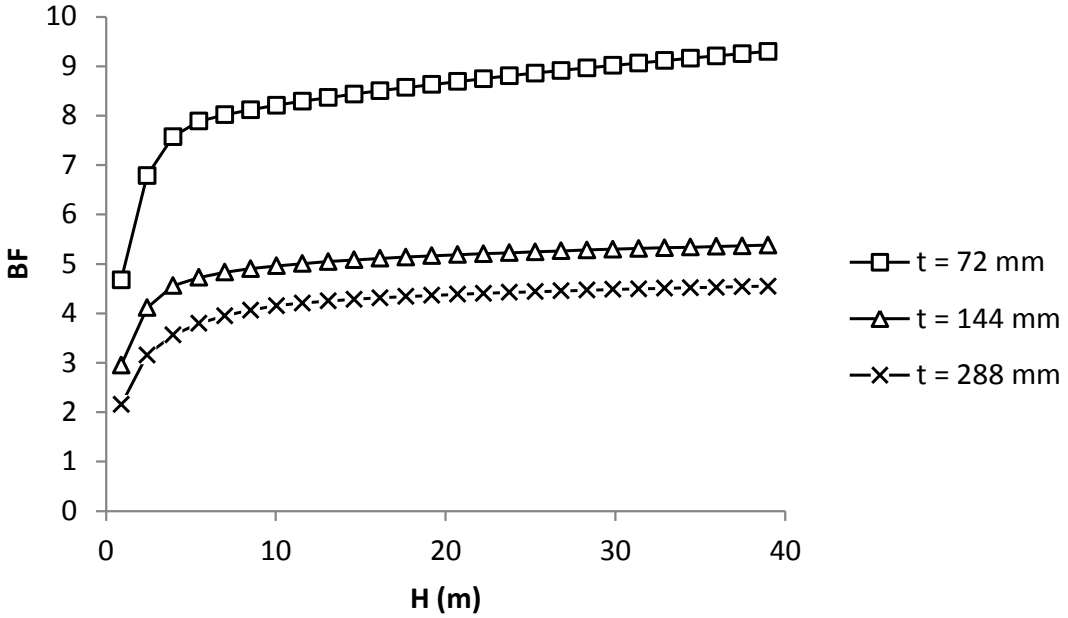

Figure A.14: Effect of backfill height on the soil load bedding factor for a pipe diameter of 1.2 m buried in Type 2 installation

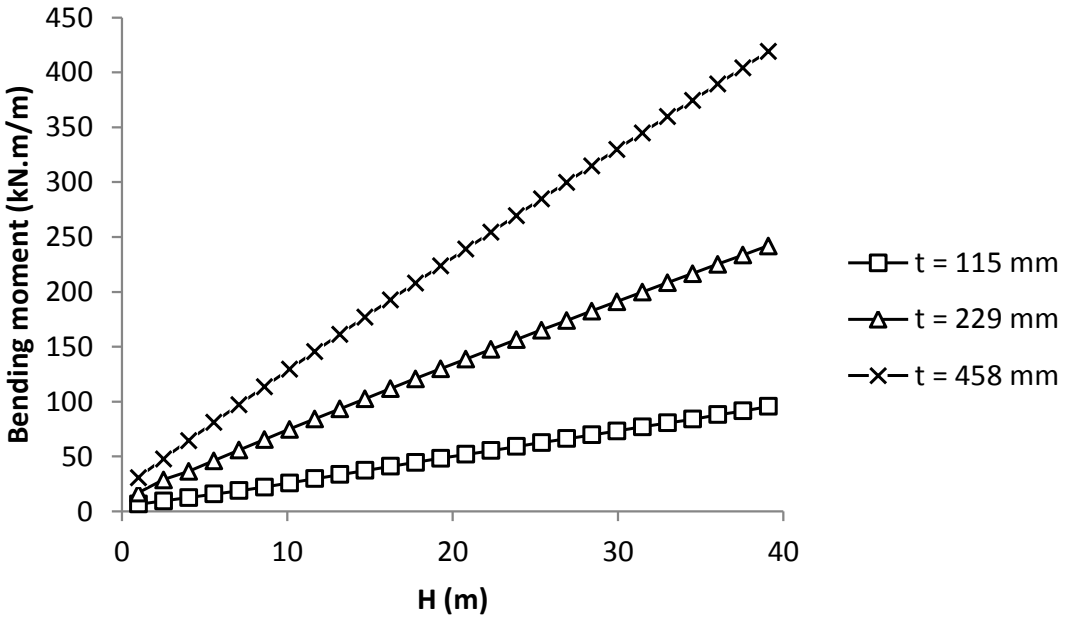

Figure A.15: Effect of backfill height on the developed maximum bending moment for a pipe with a diameter of 2.4 m buried in Type 2 installation

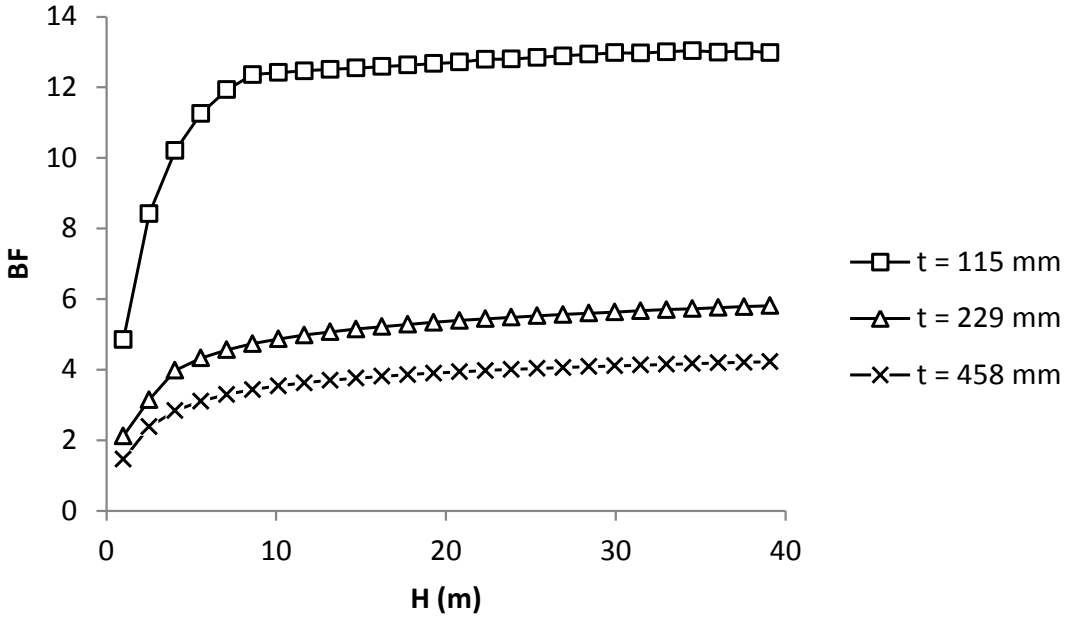

Figure A.16: Effect of backfill height on the soil load bedding factor for a pipe diameter of 2.4 m buried in Type 2 installation

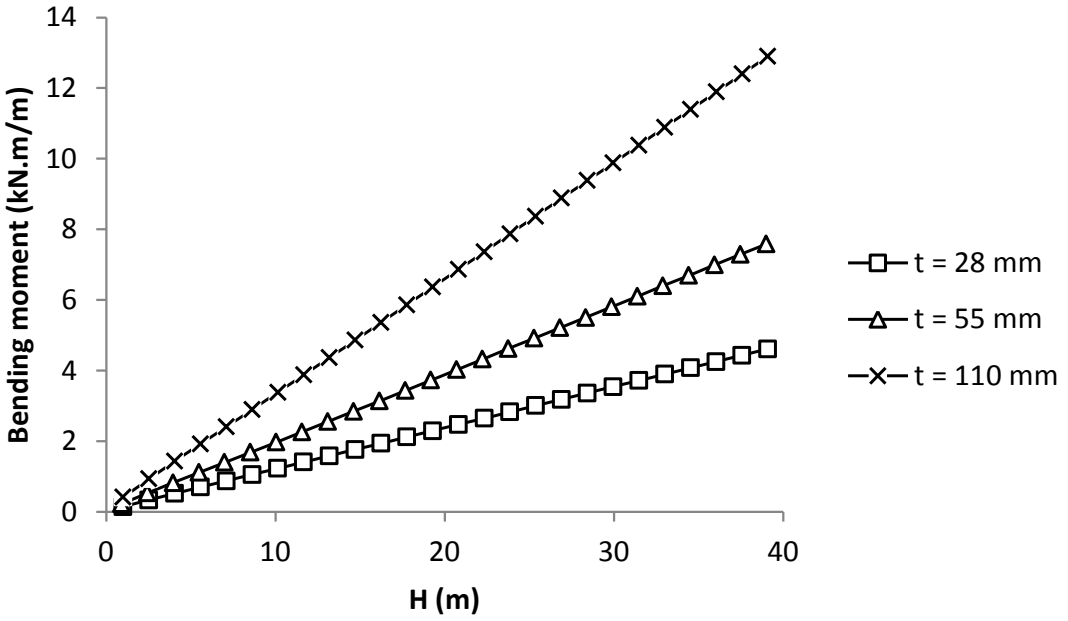

Figure A.17: Effect of backfill height on the developed maximum bending moment for a pipe with a diameter of 0.3 m buried in Type 3 installation

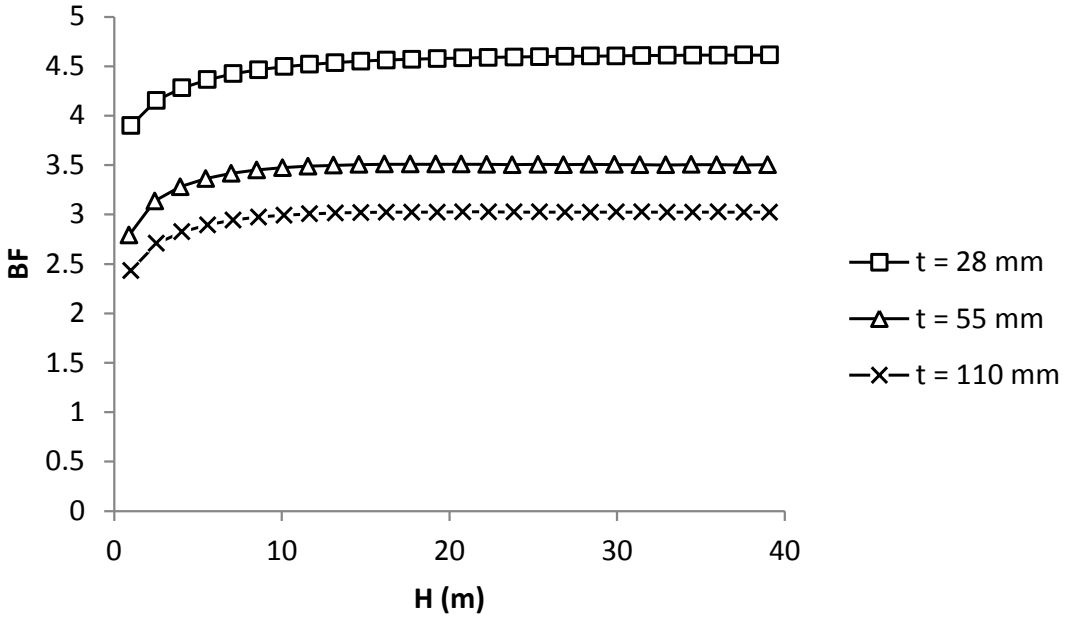

Figure A.18: Effect of backfill height on the soil load bedding factor for a pipe diameter of 0.3 m buried in Type 3 installation

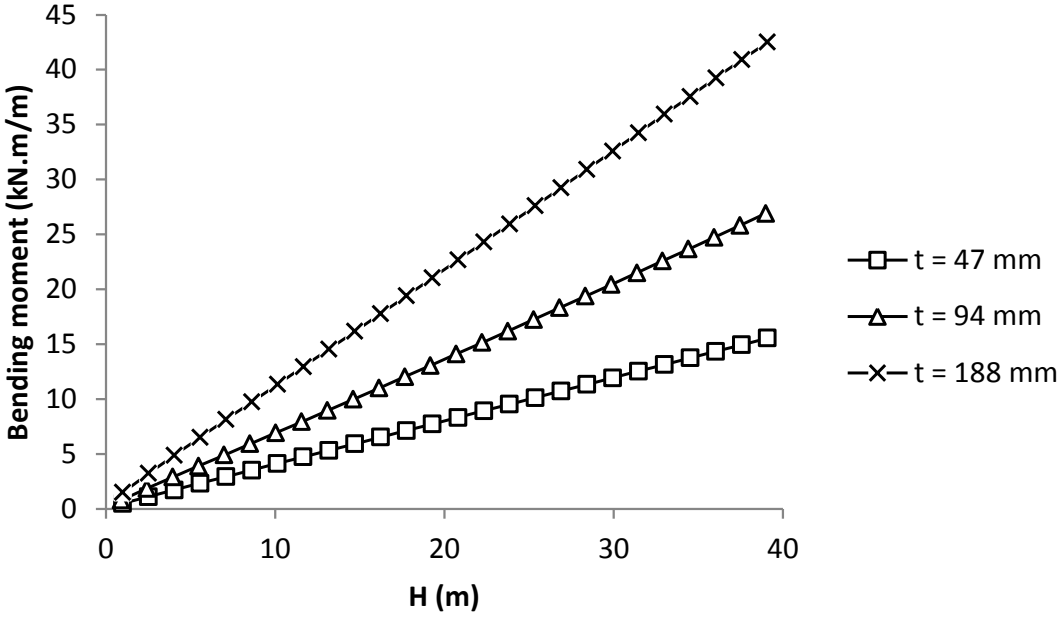

Figure A.19: Effect of backfill height on the developed maximum bending moment for a pipe with a diameter of 0.6 m buried in Type 3 installation

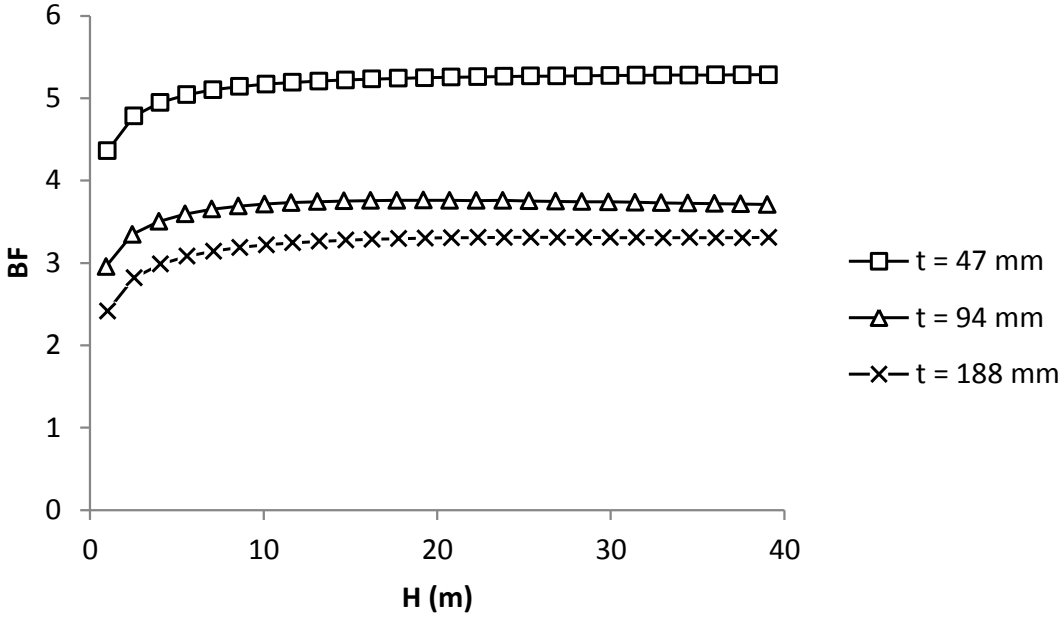

Figure A.20: Effect of backfill height on the soil load bedding factor for a pipe diameter of 0.6 m buried in Type 3 installation

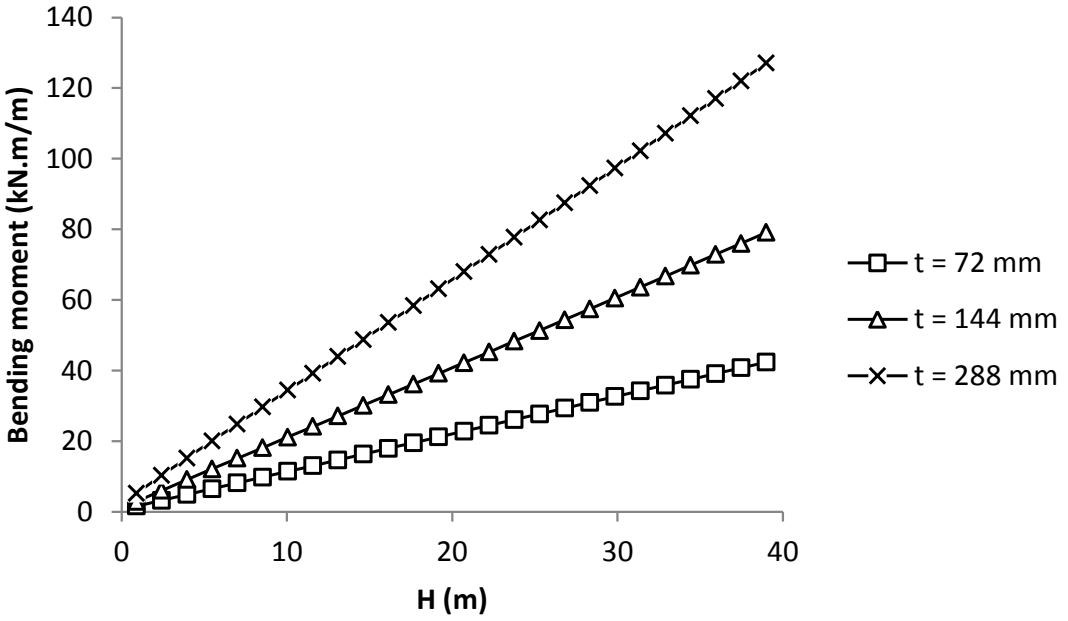

Figure A.21: Effect of backfill height on the developed maximum bending moment for a pipe with a diameter of 1.2 m buried in Type 3 installation

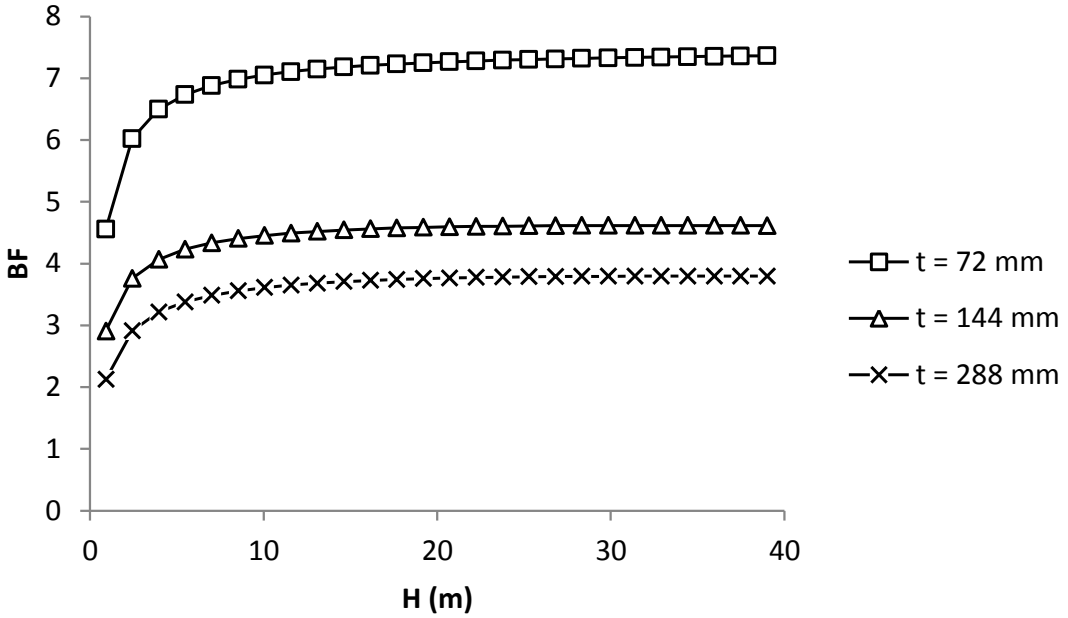

Figure A.22: Effect of backfill height on the soil load bedding factor for a pipe diameter of 1.2 m buried in Type 3 installation

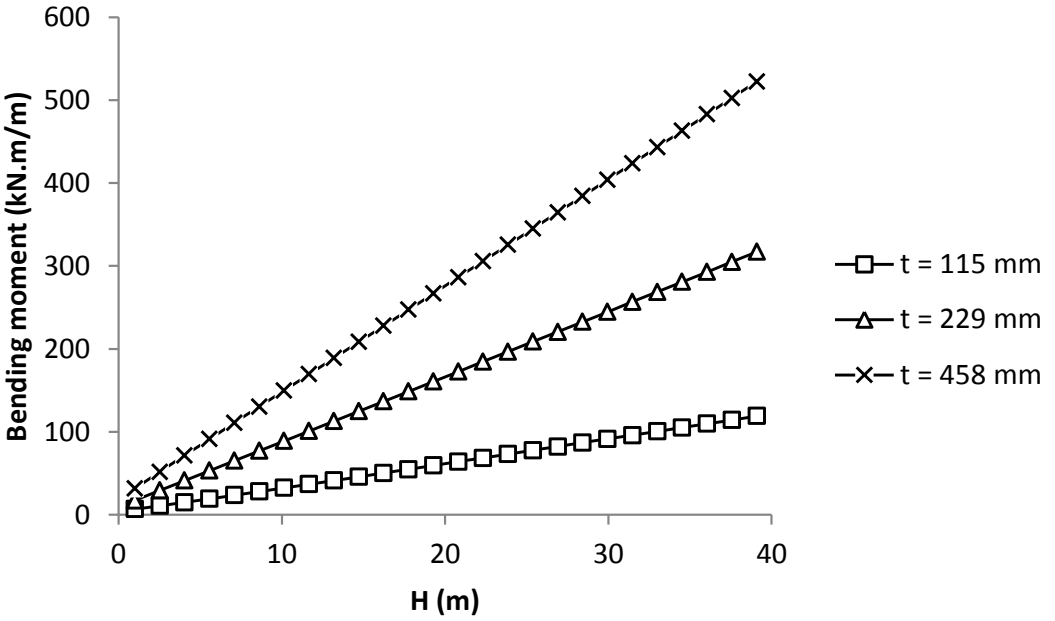

Figure A.23: Effect of backfill height on the developed maximum bending moment for a pipe with a diameter of 2.4 m buried in Type 3 installation

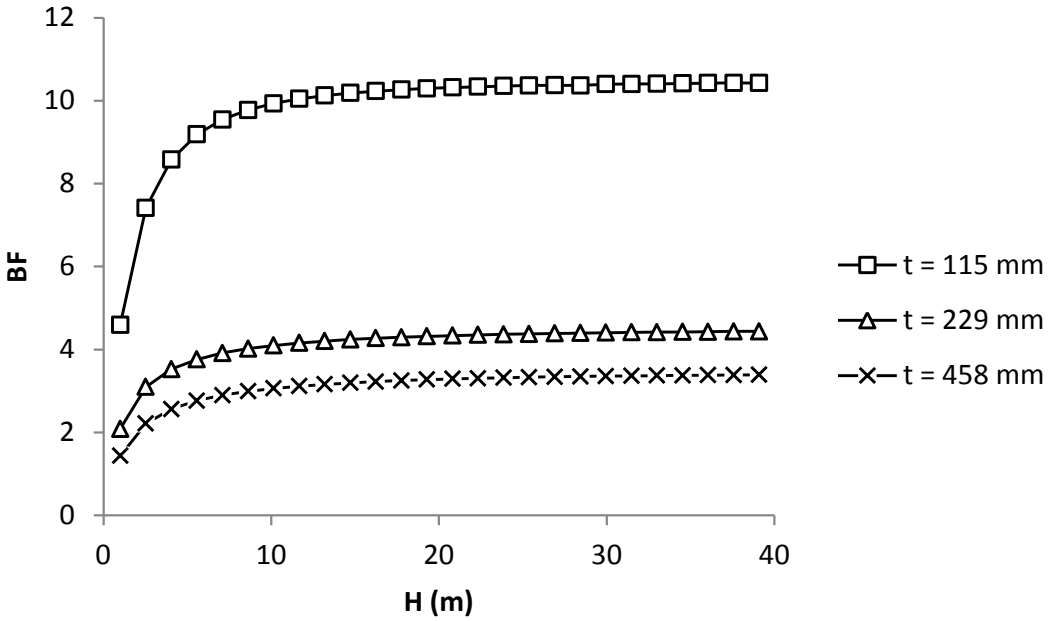

Figure A.24: Effect of backfill height on the soil load bedding factor for a pipe diameter of 2.4 m buried in Type 3 installation

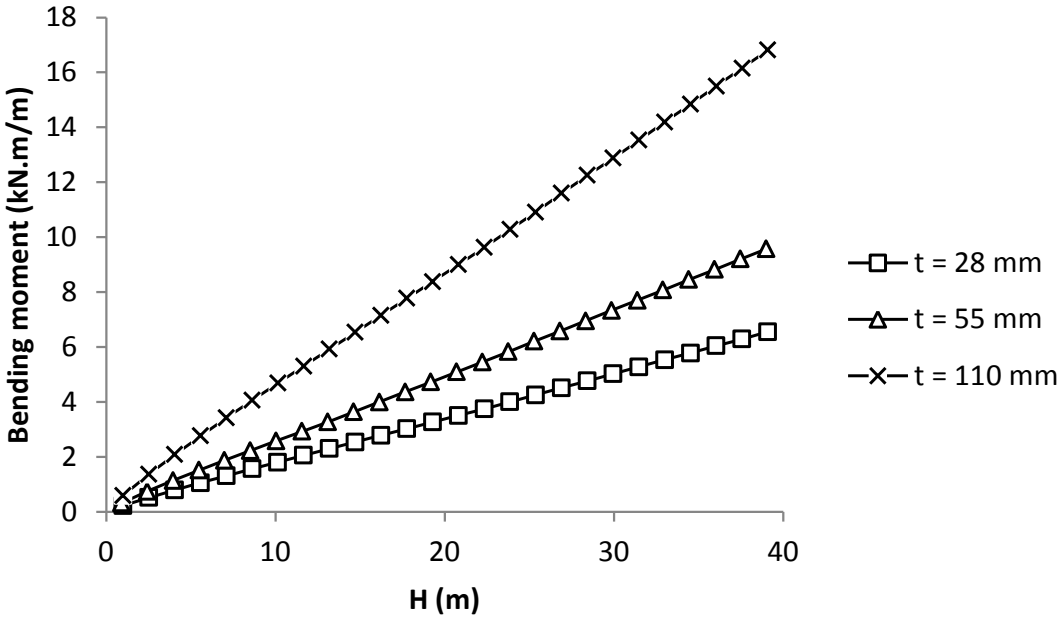

Figure A.25: Effect of backfill height on the developed maximum bending moment for a pipe with a diameter of 0.3 m buried in Type 4 installation

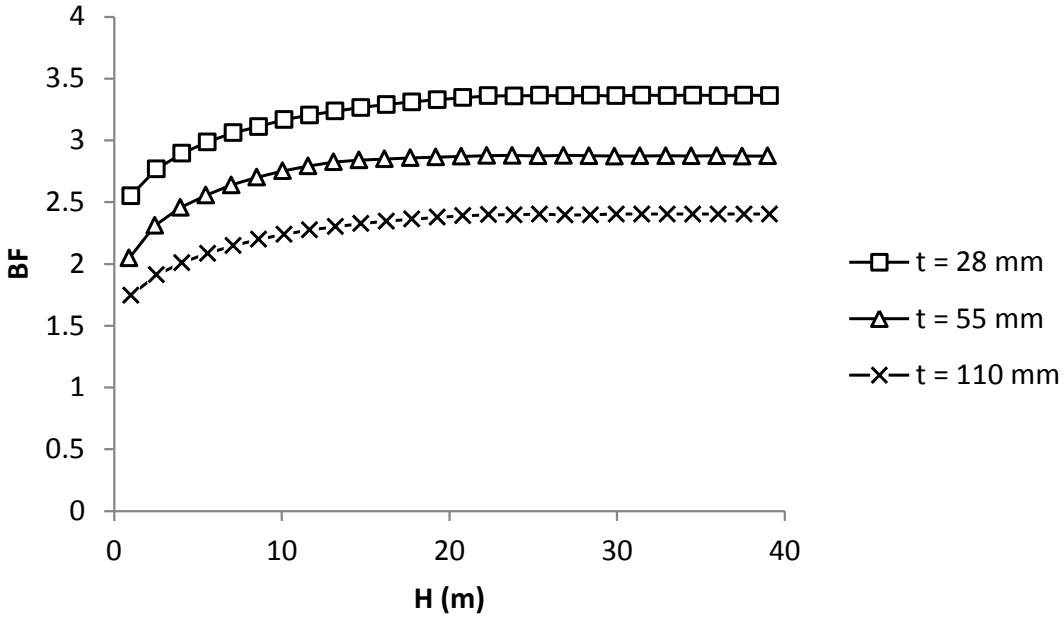

Figure A.26: Effect of backfill height on the soil load bedding factor for a pipe diameter of 0.3 m buried in Type 4 installation

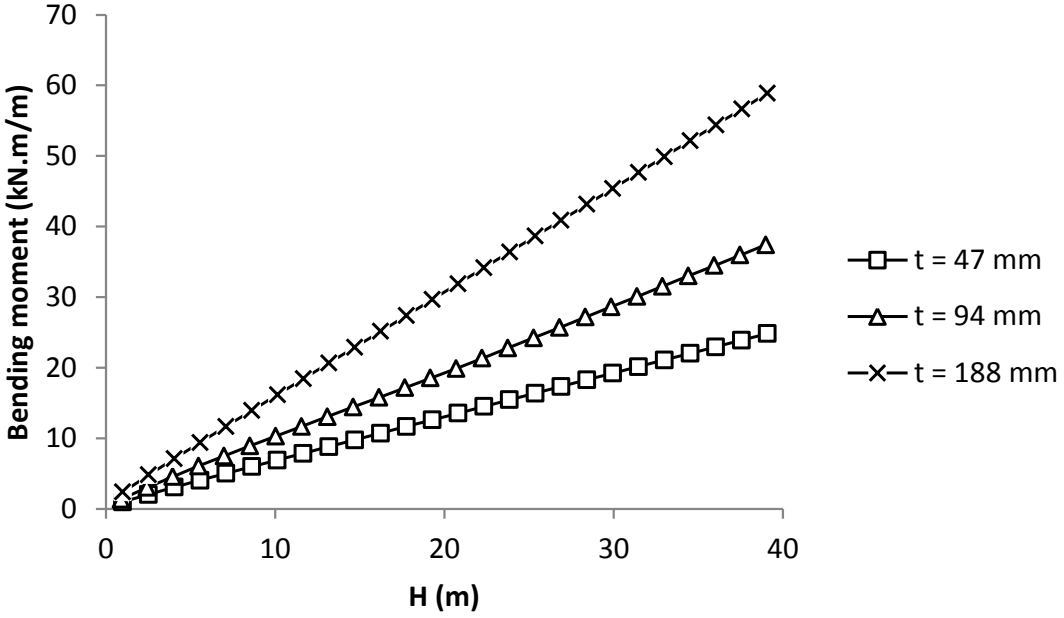

Figure A.27: Effect of backfill height on the developed maximum bending moment for a pipe with a diameter of 0.6 m buried in Type 4 installation

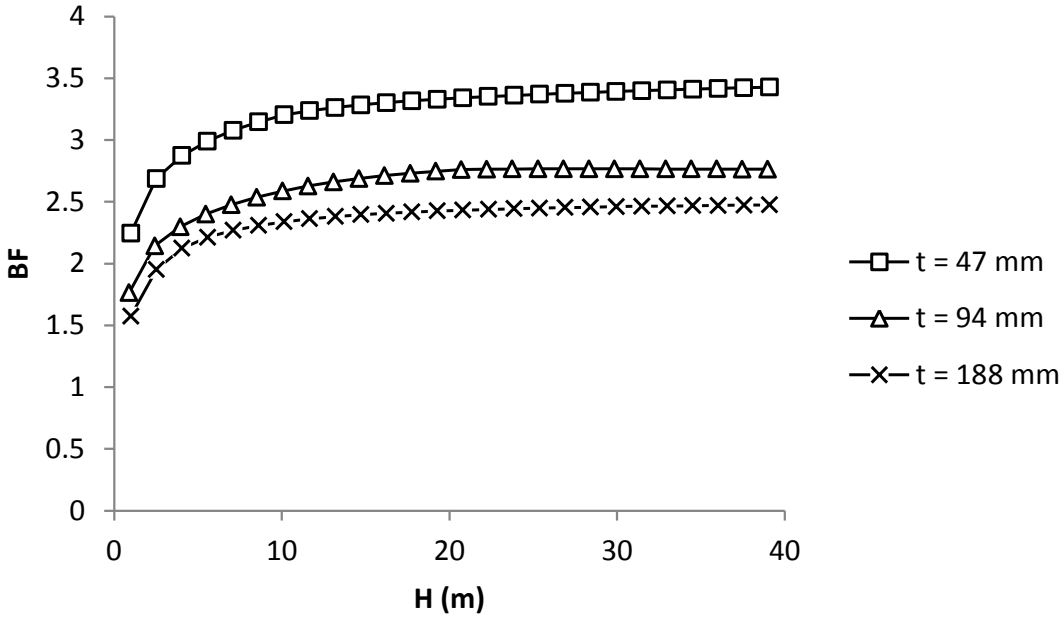

Figure A.28: Effect of backfill height on the soil load bedding factor for a pipe diameter of 0.6 m buried in Type 4 installation

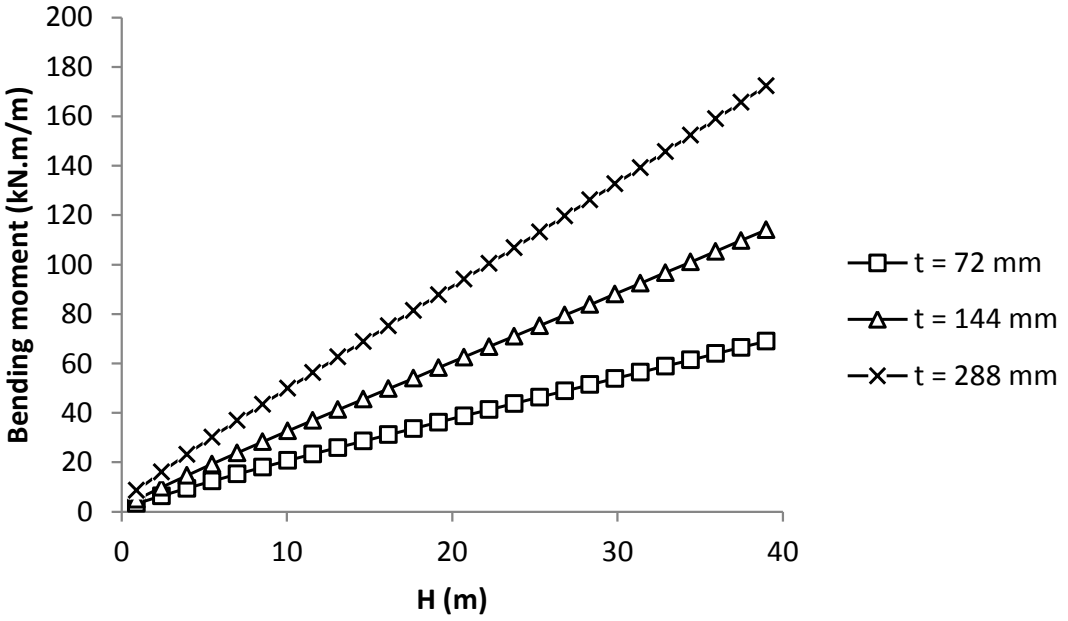

Figure A.29: Effect of backfill height on the developed maximum bending moment for a pipe with a diameter of 1.2 m buried in Type 4 installation

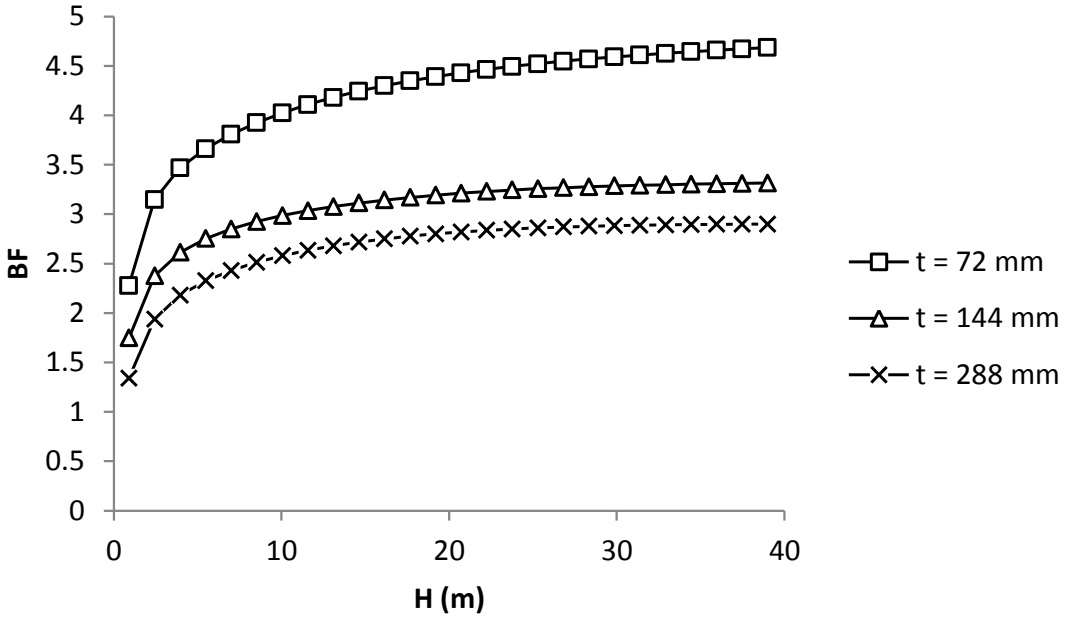

Figure A.30: Effect of backfill height on the soil load bedding factor for a pipe diameter of 1.2 m buried in Type 4 installation

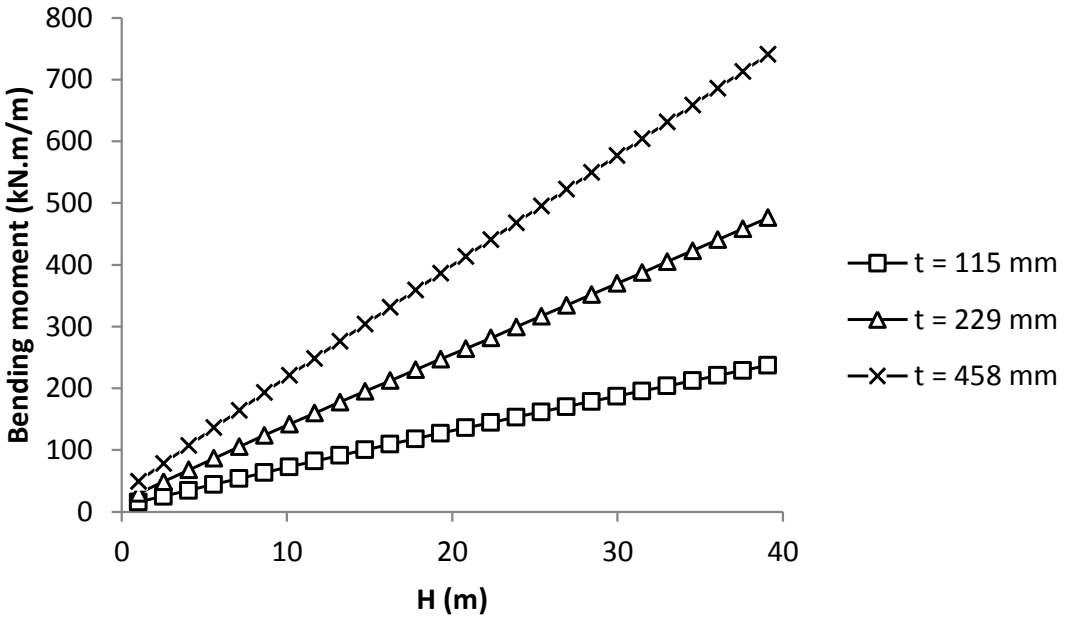

Figure A.31: Effect of backfill height on the developed maximum bending moment for a pipe with a diameter of 2.4 m buried in Type 4 installation

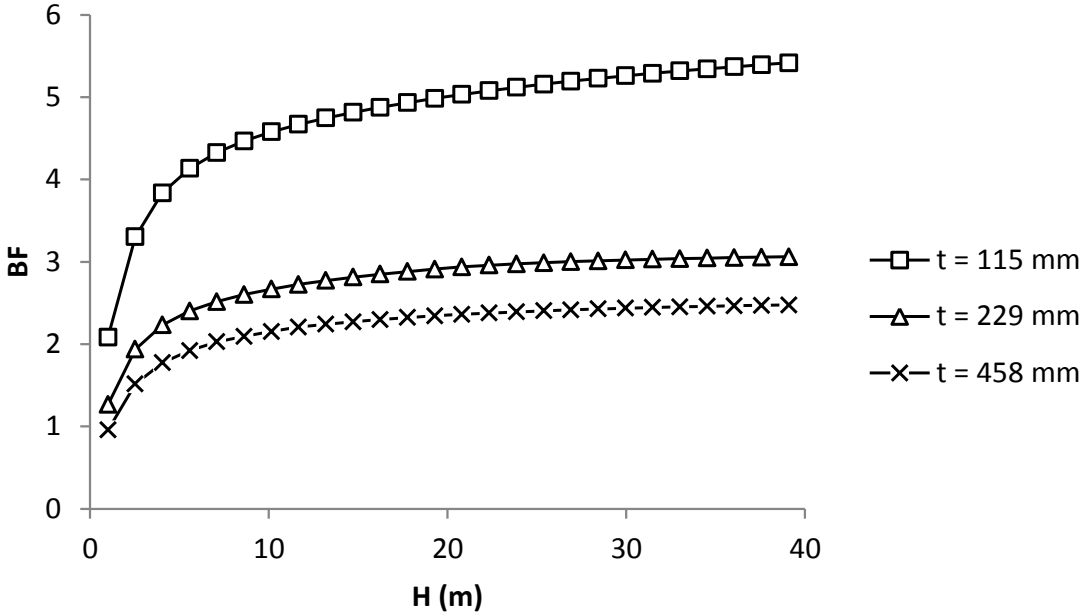

Figure A.32: Effect of backfill height on the soil load bedding factor for a pipe diameter of 2.4 m buried in Type 4 installation

Appendix B: Calculation of total force based on the BS design methodology

Table B1: Calculation of total force based on the BS design methodology for the good installation condition

D	t	$Dout$	H	$H/Dout$	C_c*	$F1$**	T_w	H/T_w	Ka × μ′	C_d ***	$F2$ ****	Min. of $F1$ and $F2$	$W_{traffic}$ *****	W_t ******
0.30	0.03	0.35	1.00	2.85	4.21	10.87	0.83	1.21	0.17	1.00	14.30	10.87	27.30	38.17
0.30	0.03	0.35	1.50	4.28	6.34	16.39	0.83	1.82	0.17	1.37	19.58	16.39	18.85	35.24
0.30	0.03	0.35	2.00	5.70	8.48	21.92	0.83	2.42	0.17	1.67	23.90	21.92	14.11	36.03
0.30	0.03	0.35	2.50	7.13	10.62	27.44	0.83	3.03	0.17	1.91	27.44	27.44	11.04	38.47
0.30	0.05	0.40	1.00	2.49	3.67	12.41	0.90	1.11	0.17	0.93	15.87	12.41	31.26	43.67
0.30	0.05	0.40	1.50	3.74	5.53	18.74	0.90	1.66	0.17	1.28	21.88	18.74	21.58	40.31
0.30	0.05	0.40	2.00	4.98	7.40	25.06	0.90	2.22	0.17	1.57	26.88	25.06	16.15	41.21
0.30	0.05	0.40	2.50	6.23	9.27	31.39	0.90	2.77	0.17	1.82	31.05	31.05	12.64	43.68
0.30	0.10	0.50	1.00	1.98	2.91	15.50	1.06	0.95	0.17	0.81	19.05	15.50	39.23	54.73
0.30	0.10	0.50	1.50	2.98	4.39	23.44	1.06	1.42	0.17	1.13	26.56	23.44	27.08	50.52
0.30	0.10	0.50	2.00	3.97	5.88	31.38	1.06	1.89	0.17	1.41	32.98	31.38	20.27	51.65
0.30	0.10	0.50	2.50	4.96	7.37	39.32	1.06	2.37	0.17	1.64	38.47	38.47	15.86	54.33
0.60	0.04	0.68	1.00	1.48	2.15	20.62	1.31	0.76	0.17	0.67	24.40	20.62	52.62	73.24
0.60	0.04	0.68	1.50	2.22	3.26	31.27	1.31	1.14	0.17	0.95	34.49	31.27	36.32	67.59
0.60	0.04	0.68	2.00	2.96	4.37	41.92	1.31	1.52	0.17	1.20	43.38	41.92	27.18	69.10

0.60	0.04	0.68	2.50	3.70	5.48	52.56	1.31	1.90	0.17	1.41	51.23	51.23	21.27	72.50
0.60	0.08	0.75	1.00	1.33	1.92	22.87	1.43	0.70	0.17	0.63	26.79	22.87	58.56	81.43
0.60	0.08	0.75	1.50	1.99	2.92	34.72	1.43	1.05	0.17	0.89	38.03	34.72	40.42	75.14
0.60	0.08	0.75	2.00	2.66	3.92	46.57	1.43	1.40	0.17	1.12	48.05	46.57	30.26	76.83
0.60	0.08	0.75	2.50	3.32	4.91	58.42	1.43	1.75	0.17	1.33	56.98	56.98	23.67	80.65
0.60	0.15	0.90	1.00	1.11	1.59	27.27	1.66	0.60	0.17	0.55	31.53	27.27	70.36	97.64
0.60	0.15	0.90	1.50	1.66	2.42	41.51	1.66	0.91	0.17	0.78	45.09	41.51	48.57	90.08
0.60	0.15	0.90	2.00	2.21	3.25	55.75	1.66	1.21	0.17	1.00	57.36	55.75	36.35	92.10
0.60	0.15	0.90	2.50	2.77	4.08	69.99	1.66	1.51	0.17	1.19	68.47	68.47	28.44	96.91
1.20	0.06	1.33	1.00	0.75	1.06	39.21	2.29	0.44	0.17	0.41	44.80	39.21	103.28	142.50
1.20	0.06	1.33	1.50	1.13	1.63	60.11	2.29	0.65	0.17	0.59	64.89	60.11	71.29	131.41
1.20	0.06	1.33	2.00	1.51	2.19	81.01	2.29	0.87	0.17	0.76	83.58	81.01	53.36	134.38
1.20	0.06	1.33	2.50	1.88	2.76	101.91	2.29	1.09	0.17	0.92	100.98	100.98	41.75	142.73
1.20	0.13	1.45	1.00	0.69	0.96	42.69	2.48	0.40	0.17	0.38	48.78	42.69	113.17	155.86
1.20	0.13	1.45	1.50	1.03	1.48	65.59	2.48	0.60	0.17	0.55	70.85	65.59	78.12	143.71
1.20	0.13	1.45	2.00	1.38	1.99	88.49	2.48	0.81	0.17	0.71	91.49	88.49	58.47	146.96
1.20	0.13	1.45	2.50	1.72	2.51	111.39	2.48	1.01	0.17	0.86	110.81	110.81	45.75	156.56
1.20	0.25	1.71	1.00	0.59	0.81	49.51	2.86	0.35	0.17	0.33	56.77	49.51	132.94	182.45
1.20	0.25	1.71	1.50	0.88	1.25	76.41	2.86	0.52	0.17	0.48	82.79	76.41	91.76	168.18
1.20	0.25	1.71	2.00	1.17	1.69	103.32	2.86	0.70	0.17	0.62	107.35	103.32	68.68	172.00

1.20	0.25	1.71	2.50	1.46	2.13	130.22	2.86	0.87	0.17	0.76	130.54	130.22	53.74	183.95
2.40	0.11	2.63	1.00	0.38	0.50	72.63	4.24	0.24	0.17	0.23	85.71	72.63	204.55	277.18
2.40	0.23	2.86	1.00	0.35	0.45	78.02	4.59	0.22	0.17	0.21	92.94	78.02	222.45	300.47
2.40	0.46	3.31	1.00	0.30	0.38	88.26	5.27	0.19	0.17	0.18	107.31	88.26	257.97	346.23

* Equation 1.3

** $F_1 = C_c \times \gamma \times D_{out}^2$

*** Equation 1.4

**** $F2 = (C_d \times \gamma \times T_w^2)$

***** Equation 1.5

****** Equation 1.1

REFERENCES

AASHTO. (1998) **AASHTO LRFD bridge design specifications**. Washington, D.C.: AASHTO.

AASHTO. (2004) **AASHTO LRFD bridge design specifications**. 3rd ed. Washington, D.C.: AASHTO.

AASHTO. (2007) **AASHTO LRFD bridge design specifications**. 4th ed. Washington, D.C.: AASHTO.

AASHTO. (2013) **AASHTO LRFD bridge design specifications**. 6th ed. Washington, D.C.: AASHTO.

AASHTO. (2016) **AASHTO LRFD Bridge Design Specifications**. 7th ed. Washington, D.C.: AASHTO.

Abadi, T., Le Pen, L., Zervos, A. and Powrie, W. (2015) Measuring the area and number of ballast particle contacts at sleeper/ballast and ballast/subgrade interfaces. **International Journal of Railway Technology**, 4 (2): 45-72

Abolmaali, A. and Kararam, A. (2010) Nonlinear finite-element-based investigation of the effect of bedding thickness on buried concrete pipe. **Journal of Transportation Engineering**, 136 (9): 793-799.

Abolmaali, A. and Kararam, A. (2013) Nonlinear finite-element modeling analysis of soil-pipe interaction. **International Journal of Geomechanics**, 13 (3): 197-204.

ACI. (2014) B**uilding code requirements for structural concrete (ACI 318-14) and commentary (ACI 318R-14)**. Farmington Hills, MI: American Concrete Institute.

ACPA. (2011) **Concrete pipe design manual**. Irving: ACPA.

Ahangar Asr, A. and Javadi, A.A. (2016) Air losses in compressed air tunnelling: a prediction model. **Proceedings of the Institution of Civil Engineers - Engineering and Computational Mechanics**, 169 (3): 140-147.

Ahangar-Asr, A., Javadi, A.A., Johari, A. and Chen, Y. (2014) Lateral load bearing capacity modelling of piles in cohesive soils in undrained conditions: An intelligent evolutionary approach. **Applied Soft Computing**, 24: 822-828.

Alani, A.M. and Faramarzi, A. (2014) An evolutionary approach to modelling concrete degradation due to sulphuric acid attack. **Applied Soft Computing**, 24: 985-993.

Alani, A.M., Faramarzi, A., Mahmoodian, M. and Tee, K.F. (2014) Prediction of sulphide build-up in filled sewer pipes. **Environmental Technology**, 35 (14): 1721-1728.

Allard, E. and El Naggar, H. (2016) Pressure distribution around rigid culverts considering soil-structure interaction effects. **International Journal of Geomechanics**, 16 (2), 04015056.

Arockiasamy, M., Chaallal, O. and Limpeteeprakarn, T. (2006) Full-scale field tests on flexible pipes under live load application. **Journal of Performance of Constructed Facilities**, 20 (1): 21–27.

ASTM. (2016) **C 76: Standard specification for reinforced concrete culvert, storm drain, and sewer pipe**. West Conshohocken: ASTM International.

Balkaya, M., Moore, I.D. and Sağlamer, A. (2012a) Study of non-uniform bedding due to voids under jointed PVC water distribution pipes. **Geotextiles and Geomembranes**, 34: 39-50.

Balkaya, M., Moore, I.D. and Sağlamer, A. (2012b) Study of nonuniform bedding support because of erosion under cast iron water distribution pipes. **Journal of Geotechnical and Geoenvironmental Engineering**, 138 (10): 1247-1256.

Balkaya, M., Moore, I.D. and Sağlamer, A. (2013) Study of non-uniform bedding support under continuous PVC water distribution pipes. **Tunnelling and Underground Space Technology**, 35: 99-108.

Bian X., Tang X., Shen, W., Ling, D. and Chen, Y. (2012) An experimental study on a culvert buried in granular soil subjected to vehicle loads. **Advances in Structural Engineering**, 15 (6): 1031-1040.

Boscardin, M.D., Selig, E.T., Lin, R.S. and Yang, G.R. (1990) Hyperbolic parameters for compacted soils. **Journal of Geotechnical Engineering ASCE**, 116 (1): 88-104.

Boschert, J. and Howard, A. (2014) “Importance of haunching.” In Rahman, S. and McPherson, D. (eds.) **Pipelines 2014: From Underground to the Forefront of Innovation and Sustainability**, Portland: ASCE. pp. 393-404.

Brown, S.F. and Selig, E.T. (1991) “The design of pavement and rail track foundations.” In O’Reilly, M. P. and Brown, S. F. (eds.) **Cyclic loading of soils: from theory to practice**. Glasgow and London: Blackie and Son Ltd. pp. 249-305.

Bryden, P., El Naggar, H. and Valsangkar, A. (2015) Soil-structure interaction of very flexible pipes: centrifuge and numerical investigations. **International Journal of Geomechanics**, 15 (6): 04014091.

BSI. (1997) **BS EN 1295-1: Structural design of buried pipelines under various conditions of loading – part 1: general requirements**. London: BSI.

BSI. (2002) **BS EN 1916: Concrete pipes and fittings, unreinforced, steel fibre and reinforced**. London: BSI.

BSI. (2009) **BS EN 1401-1: Plastic piping systems for non-pressure underground drainage and sewerage– Unplasticized poly (vinyl chloride) (PVC-U)- part 1**. London: BSI.

BSI. (2010) **BS 9295: Guide to the structural design of buried pipelines**. London: BSI.

BSI. (2016) **BS ISO 19469-1: Plastic piping systems for non pressure underground drainage – single wall corrugated piping systems of polyethylene (PE), polypropylene (pp) and unplasticized poly (vinyl chloride) (PVC-U)- Part 1: General requirements and performance characteristics**. London: BSI.

Chaallal, O., Arockiasamy, M. and Godat, A. (2015a) Field test performance of buried flexible pipes under live truck loads. **Journal of Performance of Constructed Facilities**, 29 (5): 04014124.

Chaallal, O., Arockiasamy, M. and Godat, A. (2015b) Numerical finite-element investigation of the parameters influencing the behavior of flexible pipes for culverts and storm sewers under truck load. **Journal of Pipeline Systems Engineering and Practice**, 6 (2): 04014015.

Chapman, D. N, Fleming, P. R., Rogers, C. D. F. and Talby, R. T. (2007) The response of flexible pipes buried in sand to static surface stress. **Geomechanics and Geoengineering: An International Journal**, 2 (1): 17-28.

CSA. (2006) **CAN/CSA-S6-06: Canadian highway bridge design code**. Mississauga: CSA.

Cui, X., Li, J., Chan, A. and Chapman, D. (2012) A 2D DEM–LBM study on soil behaviour due to locally injected fluid. **Particuology**, 10 (2): 242-252.

De Beer, M., Fisher, C. and Jooste, F.J. (1997). "Determination of pneumatic tyre/pavement interface contact stresses under moving loads and some effects on pavements with thin asphalt surfacing layers." In **8th International Conference on Asphalt Pavements**. Seattle: pp.179-227. (Volume 1)

Dhar, A. S., Moore, I. D. and McGrath, T. J. (2004) Two-dimensional analyses of thermoplastic culvert deformations and strains. **Journal of Geotechnical and Geoenvironmental Engineering**, 130 (2): 199-208.

Duncan, J. M. and Chang, C. (1970) Nonlinear analysis of stress and strain in soils. **Journal of the Soil Mechanics and Foundations Division ASCE**, 96 (5): 1629-1653.

Elshimi, T. M. and Moore, I. D. (2013) Modeling the effects of backfilling and soil compaction beside shallow buried pipes. **Journal of Pipeline Systems Engineering and Practice**, 4 (4): 04013004.

Elshimi, T.M. (2011) **Three-dimensional nonlinear analysis of deep-corrugated culverts**. PhD thesis, Queen's University.

Faramarzi, A, Javadi, A. A. and Alani, A. M. (2012) EPR-based material modelling of soils considering volume changes. **Computers and Geosciences**, 48: 73-85.

Faramarzi, A., Alani, A. M. and Javadi, A. A. (2014) An EPR-based self-learning approach to material modelling. **Computers and Structures**, 137: 63-71.

Faramarzi, A., Javadi, A. A. and Ahangar-Asr, A. (2013) Numerical implementation of EPR-based material models in finite element analysis. **Computers and Structures**, 118, 100-108.

Galavi, V. and Brinkgreve, R.B.J. (2014) "Finite element modelling of geotechnical structures subjected to moving loads." In Hicks, M.A., Brinkgreve, R.B.J. and Rohe, A (eds.) **Numerical methods in geotechnical engineering**. London: pp. 235-40.

Gallage, C. P. K., Chan, D. and Kodikara, J. (2012) Response of a plastic pipe buried in expansive clay. **Proceedings of the Institution of Civil Engineers - Geotechnical Engineering**, 165 (1): 45-57.

García, D.B. (2012) **Investigation of culvert joints employing large scale tests and numerical simulations**. PhD thesis, Queen's University.

García, D.B. and Moore, I.D. (2015a) Performance of deteriorated corrugated steel culverts rehabilitated with sprayed-on cementitious liners subjected to surface loads. **Tunnelling and Underground Space Technology**, 47: 222-232.

García, D.B. and Moore, I.D. (2015b). Behaviour of bell and spigot joints in buried reinforced concrete pipelines. **Canadian Geotechnical Journal**, 52 (5): 609-625.

Giustolisi, O. and Savic, D.A. (2006) A symbolic data-driven technique based on evolutionary polynomial regression. **Journal of Hydroinformatics**, 8 (3): 207-222.

Giustolisi, O. and Savic, D.A. (2009) Advances in data-driven analyses and modelling using EPR-MOGA. **Journal of Hydroinformatics**, 11 (3-4): 225-236.

Gray, H.F. (1940) Sewerage in ancient and medieval time. **Sewage Works Journal**, 12 (5): 939-946.

Gumbel, J.E., O'Reilly, M.P., Lake, L.M. and Carder, D.R. (1982). "The development of a new design method for buried flexible pipes." In **Europipe 82: European Conference for the Construction and Maintenance of Pipelines**. Basel: pp.87-98.

HA (2001). **Design Manual for Roads and Bridges – Volume 4, Section 2, Part 5: HA 40/01: Determination of Pipe and Bedding Combination for Drainage Work**. London: The Stationery Office.

Janbu, N. (1963). “Soil compressibility as determined by odometer and triaxial tests.” In **the European Conference on Soil Mechanics and Foundation Engineering**. Wiesbaden: 19–25 (Volume 1).

Javadi, A.A., Ahangar-Asr, A., Johari, A., Faramarzi, A. and Toll, D. (2012b) Modelling stress–strain and volume change behaviour of unsaturated soils using an evolutionary based data mining technique, an incremental approach. **Engineering Applications of Artificial Intelligence**, 25 (5): 926-933.

Javadi, A.A., Faramarzi, A. and Ahangar-Asr, A. (2012a) Analysis of behaviour of soils under cyclic loading using EPR-based finite element method. **Finite Elements in Analysis and Design**, 58: 53-65.

Kamel, S. and Meguid, M.A. (2013). Investigating the effects of local contact loss on the earth pressure distribution on rigid pipes. **Geotechnical and Geological Engineering**, 31(1): 199-212.

Kang, J. S., Stuart, S.J. and Davidson, J.S. (2013a) Analytical evaluation of maximum cover limits for thermoplastic pipes used in highway constructions. **Structure and Infrastructure Engineering**, 9 (7): 667-674.

Kang, J., Jung, Y. and Ahn, Y. (2013b) Cover requirements of thermoplastic pipes used under highways. **Composites Part B: Engineering**, 55: 184-192.

Kang, J., Parker, F. and Yoo, C.H. (2007) Soil-structure interaction and imperfect trench installations for deeply buried concrete pipes. **Journal of Geotechnical and Geoenvironmental Engineering**, 133 (3): 277-285.

Kang, J., Parker, F. and Yoo, C.H. (2008a) Soil–structure interaction for deeply buried corrugated steel pipes Part I: Embankment installation. **Engineering Structures**, 30 (2): 384-392.

Kang, J., Parker, F. and Yoo, C.H. (2008b) Soil–structure interaction for deeply buried corrugated steel pipes Part II: Imperfect trench installation. **Engineering Structures**, 30 (3): 588-594.

Kang, J., Stuart, S. J. and Davidson, J. S. (2014) Analytical study of minimum cover required for thermoplastic pipes used in highway construction. **Structure and Infrastructure Engineering**, 10 (3): 316-327.

Katona, M.G. (1976). **FHWA-RD Report 77-5: CANDE: a Modern Approach for the Structural Design and Analysis of Buried Culverts**. Washington: Federal Highway Administration Office of Research and Development.

Katona, M.G. (1990) Minimum cover heights for corrugated plastic pipe under vehicle loading. **Transportation Research Record: Journal of the Transportation Research Board**, 1288: 127-135.

Katona, M.G. (2010) Seismic design and analysis of buried culverts and structures. **Journal of Pipeline Systems Engineering and Practice**, 1 (3): 111-119.

Katona, M.G. (2017) Influence of soil models on structural performance of buried culverts. **International Journal of Geomechanics**, 17 (1): 04016031.

Kraus, E., Oh, J. and Fernando, E.G. (2014) Impact of repeat overweight truck traffic on buried utility facilities. **Journal of Performance of Constructed Facilities**, 28 (4): 04014004.

Lay, G.R. and Brachman, R.W.I. (2014) Full-scale physical testing of a buried reinforced concrete pipe under axle load. **Canadian Geotechnical Journal**, 51 (4): 394-408.

Liu, G.R. and Quek Jerry, S.S. (2003) A non-reflecting boundary for analyzing wave propagation using the finite element method. **Finite Elements in Analysis and Design**, 39: 403-417.

MacDougall, K. (2014) **Behaviour and design of reinforced concrete pipes**. MASc thesis, Queen's University.

MacDougall, K., Hoult, N.A. and Moore, I.D. (2016) Measured load capacity of buried reinforced concrete pipes. **ACI Structural Journal**, 113 (1): 63-73.

Mai, V.T., Moore, I.D. and Hoult, N.A. (2014) Performance of two-dimensional analysis: Deteriorated metal culverts under surface live load. **Tunnelling and Underground Space Technology**, 42: 152-160.

Masada, T. and Zhu, J. (2015) Computer analysis of buried stormwater chamber structures. **Journal of Pipeline Systems Engineering and Practice**, 6 (2): 04014013.

Meguid, M.A. and Kamel, S. (2014) A three-dimensional analysis of the effects of erosion voids on rigid pipes. **Tunnelling and Underground Space Technology**, 43: 276-289.

Mehrjardi, G.T., Tafreshi, S.N.M. and Dawson, A.R. (2015) Numerical analysis on buried pipes protected by combination of geocell reinforcement and rubber-soil mixture. **International Journal of Civil Engineering**, 13 (2): 90-104.

Mellat, P., Andersson, A., Pettersson, L. and Karoumi, R. (2014) Dynamic behaviour of a short span soil–steel composite bridge for high-speed railways–Field measurements and FE-analysis. **Engineering structures**, 69 (15): 49-61.

Mohamedzein, Y. and Al-Aghbari, M.Y. (2016) Experimental study of the performance of plastic pipes buried in dune sand. **International Journal of Geotechnical Engineering**, 10 (3): 236-245.

Moore, I. D. (2001) "Buried pipes and culverts." In Rowe, R. K. (ed.) **Geotechnical and Geoenvironmental Engineering Handbook**. Norwell: Kluwer Academic Publishing. pp. 539‑566.

Moore, I.D., Hoult, N.A. and MacDougall, K. (2014) **Establishment of Appropriate Guidelines for Use of the Direct and Indirect Design Methods for Reinforced Concrete Pipe: Contractor's Final Report for NCHRP Project 20-07 Task 316**. Washington: Transportation Research Board.

Moser, A.P. and Folkman, S. (2008) **Buried pipe design**. 3rd ed. New York: The McGraw-Hill.

Motahari, A. and Abolmaali, A. (2010) Effect of bedding thickness on behavior of rigid pipes as determined by using numerical crack modeling. **Transportation Research Record: Journal of the Transportation Research Board**, 2172: 182-191.

Nath, P. (1983) Trench excavation effects on adjacent buried pipes: finite element study. **Journal of Geotechnical Engineering**, 109 (11): 1399-1415.

Ognedal, A.S., Clausen, A.H., Polanco-Loria, M., Benallal, A., Raka, B. and Hopperstad, O.S. (2012) Experimental and numerical study on the behaviour of PVC and HDPE in biaxial tension. **Mechanics of Materials**, 54: 18-31.

Petersen, D.L., Nelson, C.R., Li, G., McGrath, T.J. and Kitane, Y. (2010) **NCHRP Report 647: Recommended design specifications for live load distribution to buried structures**. Washington: Transportation Research Board.

Pettibone, H.C. and Howard, A.K. (1967) Distribution of soil pressures on concrete pipe. **Journal of the pipeline division**, 93 (2): 85-102.

Rakitin, B. and Xu, M. (2014) Centrifuge modeling of large-diameter underground pipes subjected to heavy traffic loads. **Canadian Geotechnical Journal**, 51 (4): 353-368.

Rakitin, B. and Xu, M. (2015) Centrifuge testing to simulate buried reinforced concrete pipe joints subjected to traffic loading. **Canadian Geotechnical Journal**, 52 (11): 1762-1774.

Robert, D.J. (2010) **Soil-pipeline interaction in unsaturated soils**. PhD thesis, University of Cambridge.

Robert, D.J., Rajeev, P., Kodikara, J. and Rajani, B. (2016) Equation to predict maximum pipe stress incorporating internal and external loadings on buried pipes. **Canadian Geotechnical Journal**, 53 (8): 1315-1331.

Rogers, C.D.F. (1985) **The response of buried uPVC pipes to surface loading**. PhD thesis, The University of Nottingham.

Rogers, C.D.F. (1987) The influence of the surrounding soil on flexible pipe performance. **Transportation Research Record**, 1129: 1-11.

Rogers, C.D.F. (1988) Some observations on flexible pipe response to load. **Transportation Research Record**, 1191: 1-11.

Rogers, C.D.F., Fleming, P. R. and Talby, R. (1996) Use of visual methods to investigate influence of installation procedure on pipe-soil interaction. **Transportation Research Record: Journal of the Transportation Research Board**, 1541: 76-85.

Sargand, S.M., Hazen, G.A., White, K. and Moran, A. (2001a) Time-dependent deflection of thermoplastic pipes under deep burial. **Transportation Research Record: Journal of the Transportation Research Board**, 1770: 236-242.

Sargand, S.M., Masada, T. and Schehl, D.J. (2001b) Soil pressure measured at various fill heights above deeply buried thermoplastic pipe. **Transportation Research Record: Journal of the Transportation Research Board**, 1770: 227-235.

Savic, D., Giustolisi, O., Berardi, L., Shepherd, W., Djordjevic, S. and Saul, A. (2006) Modelling sewer failure by evolutionary computing. **Proceedings of the Institution of Civil Engineers - Water Management**, 159 (2): 111-118.

Sayeed, M.A. and Shahin, M.A. (2016) Three-dimensional numerical modelling of ballasted railway track foundations for high-speed trains with special reference to critical speed. **Transportation Geotechnics**, 6: 55-65.

Sheldon, T., Sezen, H. and Moore, I.D. (2015) Joint response of existing pipe culverts under surface live loads. **Journal of Performance of Constructed Facilities**, 29 (1): 04014037.

Sheldon, T.A. (2011) **Beam-on-springs modeling of jointed culvert systems**. MSc thesis, The Ohio State University.

Shenton, M.J. (1978) "Deformation of railway ballast under repeated loading condition." In Kerr, A.D. (ed.) **Proceeding of Railroad Track Mechanics and Technology**. Princeton University: pp. 405-425.

Surarak, C., Likitlersuang, S., Wanatowski, D., Balasubramaniam, A., Oh, E. and Guan, H. (2012) Stiffness and strength parameters for hardening soil model of soft and stiff Bangkok clays. **Soils and Foundations**, 52 (4): 682-697.

Talby, R. (1997) **Behaviour of buried pipes and bored tunnels in sand**. PhD thesis, Loughborough University.

Taleb, B. and Moore, I. (1999) Metal culvert response to earth loading: Performance of two-dimensional analysis. T**ransportation Research Record: Journal of the Transportation Research Board**, 1656: 25-36.

Tan, Z. and Moore, I.D. (2007). “Effect of backfill erosion on moments in buried rigid pipes.” In **Transportation Research Board Annual Conference**. Washington: Transportation Research Board.

Tee, K.F., Khan, L.R. and Chen, H.P. (2013) Probabilistic failure analysis of underground flexible pipes. **Structural Engineering and Mechanics**, 47 (2):167-183.

The sewage networks in UR city 4000 BC. (2016). Baghdad: Al-Masalah.

Trickey, S.A. and Moore, I.D. (2007) Three-dimensional response of buried pipes under circular surface loading. **Journal of Geotechnical and Geoenvironmental Engineering**, 133 (2): 219-223.

Turan, A., El Nagger, M.H. and Dundas, D. (2013) Investigation of induced trench method using a full scale test embankment. **Geotechnical and Geological Engineering**, 31 (2): 557-568.

Turney, M.S., Howard, A. and Bambei, J.H. (2015) “Compacting pipeline embedment soils with saturation and vibration.” In Sever, V.F. and Osborn, L. (eds.) **Pipelines 2015: Recent Advances in Underground Pipeline Engineering and Construction**. Baltimore: pp. 615-625.

Vivek, P. (2011) **Static and dynamic interference of strip footings in layered soil**. MTech thesis, Indian Institute of Technology, Kanpur.

Witthoeft, A.F. and Kim, H. (2016) Numerical investigation of earth pressure reduction on buried pipes using EPS geofoam compressible inclusions. **Geosynthetic International**, 23 (4): 287-300.

Wong, L.S., Allouche, E.N., Dhar, A.S., Baumert, M. and Moore, I.D. (2006) Long-term monitoring of SIDD type IV installations. **Canadian Geotechnical Journal**, 43 (4): 392-408.

Xu, M., Shen, D. and Rakitin, B. (2017). The longitudinal response of buried large-diameter reinforced concrete pipeline with gasketed bell-and-spigot joints subjected to traffic loading. **Tunnelling and Underground Space Technology**, 64: 117-132.

Yeau, K.Y., Sezen, H. and Fox, P.J. (2014) Simulation of behavior of in-service metal culverts. **Journal of Pipeline Systems Engineering and Practice**, 5 (2): 04013016.

Yoo, C.S., Lee, K.M., Chung, S.W. and Kim, J.S. (1999) Interaction between flexile buried pipe and surface load. **Journal of Korean Geotechnical Society**, 15 (3): 83-97.

Young, O.C. and O'Reilly, M.P. (1987) **A guide to design loadings for buried rigid pipes**. London: Department of Transport.

Zhan, C. and Rajani, B. (1997) Load transfer analyses of buried pipe in different backfills. **Journal of Transportation Engineering**, 123 (6): 447-453.

BIBLIOGRAPHY

Abuhajar, O., El Naggar, H. and Newson, T. (2015) Seismic soil–culvert interaction. **Canadian Geotechnical Journal**, 52(11): 1649-1667.

Abuhajar, O., El Naggar, H. and Newson, T. (2015) Static soil culvert interaction the effect of box culvert geometric configurations and soil properties. **Computers and Geotechnics**, 69: 219-235.

Abuhajar, O., El Naggar, H. and Newson, T. (2016) Numerical modeling of soil and surface foundation pressure effects on buried box culvert behavior. **Journal of Geotechnical and Geoenvironmental Engineering**, 142 (12): 04016072.

Acharya, R., Han, J. and Parsons, R.L. (2016) Numerical analysis of low-fill box culvert under rigid pavement subjected to static traffic loading. **International Journal of Geomechanics**, 16 (5): 04016016.

Acharya, R., Han, J., Brennan, J.J., Parsons, R.L. and Khatri, D.K. (2014) Structural response of a low-fill box culvert under static and traffic loading. **Journal of Performance of Constructed Facilities**, 30 (1): 04014184.

Alani, A.M. and Faramarzi, A. (2015) Predicting the probability of failure of cementitious sewer pipes using stochastic finite element method. **International journal of environmental research and public health**, 12 (6): 6641-6656.

Al-Shayea, N., Abduljauwad, S., Bashir, R., Al-Ghamedy, H. and Asi, I. (2003) Determination of parameters for a hyperbolic model of soils. **Proceedings of the Institution of Civil Engineers - Geotechnical Engineering**, 156 (2): 105-117.

Ban, H., Park, S. W. and Kim, Y. R. (2013) Performance evaluation of buried concrete pipe under heavy traffic load. **Journal of the Korean Geotechnical Society**, 29 (12): 69-75. (In Korean).

Beben, D. (2013) Dynamic amplification factors of corrugated steel plate culverts. **Engineering Structures**, 46: 193-204.

Blanco, A., Pujadas, P., Cavalaro, S.H.P. and Aguado, A. (2014) Methodology for the design of controlled low-strength materials. Application to the backfill of narrow trenches. **Construction and Building Materials**, 72: 23-30.

Brachman , R.W.I. and Krushelnitzky, R.P. (2005) Response of a landfill drainage pipe buried in a trench. **Canadian Geotechnical Journal**, 42 (3): 752–762.

Celebi, E. and Schmid, G. (2005) Investigation of ground vibrations induced by moving loads**. Engineering Structures**, 27 (14): 1981-1998.

Chen, B. and Sun, L. (2013) The impact of soil properties on the structural integrity of high-fill reinforced concrete culverts. **Computers and Geotechnics**, 52: 46-53.

Chen, Y., Zhang, H., Zhang, J., Liu, X., Li, X. and Zhou, J. (2015) Failure assessment of X80 pipeline with interacting corrosion defects. **Engineering Failure Analysis**, 47: 67-76.

Clayton, C.R.I., Xu, M., Whiter, J.T., Ham, A. and Rust, M. (2010) Stresses in cast-iron pipes due to seasonal shrink-swell of clay soils. **Proceedings of the Institution of Civil Engineers - Water Management**, 163 (3): 157-162.

Corey, R., Han, J., Khatri, D.K. and Parsons, R.L. (2014) Laboratory study on geosynthetic protection of buried steel-reinforced HDPE pipes from static loading. **Journal of Geotechnical and Geoenvironmental Engineering**, 140 (6): 04014019.

Cui, X., Li, J., Chan, A. and Chapman, D. (2014) Coupled DEM–LBM simulation of internal fluidisation induced by a leaking pipe. **Powder Technology**, 254: 299-306.

Darestani, M.Y., Thambiratnam, D.P., Nataatmadja, A. and Baweja, D. (2007) Structural response of concrete pavements under moving truck loads. **Journal of Transportation Engineering**, 133 (12): 670-676.

Dezfooli, M.S., Abolmaali, A. and Razavi, M. (2014). Coupled nonlinear finite-element analysis of soil–steel pipe structure interaction. **International Journal of Geomechanics**, 15 (1): 04014032.

Dezfooli, M.S., Abolmaali, A., Park, Y., Razavi, M. and Bellaver, F. (2014) Staged construction modeling of steel pipes buried in controlled low-strength material using 3D nonlinear finite-element analysis. **International Journal of Geomechanics**, 15 (6): 04014088.

El-Sawy, K.M. (2003) Three-dimensional modeling of soil-steel culverts under the effect of truckloads. **Thin-walled structures**, 41 (8): 747-768.

Elshimi, T.M., Brachman, R.W.I. and Moore, I.D. (2013) Effect of truck position and multiple truck loading on response of long-span metal culverts. **Canadian Geotechnical Journal**, 51 (2): 196-207.

Erdogmus, E., Skourup, B.N. and Tadros, M. (2010) Recommendations for design of reinforced concrete pipe. **Journal of Pipeline Systems Engineering and Practice**, 1 (1): 25-32.

Flener, E.B. and Karoumi, R. (2009) Dynamic testing of a soil–steel composite railway bridge. **Engineering structures**, 31 (12): 2803-2811.

García, D.B. and Moore, I.D. (2015) Evaluation and application of the flexural rigidity of a reinforced concrete pipe. **Journal of Pipeline Systems Engineering and Practice**, 7 (1): 04015015.

Hegde, A.M. and Sitharam, T.G. (2015) Experimental and numerical studies on protection of buried pipelines and underground utilities using geocells. **Geotextiles and Geomembranes**, 43 (5): 372-381.

Hong, W.P., Bov, M.L. and Kim, H.M. (2016) Prediction of vertical pressure in a trench as influenced by soil arching. **KSCE Journal of Civil Engineering**, 20 (7): 2711-2718.

Howard, I.L. and Warren, K.A. (2009) Finite-element modeling of instrumented flexible pavements under stationary transient loading. **Journal of Transportation Engineering**, 135 (2): 53-61.

Jung, J.K., O'Rourke, T.D. and Olson, N.A. (2013) Lateral soil-pipe interaction in dry and partially saturated sand. **Journal of Geotechnical and Geoenvironmental Engineering**, 139 (12): 2028-2036.

Kang, J., Parker, F., Kang, Y.J. and Yoo, C.H. (2008) Effects of frictional forces acting on sidewalls of buried box culverts. **International journal for numerical and analytical methods in geomechanics**, 32 (3): 289-306.

Katona, M.G. and McGrath, T.J. (2007) Guideline for Interpreting AASHTO Specifications to Design or Evaluate Buried Structures with Comprehensive Solution Methods. **Transportation Research Record: Journal of the Transportation Research Board**, 2028: 211-217.

Kenneally, B., Musimbi, O.M., Wang, J. and Mooney, M.A. (2015) Finite element analysis of vibratory roller response on layered soil systems. **Computers and Geotechnics**, 67: 73-82.

Kunert, H.G., Otegui, J.L. and Marquez, A. (2012) Nonlinear FEM strategies for modeling pipe–soil interaction. **Engineering Failure Analysis**, 24: 46-56.

Lavasan, A.A., Talsaz, A., Ghazavi, M. and Schanz, T. (2016) Behavior of shallow strip footing on twin voids. **Geotechnical and Geological Engineering**, 34 (6): 1791-1805.

Lee, Y., Feng, M.Q. and Lee, E.T. (2014) Deflection of buried prestressed concrete cylinder pipe with soil-pipe interaction. **KSCE Journal of Civil Engineering**, 18 (7): 2191-2195.

Lee, Y.G., Kim, S.H., Park, J.S., Kang, J.W. and Yoon, S.J. (2015) Full-scale field test for buried glass-fiber reinforced plastic pipe with large diameter. **Composite Structures**, 120: 167-173.

Li, L. and Aubertin, M. (2015) Numerical analysis of the stress distribution in symmetrical backfilled trenches with inclined walls. I**ndian Geotechnical Journal**, 45 (3): 278-290.

Liu, P.F., Zheng, J.Y., Zhang, B.J. and Shi, P. (2010) Failure analysis of natural gas buried X65 steel pipeline under deflection load using finite element method. **Materials & Design**, 31 (3): 1384-1391.

Luo, X., Lu, S., Shi, J., Li, X. and Zheng, J. (2015) Numerical simulation of strength failure of buried polyethylene pipe under foundation settlement. **Engineering Failure Analysis**, 48: 144-152.

Mai, V.T., Hoult, N.A. and Moore, I.D. (2014) Effect of deterioration on the performance of corrugated steel culverts. **Journal of Geotechnical and Geoenvironmental Engineering**, 140 (2): 04013007.

McGuigan, B.L. and Valsangkar, A.J. (2010) Centrifuge testing and numerical analysis of box culverts installed in induced trenches. **Canadian Geotechnical Journal**, 47 (2): 147-163.

McGuigan, B.L. and Valsangkar, A.J. (2011) Field monitoring and analysis of twin 3660 mm inside diameter induced trench culverts installed under 21.7 m of fill. **Canadian Geotechnical Journal**, 48 (5): 781-794.

McGuigan, B.L., Oshati, O.S., Parker, B.A. and Valsangkar, A.J. (2016). Post-construction performance of induced trench rigid culverts. **Canadian Geotechnical Journal**, 53 (11): 1807-1821.

Meguid, M.A. and Hussein, M.G. (2017) A numerical procedure for the assessment of contact pressures on buried structures overlain by EPS geofoam inclusion. **International Journal of Geosynthetics and Ground Engineering**, 3: 2.

Mehrjardi, G.T., Tafreshi, S.M. and Dawson, A.R. (2012) Combined use of geocell reinforcement and rubber–soil mixtures to improve performance of buried pipes. **Geotextiles and Geomembranes**, 34: 116-130.

Mohamed, N. and Nehdi, M.L. (2016) Rational finite element assisted design of precast steel fibre reinforced concrete pipes. **Engineering Structures**, 124: 196-206.

Mohamed, N., Soliman, A.M. and Nehdi, M.L. (2014) Full-scale pipes using dry-cast steel fibre-reinforced concrete. **Construction and Building Materials**, 72: 411-422.

Mohamed, N., Soliman, A.M. and Nehdi, M.L. (2015) Mechanical performance of full-scale precast steel fibre-reinforced concrete pipes. **Engineering Structures**, 84: 287-299.

Nehdi, M.L., Mohamed, N. and Soliman, A.M. (2016). Investigation of buried full-scale SFRC pipes under live loads. **Construction and Building Materials**, 102: 733-742.

Oey, H.S., Greggerson Jr, V.L. and Womack, D.P. (1984) Buried gas pipelines under vehicular crossings. **Journal of Transportation Engineering**, 110 (2): 203-222.

Ozdemir, Z., Coulier, P., Lak, M.A., François, S., Lombaert, G. and Degrande, G. (2013) Numerical evaluation of the dynamic response of pipelines to vibrations induced by the operation of a pavement breaker. **Soil Dynamics and Earthquake Engineering**, 44: 153-167.

Picoux, B., El Ayadi, A. and Petit, C. (2009) Dynamic response of a flexible pavement submitted by impulsive loading. **Soil Dynamics and Earthquake Engineering**, 29 (5): 845-854.

Poorooshasb, H.B. (1991) An analytical reevaluation of Marston theory of earth pressure on buried box structures. **Soils and foundations**, 31 (4): 1-12.

Potter, J.C., 1985. Effects of Vehicles on Buried, High-Pressure Pipe. **Journal of Transportation Engineering**, 111 (3): 224-236.

Rajeev, P. and Kodikara, J. (2011) Numerical analysis of an experimental pipe buried in swelling soil. **Computers and Geotechnics**, 38: 897-904.

Rajeev, P., Chan, D. and Kodikara, J. (2012) Ground–atmosphere interaction modelling for long-term prediction of soil moisture and temperature. **Canadian Geotechnical Journal**, 49 (9): 1059-1073.

Royal, A.C.D., Hunt, D.V.L., Rogers, C.D.F. and Chapman, D.N. (2010) Numerical simulation of the creation and performance of extruded concrete linings in microtunnelling. **Tunnelling and Underground Space Technology**, 25: 745-753.

Saadeldin, R., Hu, Y. and Henni, A. (2015) Numerical analysis of buried pipes under field geo-environmental conditions. **International Journal of Geo-Engineering**, 6: 6.

Sezen, H., Yeau, K.Y. and Fox, P.J. (2008) In-situ load testing of corrugated steel pipe-arch culverts. **Journal of Performance of Constructed Facilities**, 22 (4): 245-252.

Simpson, B., Moore, I.D. and Hoult, N.A. (2015) Experimental investigation of rehabilitated steel culvert performance under static surface loading. **Journal of Geotechnical and Geoenvironmental Engineering**, 142 (2): 04015076.

Smith, G. and Watkins, R. (2004) "The Iowa formula it's use and misuse when designing flexible pipe." In Galleher, Jr, J.J. and Stift, M.T. (eds.) **Pipeline Engineering and Construction: What's on the Horizon?**. California: pp. 1-7.

Srivastava, A., Goyal, C.R. and Raghuvanshi, A. (2013) Load settlement response of footing placed over buried flexible pipe through a model plate load test. **International Journal of Geomechanics**, 13 (4): 477-481.

Suleiman, M.T., Lohnes, R.A., Wipf, T.J. and Klaiber, F.W. (2003) Analysis of deeply buried flexible pipes. **Transportation Research Record: Journal of the Transportation Research Board**, 1849: 124-134.

Trickey, S.A., Moore, I.D. and Balkaya, M. (2016) Parametric study of frost-induced bending moments in buried cast iron water pipes. **Tunnelling and Underground Space Technology**, 51: 291-300.

Wols, B.A. and Van Thienen, P. (2014) Modelling the effect of climate change induced soil settling on drinking water distribution pipes. **Computers and Geotechnics**, 55: 240-247.

Wu, J., Liang, J. and Adhikari, S. (2014) Dynamic response of concrete pavement structure with asphalt isolating layer under moving loads. **Journal of Traffic and Transportation Engineering (English Edition)**, 1 (6): 439-447.

Yeau, K.Y., Sezen, H. and Fox, P.J. (2014) Simulation of behavior of in-service metal culverts. **Journal of Pipeline Systems Engineering and Practice**, 5 (2): 04013016.

You, Z., Xia, Y., Hu, C. and Wang, B. (2001) Finite element analysis of concrete pavements over culverts. **International Journal of Geomechanics**, 1 (3): 337-350.

Zhang, J., Liang, Z. and Han, C. (In press) Mechanical behaviour analysis of buried pressure pipeline crossing ground settlement zone. **International Journal of Pavement Engineering**.